

# Results from measurements on the PV-VENT systems at Lundebjerg



# **Results from measurements on the PV-VENT systems at Lundebjerg**

**Søren Østergaard Jensen**

**Solar Energy Centre Denmark  
Danish Technological Institute**

**May 2001**

## Preface

The present report concludes together with (Jensen, 2000a) Solar Energy Centre Denmark's (Danish Technological Institute) measuring work in the PV-VENT project. The measuring project was partly financed by EU via the JOULE project "PV-VENT – Low cost energy efficient PV-ventilation in retrofit housing", contract no. JOR3-CT97-0160 and partly by the Danish Ministry of Environment and Energy via the project "PV-VENT", journal no. 51181/97-0021.

The project group behind the project was:

Cenergia Energy Consultants, DK  
Fortum Energy (former NESTE-NAPS), SF  
AirVex Danmark (former Temovex Denmark), DK  
FSB, DK  
Danish Technological Institute, DK  
Ecofys, NL  
PA-Energy, DK  
NTNU, N  
Copenhagen Energy, DK

The following persons have participated in the measuring project:

Søren Østergaard Jensen. M.Sc., Solar Energy Centre Denmark  
Hossein Gohari, B.Sc., Heating Technology, Danish Technological Institute  
Trine Dalsgaard Jacobsen, M.Sc., Solar Energy Centre Denmark  
William Otto, laboratory technician, Solar Energy Centre Denmark  
Lars Molnit, student (B.Sc.), Solar Energy Centre Denmark  
Bertel Jensen, B.Sc., Solar Energy Centre Denmark  
Ulrik Mehr, M.Sc., Solar Energy Centre Denmark  
Hans Olsen. B.Sc., Ventilation and Environment. Technological Institute of Denmark  
Anne Rasmussen, M.Sc., Cenergia Energy Consultants  
Lisbet Michaelsen, B.Sc., Cenergia Energy Consultants

Results from measurements on the PV-Vent systems at Lundebjerg  
1<sup>st</sup> printing, 1<sup>st</sup> edition  
© Danish Technological Institute  
Energy division

ISBN: 87-7756-611-0  
ISSN: 1600-3780

## List of content

1.	Description of the PV-VENT systems at Lundebjerg .....	3
1.1.	Brief description of the PV-VENT systems .....	7
1.2.	Detailed description of the PV-VENT systems .....	8
1.2.1.	The PV-gable .....	9
1.2.2.	Ventilation systems in no. 36 B .....	13
1.2.3.	Ventilation systems in no. 40 (and 38) .....	14
1.2.3.1.	Apartment 40 A .....	14
1.2.3.2.	Apartment 40 B .....	17
1.2.3.3.	Common ventilation system in 40 C (and 38) .....	17
1.2.4.	Solar ventilation chimneys .....	19
1.2.5.	PV-mixer .....	23
1.2.6.	Control .....	26
1.2.6.1.	Staircase no. 36 .....	26
1.2.6.2.	Staircase no. 38 .....	26
1.2.6.3.	Staircase no. 40 .....	27
1.2.7.	Power to the fans .....	28
1.3.	External insulation of the facades .....	28
2.	Measuring system .....	30
2.1.	Measuring points .....	30
2.1.1.	Weather data .....	30
2.1.2.	PV-gable and ventilation system in no. 36 .....	32
2.1.3.	Apartment 40 IIA .....	36
2.1.4.	Apartment 40 IIB .....	39
2.1.5.	Common ventilation system in 40 C .....	40
2.1.6.	Solar ventilation chimneys .....	40
2.2.	Data collection .....	44
2.3.	Treatment of the measured data .....	45
3.	Measurements .....	46
3.1.	Measurements from week 5 and 6, 2001 .....	46
3.1.1.	Gable .....	46
3.1.2.	Apartment 36 IIB .....	52
3.1.3.	Apartment 40 IIA .....	52
3.1.3.	Apartment 40 IIB .....	69
3.1.4.	Common ventilation system in 40 C .....	76
3.1.5.	Solar ventilation chimneys .....	87
3.2.	Calculations based on the measurements and more general conclusions .....	108
3.2.1.	The efficiency of the air to air heat exchangers .....	108
3.2.2.	Fan power .....	121
3.2.3.	Efficiency of the solar ventilation chimneys as solar air collectors .....	123
3.2.4.	Temperatures of the PV-panels .....	128
3.2.5.	Air temperatures in the PV-gable .....	132
3.2.6.	The PV-mixer .....	135
3.3.	Obtainable savings of the systems .....	141
3.3.1.	Simulation program .....	141
3.3.2.	Simulation results .....	143



4.	Conclusions .....	149
4.1.	Aims of the PV-VENT project .....	149
4.2.	Results from the PV-VENT project .....	149
4.2.1.	Architectural results .....	149
4.2.2.	Pre-heating of fresh air – cooling of PV-panels .....	150
4.2.3.	Air to air heat exchanger .....	151
4.2.4.	Low fan power .....	151
4.2.5.	Direct coupling of PV-panels and fans .....	151
4.2.6.	Total systems .....	152
4.2.7.	General conclusions .....	152
5.	References .....	153
Appendix A	Data sheets for the PV-panels .....	154
Appendix B	Data sheets for the heat exchangers and fans .....	165

## 1. Description of the PV-VENT systems at Lundebjerg

The objective of the PV-VENT project was to research, develop and test low cost, high efficiency PV-powered ventilation systems for retrofitting of apartment blocks. Systems where the fans are powered directly by the PV panels and where the waste heat from the PV panels is utilized to pre-heat fresh air to the apartments.

The present report describes the obtained experience from measurements on the PV-VENT systems installed in an apartment building in the built-up area Lundebjerg situated in Skovlunde a small town at the outskirts of Copenhagen (approximately 12 km west of Copenhagen) – see figure 1.1. The built-up area Lundebjerg managed by FSB consists in total of 16 apartment blocks with 483 apartments. The site plan for Lundebjerg is shown in figure 1.2.



Figure 1.1. The location of Skovlunde where Lundebjerg is situated.

The whole built-up area is facing a renovation of especially the exterior surfaces. The exterior walls are poorly insulated while the windows need replacement. It was decided prior to the renovation of the whole built-up area to test the renovation on one single block – Lundebjerg 36-40. It was further decided to include PV-VENT systems in this test renovation.

The three-storied building (Lundebjerg 36-40) where the PV-VENT systems are being tested was erected in the late 60'ies and is typical for that period. The building contains three staircases with 27 apartments and has a net floor area of 1600 m<sup>2</sup>. Figure 1.3 shows the apartment blocks after the renovation while figure 1.4 shows a similar but not renovated block. The apartment blocks at Lundebjerg are situated with the facades facing east and west, while the gables are facing south and north

The renovation contained the following items:

- External insulation of the exterior walls,
- Replacement of the existing windows,
- Glaze covering of the balconies,
- PV-VENT systems

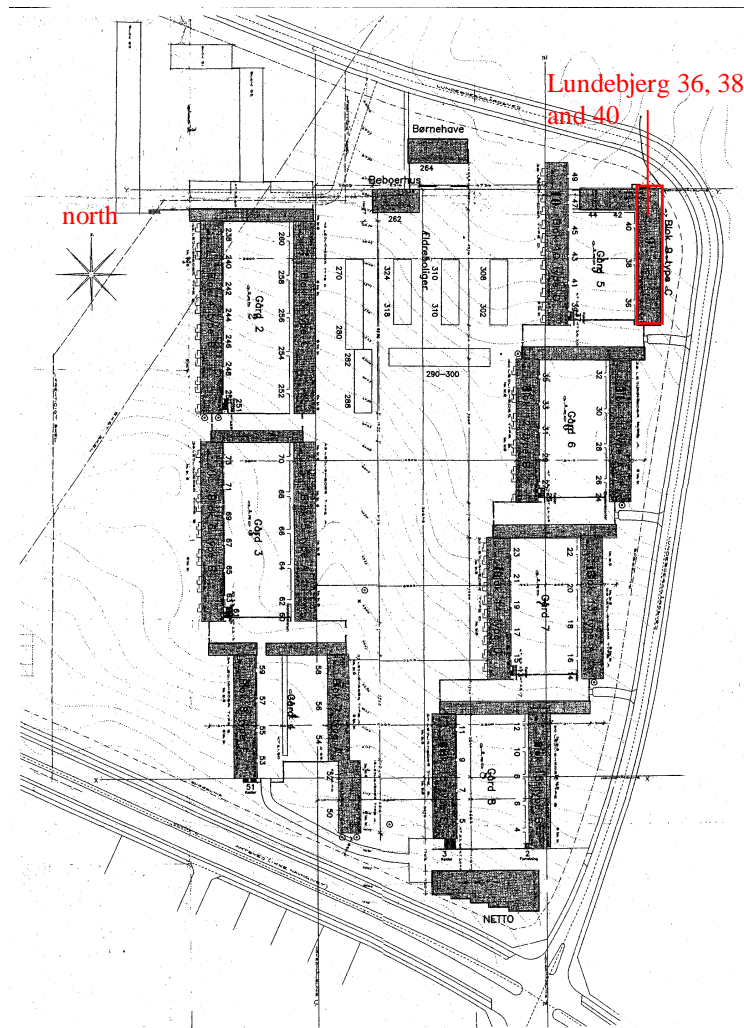


Figure 1.2. Site plan for Lundebjerg

An architectural competition on the renovation of Lundebjerg 36-40 with five well known Danish architect firms was launched in March, 1998. The winner of the competition was announced in June 1998 (Jury, 1998). The winner was the architect firm Vandkunsten Architects, which is known for its very distinct architecture – black and glass. One of the reasons why Vandkunsten Architects won the competition was their idea of solar ventilation chimneys on the roof as shown on figure 1.3. The solar ventilation chimneys overcome the problem of only the gable facing south resulting in less well-oriented area for location of the PV-panels. The architect competition is described further in (Lien and Hestness, 1999).

However, the tenants and the housing organisation did not like to change the appearance of the block from the yellow brick walls shown in figure 1.4 to black cement facade elements. After almost a year the co-operation with Vandkunsten Architects was given up and the job was given on to another of the participants of the architectural competition – Suensons Architects, which in their competition proposal had used yellow brick cladding on the exterior walls. Suensons Architects was asked to combine their yellow brick walls with the solar ventilation chimneys and French balconies proposed by Vandkunsten Architects.

The actual renovation started by the beginning of 2000 and lasted due to several difficulties most of 2000 and not the foreseen 4 months.



Figure 1.3. East facade and south gable of Lundebjerg 36-40 after the renovation.



Figure 1.4. The east facade of a non-renovated building similar to Lundebjerg 36-40.



Figures 1.5 and 1.6 show the west facade of Lundebjerg 36-40 and a similar not renovated block. Some of the balconies were as seen in figure 1.6 glazed prior to the renovation.



Figure 1.5. The west facade of Lundebjerg 36-40.



Figure 1.6. The west facade of a non-renovated block.

The apartment block consists as mentioned of 3 staircases each with 9 dwellings – 3 on each floor. The three apartments of each floor are different not only in orientation to the staircase but also in size and thereby also number of rooms. Figure 1.7 shows a plan of one of the floors of a staircase. The dwellings are labelled A, B and C. Apartments A and B have a living room and 2 rooms, while apartments C have a living room and one room. The net floor area of the three apartment types is: A: 64.5 m<sup>2</sup>, B: 64.5 m<sup>2</sup> and C: 49 m<sup>2</sup>.

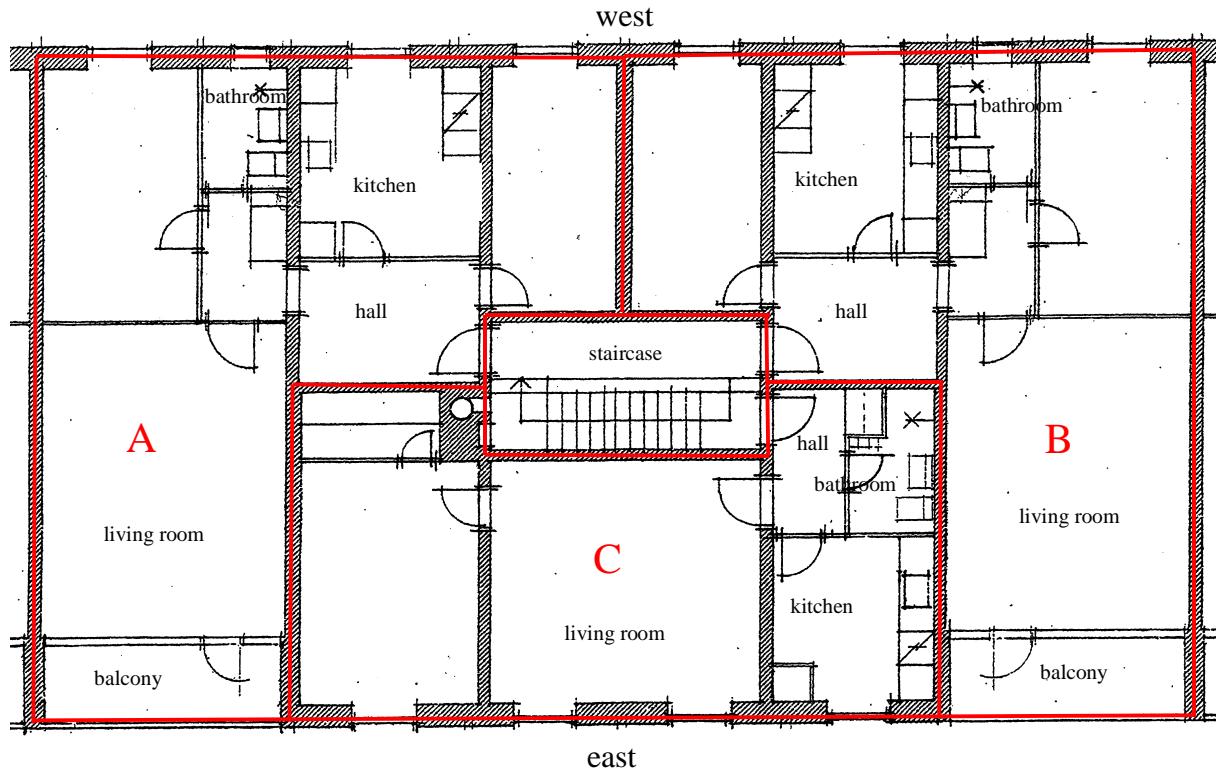


Figure 1.7. Plan of one floor of one of the staircases in Lundebjerg 36-40

The following description of the renovation will mainly focus on the PV-VENT systems.

### 1.1. Brief description of the PV-VENT systems

Several PV-VENT systems were tested in Lundebjerg – in total 5 different systems. The five systems are schematically shown in figure 1.8.

- Type 1: 3 systems in no. 40 (the A apartments) with individual heat exchangers and air intake behind 1.7 m<sup>2</sup> polycrystalline (c-Si) PV-panels in the facades. The fans are powered directly by the PV-panels in the facades.
- Type 2: 3 systems in no. 40 (the B apartments) with individual heat exchangers and air intake behind the in total 7.7 m<sup>2</sup> polycrystalline (c-Si) PV-panels in the ventilation chimney on the roof. Each of the three fans is powered directly by 1.28 m<sup>2</sup> PV-panels on the ventilation chimney.

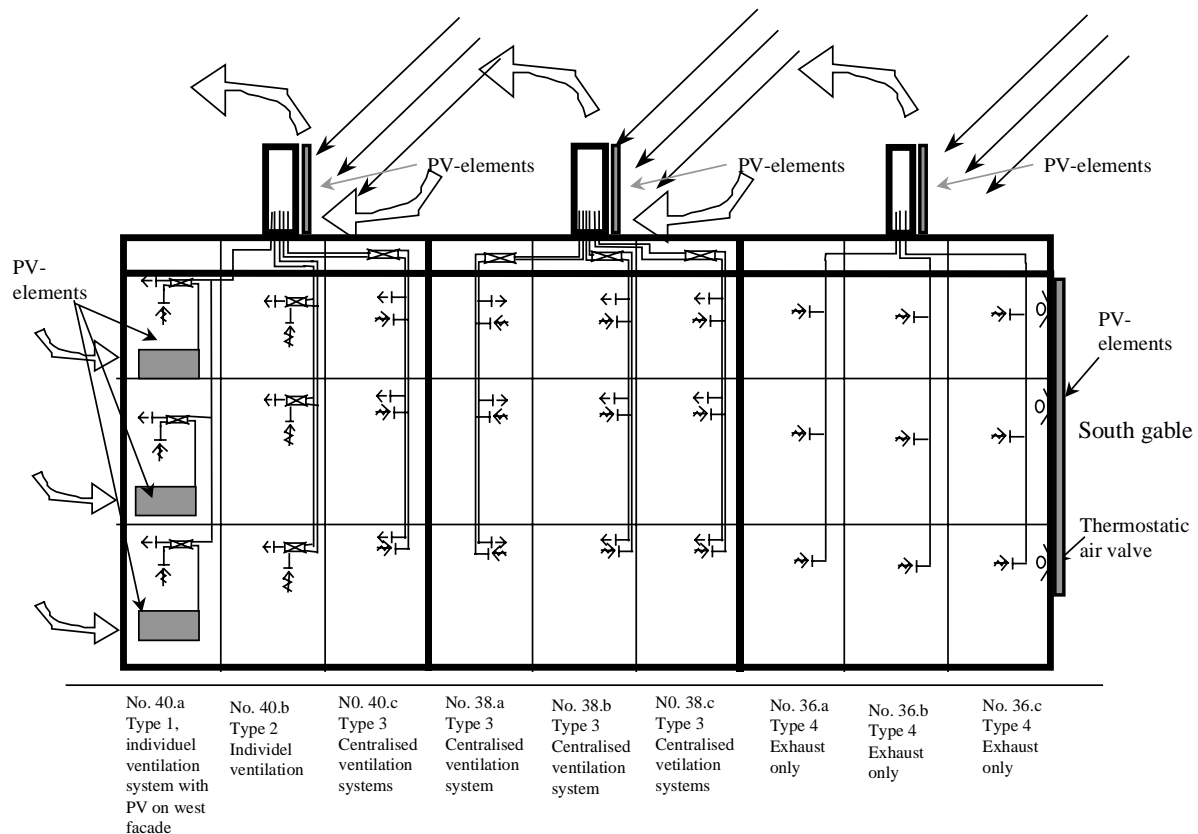


Figure 1.8. The five different PV-VENT systems at Lundebjerg.

- Type 3: 3 dwellings in no. 40 (the C apartments) and 9 dwellings in no. 38 with a common heat exchanger per 3 dwellings in the attic and air intake behind the in total  $7.7 \text{ m}^2$  polycrystalline (c-Si) PV-panels in the ventilation chimneys on the roof. Each of the three fans is powered directly by  $2.56 \text{ m}^2$  ( $3.84 \text{ m}^2$  for the C apartments in no. 40) PV-panels on the ventilation chimney.
- Type 4a: 3 dwellings in no. 36 (the B apartments) with exhaust ventilation and air intake behind PV-panels in the gable.  $52 \text{ m}^2$  thin-film (a-Si) PV-panels on the gable are grid connected. The fan for the three dwellings is powered directly by  $2.56 \text{ m}^2$  crystalline PV-panels on the ventilation chimney.
- Type 4b: 6 dwellings in no. 36 (the A and C apartments) with exhaust ventilation and no pre-heating of the fresh air. Each of the two fans is powered directly by  $2.56 \text{ m}^2$  PV-panels on the ventilation chimney on the roof.

## 1.2. Detailed description of the PV-VENT systems

The five different PV-VENT systems will in the following be described in more details. The description will be divided in different subdescriptions of the: PV-gable, the systems in no. 36, the systems in no. 40 and the solar ventilation chimneys.

### 1.2.1. The PV-gable

Figure 1.9 shows the south facing PV-gable. The PV-array consists of 180 thin-film (a-Si) PV-panels (see appendix A) with the dimensions 313 x 923 mm (w x h) (in total 52 m<sup>2</sup>) delivered by Fortum Energy each with a peak power of 12 W<sub>p</sub> resulting in total 2160 W<sub>p</sub>. The PV-array is split into three arrays as shown in figure 1.10 each connected to the grid via an inverter situated in the three apartments next to the gable.



Figure 1.9. The PV-gable.

Figure 1.11 shows the constructions of the PV-gable. The PV-panels are mounted in horizontal aluminium profiles (Leppänen, 1999) which again are mounted on vertical wooden laths giving a air gap behind the PV-panels of between 75 and 110 mm as seen in figure 1.11. Between the air gap and the existing wall is situated 100 mm of mineral wool in a wooden skeleton with a cladding of 9 mm fibre concrete plates.

Besides electricity production the aim of the PV-gable is to pre-heat fresh air to the three dwellings next to the gable. For this reason ducts are located between the air gap behind the PV-panels and the living room and the room next to the gable at each floor as shown in the in figure 1.12. In order to prevent cold draft during periods with low ambient temperature and no sun and to prevent overheating during periods with high solar radiation a Zachomatik inlet diffuser is located in each duct in the wall. A wax motor controlled by a control panel and an electrical resistance-heating element in the wax where the opening and closing temperature set point may be adjusted operates the inlet diffuser. At the installation the inlet diffuser were set to open at a temperature in the air gap behind the PV-panels of 16°C and close again at a temperature at 24°C. Figure 1.13 shows a inlet diffuser.



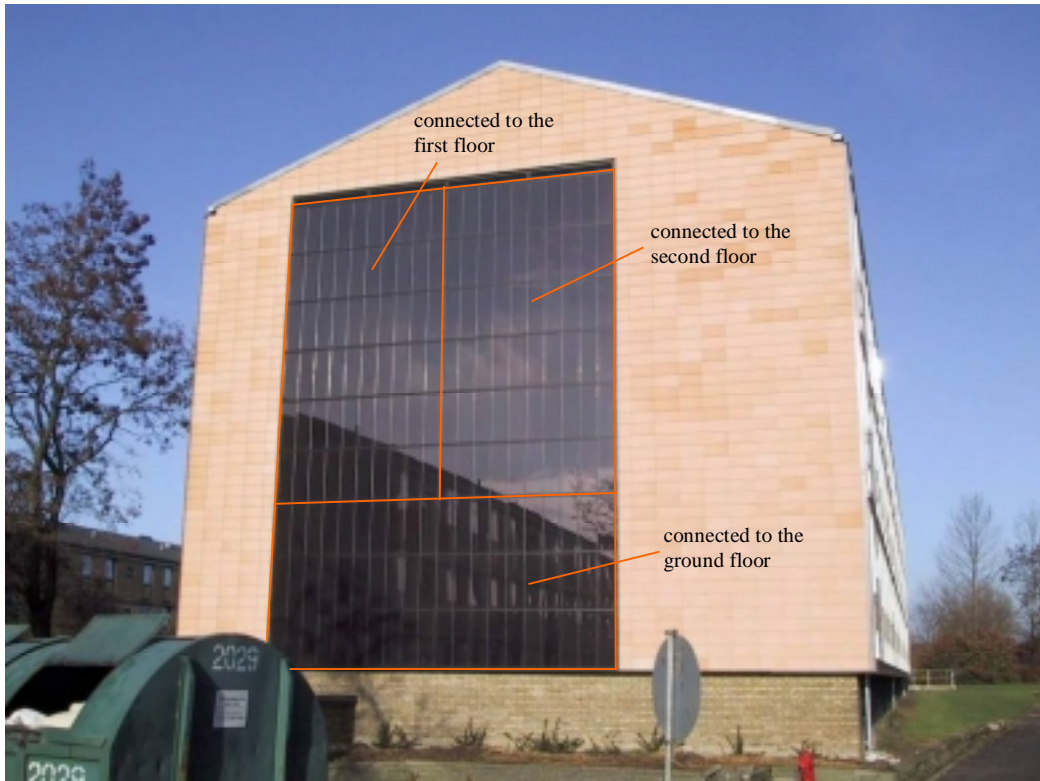


Figure 1.10. The 3 arrays of the PV-gable.

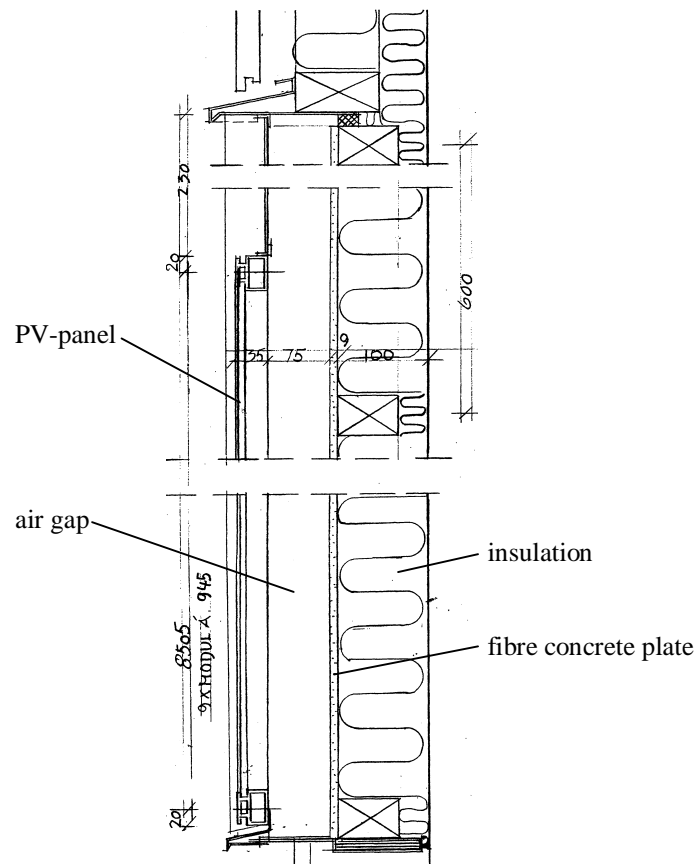


Figure 1.11. The construction of the PV-gable.

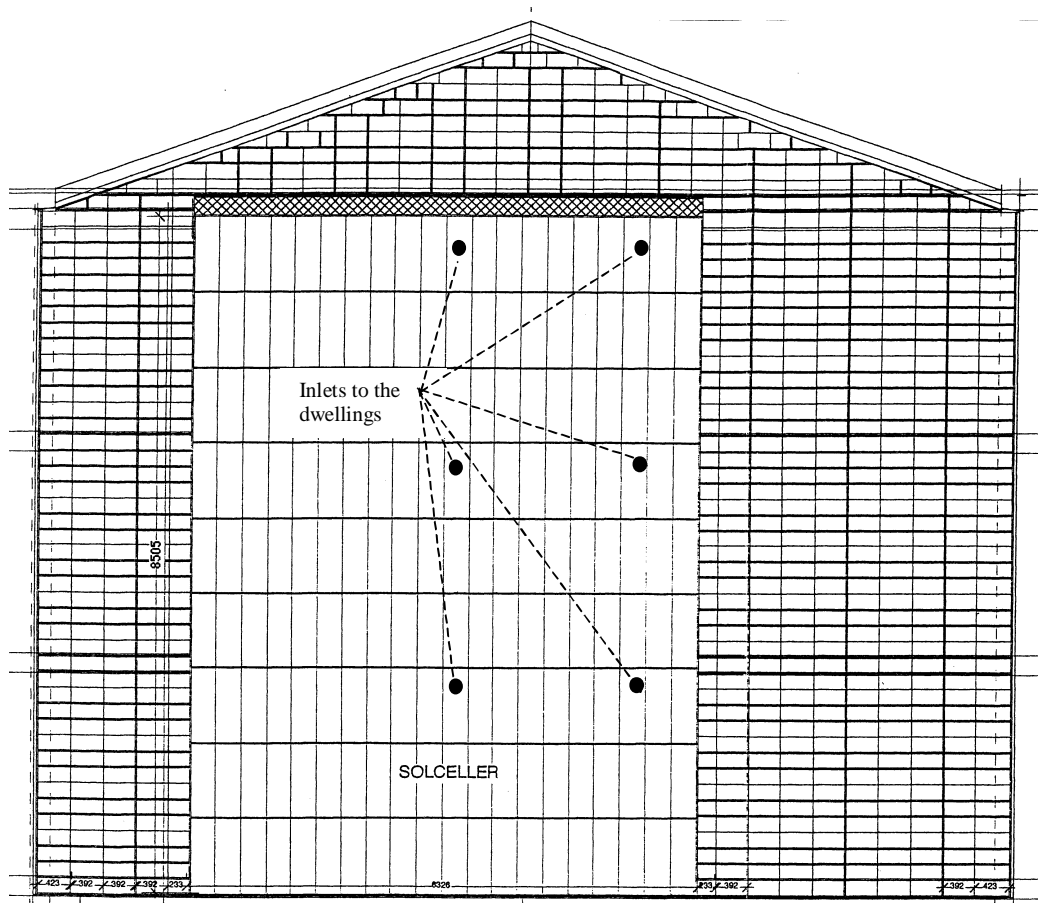


Figure 1.12. Drawing of the PV-gable with locations of the inlets to the dwellings.



Figure 1.13. Inlet diffuser for letting pre-heated air in from the air gap behind the PV-panels in the south gable.

The stream of air from the air gap behind the PV-panels is driven by the under pressure created by the exhaust ventilation from the kitchen and bathroom.

The inlet to the air gap behind the PV-panel is at the bottom of the PV-gable as shown in figure 1.14. Metal plates with holes are located at the inlet in order to prevent birds and larger objects in getting into the air gab.



Figure 1.14. The inlet at the bottom of the PV-gable.

However, during warm periods with sunshine the inlet diffusers to the dwellings will be closed and the air gap behind the PV-panels will overheat, which will reduce the electricity production of the PV-panels. So in order to cool the PV-panels during these periods Orbesen dampers driven by wax motors are installed in the top of the PV-gable. The dampers may be seen at the top of the PV-area in figure 1.9 and figure 1.12 – a close up of one damper is shown in figure 1.15. The dampers start to open at a temperature of 23°C and is fully open at a temperature of 27°C – the dampers starts to close again at a temperature of 24°C and are closed at 21°C. When the dampers start to open the intention is that the PV-panels will be cooled by a buoyancy driven air stream in the air gab.



Figure 1.15. Orbesen damper for summer ventilation of the air gap in the PV-gable.

### 1.2.2. Ventilation systems in no. 36 B

Figure 1.16 shows the ventilation systems in the apartments in no. 36. The exhaust ventilation system extract air from the kitchen and the bathroom with an intended air flow of 72 m<sup>3</sup>/h (kitchen) and 54 m<sup>3</sup>/h (bathroom) = 126 m<sup>3</sup>/h in total which is the flow rate given in the Danish building regulation.

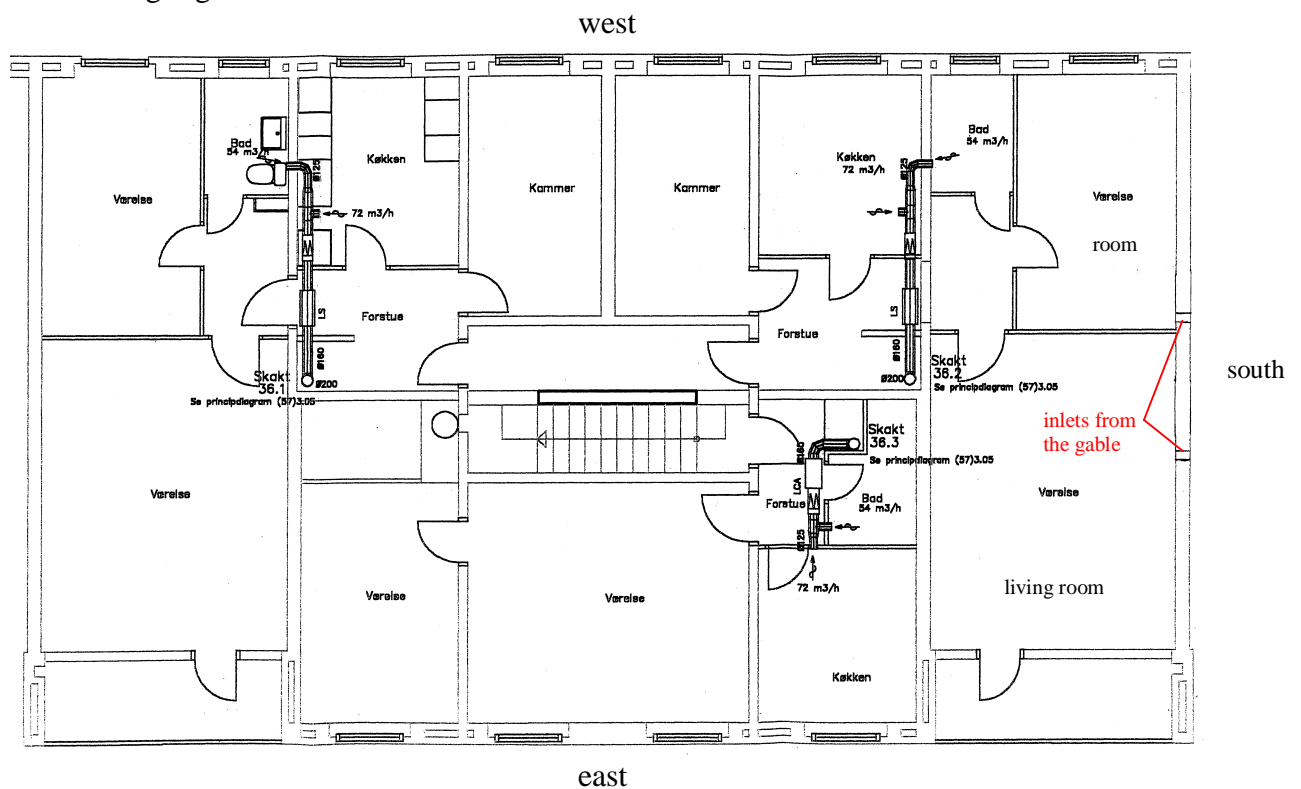


Figure 1.16. Plan of the apartments of one floor in no. 36 with exhaust ventilation.

There is one common exhaust system for each apartment type – i.e. all A apartments, all B apartments and all C apartments in no. 36 share one exhaust ventilation system with the fan developed by AirVex type 280 (56 dc) (Jensen and Peersen, 1999) (see also appendix B) located in the attic and exhaust out through the top of the solar ventilation chimney.

The exhaust fans obtain power via a so-called PV-mixer (the PV-mixer is described later) from the PV-panels on the solar ventilation chimney.

### 1.2.3. Ventilation systems in no. 40 (and 38)

Figure 1.17 shows the ventilation systems in the apartments in no. 40. The A and B apartments has individual ventilation systems with the heat exchanger and fans situated above a new suspended ceiling in the hall, while the C apartments has a common ventilation system with the heat exchanger and fans in the attic. The systems in no. 38 are identical to the system in the C apartment in no. 40 – i.e. three apartments above each other per unit.

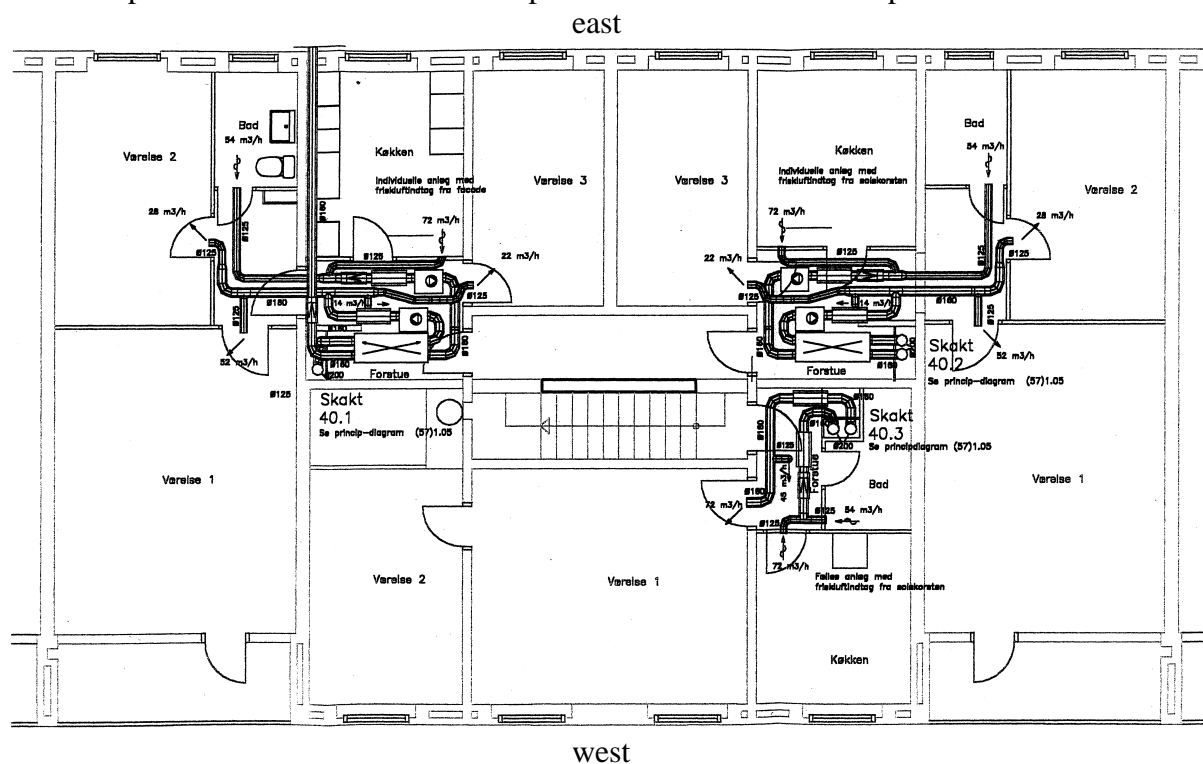


Figure 1.17. Plan of the apartments of one floor in no. 40.

The volume of extracted air is as in the dwellings in no. 36 intended to be  $126 \text{ m}^3/\text{h}$  – i.e.  $72 \text{ m}^3/\text{h}$  from the kitchen and  $54 \text{ m}^3/\text{h}$  from the bathroom. Fresh air is blown into the living room, rooms and the hall. The intended volume flow rate is  $116 \text{ m}^3/\text{h}$  or 8% less than the extracted exhaust air. The air flow rate of fresh air is less than the air flow rate of exhaust air in order to prevent humid air being forced into the constructions.

#### 1.2.3.1. Apartments 40 A

The fresh air to the apartments A in no. 40 is drawn from the facade behind the PV-panels shown in figure 1.18.



Figure 1.18. The three PV-arrays (one for each floor) at the east facade are connected to the ventilation systems in the A apartments in no. 40.

The PV-array for each dwellings consists of two polycrystalline (c-Si) PV-panels (see appendix A) with the dimensions 773 x 1116 mm (w x h) from Fortum Energy with a total area of 1.7 m<sup>2</sup> and a total peak power of 100 W<sub>p</sub>. The PV-panels are via PV-mixers (see later) powering the fans of the systems in the A apartments.

The fresh air to the dwellings is drawn from behind the PV-panels through a 70 mm wide air gap behind the PV-panels as shown in figure 1.19. Figure 1.20 shows the inlets of one PV-array – the bottom inlet should be used during the heating season, while the top inlet should be used during the warm season or when the sun heats the fresh air too much behind the PV-panels. It was originally the intention to locate Orbesen dampers in the top of the PV-panels for overheat protection as in the PV-gable. However, due to a mistake the space for location of the dampers got too small so that the dampers could not be installed. This means that air is always drawn both from behind the PV-panels and directly from outside. The fresh air is, therefore, less preheated than originally intended.





The heat exchanger and fans of the systems are located above the suspended ceiling in the hall of the apartments as shown in figure 1.21. The heat exchangers type JoVex H300 and fans type 175 (56 V dc) where all developed in the project by AirVex (Pedersen, 2001) (see also appendix B).



Figure 1.21. The fans and heat exchanger in the hall of the A apartments.

The exhaust air from the systems is blown out though the solar ventilation chimneys – see later.

### **1.2.3.2. Apartments 40 B**

The ventilation systems in the B apartments are similar to the systems in the A apartments except that the fresh air is not drawn from the facade, but from the solar ventilation chimney. PV-panels at the solar ventilation chimneys are via PV-mixers powering the fans of the systems in the B apartments. The solar ventilation chimneys are described in section 1.2.4

Figure 1.22 shows the ventilation system above the suspended ceiling in the hall (before the ceiling was installed). It is as seen in the figure very crowded above the suspended ceiling.

### **1.2.3.3. Common ventilation system in 40 C (and 38)**

The ventilation system for the C apartments (and all the apartments in no. 38) are common systems for the three C apartments with the fans and the heat exchanger located in the attic as shown in figure 1.23. The fans type 280 (56 V dc) and heat exchangers JoVex L1000 were as for the A and B apartments developed within the project by AirVex (Pedersen, 2001) (see also appendix B).





Figure 1.22. The ventilation systems in the B apartments in no. 40.



Figure 1.23. The common ventilation system for the C apartments in no. 40 and all the apartments in no. 38.

The fresh air and power (via PV-mixers) to the fans are as for the B apartments supplied by the solar ventilation chimney on the roof. The exhaust is as for the A and B apartments blown out through the solar ventilation chimney

#### 1.2.4. Solar ventilation chimneys

Figure 1.24 shows the three solar chimneys – one for each staircase and located above each staircase as shown in figure 1.25. The staircases have obtained a new larger roof light as part of the renovation leading to more daylight in the staircases. The old roof light is shown in figure 1.26.



Figure 1.24. Three solar ventilation chimneys on the roof.

The principle of the solar ventilation chimney for no. 38 and 40 is shown in figure 1.27. The solar ventilation chimney for no. 36 is different from no. 38 and 40 as no air is preheated in the chimney. Fresh air is in no. 38 and 40 drawn from behind the PV-panels in order to pre-heat the fresh air to the dwellings in no. 38 and the B and C dwellings in no. 40. The exhaust air from the dwellings is blown out through the top of the chimneys. An Orbesen damper controlled by a wax motor is situated in the top of the chimneys in order to prevent overheating. The function of the Orbesen dampers is identical to the dampers located in the PV-gable – see section 1.2.1.

The 160 mm wide air gap for the air stream behind the PV-panels is created by a set of vertical profiles as shown in figure 1.28 and 1.29. The mounting systems for the PV-panels was developed within the project and is described in (Leppänen, 1999). There are as shown in figure 1.29 large holes in the profiles in order to allow the air to flow not only vertically but also horizontally in order to allow a more even air flow behind all PV-panels. This is necessary as

the inlet from the air gap behind the PV-panels to the ventilation systems is centred horizontally in the top of the solar ventilation chimney as seen in figure 1.27.

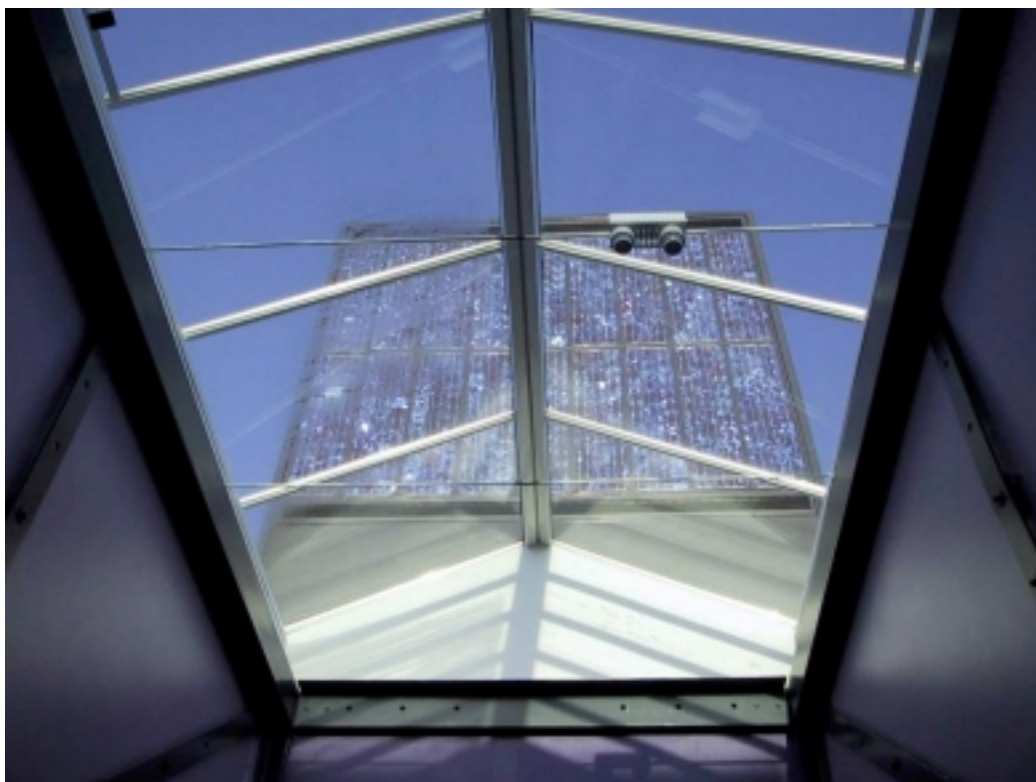


Figure 1.25. One of the solar ventilation chimneys seen through the roof light of a staircase.



Figure 1.26. The original roof light of the staircases.

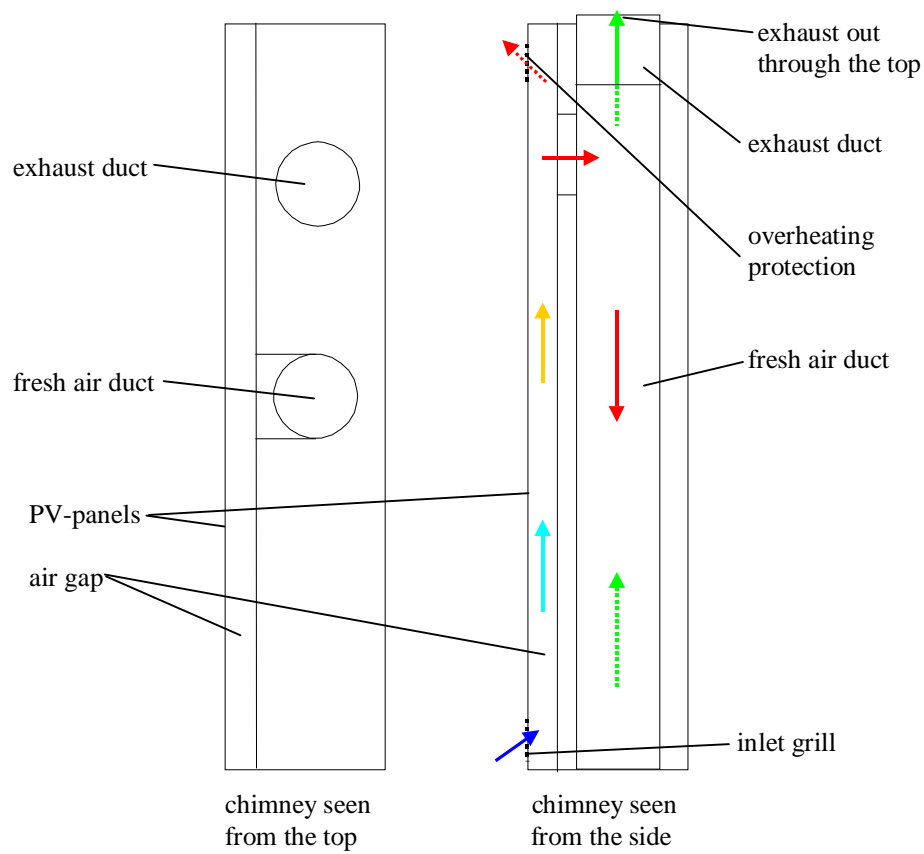


Figure 1.27. The principle of the solar ventilation chimneys.



Figure 1.28. Top of the PV-area of one of the solar ventilation chimneys during mounting.





Figure 1.29. View down the air gap behind the PV-panels of the solar ventilation chimneys.

Figure 1.30 shows the ductworks in the attic to and from one solar ventilation chimney. Figure 1.31 shows the inside of a solar ventilation chimney seen from the attic.



Figure 1.30. Ductworks in the attic to and from one solar ventilation chimney.

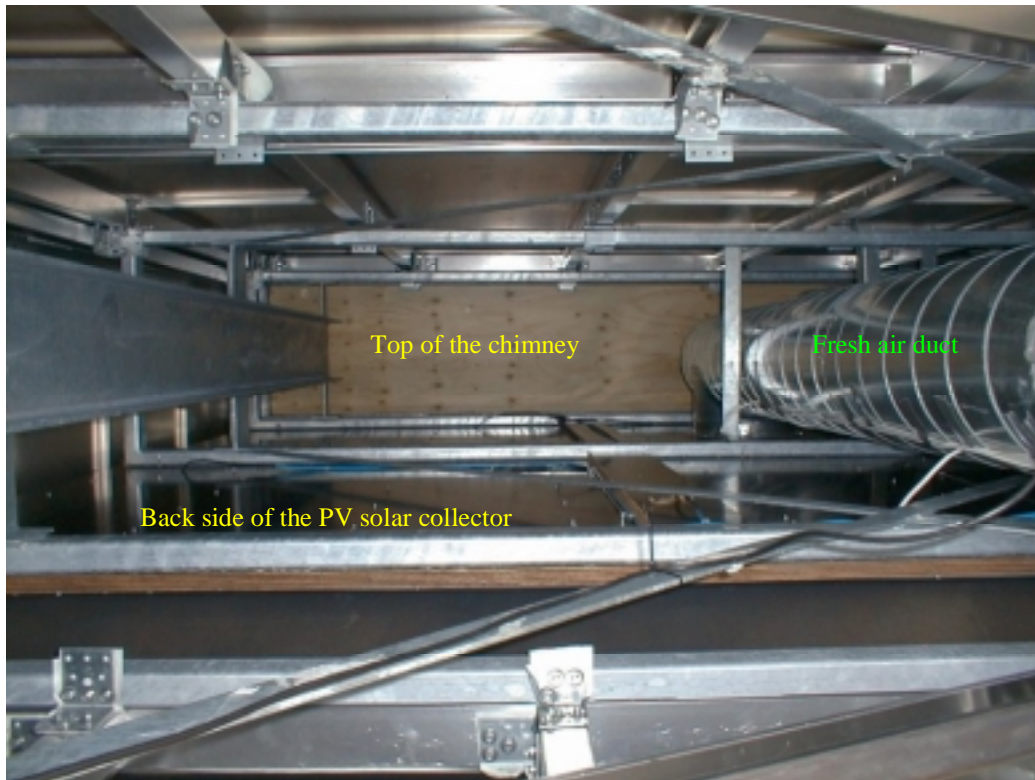


Figure 1.31. The interior of a solar ventilation chimney.

The 18 PV-panels on each chimney are polycrystalline (c-Si) PV-panels (see appendix A) delivered by Fortum Energy. The dimensions of the panels are 330 x 1293 mm (w x h) with a peak power of 50 W<sub>p</sub> each. Figure 1.32 and 1.33 shows the connection of the PV-panels. For the chimney above no. 36 and 38 the PV-panels are connected electrically as shown in figure 1.32. 6 panels are connected to the fans of either the A, B or C apartments. For the chimney at no. 40 the PV-panels are electrically connected into 4 arrays as shown in figure 1.33. 3 panels are connected to each of the B apartments, while the remaining 9 panels are connected to the system of the C apartments.

### 1.2.5. PV-mixer

The dc fans of the ventilation systems are directly connected to the PV-panels. However, the PV-panels are not during the night and during overcast conditions able to run the fans at the required speed. A so-called PV-mixer has, therefore, been developed as part of the project. The function of the PV-mixer is to ensure that as much electricity from the PV-panels as possible is used for running the fans. If the PV-power is too low to run the fans the PV-mixer top up with electricity from the grid via a transformer.

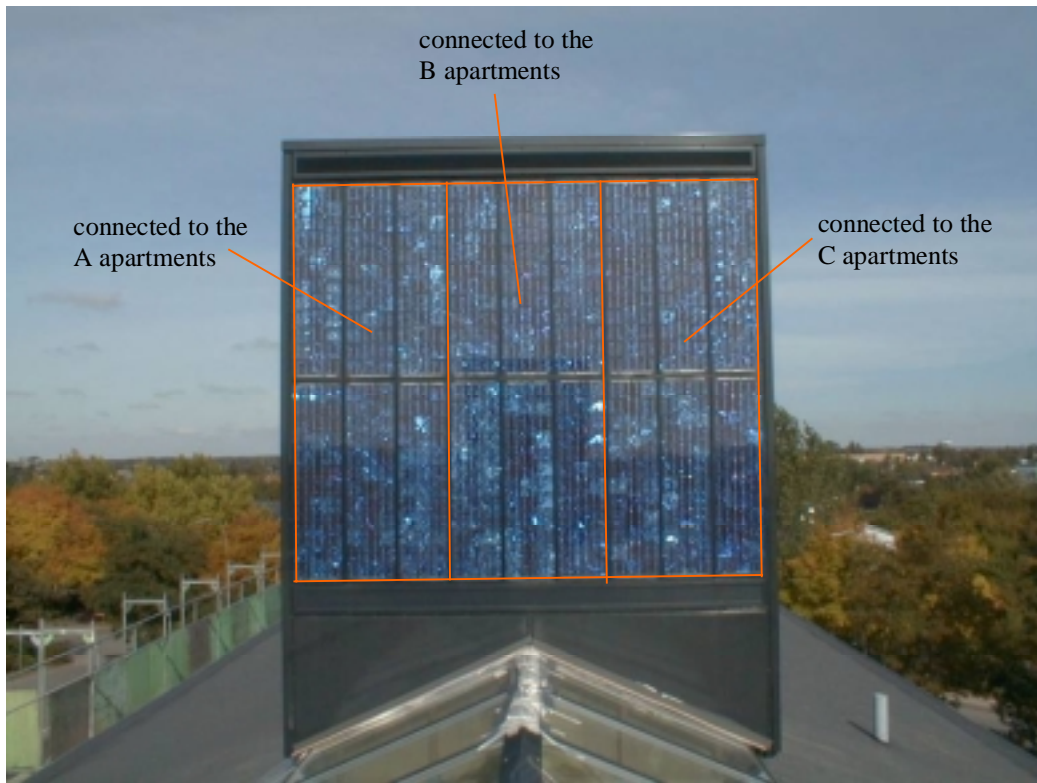


Figure 1.32. The electrical connection of the PV-panels at the solar ventilation chimney of no. 36 and 38.

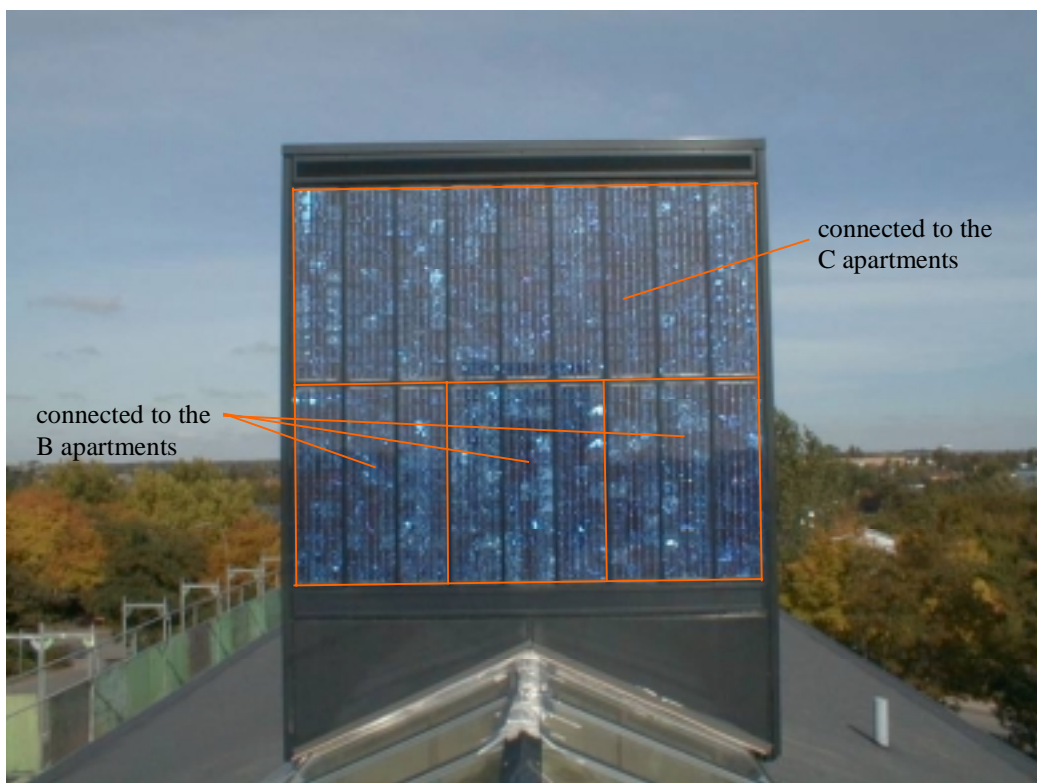


Figure 1.33. The electrical connection of the PV-panels at the solar ventilation chimney of no. 40.

The development of the PV-mixer was unfortunately delayed. The first company chosen for the development came up with a solution as late as in January 2000. The Danish Technological Institute obtained one sample for evaluation (Mehr, 2000). It was judged that the principle chosen for controlling the power from the PV-panels and the grid didn't give enough credit to the PV-panels leading to too high power consumption from the grid even if enough power could be delivered by the PV-panels. The PV-mixers was further of a very poor quality. The soldering of the components looked to be made by a plumber rather than by an electrotechnician.

The PV-mixer was, therefore, rejected and a new firm for developing the PV-mixer was found. They came up with a new design in August 2000 which also was evaluated and further tested by the Danish Technological Institute (Jensen, 2000b). This concept was approved. The test results are shown in tables 1.2-4.

Supply from PV and grid		test 1	test 2	test 3	unit
Measured	U pv	12.11	12.20	48.10	Volt
	I pv	5.00	8.00	3.50	Ampere
	U grid	54.60	54.70	55.20	Volt
	I grid	4.10	3.55	2.35	Ampere
	U consumption fans	53.40	53.70	54.20	Volt
	I consumption fans	5.10	5.15	5.10	Ampere
Calculated	P1 pv + grid	284.4	291.8	298.1	Watt
	P2 consumption fans	272.3	276.6	276.4	Watt
	Efficiency	95.8	94.8	92.7	%
	PV ratio	22.2	35.3	60.9	%

Table 1.2. Results from tests of the PV-mixer in mixed mode.

Only supply from grid		test 1	unit
Measured	U grid	56.10	Volt
	I grid	5.20	Ampere
	U consumption fans	54.90	Volt
	I consumption fans	5.10	Ampere
Calculated	P1 grid	291.7	Watt
	P2 consumption fans	280.0	Watt
	Efficiency	96.0	%

Table 1.3. Results from tests of the PV-mixer in grid mode.

Only supply from PV		test 1	test 2	test 3	unit
Measured	U pv	12.24	12.30	47.90	Volt
	I pv	7.97	10.05	7.08	Ampere
	U consumption fans	25.35	27.80	57.80	Volt
	I consumption fans	3.10	3.49	5.30	Ampere
Calculated	P1 pv	97.6	123.6	339.1	Watt
	P2 consumption fans	78.6	97.0	306.3	Watt
	Efficiency	80.6	78.5	90.3	%

Table 1.4. Results from tests of the PV-mixer in PV mode.



The tests showed an efficiency of the PV-mixer of between 93 and 96% for mixed PV and grid mode, which is in the same area of the efficiency of inverters. In purely grid mode the efficiency of the PV-mixer is 96% which is the max efficiency that can be expected for this concept based on the switch mode technology. For the purely PV mode the efficiency lay in the tests between 81 and 90% depending on the power needed for the fans. Table 1.4 indicates that the efficiency of the PV-mixer in only PV mode may get lower at lower fan power than shown in table 1.4.

The PV-mixers for the Lundebjerg project was delivered and installed in October 2000.

### **1.2.6. Control**

The PV-VENT system is controlled in several different ways – some already mentioned.

#### **1.2.6.1. Staircase no. 36**

The exhaust ventilation in the apartments in no. 36 is controlled as a constant pressure system. A pressure transducer measures the pressure in the system and the fan speed is adjusted to obtain a pre-set pressure in the system. The outlet fittings have all been pre-set by the ventilation firm and glued in a position where the desired air flow rates are obtained. The intended flow rate per dwelling was 126 m<sup>3</sup>/h.

For the B apartments the fresh air inlet from the PV-gable is as mentioned earlier controlled by a wax motor driven inlet diffuser. The diffuser opens and closes at a temperature of 16°C. The diffuser will also close if the temperature of the air from the PV-gable exceeds 24°C. The two set points may be changed by the tenants.

Orbesen dampers open in the top of the PV-gable when the temperature in the PV-gable reaches a predefined set point: the dampers start to open at a temperature of 23°C and is fully open at a temperature of 27°C – the dampers starts to close again at a temperature of 24°C and are closed a 21°C. When the dampers start to open the PV-panels will be cooled by a buoyancy driven air stream in the air gab.

#### **1.2.6.2. Staircase no. 38**

The ventilation systems in no. 38 are balanced systems with heat recovery. The air flow rates are as for the apartments in no. 36 controlled as a constant pressure system where the inlet diffusers and outlet fittings have been pre-set in order to obtain the required air flow rates and glued in that position.

The system is further controlled by the building energy management system of the building. The building energy management system measures the temperature of the exhaust air. If the temperature of the exhaust air exceeds 22°C the fresh air is bypassed the heat exchangers in order to avoid overheating of the dwellings. During summertime and other periods it is possible via the building energy management system to turn of the fresh air fan of the systems – also in order to prevent overheating during these periods.

### 1.2.6.3. Staircase no. 40

#### A apartments

The ventilation systems in the A apartments no. 40 are individual balanced systems with heat recovery. The systems are individual controlled by a control panel in the hall. The control panel is shown in figure 1.34. Table 1.5 shows the ventilation modes the tenants are able to chose among including the intended air flow rates in each mode.



Figure 1.34. The control panel from which the occupants of the A apartments in no 40 may control their ventilation systems.

Mode	Winter		Summer	
	Exhaust m <sup>3</sup> /h	Fresh air m <sup>3</sup> /h	Exhaust m <sup>3</sup> /h	Fresh air m <sup>3</sup> /h
Max	198	178	198	0
Normal	126	116	126	0
Min	60	56	60	0

Table 1.5. Ventilation modes and intended air flow rates, which can be chosen via the control panel in the apartments.

The inlet diffusers and outlet fittings have all been pre-set by the ventilation firm and glued in a position where the desired air flow rates are obtained.

It was further the intention to control the air intake from the facade – either from behind the PV-panels or directly from outside, if the heating by the PV-panels is too high, or if the ventilation system is run in summer mode without an air stream behind the PV-panels. In the latter case the PV-panels may be cooled by a buoyancy driven air stream behind the PV-panels.

However, due to a mistake it was as earlier mentioned not possible to install the dampers. The collector is thus always open at the top.

### **B apartments**

The B apartments in no. 40 are controlled in the same way as the A apartments except that the fresh air is drawn from the solar ventilation chimney.

### **C apartments**

The C apartments in no. 40 are controlled in the same way as the apartments in no. 38.

#### **1.2.7. Power to the fans**

Table 1.6 shows the max power consumption of the fans in the different systems and the peak power of the connected PV-panels.

Staircase	Apartment type	Apartments per fan	Max power of the fan W		Peak power of the connected PV-panels $W_p$
			Exhaust	Fresh air	
36	A-C	3	150		300
38	A-C	3	150	150	300
40	A	1	45	45	100
40	B	1	45	45	150
40	C	3	150	150	450

Table 1.6. Max power consumption of the fans and peak power of the connected PV-panels.

### **1.3. External insulation of the facades**

The facades have externally been insulated with 100 mm mineral wool in a wooden skeleton with 9 mm gypsum plates on top. The outer skin of the walls is external brick cladding maintained to the walls by aluminium profiles as shown in figure 1.35.



Figure 1.35. The external cladding of the externally insulated facades.

## **2. Measuring system**

The objective of the measuring campaign at Lundeberg 36-40 was to gain experience on the different types of PV-VENT systems. The measuring program was, therefore, concentrated on the PV-systems as described in the following sections.

The experiments at Lundeberg 36-40 consisted as mentioned on page 7-8 of five different ventilation systems, a PV-gable, three solar ventilation chimneys and a PV-facade. Monitoring of all systems demanded an unrealistic numbers of measuring points. In order to decrease the measuring system to a realistic size, measurements has only been carried out on one of each of the four different ventilation systems (no measurements have been carried out on type 4b – as it is similar to 4a expect for no solar pre-heating of the fresh air. It was judged that measurements on this type of system only would add marginal information), the PV-gable, the solar ventilation chimneys and one third of the PV-facade.

### **2.1. Measuring points**

The following sections describe the location and type of the different measuring sensors of the 54 point large measuring system.

#### **2.1.1. Weather data**

The measured weather data consisted of the total solar radiation on vertical south and vertical east and the ambient temperature at the north gable.

##### ***Solar radiation***

The total solar radiation on south and east was measured as the PV-panels are facing these two directions. Both the applied pyranometers were calibrated PV-pyranometers type 80SP from SolData. The south facing pyranometer was located on the solar ventilation chimney above no. 36 as seen in figure 2.1. While the east facing pyranometer was located on the railing of the French balcony of apartment A, second floor of no. 40 as shown in figure 2.2.

##### ***Ambient temperture***

The ambient temperature was measured by a class A PT100 temperature sensor located at the north gable in a standard double shield. The purpose of the double shield was to avoid the sensor in being heated up by the sun in the early morning and late evening. The sensor is shown in figure 2.3 together with the ambient temperature sensors of the building energy management system of the building.

Other ambient temperatures are also being measured. The sensors for this were located in the inlets of the PV-gable, the PV-facade and the solar ventilation chimneys and will be described in connection with these.



Figure 2.1. The location of the south facing pyranometer.

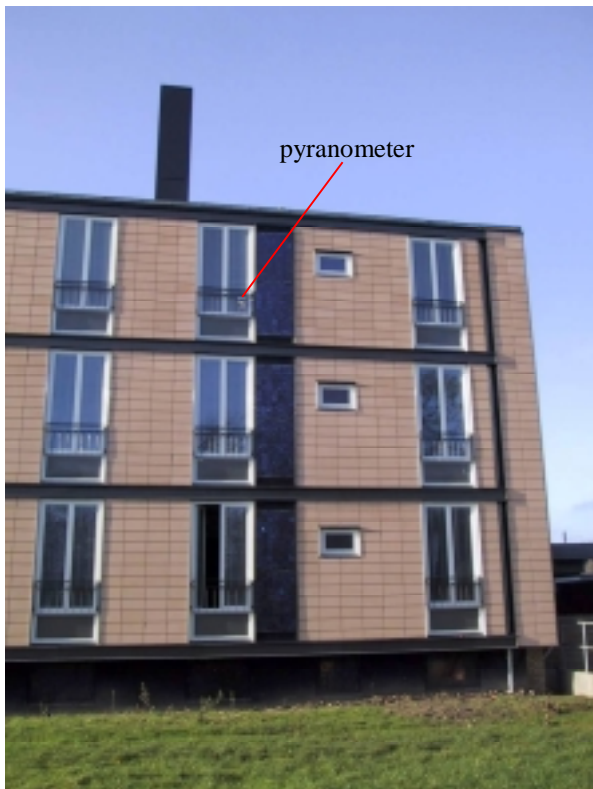


Figure 2.2. The location of the east facing pyranometer.



Figure 2.3. The double shielded ambient temperature sensor.

### 2.1.2. PV-gable and ventilation system in no. 36

There is as earlier mentioned an air gap behind the PV-panels in the gable where air is able to flow from bottom to top. On each floor there is two inlets to the two rooms behind the wall through which fresh air to the dwellings may be drawn due to the under pressure in the dwellings created by the exhaust ventilation.

#### *Air temperature sensors*

Several air temperature sensors and one surface temperature on a PV-panel were located in the PV-gable. All temperature sensors were class A PT100 temperature sensors. Figure 2.4 shows the location of the air temperature sensors in the air gab. There was located one temperature sensor in the inlet at the bottom of the PV-gable and one temperature sensor in front of the inlet to the living room on each floor and further one sensor in front of the inlet to the other room on the 2<sup>nd</sup> floor. The reason for the extra sensor on the 2<sup>nd</sup> floor was that measurements also were performed on the ventilation system for this apartment.

#### *Temperature sensor on a PV-panel*

Figure 2.5 shows the location of the surface temperature sensor at the back of one of the PV-panels of the PV-gable. The sensor was installed with aluminium tape with thermo pasta between the PV-panel and the sensor in order to ensure a good thermal contact in the same way as shown in figure 2.18. The objective of the sensor was to give an idea of the temperature level of the PV-panels.



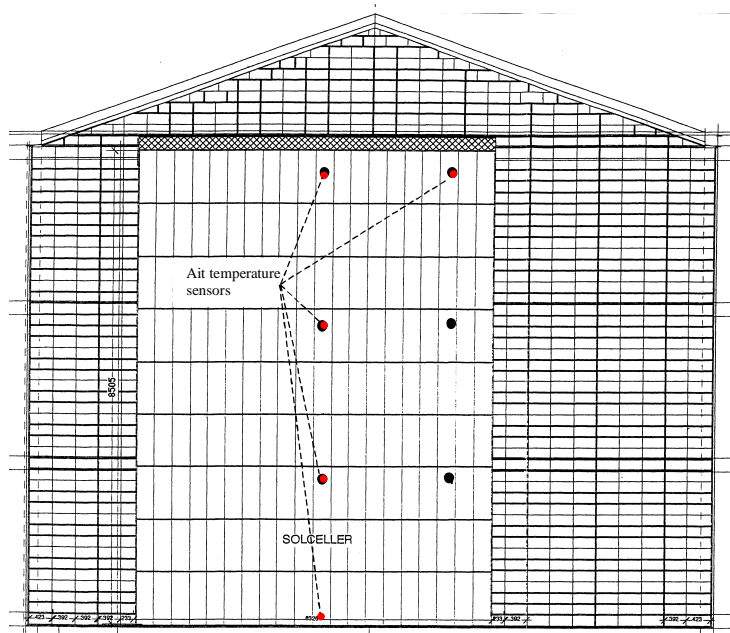


Figure 2.4. The location of the air temperature sensors in the air gap behind the PV-panels on the gable.

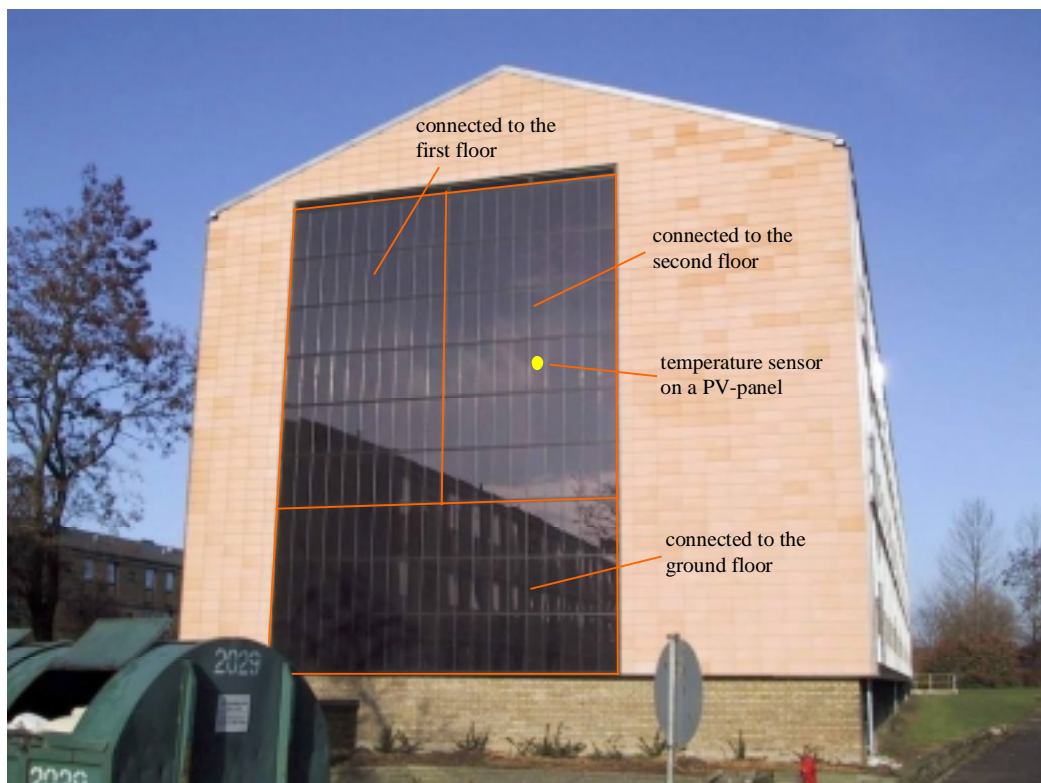


Figure 2.5. The location of the surface temperature sensor at the back of a PV-panel on the PV-gable.



### ***Power from the PV-gable***

The PV-panels at the gable are electrically connected in arrays as shown in figure 2.5. The arrays are connected to the grid via an inverter located in the apartments next to the existing energy meter. The power from each array is measured by a electrical power meter from ABB – shown in figure 2.6. The readings by the power meter in the apartment at the 2<sup>nd</sup> floor were transferred to the measuring system by counting the pulses give out by the power meter.



Figure 2.6. The power meter for measuring the energy production of one of the three arrays of PV-panels on the to the 2<sup>nd</sup> floor.

The temperature at the back side of on of the PV-panels was as shown in figure 2.5 situated in more or less the middle of the PV-array connected to the dwelling at the second floor, which was the array the power measurement was performed on. The two measurements establish together a possibility of evaluating the temperature dependency of the power from the PV-panels

### ***Air flows from the PV-gable to the dwelling***

The air flow in the PV-gable is combined buoyancy driven and driven by the under pressure in the dwellings. This means that the air speed is low which again means that it is difficult to measure the volume flow rate of air in the gable. The air speeds were, therefore, only measured in the inlets to the dwelling at the second floor. The air speed was as seen in figure 2.7 measured by an air speed sensor (VentCaptor) located in the duct between the air gap behind the PV-panels and the room. The applied air speed sensors were calibrated on location. Calibration on location was necessary as the inlet condition to the duct don't give a steady air stream at the measuring point. The air speed sensors were after finilazation of the gable calibrated by a duct with a fan with adjustable speed and a calibrated air speed sensor as seen in

figure 2.8. A correlation between the sensor signal and the volume flow rate was in this way established.

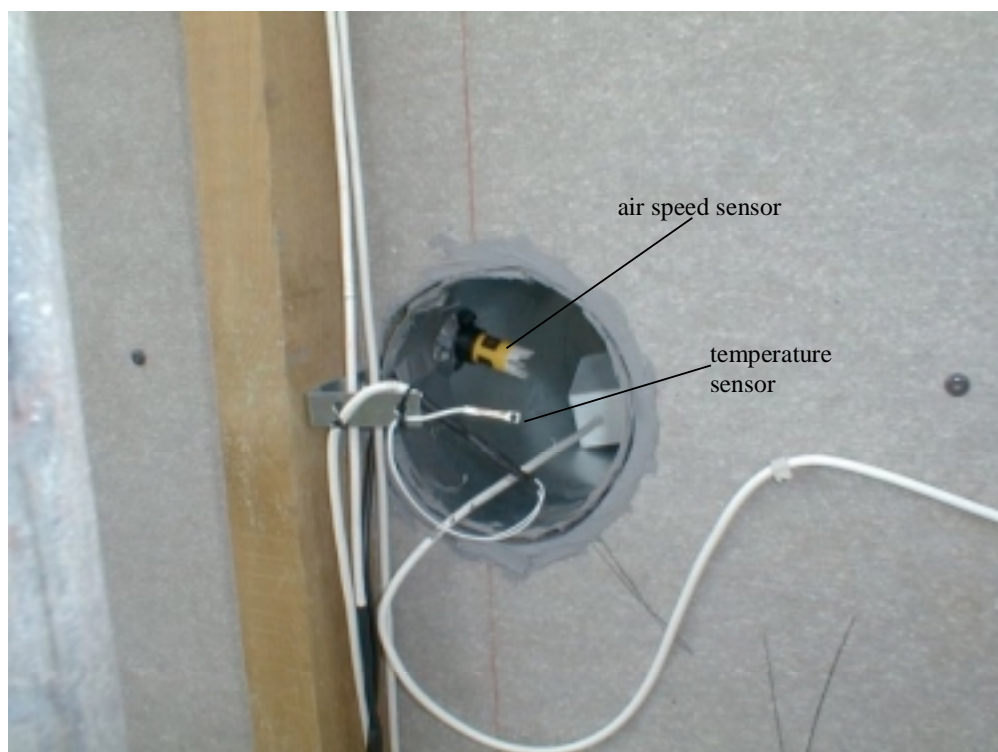


Figure 2.7. Temperature sensor and air speed sensor in the duct between the air gap behind the PV-panels in the gable and the room behind the gable.



Figure 2.8. Calibration of the air speed sensors in the inlet from the PV-gable.

### ***Flow rate of exhaust air***

The volume flow rate of exhaust air from the apartment was measured by means of a calibrated air speed sensor (VentCaptor) located in the exhaust duct from the dwelling as seen in figure 2.9. In order to determine the amount of energy extracted by the exhaust air, the temperature of the exhaust air was measured with a class A PT100 temperature sensor – the location of this is also shown in figure 2.9.



Figure 2.9. The air speed sensor and temperature sensor in the exhaust duct.

### ***All sensors in connection with apartment B, second floor, no. 36***

Figure 2.10 shows the location of all the applied sensors on the floor plan of the B apartment in no. 36.

#### **2.1.3. Apartment 40 IIA**

There is as earlier mentioned an air gap behind the PV-panels in the facade where air is able to flow from bottom to top. The ventilation systems of the A apartments draw fresh air from the facade.

### ***Temperature sensors in the PV-facade***

Figure 2.11 shows the location the three temperature sensors in the PV-facade. There was one air temperature sensor at the bottom (inlet) of the air gap and one in the inlet to the ventilation duct. There was further one surface temperature sensor mounted on the lower part of the top panel of the PV-array. The sensor was mounted behind one cell with aluminium tape with thermo pasta between the PV-panel and the sensor in order to ensure a good thermal contact in the same way as shown in figure 2.18. The objective of this sensor was to give an idea of the temperature level of the PV-panels.

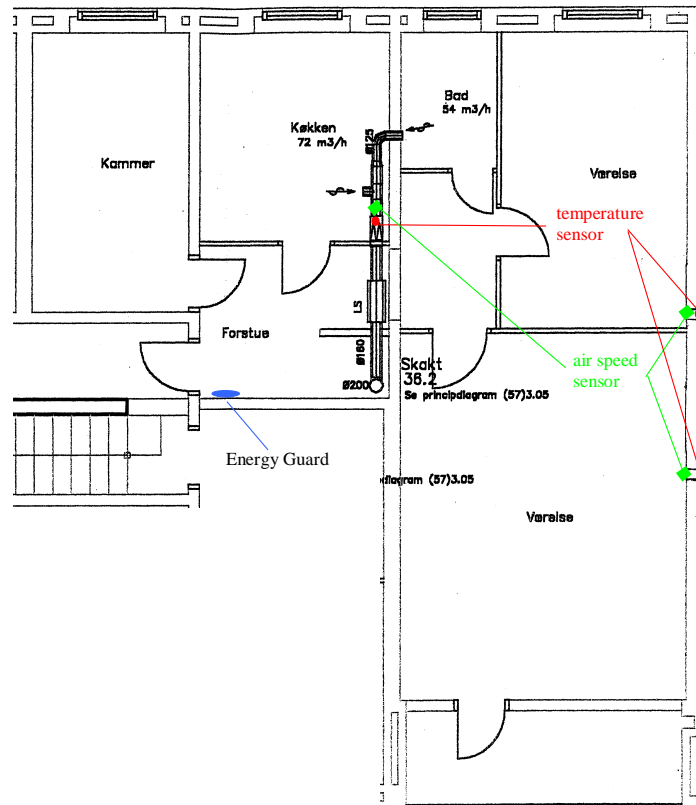


Figure 2.10. Location of the sensors in apartment B, second floor, no. 36.

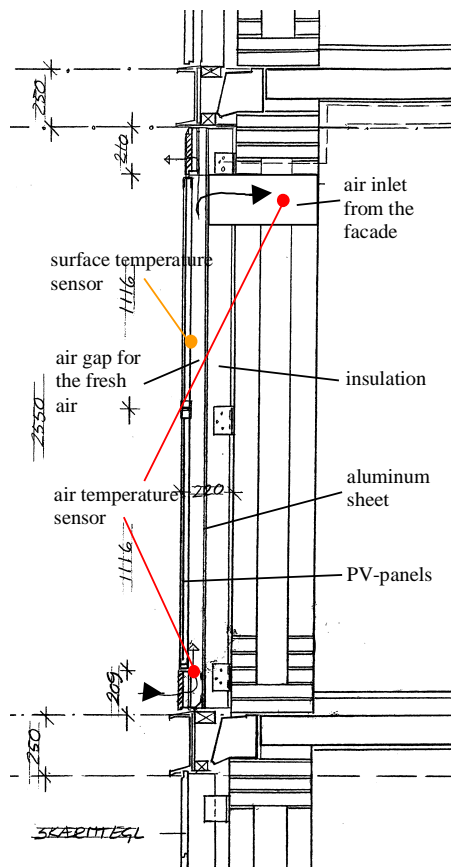


Figure 2.11. The location of the temperature sensors in the PV-facade.

All sensors used were class A PT100 temperature sensors.

### *Sensors around the heat exchanger*

Figure 2.12 show the temperature sensors and air speed sensors applied to measure the conditions around the heat exchanger unit of the system. The sensor for measuring the temperature of the fresh air to the dwelling mentioned above is also shown.

The following three air temperatures were measured: Temperature of the fresh air to and from the heat exchange and the temperature of the exhaust air to the heat exchanger. All sensors were class A PT100 temperature sensors.

Two air speeds were measured in the system: The air speed of fresh and exhaust air. Both air speeds were measured using calibrated VentCaptors.

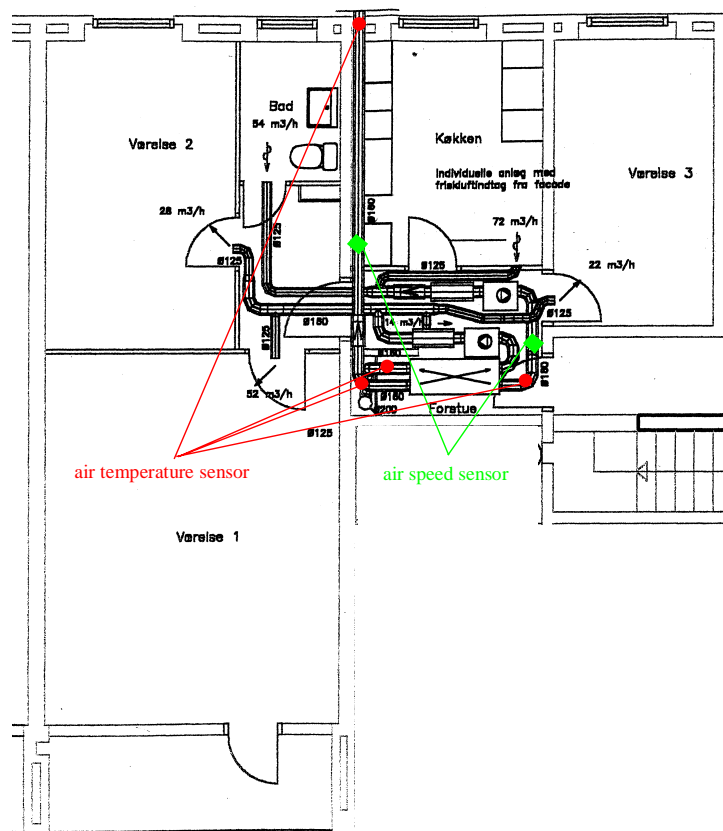


Figure 2.12. The location of the sensors applied on the ventilation system in apartment A, second floor, no. 40.

### *Energy streams around the PV-mixer*

The fans of the system are partly powered by the PV-panels in the facade. At low or no PV-power the fans run partly or only on power from the grid. A PV-mixer is in charge of assuring that the fans are supplied with as much PV-power as possible.

The PV-mixer is one of the new parts developed in the project. It is, therefore, important to establish knowledge of the function of the PV-mixer.



It is, however, a non-trivial task to determine the performance of the PV-mixer as it has two power inputs and one power output. Especially the inputs may change rapidly over time e.g. if a cloud gets in front of the sun and if the regulation of the power from the grid is performed by “cutting” the current. It is, thus, extremely important that the voltage and current is measured at the same time – even a small time shift between the measuring of the two values for all in and outputs may lead to a wrong picture of the performance of the PV-mixer and the PV-panels.

At first it was tried to find an existing sensor/meter that was able to perform the measurements with the necessary accuracy on the first version of the PV-mixer. However, no such was found as it was very difficult to measure connected values of voltage and current to and from the PV-mixer in order to get a true picture of the power to and from the first version of the PV-mixer. Finally Solar Energy Centre Denmark decided to develop the sensor. The sensor consisted basically of a 4-quadrant analogue multiplier, which at a high frequency measure the voltage and current going either in or out of the PV-mixer and multiply the two values in order to obtain the power. The measuring frequency is higher than the fastest variation of either in or output of the PV-mixer – this ensures precise and correct measurements of the power. This design of the sensor was maintained although the new version of the PV-mixer made it much easier to measure connected values of voltage and current to and from the PV-mixer. The developed sensors was installed and calibrated by the end of 2000. However, it was discovered that the readings from the sensors unfortunately didn’t give much meaning. After a careful investigation it was discovered that the 4-quadrant analogue multiplier is rather temperature dependent (not mentioned in the data sheet for the chip). This means that the calibration equation changes with the temperature meaning that the readings cannot be transferred to meaningful measurements.

The new version of the PV-mixer made it fortunately easier to measure connected values of voltage and current to and from the PV-mixer. A new marked survey showed that signal calculators from PRelectronics type 2289 could measure connected voltage and current to and from the PV-mixers. The new sensors – see figure 2.13 - were installed and calibrated by the end of January 2001.



Figure 2.13. Sensor for measuring the power in or output of the PV-mixers.

#### **2.1.4. Apartment 40 IIB**

The measurements on the ventilation system in this apartments was as shown in figure 2.14 similar to the measurements on the above A apartment except for the measurements in the facade. Identical sensors as in A were applied.

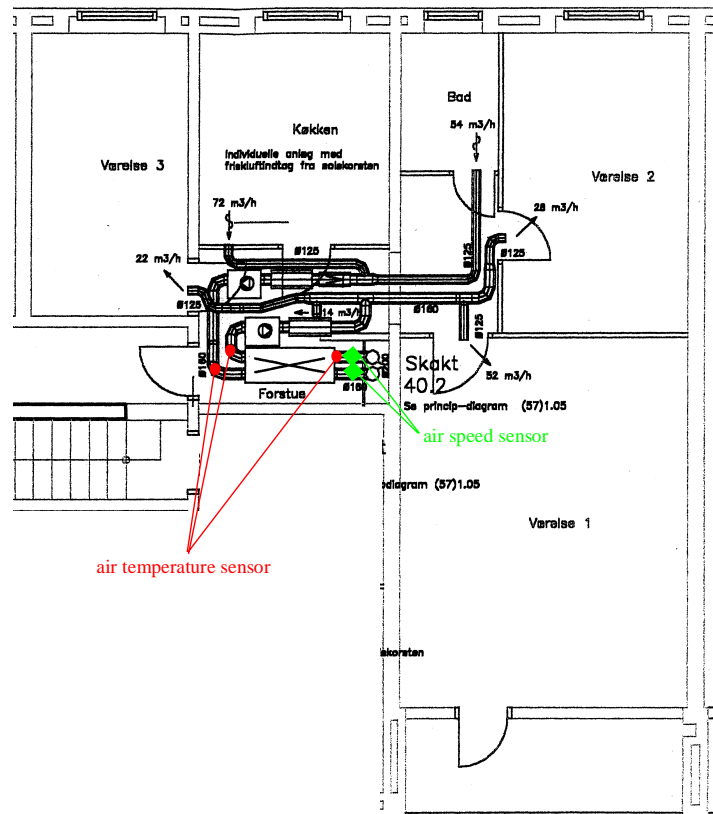


Figure 2.14. The location of the sensors applied on the ventilation system in apartment B, second floor, no. 40.

### 2.1.5. Common ventilation system in 40 C

The measurements on the common ventilation system for the C apartments in no. 40 were carried out in the attic where the heat exchanger of this system is located. The applied measuring points were similar to the ones applied on the heat exchanger in the A and B apartments as seen in figure 2.15: three temperature sensors and two volume flow rates. The temperature sensors were all class A PT100 sensors while the volume flow rate of air were measured as pressure drops over calibrated bendings. The pressure drops were measured by calibrated pressure transducers from Huba control type 694 as shown in figure 2.16.

### 2.1.6. Solar ventilation chimneys

Several things were measured in connection with the solar ventilation chimneys.

#### *Surface temperatures on the PV-panels*

Figure 2.17 shows the location of the surface temperatures on the backside of one of the PV-panels of the solar ventilation chimneys. One surfaces sensor was located at the back of the middle PV-panel in the top row on each chimney. One more sensor was located at the back of the middle PV-panel in the bottom row on the chimney above no. 40 (this sensor turned, however, out to be of little use as it fluctuated very much and was further not possible to replace). The sensors were mounted on the backside of the PV-panel behind one cell by means of alu-

minium tape as seen in figure 2.18. Thermo pasta was located between the PV-panel and the sensor in order to obtain a good thermal connection between the PV-panel and the sensor.

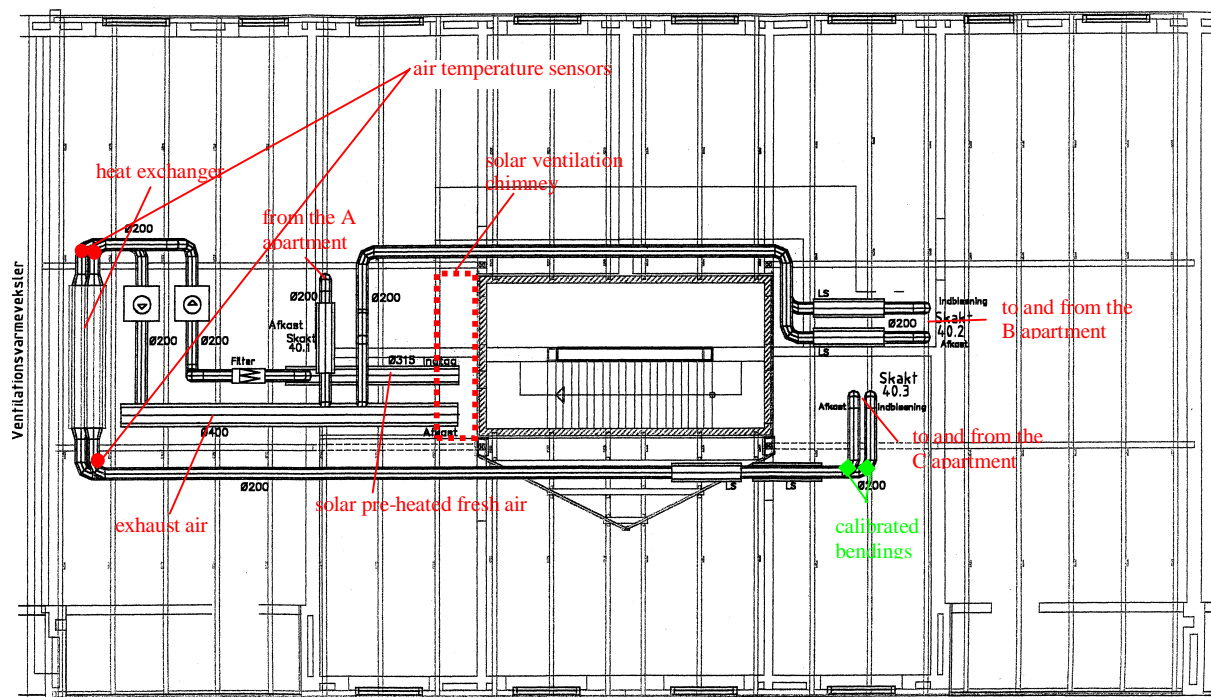


Figure 2.15. The location of the sensors applied on the ventilation system of the C apartments in no. 40.



Figure 2.16. The applied pressure transducers for determination of the volume flow rates.

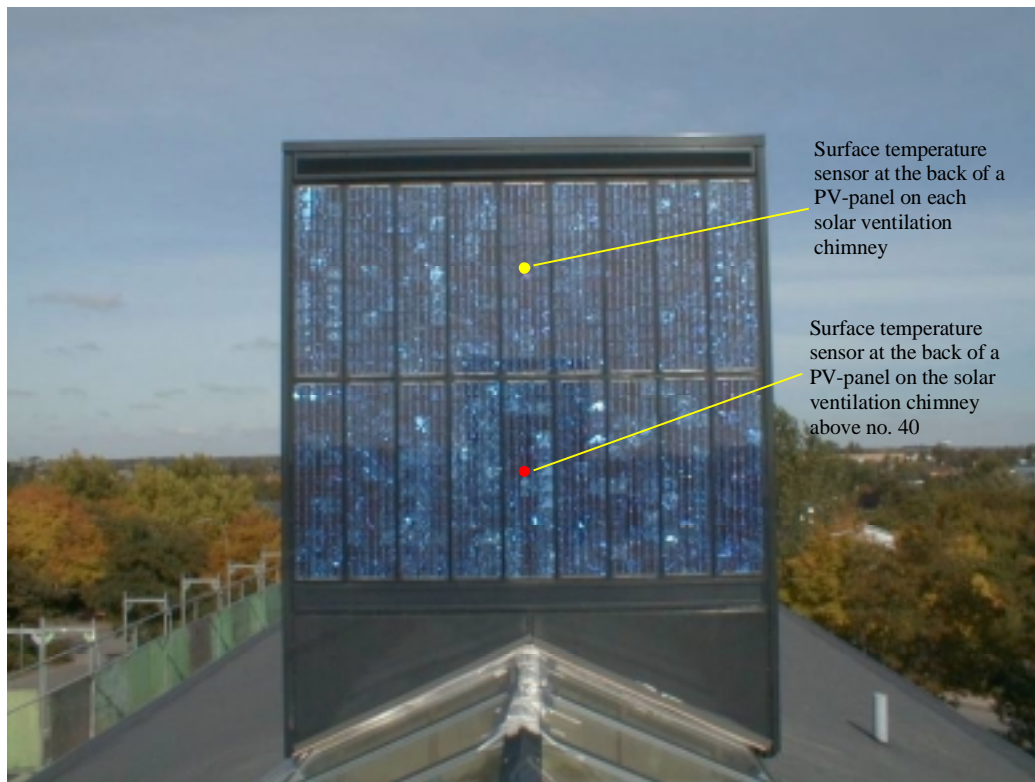


Figure 2.17. The location of the surface temperature sensors at the backside of one of the PV-panels on the solar ventilation chimneys.



Figure 2.18. A surface sensor mounted at the back of a PV-panel.



### *Temperature and air speed measurements*

Fresh air is pre-heated in the solar ventilation chimney above no. 38 and 40. Figure 2.19 shows the location of the temperature sensors used to determine the heating of the air in the chimneys. The two air temperature sensors were class A PT100 sensors, while the air speeds were measured by means of calibrated VentCaptors. Figure 2.20 shows the location of one of the air temperature sensors in the inlet, while figure 2.21 shows an example of an outlet sensor.

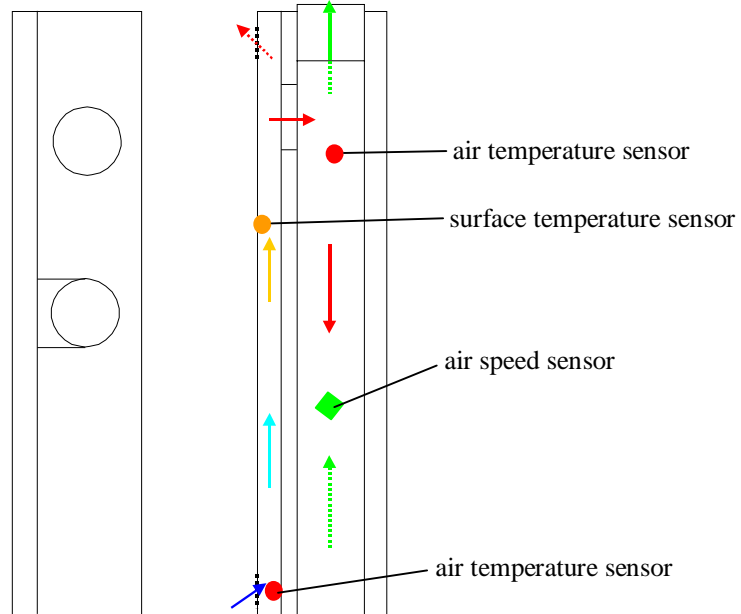


Figure 2.19. The location of air temperature and air speed sensors in the solar ventilation chimneys above no. 38 and 40.

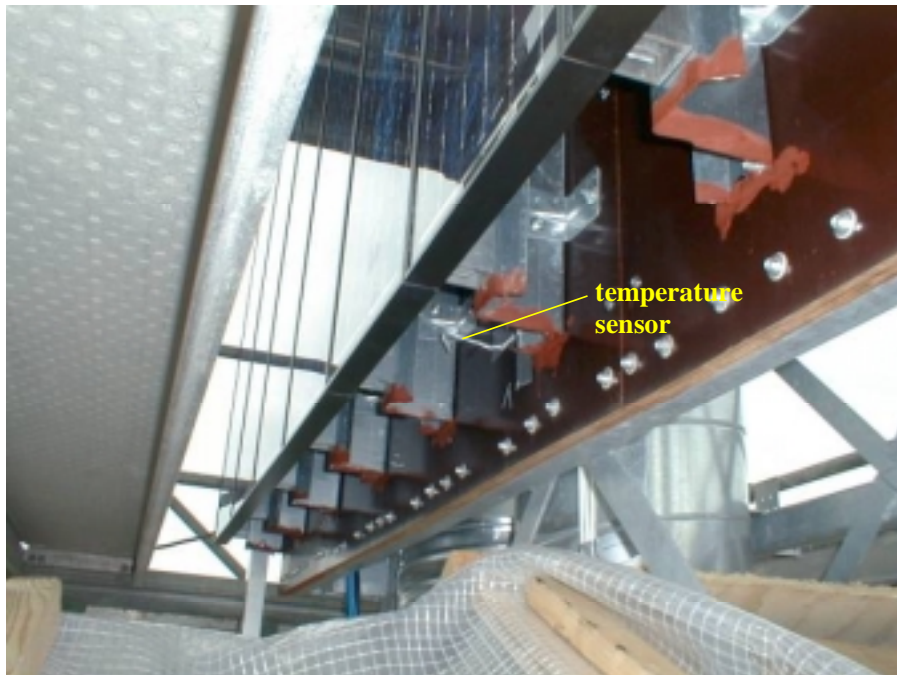


Figure 2.20. Example of the location of an air temperature sensor in the inlet of a solar ventilation chimney.





Figure 2.21. Example of the location of an air temperature sensor in the outlet of a solar ventilation chimney.

### ***Energy streams around the PV-mixer***

The power from the solar ventilation chimneys is used to run the fans of the ventilation systems. The power from the PV-panels and the grid to the PV-mixers and the power from the PV-mixers to the fans were measured as described in section 2.1.3. One PV-array including PV-mixer was monitored on each chimney: the PV-mixer for the B apartments in no. 36 and 38 (see figure 1.32) and the PV-mixer for the C-apartment in no. 40 (see figure 1.33) as the surface temperature sensors were located at the back of one PV-panel in these arrays – compare figures 1.32-33 with figure 2.17.

### ***Purpose of the measurements on the solar ventilation chimneys***

The three solar ventilation chimneys are very similar except that no fresh air is heated in the chimney above n. 36. The PV-panels are here, thus, only cooled by an buoyancy driven air flow. The chimney above no. 38 supplies air to 9 apartments while the chimney above no. 40 supply air to 6 dwellings. The PV-panels on the chimney above no. 38 is, thus, cooled more by the fresh air to the dwellings than the PV-panels on the chimney above no. 40. It is, therefore, of interest to determine the influence of the air flow rate on the power generated by the PV-panels and the influence of the air flow rate on the solar ventilation chimneys acting as solar air collector.

## **2.2. Data collection**

All sensors were connected to a data logger system with modules from Analog Devices. Each sensor were scanned each 5<sup>th</sup> second and averaged into 10 minutes mean values and stored on the hard disk of a PC.

The PC via the software Labview 5.0 controlled the data logger system. Spot values of the sensor readings were continuously shown on the screen of the PC. The PC/data logger system was mainly located in the attic above no. 40 as seen in figure 2.22.



Figure 2.22. The PC/data logger system in the attic above no. 40.

## **2.6. Treatment of measured data**

Using the data logger system/PC some of the measured values were directly translated into physical understandable values like temperatures and solar radiation.

Using the calibration equations other measured values were later transformed to air flow rates and power. The thermal performance of the heat exchanger, the PV-gable, the PV-facade and the solar ventilation chimneys were likewise later evaluated using the measured temperatures, air flow rates and power.

### 3. Measurements

Measurements have been carried out at Lundebjerg for a little less than one half year from mid October 2000 to end March 2001. The rather short measuring period was due to problems in the actual renovation process of the building, which lasted longer than anticipated. For the same reason the sensors has been installed successively when possible according to the building process. The last sensors where installed as late as in February 2001. The measurements was further made difficult as many of the systems were run improperly for most of the measuring period

Although the very short measuring period and the often not correct running of the PV-VENT systems it is still believed that the measuring camping has been successful as it has been possible to extrapolate the findings from the measurements in order to obtain important information on the potential yearly savings when applying PV-VENT systems. The main drawback of the short measuring period is that no information on the performance of the systems during summer conditions has been obtained.

The first section of this chapter contains graphs showing the measurements from two weeks in order to illustrate the function of the PV-VENT system – the two chosen weeks are week 5 and 6 of 2001 (January 29 – February 11) and in some cases also graphs for other periods in order to show other features not present in week 5-6, 2001. The second section contains more general conclusions on the different components of the system, while in the third section the savings of the system are calculated.

#### 3.1. Measurements from week 5 and 6, 2001

Figures 3.1-2 show the weather conditions during these specific weeks – i.e. total solar radiation at the south facing chimney above no. 36 (see figure 2.1), the total solar radiation on vertical east at apartment 40 IIA (figure 2.2) and the ambient temperature at the north gable (figure 2.3). The two weeks are characterised by days with clear sky conditions and days with cloudy conditions. The ambient temperature was between  $-10$  and  $11^{\circ}\text{C}$ .

The measuring system was very large, so in order to make it easier to interpret the graphs the graphs have been grouped. The data are grouped in the following groups: gable, apartment 36 IIB, apartment 40 IIA, apartment 40 IIB, ventilation system 40C and the solar ventilation chimneys.

##### 3.1.1. Gable

Figures 3.3-4 show the temperatures in the gable during the two considered weeks. The location of the temperature sensors is shown in figure 2.4-5. The figures show that the temperature of the PV-panel during this period reaches temperatures of up to  $50^{\circ}\text{C}$ , which is 40 K above the ambient temperature. The temperature at the inlet to the apartment 36 IIB reaches a max. temperature of  $37^{\circ}\text{C}$ , which is 27 K above ambient. The temperatures at the inlet to the lower floors are of course lower with at peak temperature of 14 K lower at the ground floor than at the second floor. The second floor seems thus to benefit more from the PV-gable – this may, however, not be the case as the inlet diffusers to the dwellings closes (intended) at  $24^{\circ}\text{C}$ . Figures 3.5-6 show the measured PV-power from on third of the PV-gable (se figure 2.5) delivered by the inverter to the grid. Due to a malfunction of the power sensor on the PV-gable,

measurements are here first obtained from the following two weeks (February 15-26). The total radiation is also shown in figure 3.5-6. The measured PV power in figures 3.5-6 fluctuates very much also during periods with stable radiation levels. The reason for this is shown in figure 3.7 showing the power from the PV-gable and the total solar radiation for February 18. Although clear sky conditions, the inverter fails regularly to deliver power to the grid. The reason for this is assumed to be the condition of the grid to which the inverter delivers the PV power. The inverter measures the conditions of the grid and if e.g. the impedance of the grid is too high the inverter stops to deliver PV power to the grid and first start again when the impedance drops below a certain level. One solution to overcome the problem is to disable the inverters check of the grid – the check of the grid is not a demand.

Figure 3.7 shows a strange phoneme. There is a peak in the measured total radiation around noon. This is due to the location of the pyranometer at the chimney above no. 36. Solar radiation is reflected up to the pyranometer from the roof light in front of the chimney (figure 1.24). For that reason only values at radiation levels below 800 W/m<sup>2</sup> is considered in the following figure 3.8.

Figures 3.5-6 show peak values of above 300 W. In order to compare this with the peak value informed by the manufacture, the peak value informed by the manufacture has to be corrected for the actual irradiation and the actual temperature of the PV-panels in the following way:

$$P_{\text{potential}} = P_p \cdot E_{\text{useful}} / E_p \cdot (1 - (T_{\text{actual}} - T_p) \cdot 0.004) \quad (3.1)$$

where  $P_p$  is the peak power found with a solar radiation  $E_p$  of 1000 W/m<sup>2</sup> and a cell temperature  $T_p$  of 25°C.  $P_p$  is in the considered case 2160 / 3 = 720 W<sub>p</sub>  
 $E_{\text{useful}}$  is the useful solar radiation calculated as described below  
 $T_{\text{actual}}$  is the temperature measured at the backside of the PV-panel – see figures 3.4-5.  
 0.004 is the temperature dependence of the PV-panels

The total radiation on the PV-panel is transformed to useful radiation by taking into account the reflection of the solar radiation in glazing of the PV-panels at periods with a non zero incidence angle for the solar radiation. In order to correct for the reflections it is necessary to calculate the split between direct and diffuse radiation based on the measured total radiation. This was done using the equations in (Duffie and Beckman, 1991). The calculated split introduces a small uncertainty compared to a case where both total and diffuse radiation is measured. The following correction factor has been applied to account for the reflection in the:

$$k = 1 - \tan^a(\theta/2) \quad (3.2)$$

where  $\theta$  is the incidence angle for the radiation: the actual incidence angle for the direct radiation and 60° for the diffuse radiation.  $a$  is 3.7 (Nielsen, 1995).

The potential power further has to be corrected for the efficiency of the inverter – here 0.95.

Figure 3.8 shows the measured PV-power together with the calculated potential PV-power for the available data (February 15 – April 1). Figure 3.8 shows a measured peak power of about 375 W (the red line) at an irradiation of 800 W/m<sup>2</sup>. The potential peak power is calculated to be about 500 W. The measured power is thus 25 % lower than the potential power. This may be explained by losses due to bad matching of the PV-panels (too large differences in performance), losses in the wiring, dirt on the cover, etc but may also partly be due to the im-

proper operation of the inverter – i.e. that the PV-panels never were allowed to produce at their maximum.

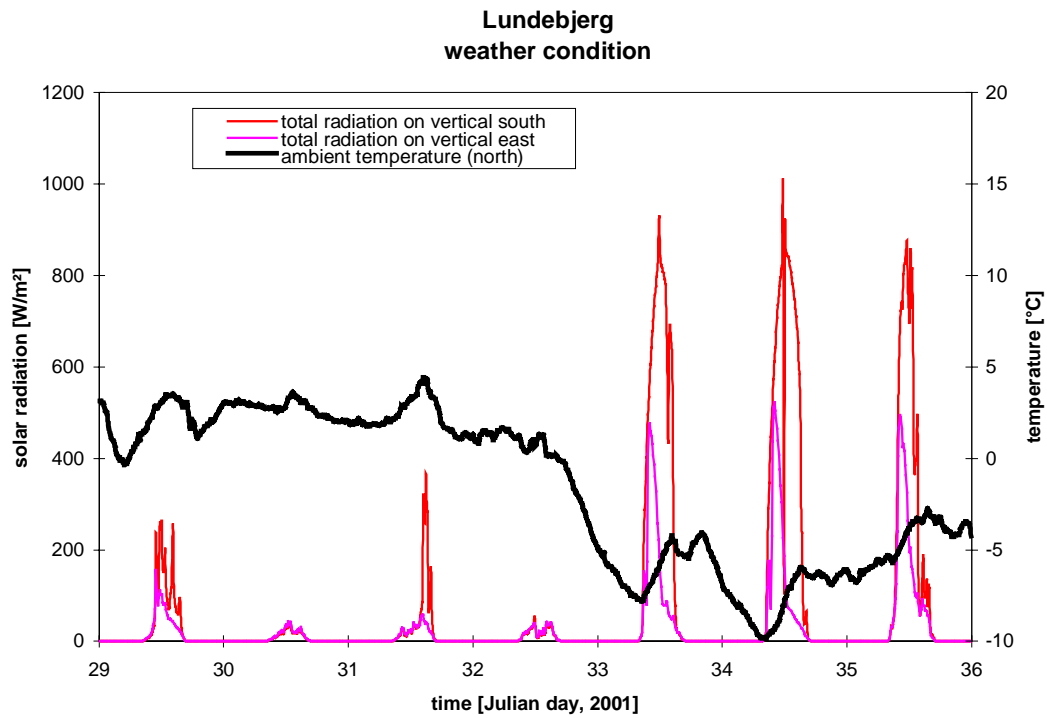


Figure 3.1. The weather conditions during week 5, 2001 (January 29 – February 4).

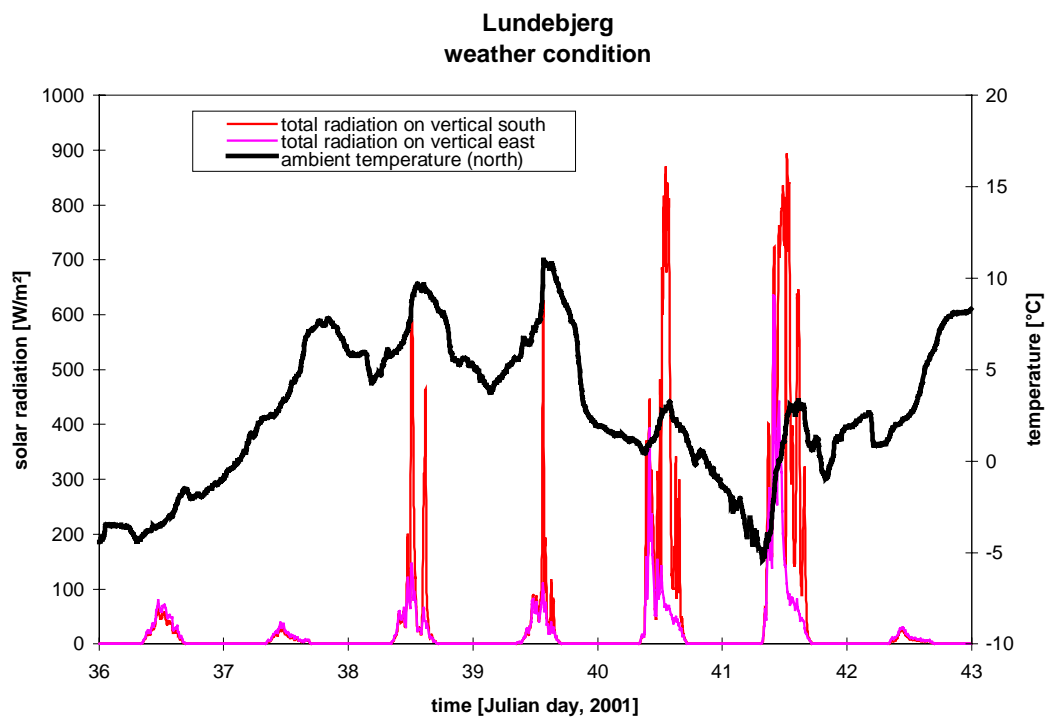


Figure 3.2. The weather conditions during week 6, 2001 (February 5 – February 11).



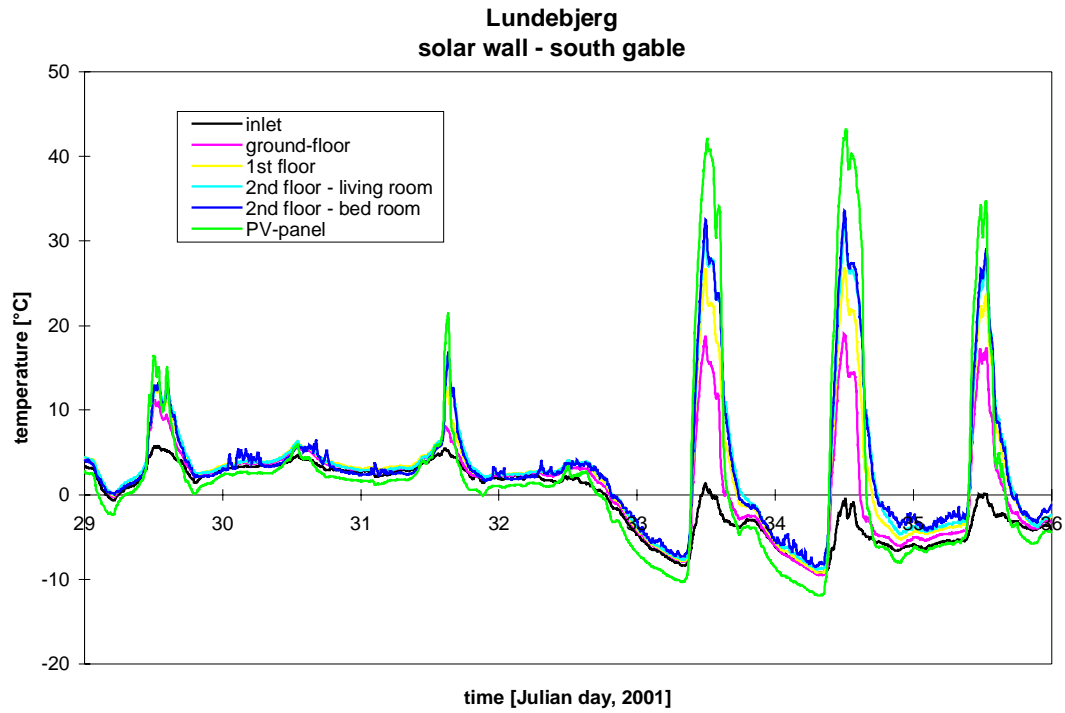


Figure 3.3. Temperatures in the PV-gable during week 5, 2001 (January 29 – February 4).

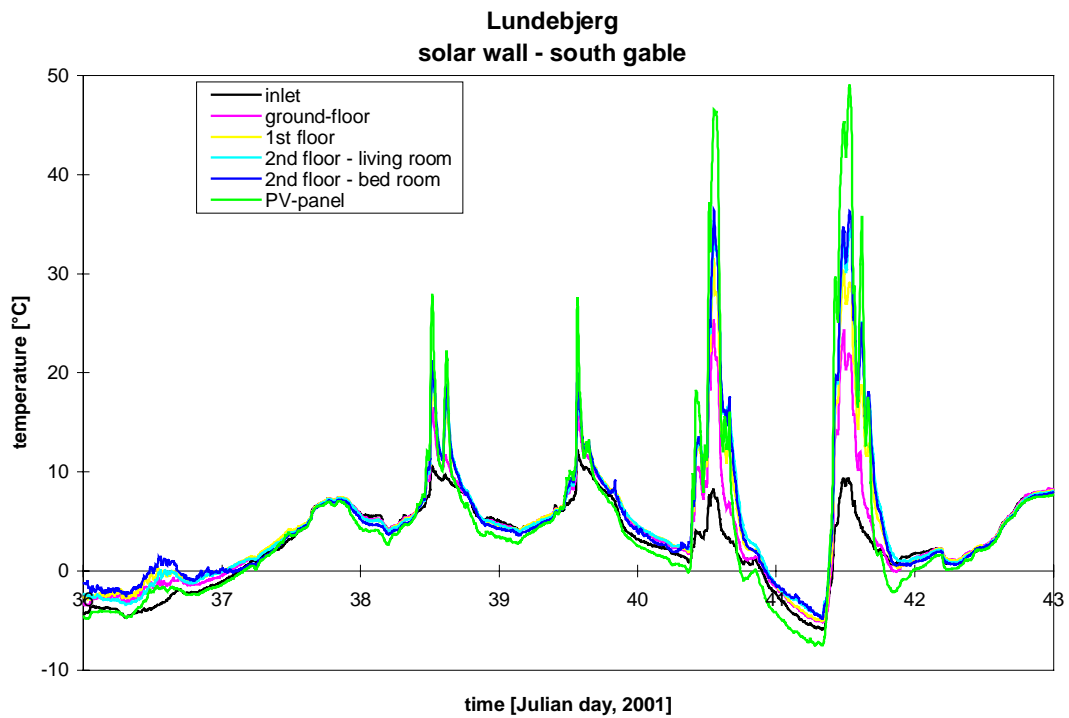


Figure 3.4. Temperatures in the PV-gable during week 6, 2001 (February 5 – February 11).

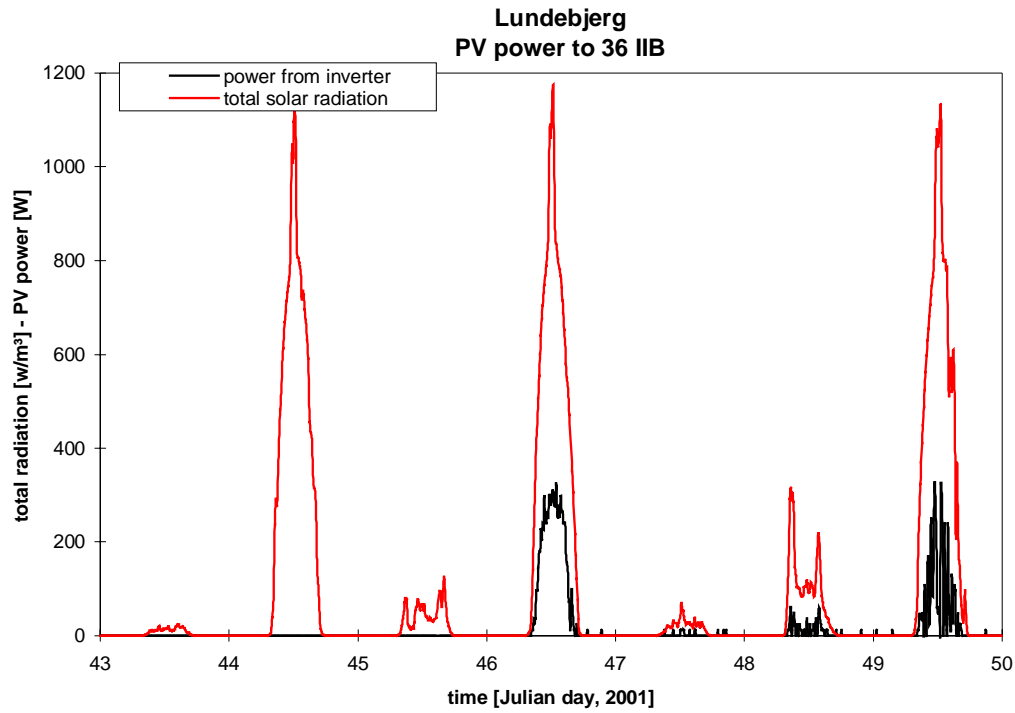


Figure 3.5. Power from one third of the PV-gable and total radiation on vertical south during week 7, 2001 (February 12 – February 18).

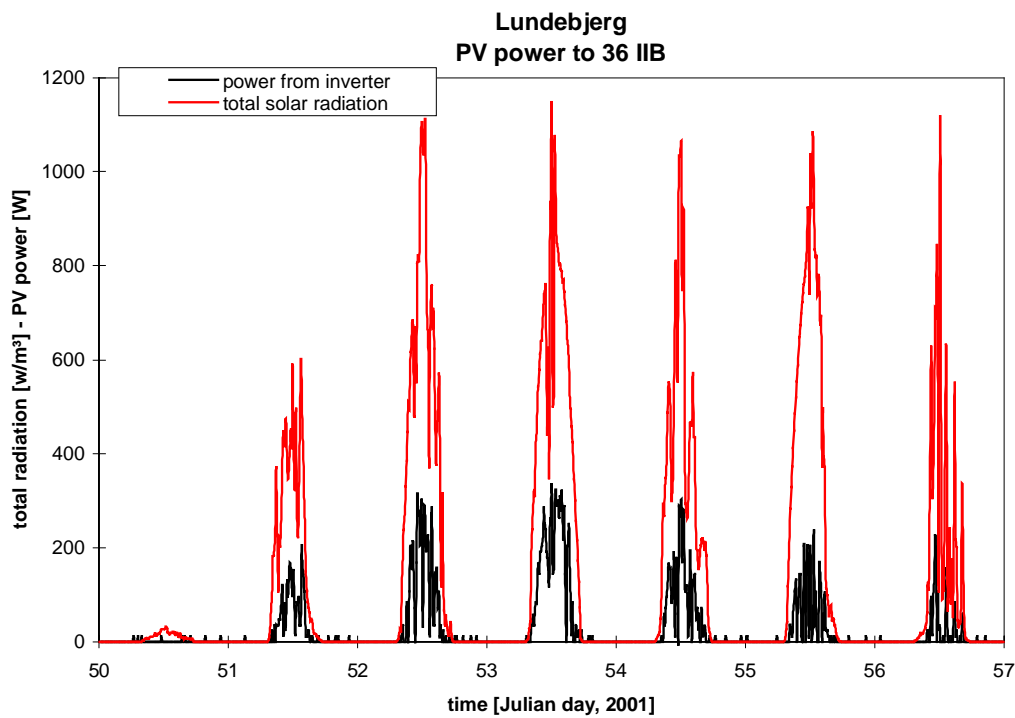


Figure 3.6. Power from one third of the PV-gable and total radiation on vertical south during week 8, 2001 (February 19 – February 25).

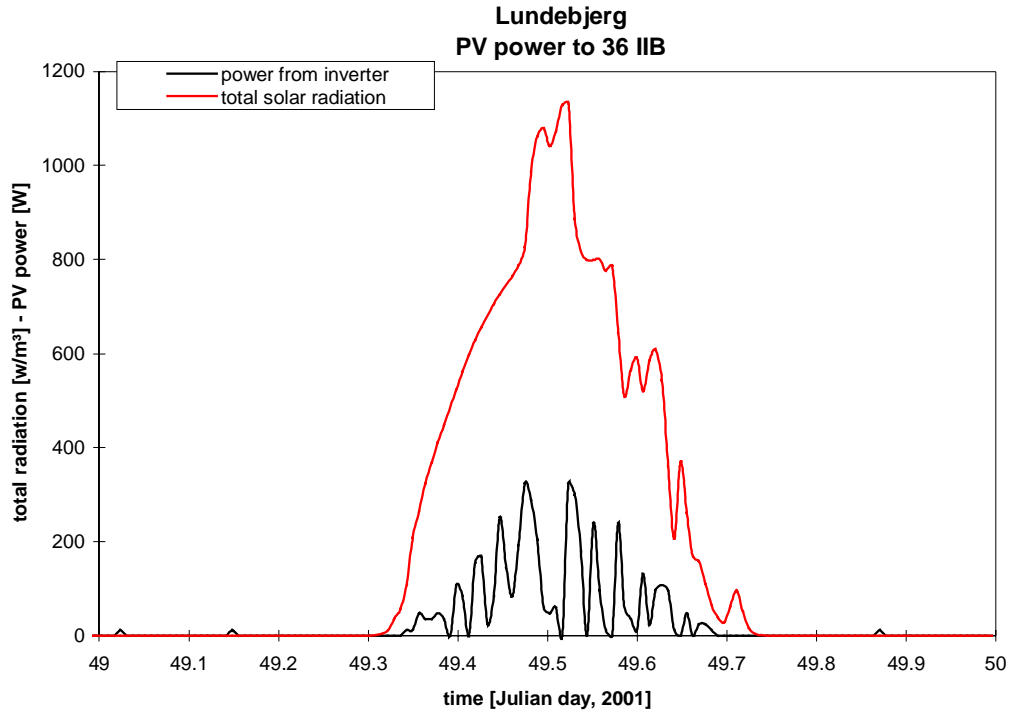


Figure 3.7. Power from one third of the PV-gable and the total radiation on vertical south for February 18

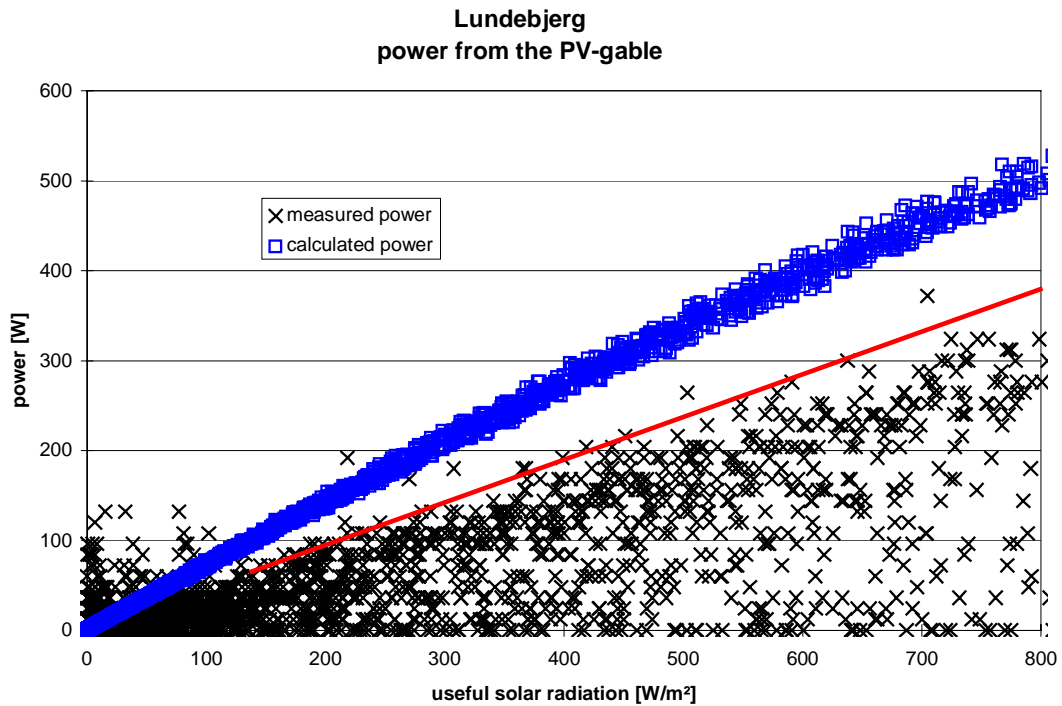


Figure 3.8. The measured and calculated PV power from one third of the PV-gable as a function of the useful solar radiation.

### 3.1.2. Apartment 36 IIB

Figures 3.9-10 show the measured air flow rates to the apartment from the PV-gable and the flow rate and temperature of the exhaust air from the apartment. Figures 3.9-10 show that hardly any air is sucked into the living room. This was also the experience when calibrating the air speed sensors (figure 2.8) – although almost similar calibration equation almost no incoming air was felt when putting the hand in front of the open inlet diffuser in the living room, while a strong air flow was felt from the inlet diffuser in the room. Probably there is something blocking the air in the gable in front of the inlet diffuser to the living room. However, it is believed that if air also was coming in by the diffuser in the living room, the total air flow rate to the dwelling wouldn't be much higher than the shown total air flow rate shown in figures 3.9-10 as the air flow rate to the room will decrease as the underpressure in dwelling only are able to maintain a certain total air flow rate to the dwelling depending on the pressure drop over the diffusers and gable. Figure 3.10 further shows a problem when measuring the air speed in the duct between the gable and the dwelling – the measured air speed fluctuated very much and air speeds were measured when the inlet diffusers could not have been open due to a too low temperature level in the gable as seen when comparing figure 3.10 with figure 3.4. The temperature is too low to be able to open the inlet diffusers on e.g. day 36-37.

Figures 3.9-10 show that the air flow rate of exhaust air is rather low – 80-90 m<sup>3</sup>/h. The flow rate should according to the Danish Building regulations have been 126 m<sup>3</sup>/h. By the installation/start of the system the flow rate was above 100 m<sup>3</sup>/h but has slowly decreased to about 60 m<sup>3</sup>/h by the end of March, 2001. It has been checked that this is not due to an increasing layer of smudge on the sensor. The filters of the system should most probably be replaced. The flow rate is further a bit fluctuating which is caused by the constant pressure control of the system. The control makes the fan overreact a bit.

Figures 3.9-10 also show that the temperature of the exhaust air is between 20 and 22°C, which is as expected as the temperature just below the ceiling is a bit higher than the air temperature in the living zone.

The problem with the often non-realistic air flow rates to the dwelling is almost eliminated in figures 3.11-12 showing the power flow to and from the dwelling. Due to the very low temperature increase between the inlet at the bottom of the gable and the inlet to the dwelling the calculated power to the dwelling becomes almost negligible.

Figures 3.13-14 show how large a percentage the pre-heated air from the gable covers of the energy lost by the exhaust ventilation. For the measured period mid October 2000 – end March 2001 the pre-heating of the fresh air in the gable has been less than 1 % of the energy lost by the exhaust ventilation. The possible savings will further be evaluated in section 3.3.

### 3.1.3. Apartment 40 IIA

Figures 3.15-16 show the air flow rates to and from apartment 40 IIA, while figures 3.17-18 show the temperatures in the PV-facade and around the air to air heat exchanger in apartment 40 IIA. The location of the sensors is shown in figures 2.11-12.

Figures 3.15-16 show that the system mainly has been run in min. air flow mode/summer mode during the shown period – i.e. min. exhaust flow rate and close to zero flow rate of fresh air. Figure 3.16 further shows that the tenant is able to trick the control to what should

be an impossible mode – i.e. normal exhaust/min. fresh air. For this reason another set of graphs are shown for the air flows and temperatures in figures 3.19-22, where the system also has been run in normal flow rates.

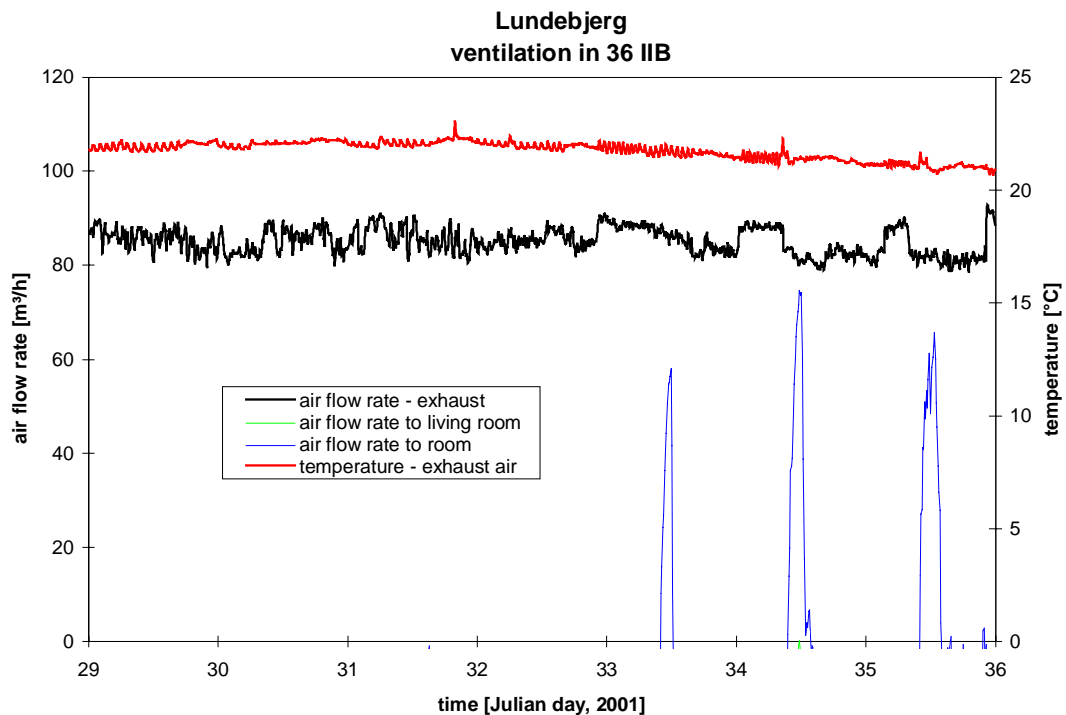


Figure 3.9. Measured air flow rates to and from apartment 36 IIB during week 5, 2001 (January 29 – February 4).

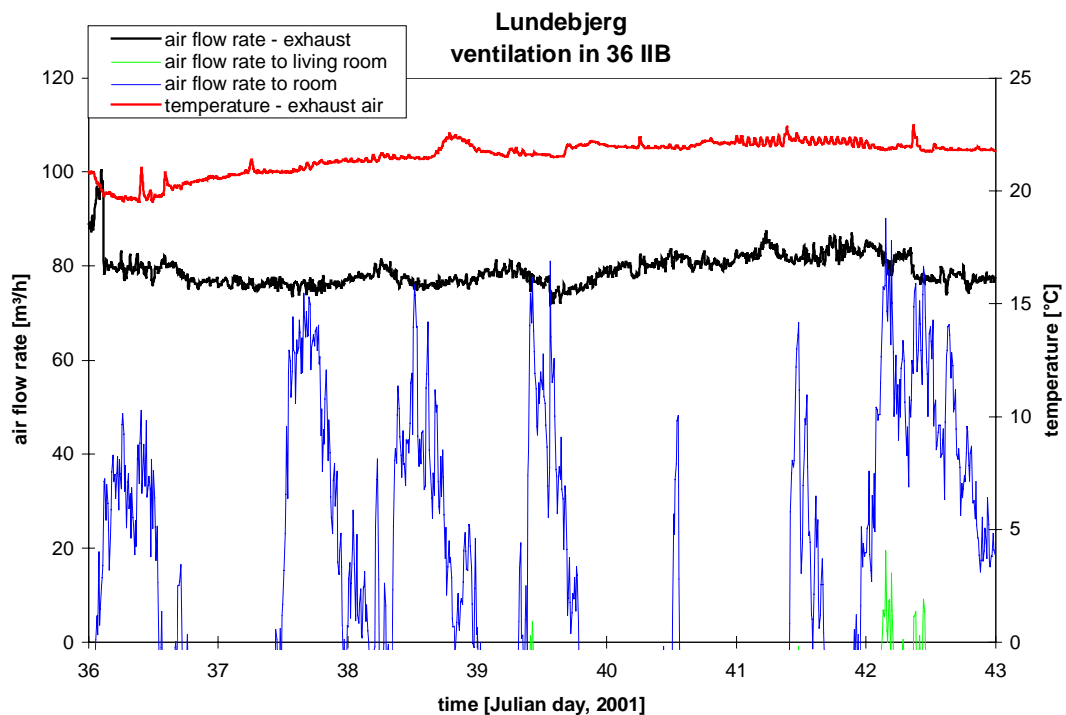


Figure 3.10. Measured air flow rates to and from apartment 36 IIB during week 6, 2001 (February 5 – February 11).



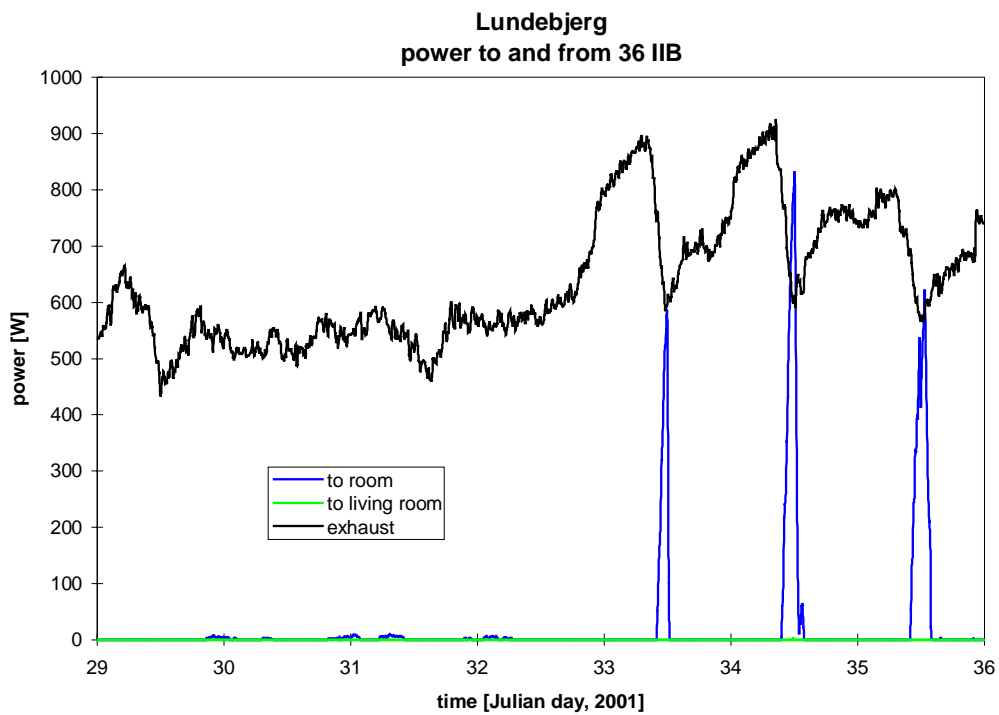


Figure 3.11. Power in the air to and from apartment 36 IIB during week 5, 2001 (January 29 – February 4).

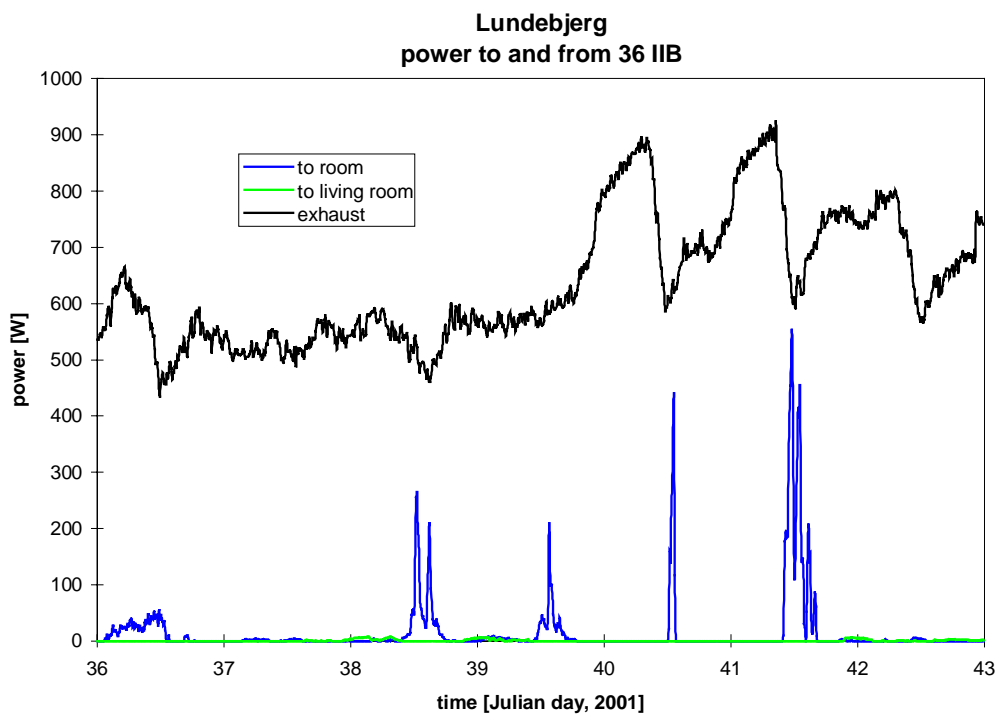


Figure 3.12. Power in the air to and from apartment 36 IIB during week 6, 2001 (February 5 – February 11).

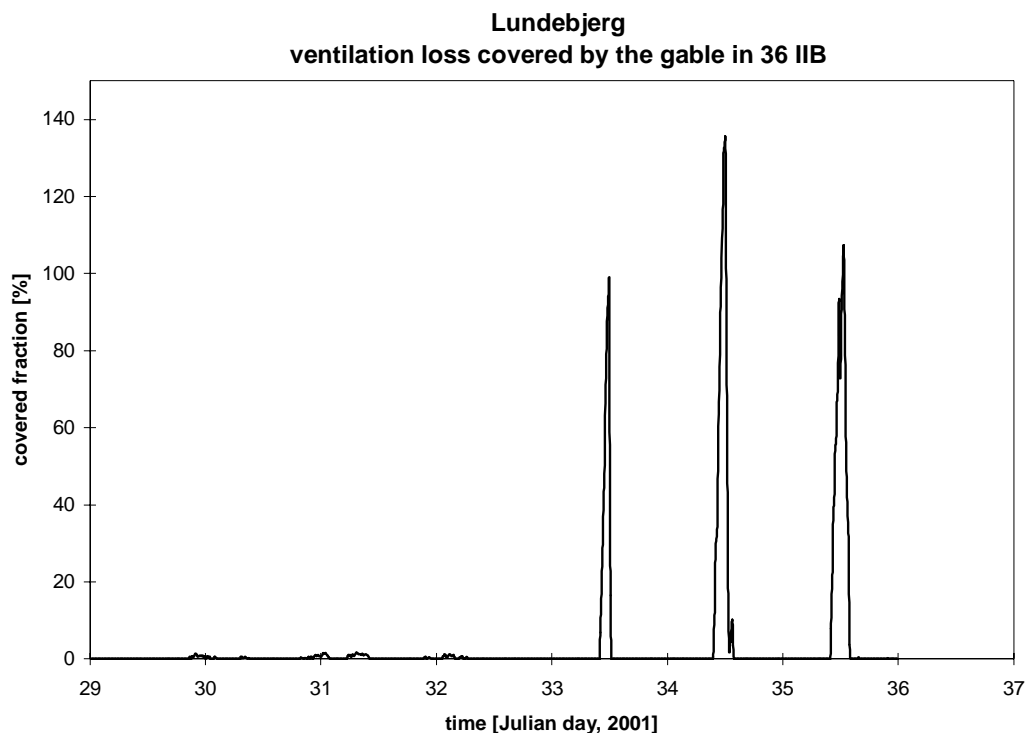


Figure 3.13. The fraction the per-heating of the fresh air to apartment 36 IIB is able to cover of the loss due to the exhaust ventilation during week 5, 2001 (January 29 – February 4).

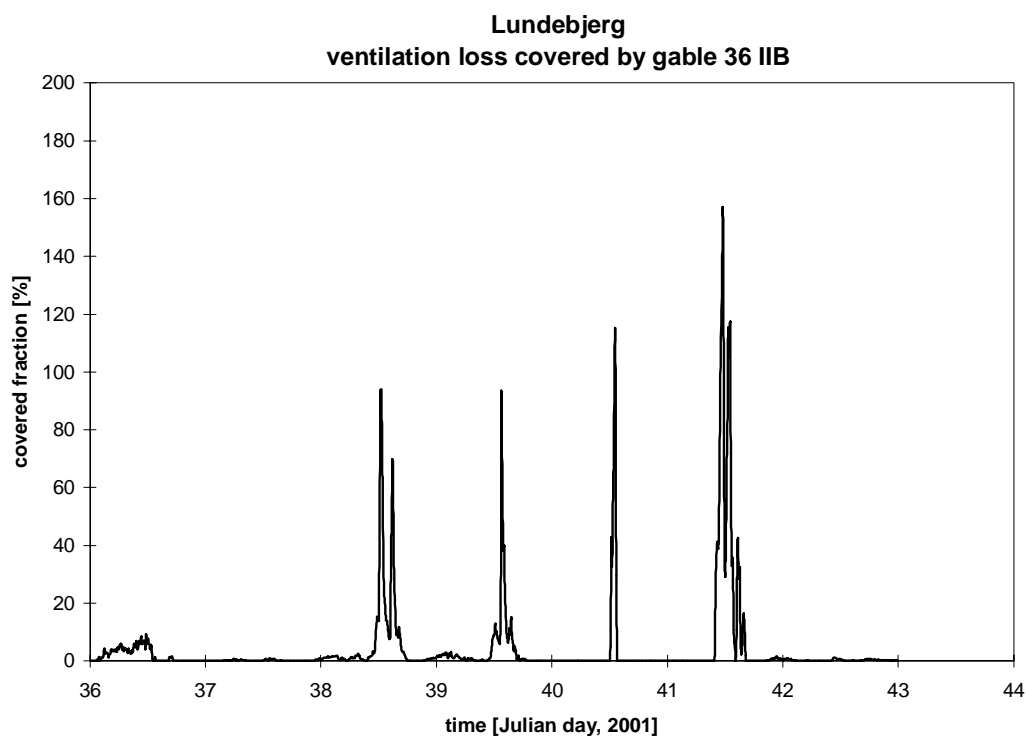


Figure 3.14. The fraction the per-heating of the fresh air to apartment 36 IIB is able to cover of the loss due to the exhaust ventilation during week 6, 2001 (February 5 – February 11).

Figures 3.15-16 clearly show the problem in letting the tenants be able to control the ventilation system: the system will most probably not be run in the most efficient and/or intended mode – this is also shown in the next section and by the measurements at Sundevedsgade/Tøndergade (Jensen, 2001). The reason for running the ventilation system in min. air flow mode is the noise from the ventilation system. The tenant of the dwelling is very sensitive to the noise from the ventilation system.

Figures 3.21-22 show an temperature increase of the air out of the PV-facade of around 1 K at normal flow rate of fresh air, while the temperature of the PV-panel shows an increase compared to ambient of 10 K. The reason for the very low temperature increase over the PV-facade is first of all that the PV-facade is not constructed as intended. Air is as explained in section 2.1.3 taken both from behind the PV-facade and directly from ambient. The radiation level on the PV-facade is further rather low as seen in figures 3.1-2.

Figures 3.19-22 further show that the fresh air is heated further when passing the apartment from the facade to the heat exchanger. The temperature raise is for the considered periods at normal flow rate around 2 K.

Based on the flow rates and the temperatures around the heat exchanger it is possible to calculate the heat flows in the system and thereby the efficiency of the system. The efficiency of the heat exchanger is calculated in the following way:

$$\eta = q_{in} / q_{out} \quad (3.3)$$

where:  $q_{in}$  is the heat transferred to the fresh air in the heat exchanger

$q_{out}$  is the energy in the exhaust air calculated based on the temperature of the exhaust air from the apartment and the temperature of the fresh air to the heat exchanger

Figures 3.23-24 show the calculated heat flows in the heat exchanger, while figures 3.25-26 show the efficiency of the heat exchanger for the same period as shown in figures 3.19-21. Figures 3.23-26 show that the heat exchanger is very efficient at normal flow rate, while much heat is lost when the fresh air fan is switched off. However, the efficiencies shown in figures 3.25-26 is only valid for the shown period as condensation may occur in the heat exchanger leading to a higher efficiency when the efficiency as shown here is based on the dry temperatures – i.e. not considering condensation. Condensation did actually occur during the period shown in figures 3.25-26. This is shown by the difference in the calculated power transferred to the fresh air (black curve in figures 3.23-24) and the calculated power transferred from the exhaust air (blue curve in figures 3.23-24). If no condensation occurs these two values should be identical, but as the power transferred to the fresh air is higher than the power transferred from the exhaust air, this indicates that condensation has taken place. This will be dealt with in details in section 3.3.

Figures 3.27-28 show the power increase of the fresh air over the different components of the system. The area between the x-axis and the red curve is the power transferred to the fresh air across the PV-solar air collector. The area between red and the blue curve gives the power increase over the ducting in the dwelling between the facade and the heat exchanger (see figure 2.12). The area between the blue and the green curve is the power transferred to the fresh air in the heat exchanger. The black curve illustrates the power which would have been transferred if the fresh air was delivered directly to the heat exchanger – i.e. not being pre-heated by the solar collector and the ducting. The black curve is calculated by multiplying the power

in the exhaust air with the actual efficiency of the heat exchanger from figures 3.25-26. The difference between the green and black curved show the benefit of the collector (and the ducting). It may be seen in figures 3.27-28 that the power transfer to the fresh air due to the PV-solar air collector in the facade is marginal which again show, that main part of the air is taken directly from outside and not from behind the PV-panel due to the missing damper in the top of the PV-solar air collector. The low power transfer to the fresh air is further due to the fact that the PV-solar air collector is facing due east leading to less solar radiation hitting the collector (see figures 3.1-2).

Figures 3.29-30 show the power transferred to the fresh air in the collector and the collector + ducting as a fraction of the total power transferred to the fresh air when passing the total system. The black curve show the actual benefit of the collector (and ducting) – i.e. the difference between the green and black curve in figures 3.27-28. Although the fresh air is pre-heated very much in the collector and duct this pre-heating only result in minor actual benefit. This is because the heat exchanger is very efficient (figure 3.25-3.26). The pre-heating before the heat exchanger compete with the pre-heating in the heat exchanger. When the pre-heating in the collector goes up the pre-heating in the heat exchanger goes almost just as much down.

Figures 3.31-32 show the electrical power to and from the PV-mixer of the PV-VENT system in apartment 40 IIA. From the figures it is seen that when solar power is available an immediate drop occurs in the power consumption from the grid. When the PV-panels can supply all the power to the fan no power is taken from the grid – i.e. the power demand of the PV-mixer itself is in these situations taken from the PV-panel. The difference between fan and grid power at no solar power gives the efficiency of the PV-mixer in grid mode, which according to table 1.3 should be 96 %. This efficiency is in figures 3.31-32 lower than 96% at low fan power (8 W) but obtained at higher fan power (25 W). The reason for the lower efficiency at low fan power is the uncertainty of the sensors ( $\pm 1$  W each) which of course makes the measurements more uncertain at low power. In pure PV mode the necessary PV power is higher than the fan power – the difference gives the efficiency of the PV-mixer in pure PV mode. From figures 3.31-32 it is seen that the efficiency in pure PV mode is lower than in pure grid mode. This is dealt with in table 1.4 and further in section 3.2.

Figures 3.33-34 show the utilized PV power and the potential power from the PV-panels (the loss in the wiring is not considered as it is in the order of 2-3% and thus far less than the uncertainty of the measurements). The potential power is calculated as for the PV-gable – see section 3.1.1, equation 3.1. Figures 3.33-34 show that the utilization of the potential PV power is very dependent on the actual demand as seen when comparing figures 3.33-34 with figures 3.31-32.

How large a fraction - that actually is utilized - is shown in figures 3.35-36. Between 30 and 90 % has been utilized during the shown period. The highest utilization is of course reached when the power demand of the fans divided with the efficiency of the PV-mixer matches the potential PV-power from the PV-panels. The yearly saving and waste are dealt with in section 3.3. However, from figures 3.33-34 it can be stated that the peak power of the PV-panels should not be higher than the demand divided with the efficiency of the PV-mixer at that specific demand.

When comparing figures 3.15-16 with 3.31-32 it is seen that the exhaust air flow rate increases when the PV-panels are able to cover the demand. This is because the voltage to the fans increases due to a bit higher voltage from the PV-panels than from the transformer.

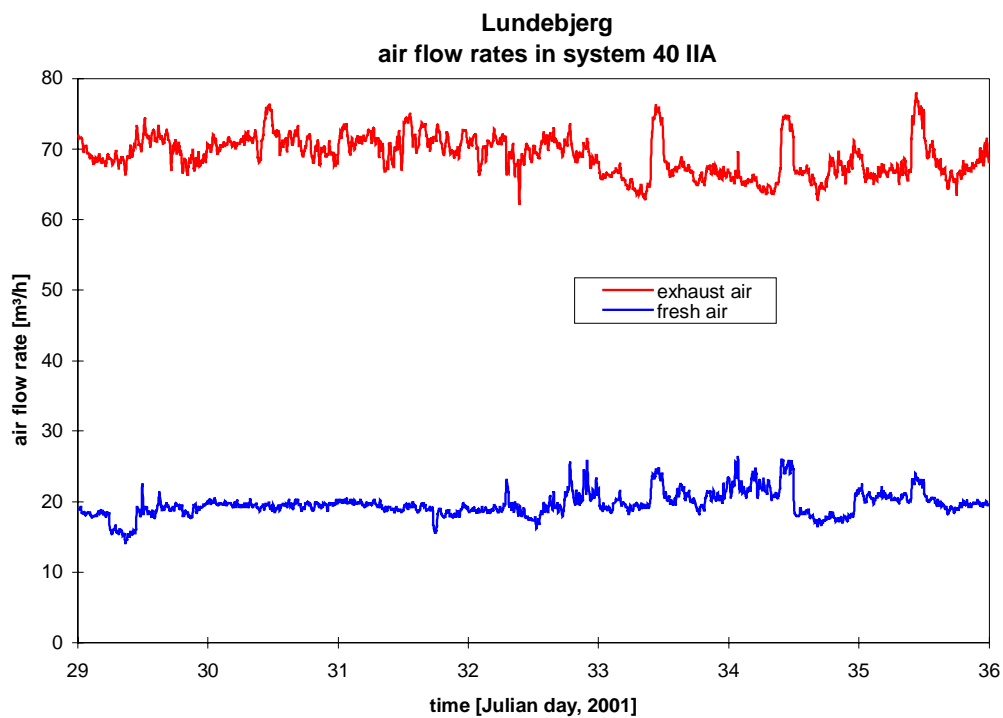


Figure 3.15. The air flow rates in the system of apartment 40 IIA during week 5, 2001 (January 29 – February 4).

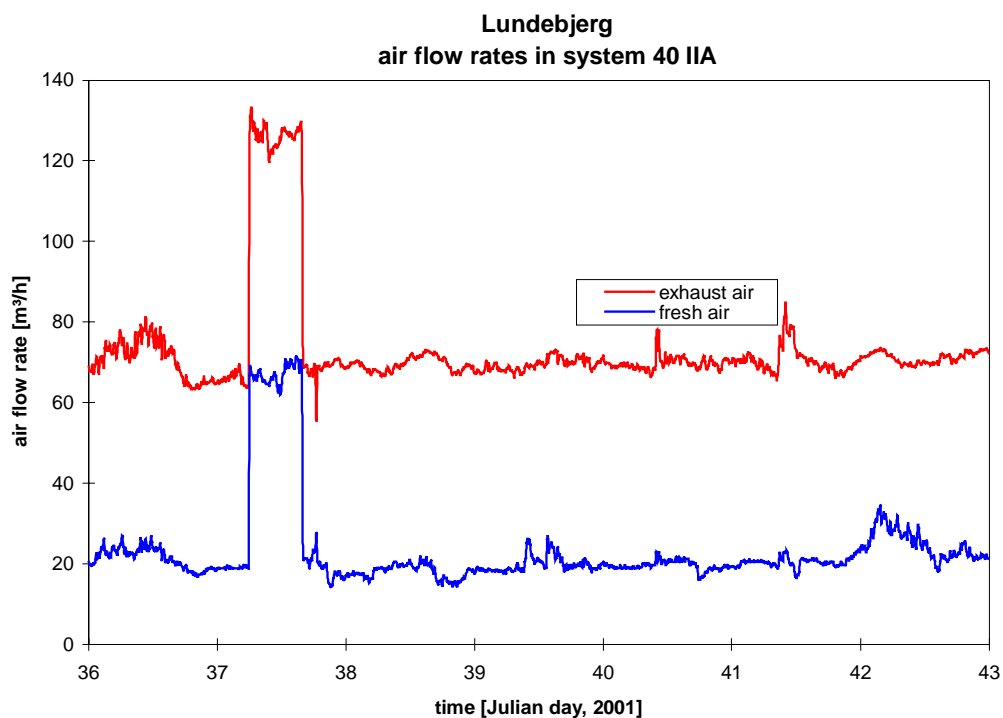


Figure 3.16. The air flow rates in the system of apartment 40 IIA during week 6, 2001 (February 5 – February 11).

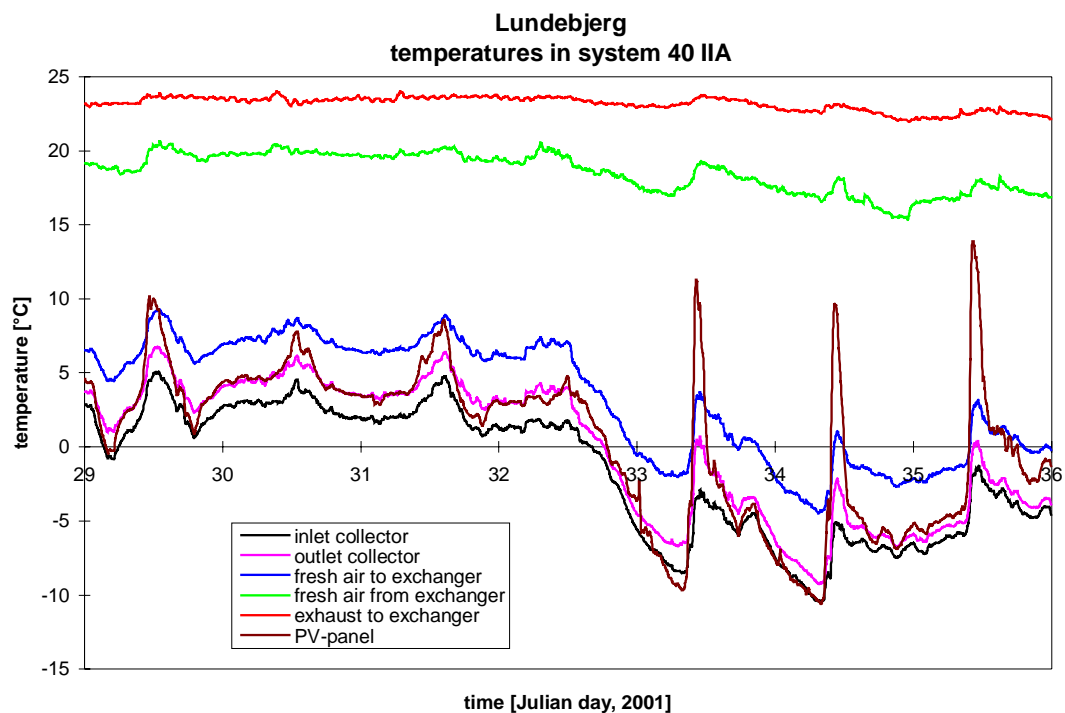


Figure 3.17. The air and PV temperatures in the system of apartment 40 IIA during week 5, 2001 (January 29 – February 4).

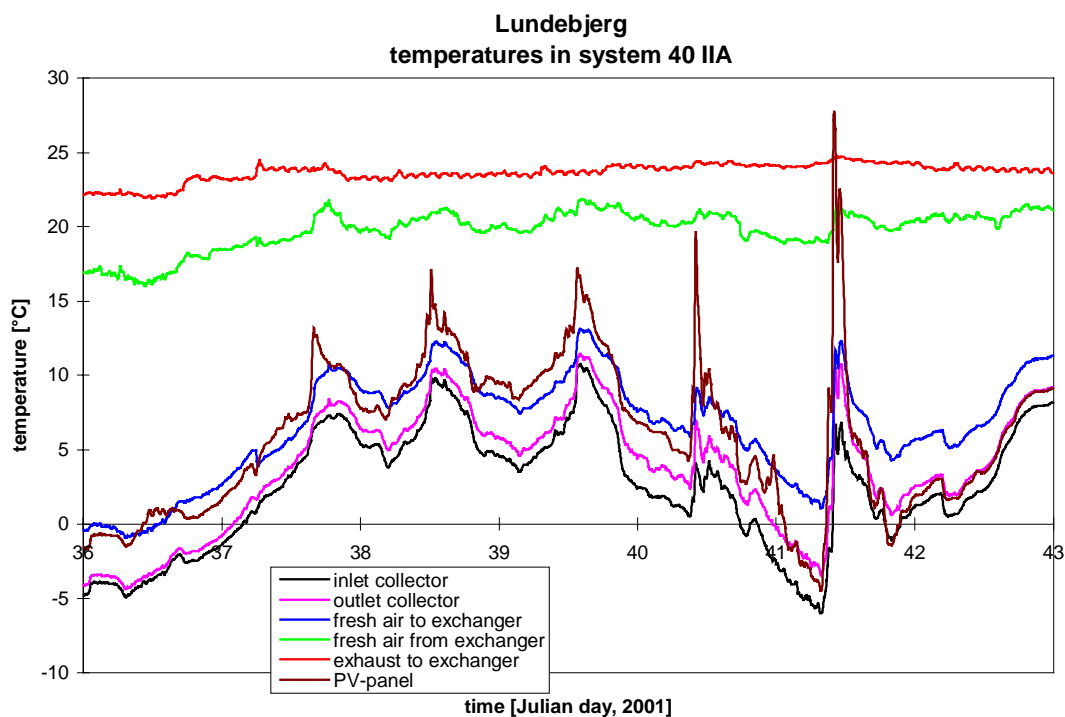


Figure 3.18. The air and PV temperatures in the system of apartment 40 IIA during week 6, 2001 (February 5 – February 11).



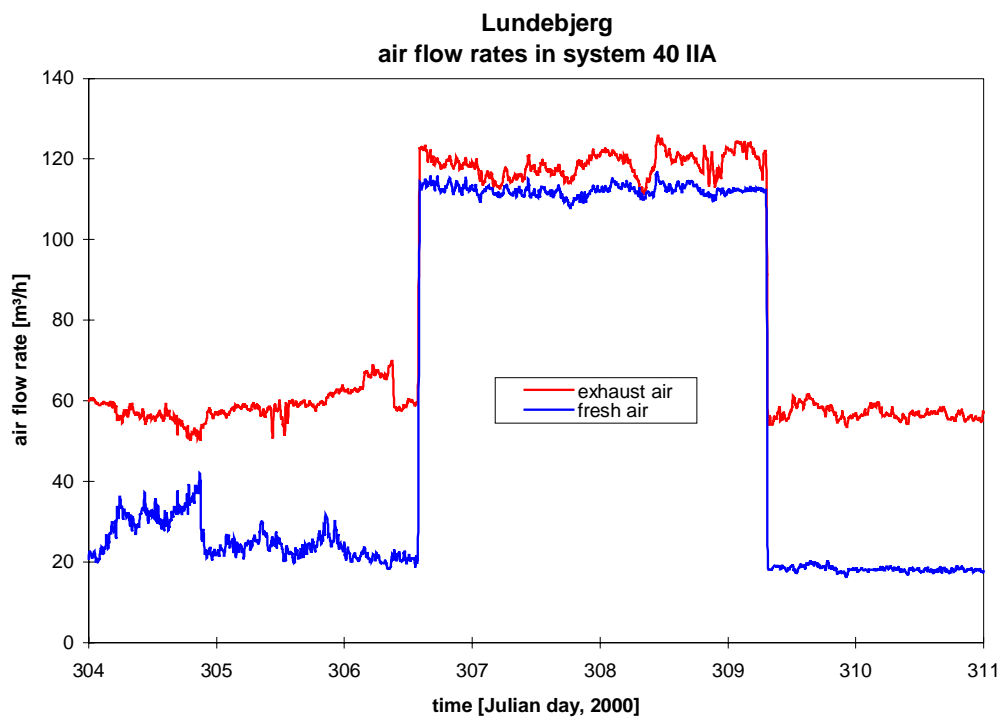


Figure 3.19. The air flow rates in the system of apartment 40 IIA during week 44, 2000 (October 30 – November 5).

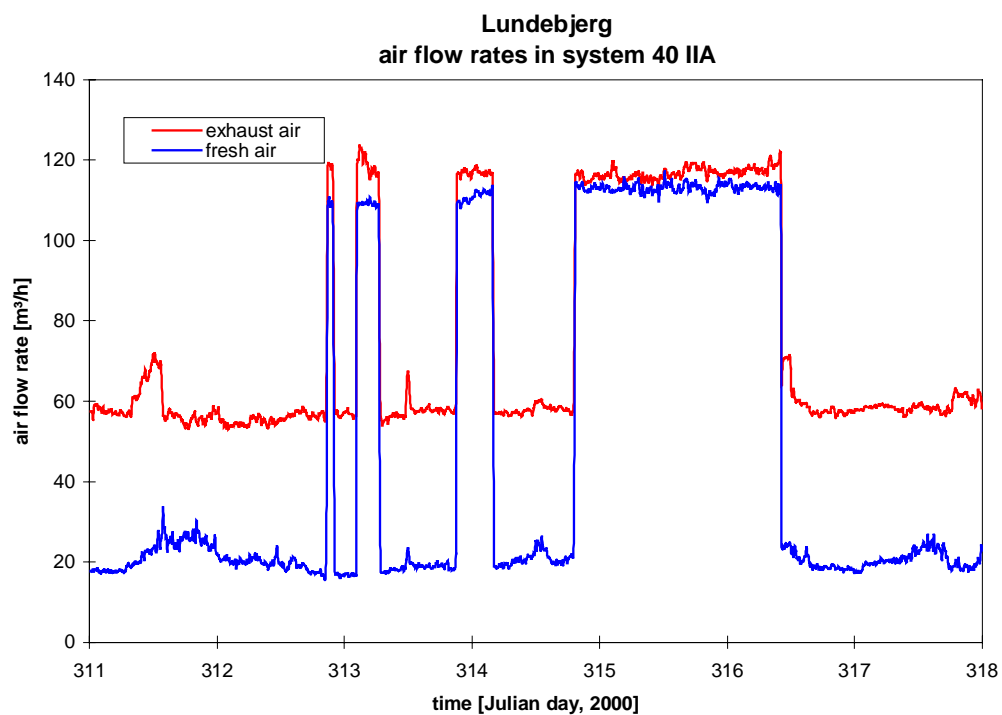


Figure 3.20. The air flow rates in the system of apartment 40 IIA during week 45, 2000 (November 6– November 12).

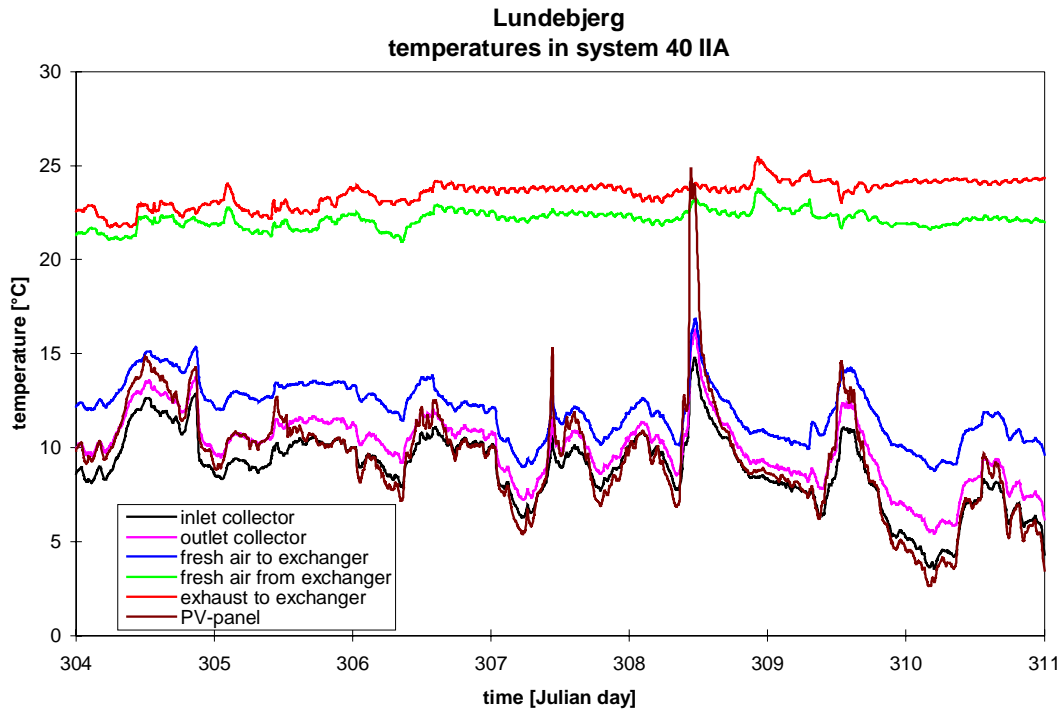


Figure 3.21. The air and PV temperatures in the system of apartment 40 IIA during week 44, 2000 (October 30 – November 5).

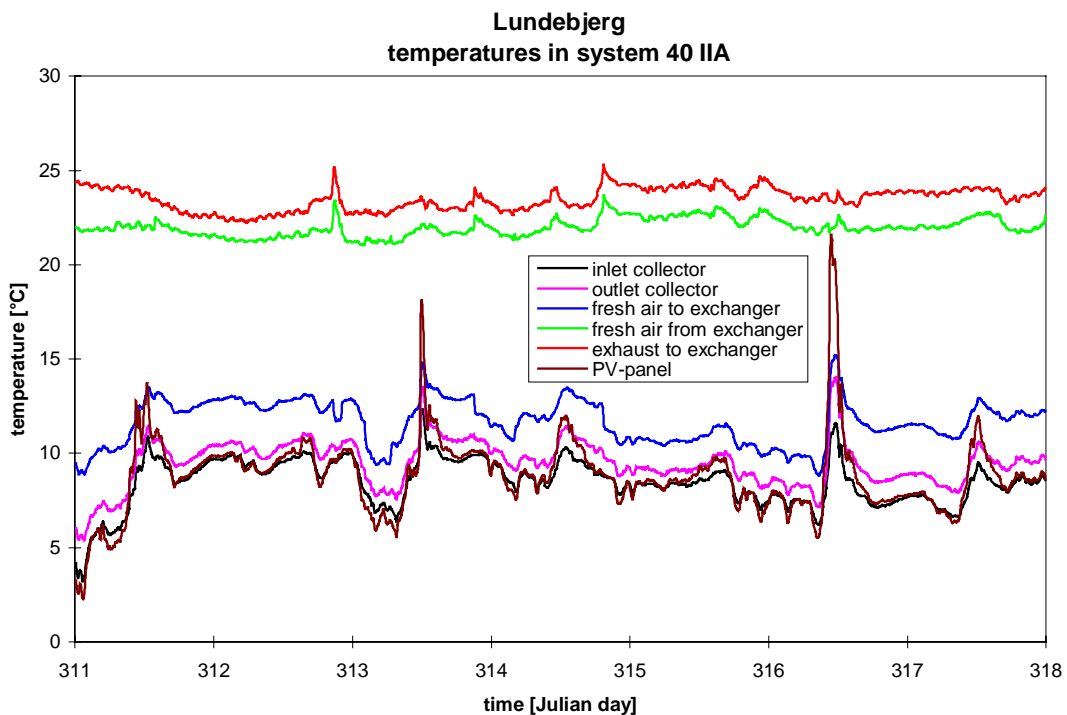


Figure 3.22. The air and PV temperatures in the system of apartment 40 IIA during week 45, 2000 (November 6– November 12).

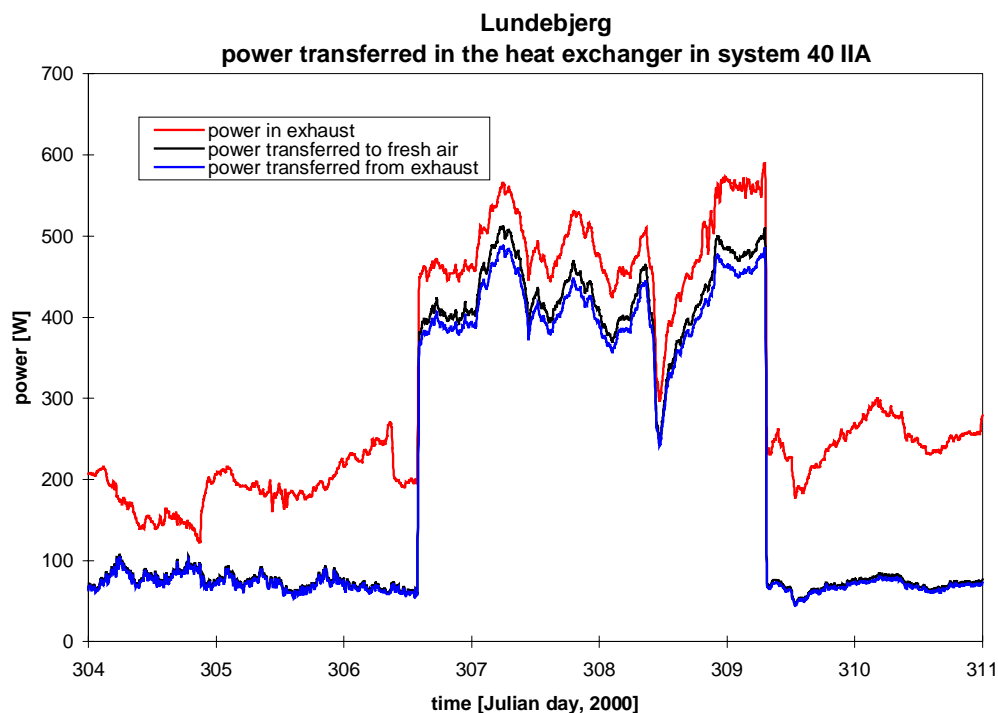


Figure 3.23. The heat flows in the heat exchanger of apartment 40 IIA during week 44, 2000 (October 30 – November 5).

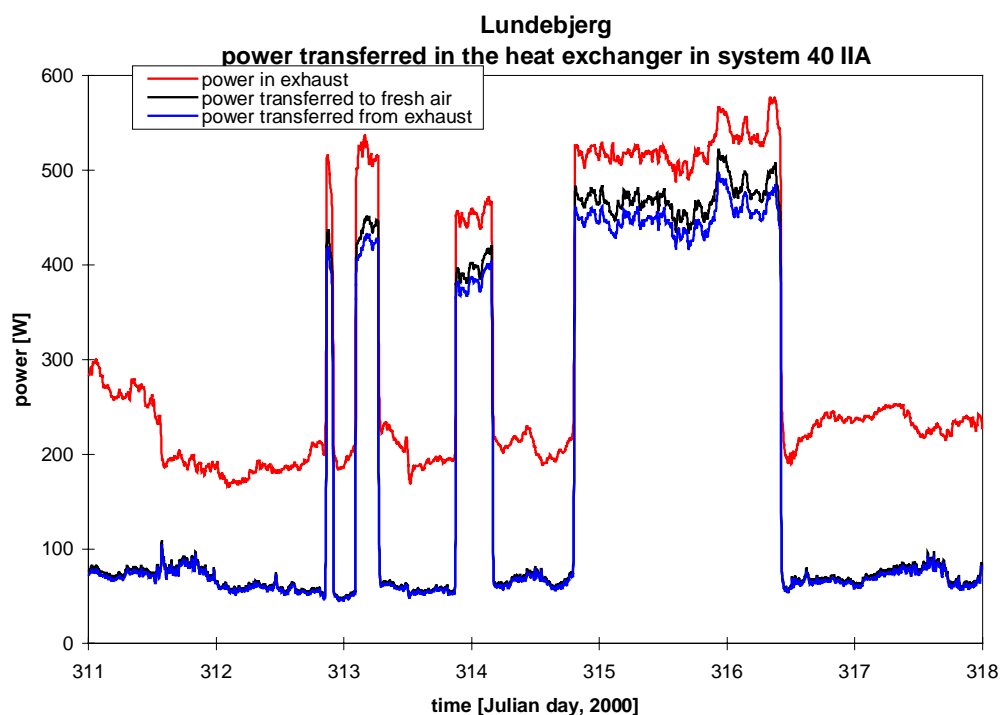


Figure 3.24. The heat flows in the heat exchanger of apartment 40 IIA during week 45, 2000 (November 6– November 12).

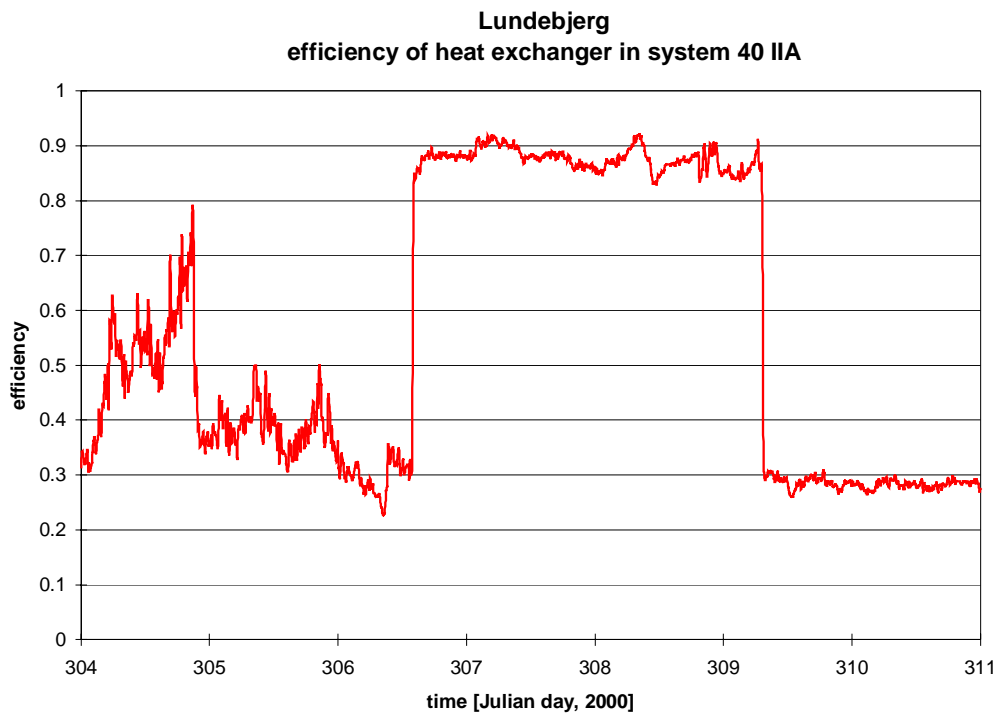


Figure 3.25. The efficiency of the heat exchanger of apartment 40 IIA during week 44, 2000 (October 30 – November 5).

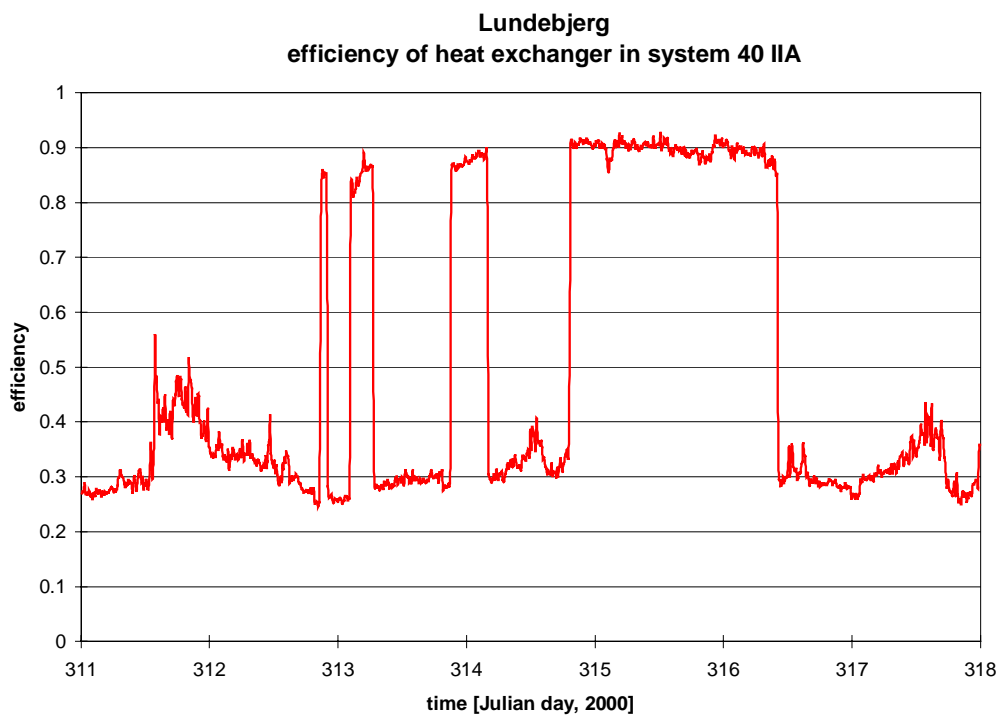


Figure 3.26. The efficiency of the heat exchanger of apartment 40 IIA during week 44, 2000 (November 6– November 12).

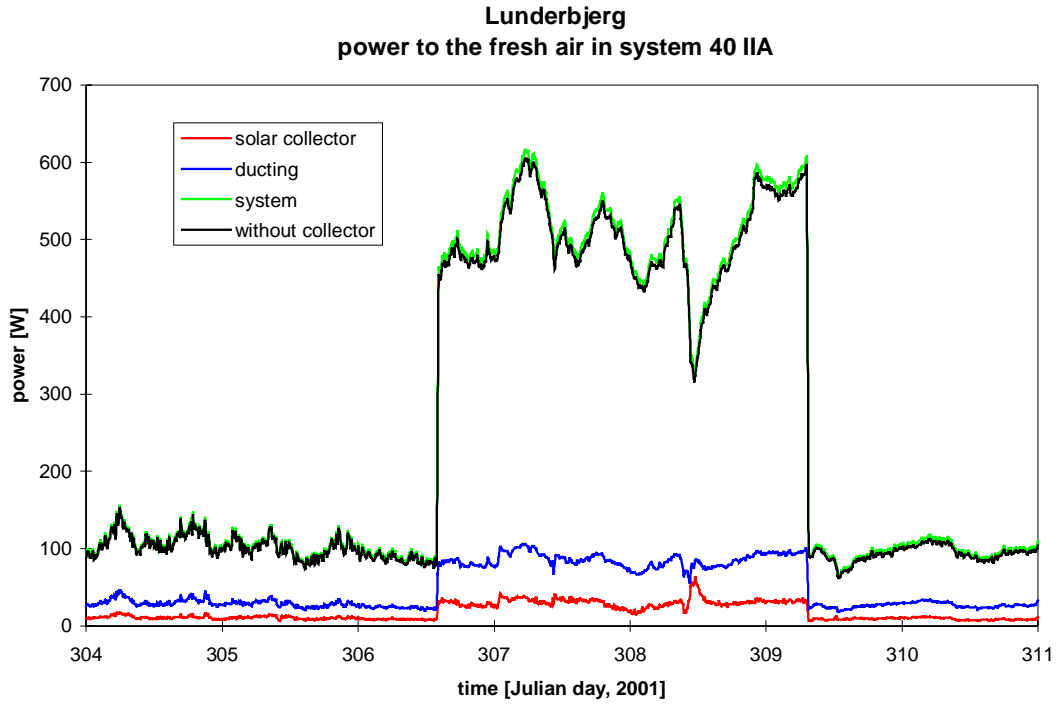


Figure 3.27. Power transferred to the fresh air in the collector, ducting and heat exchanger of apartment 40 IIA during week 44, 2000 (October 30 – November 5).

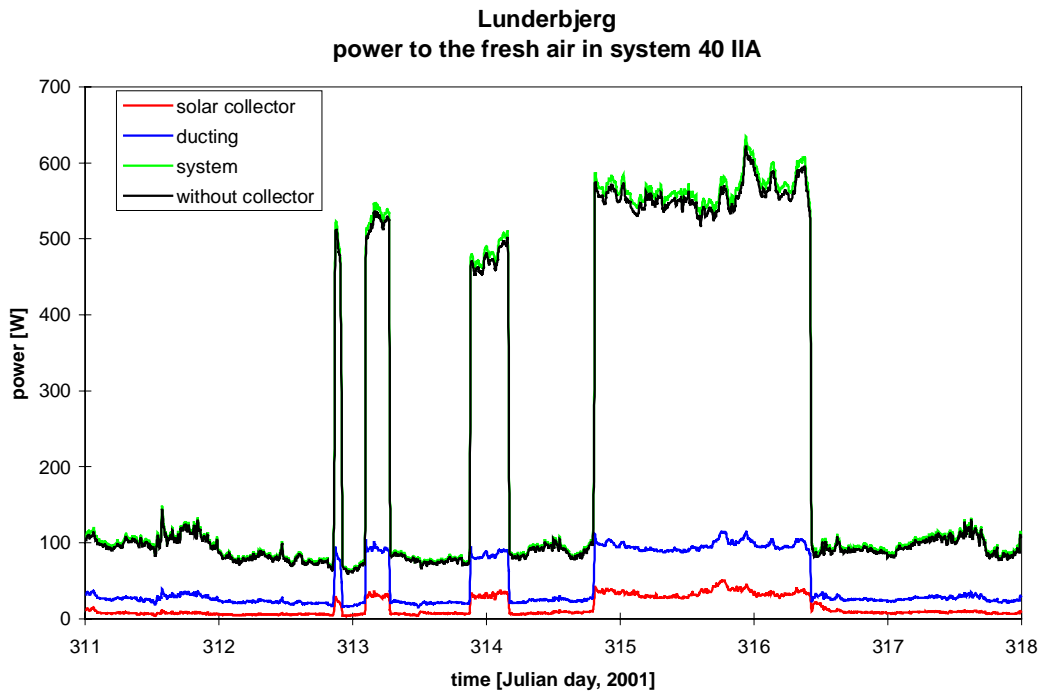


Figure 3.28. Power transferred to the fresh air in the collector, ducting and heat exchanger of apartment 40 IIA during week 45, 2000 (November 6 – November 12).

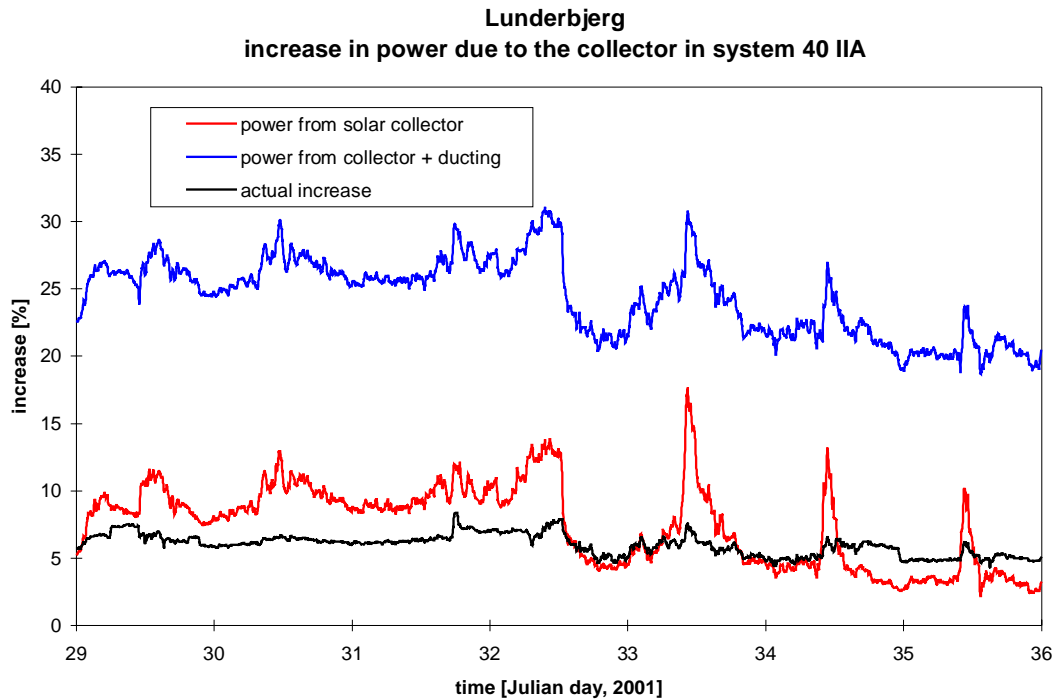


Figure 3.29. The possible and actual fraction the per-heating of the fresh air in the solar ventilation chimney and ducting is able to cover of the ventilation loss in apartment 40 IIA during week 44, 2000 (October 30 – November 5).

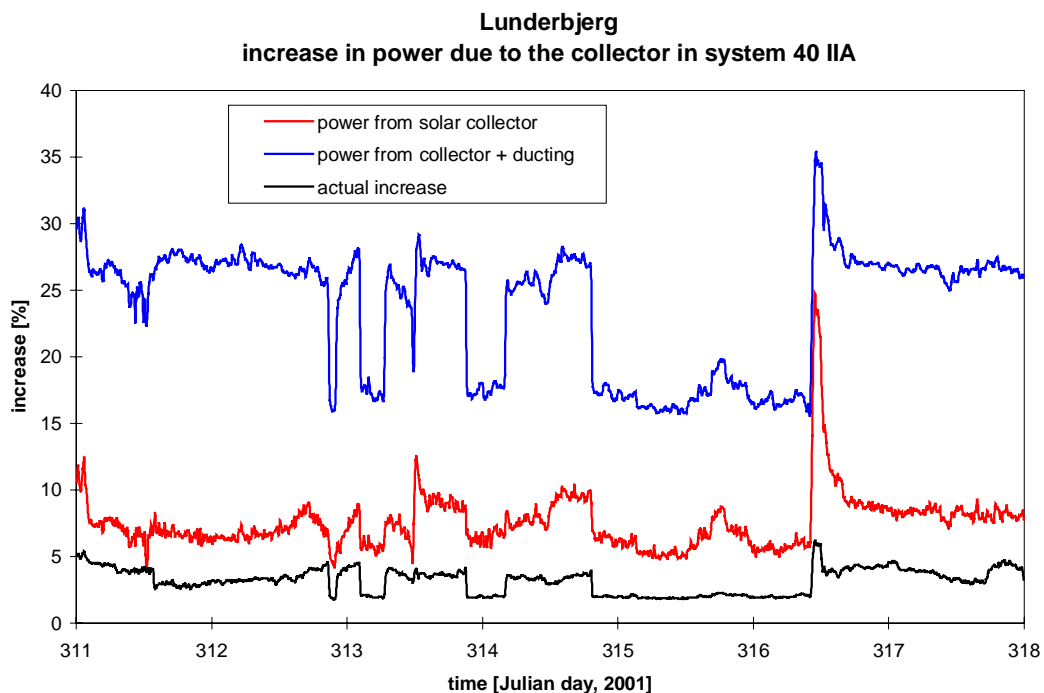


Figure 3.30. The possible and actual fraction the per-heating of the fresh air in the solar ventilation chimney and ducting is able to cover of the ventilation loss in apartment 40 IIA during week 45, 2000 (November 6 – November 12).



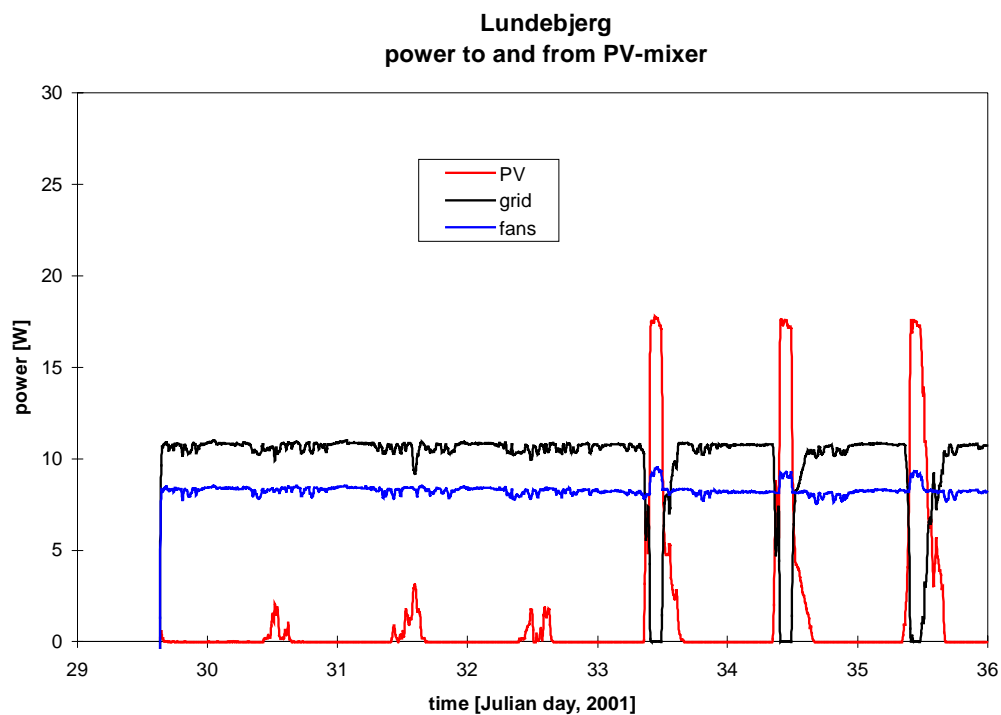


Figure 3.31. Power to and from the PV-mixer of apartment 40 IIA during week 5, 2001 (January 29 – February 4).

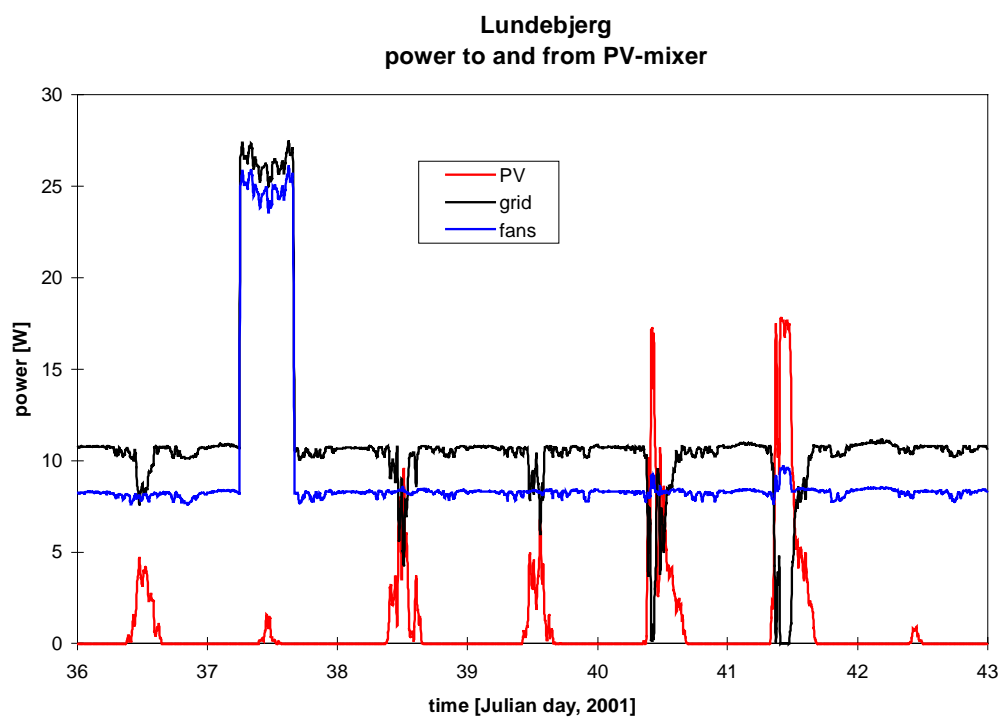


Figure 3.32. Power to and from the PV-mixer of apartment 40 IIA during week 6, 2001 (February 5 – February 11).

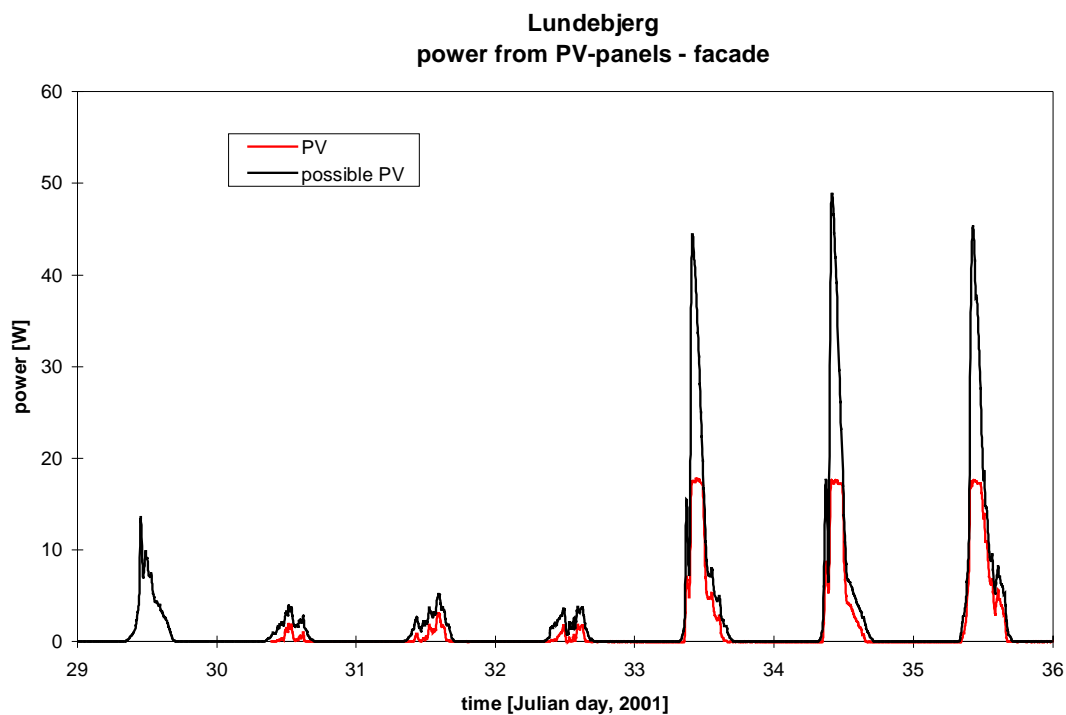


Figure 3.33. Actual power and potential power from the PV-facade of apartment 40 IIA during week 5, 2001 (January 29 – February 4).

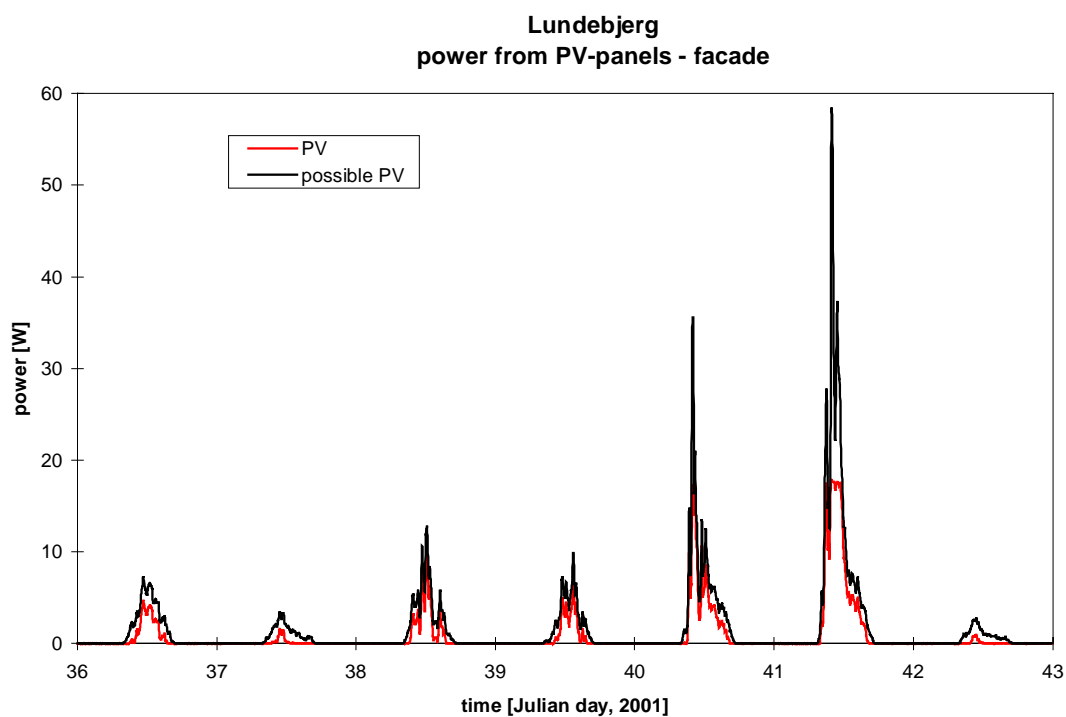


Figure 3.34. Actual power and potential power from the PV-facade of apartment 40 IIA during week 6, 2001 (February 5 – February 11).

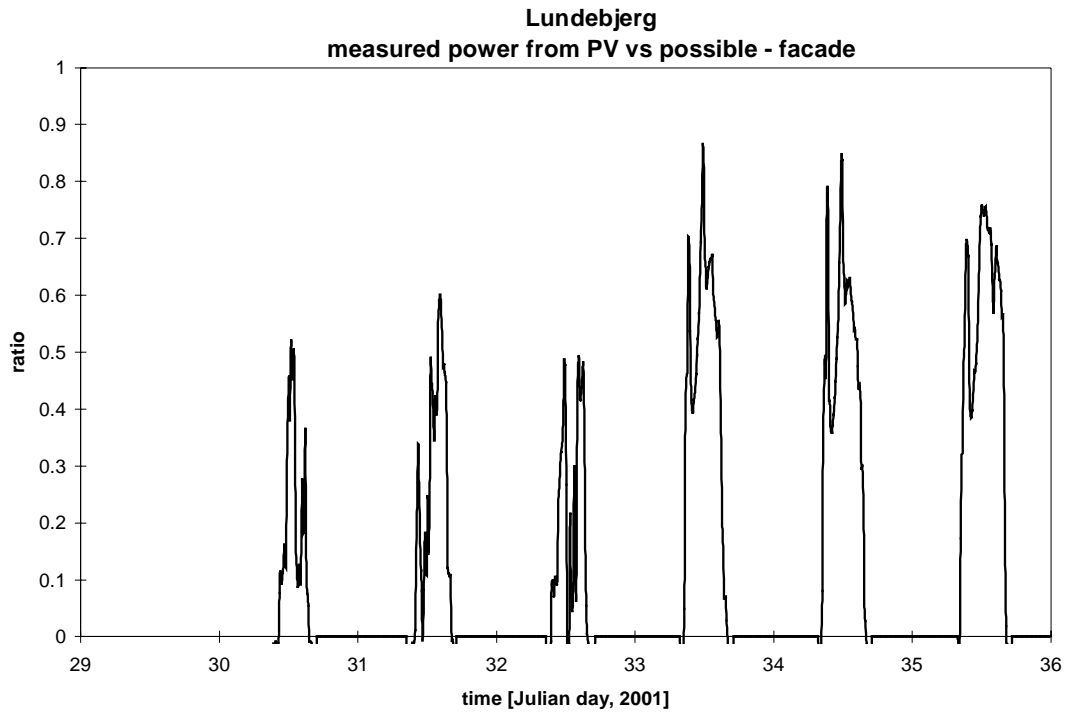


Figure 3.35. Actual power divided with potential power from the PV-facade of apartment 40 IIA during week 5, 2001 (January 29 – February 4).

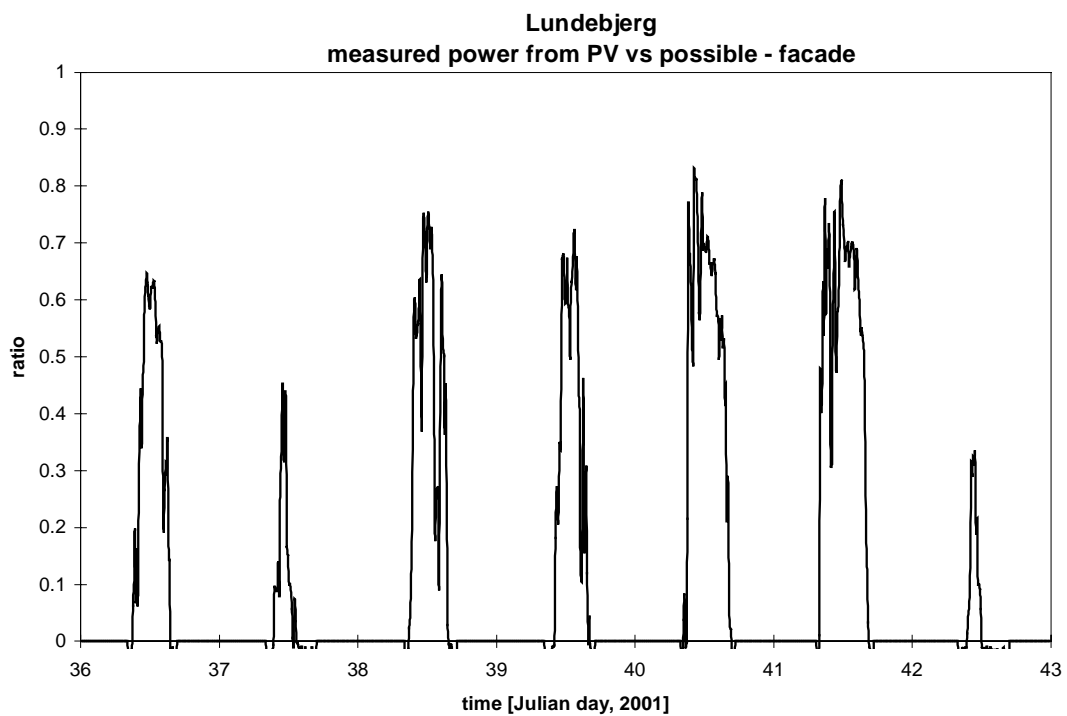


Figure 3.36. Actual power divided with potential power from the PV-facade of apartment 40 IIA during week 6, 2001 (February – February 11).

### 3.1.3. Apartment 40 IIB

Figures 3.37-38 show the air flow rates in the system of apartment 40 IIB while figures 3.39-40 show the temperatures around the air to air heat exchanger of apartment 40 IIB. The location of the sensors is shown in figure 2.14.

Figures 3.37-38 show the same problem as encountered for apartment 40 IIA – incorrect running of the ventilation system. The system has in main part of the measuring period been run in min. flow mode and only occasionally run in normal or max flow mode. The reason for this is that the tenants find the air in the dwelling too dry even at this low flow rate – they state that the humidity of the air is 20-25 %rh, so there is no need for running the system at higher flow rates except occasionally after showering where the system is run at full speed for shorter periods.

Figures 3.39-40 show that the inlet temperature of fresh air to the heat exchanger on day 41 reaches 18°C, while the ambient temperature max was 3-4°C (see figure 3.2). This illustrates that the solar ventilation chimney has a higher degree of preheating of the fresh air than the PV-facade in apartment 40 IIA. The efficiency of the solar ventilation chimneys as solar air collector is dealt with in section 3.2. When comparing the max fresh air inlet temperature on day 41 with figure 3.78 it is seen that the max outlet temperature from the solar ventilation chimney this day was 19°C, which indicate that only little heat is lost from the ductworks in the attic.

The temperature of the exhaust air is about 22°C, which is reasonable.

Figures 3.41-42 show the calculated heat flows in the heat exchanger calculated in the same manner as for apartment 40 IIA, while figures 3.43-44 shows the calculated efficiency for the period.

Figures 3.41-42 show that during sunshine when the ventilation chimney creates a high increase of the fresh air temperature the heat flows in the heat exchanger become very low and will eventually be negative when the fresh air inlet temperature to the heat exchanger gets above the temperature of the exhaust air.

Figures 3.43-44 and figures 3.37-38 show that the efficiency of the heat exchanger is very flow rate dependent. Due to the rather large relative difference between the air flow rate of fresh and exhaust air, the efficiency of the heat exchanger stays most of the time below 60%. Very high efficiencies are reached during the short periods when the air flow rate of fresh air gets higher than the air flow rate of exhaust air.

The efficiency of the heat exchanger at normal flow rates will as for apartment 40 IIA further be dealt with in section 3.2, where more general conclusions will be drawn based on the complete set of measurements rather than on two weeks of measurements. The efficiency will further be brought on a form where comparison with other heat exchangers is possible.

Figures 3.45-46 show as for apartment 40 IIA the power transfers to the fresh air in the solar ventilation chimney, the ducting and in the heat exchanger in the same way as in figures 3-27-28, while figures 3.47-48 show the fraction of the pre-heating in the solar ventilation chimney and ducting compared to the pre-heating over the total system. These fractions are compared

with the actual benefit of the solar ventilation chimney compared to a system with no pre-heating before the heat exchanger. Please be aware of different y-axis.

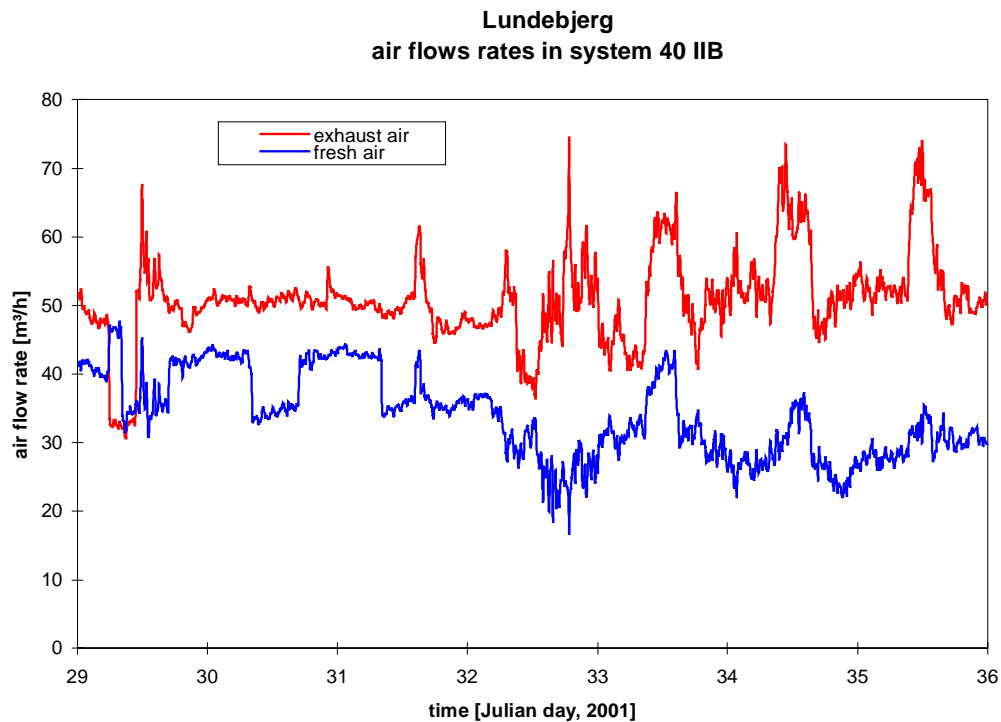


Figure 3.37. The air flow rates in the system of apartment 40 IIB during week 5, 2001 (January 29 – February 4).

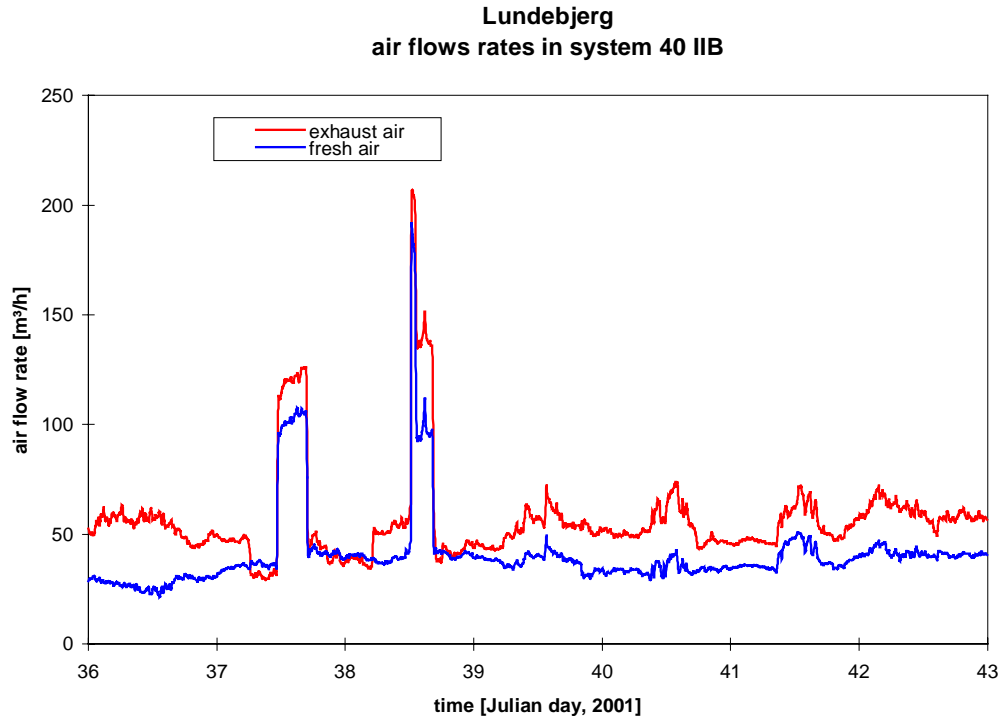


Figure 3.38. The air flow rates in the system of apartment 40 IIB during week 6, 2001 (February 5 – February 11).

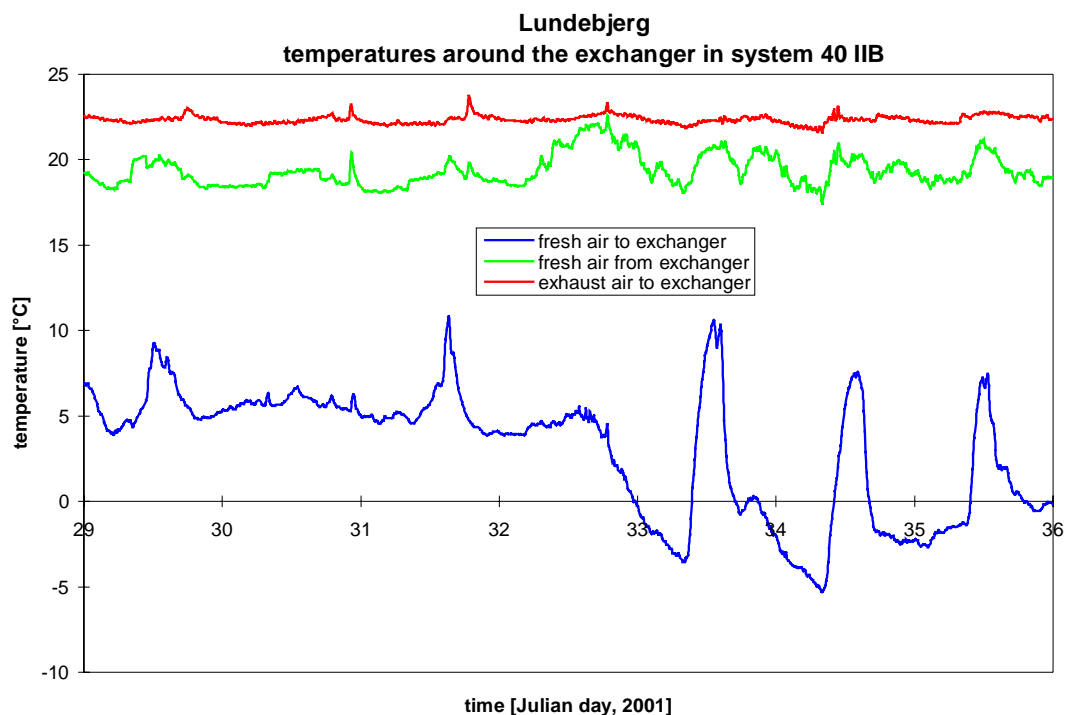


Figure 3.39. The air temperatures around the heat exchanger of apartment 40 IIB during week 5, 2001 (January 29 – February 4).

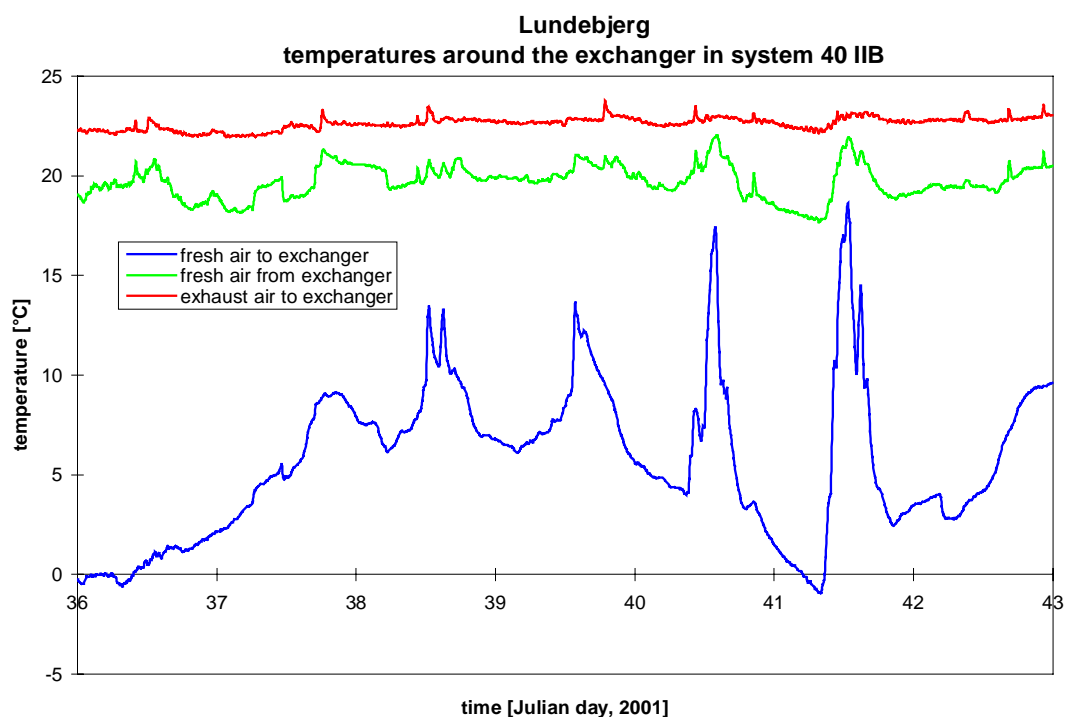


Figure 3.40. The air temperatures around the heat exchanger of apartment 40 IIB during week 6, 2001 (February 5 – February 11).



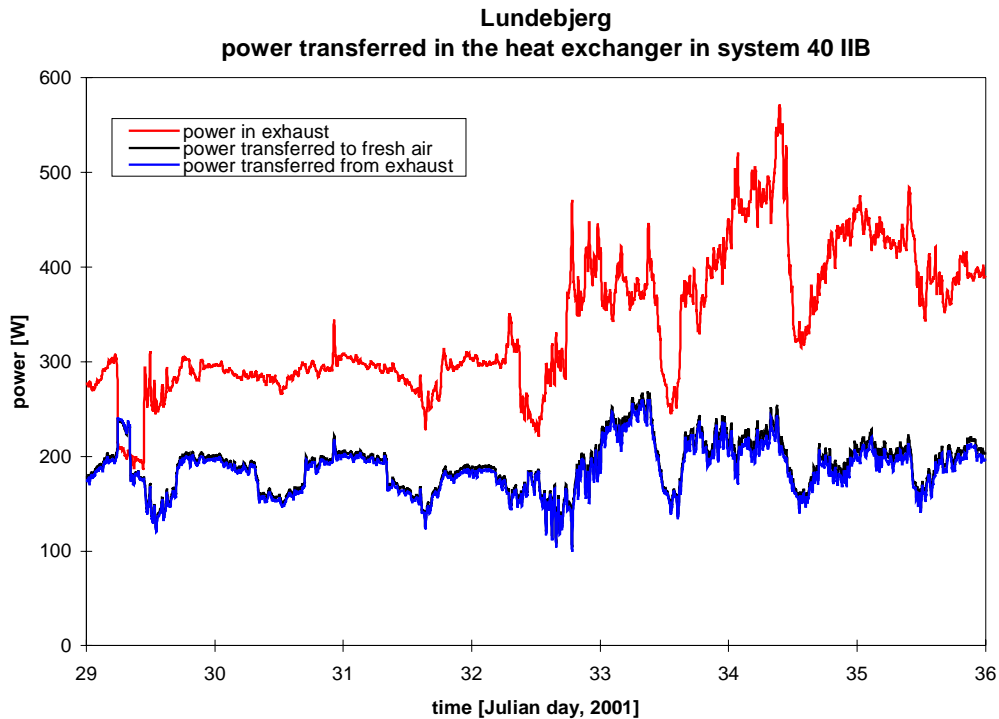


Figure 3.41. The heat flows in the heat exchanger of apartment 40 IIB during week 5, 2001 (January 29 – February 4).

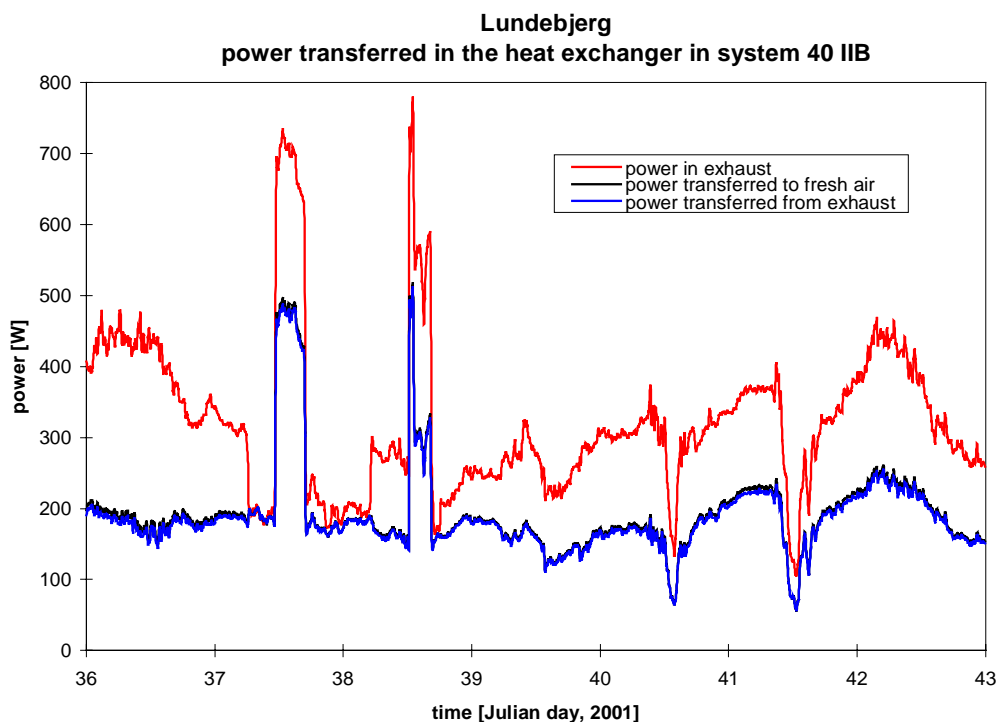


Figure 3.42. The heat flows in the heat exchanger of apartment 40 IIB during week 6, 2001 (February 5 – February 11).

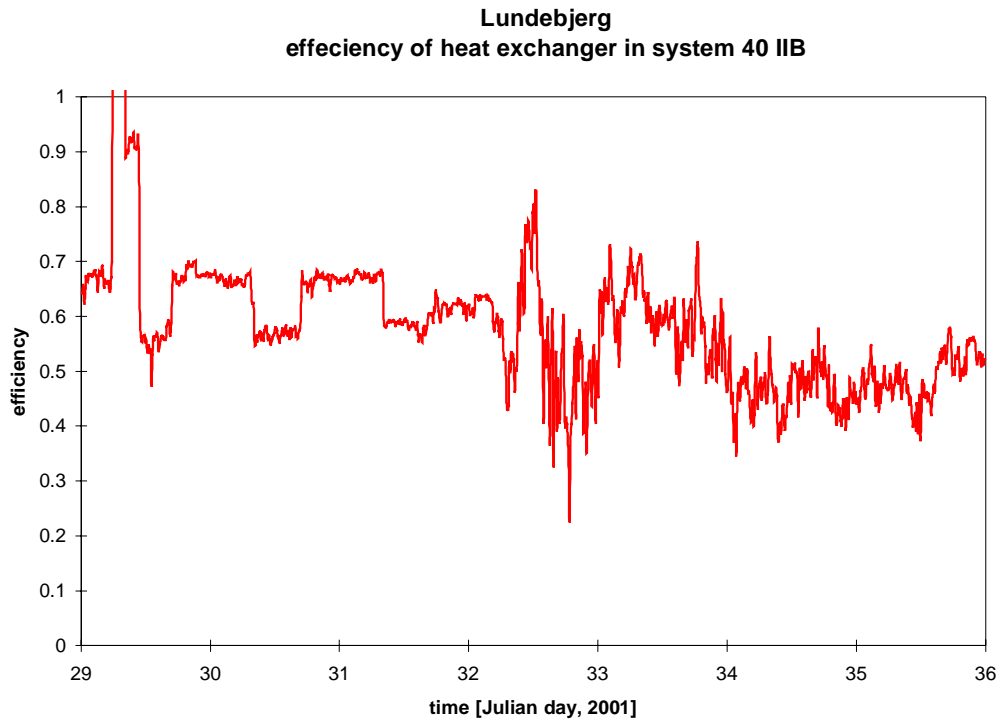


Figure 3.43. The efficiency of the heat exchanger of apartment 40 IIB during week 5, 2001 (January 29 – February 4).

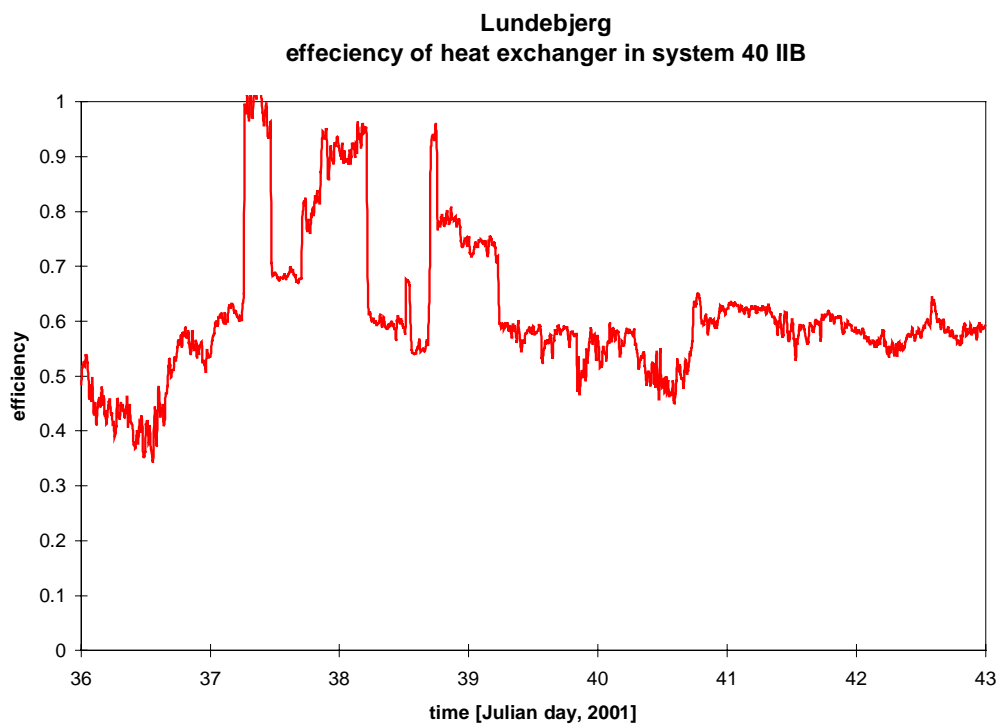


Figure 3.44. The efficiency of the heat exchanger of apartment 40 IIB during week 6, 2001 (February 5 – February 11).

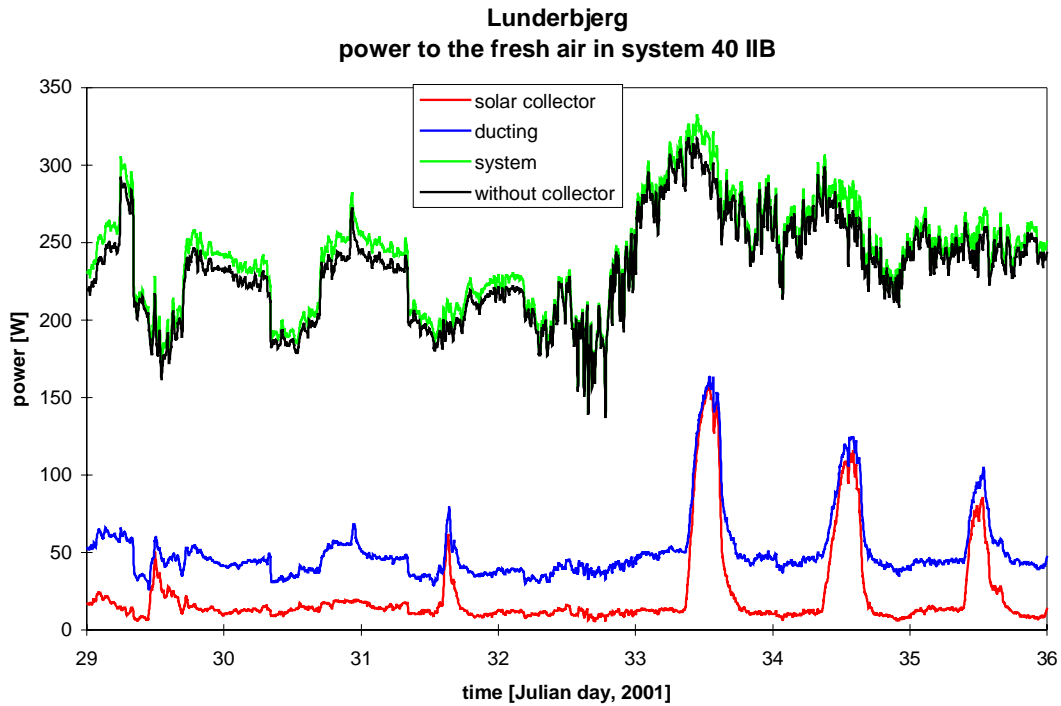


Figure 3.45. Power transferred to the fresh air in the solar ventilation chimney, ducting and heat exchanger of apartment 40 IIB during week 5, 2001 (January 29 – February 4).

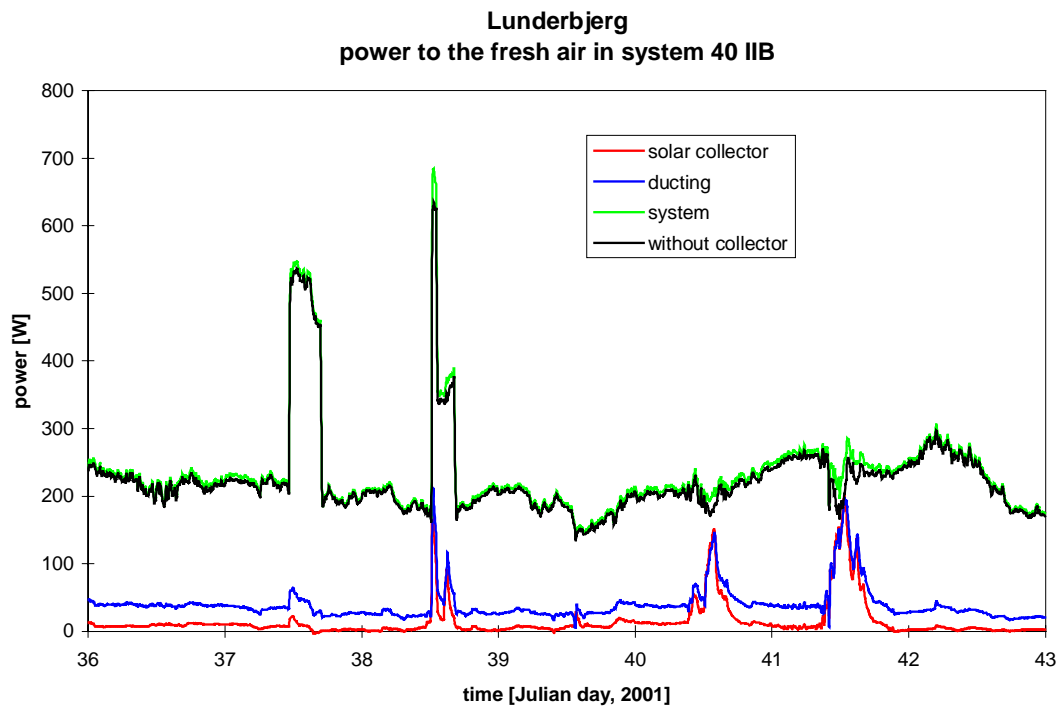


Figure 3.46. Power transferred to the fresh air in the solar ventilation chimney, ducting and heat exchanger of apartment 40 IIB during week 6, 2001 (February 5 – February 11).

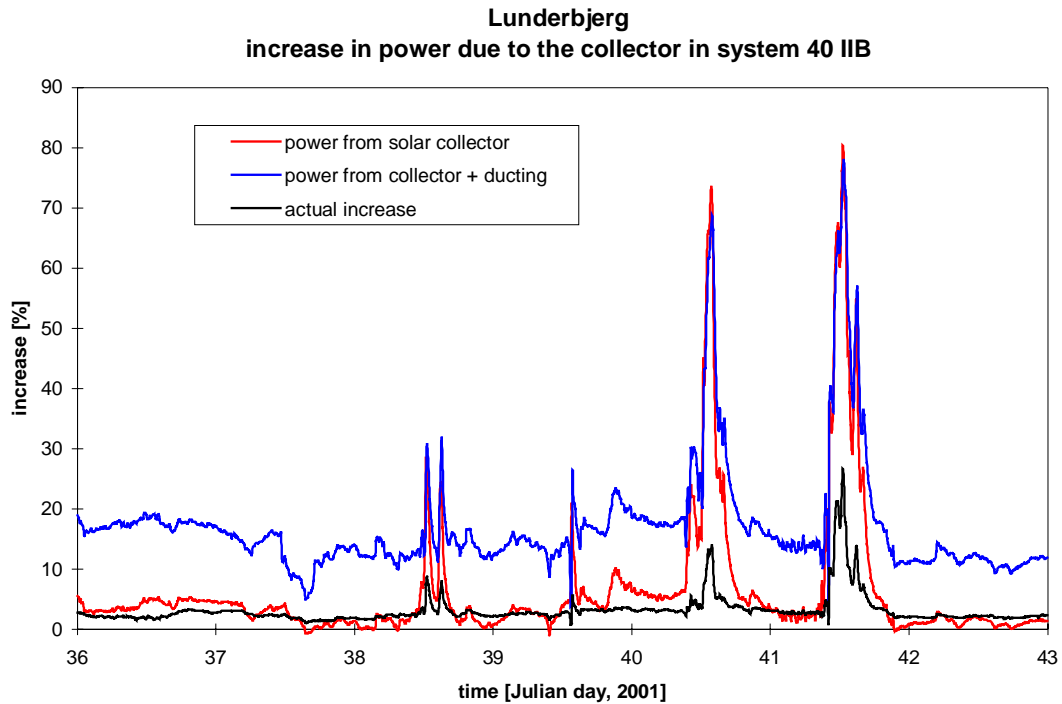


Figure 3.47. The possible and actual fraction the per-heating of the fresh air in the solar ventilation chimney and ducting is able to cover of the ventilation loss in apartment 40 IIB during week 5, 2001 (January 29 – February 4).

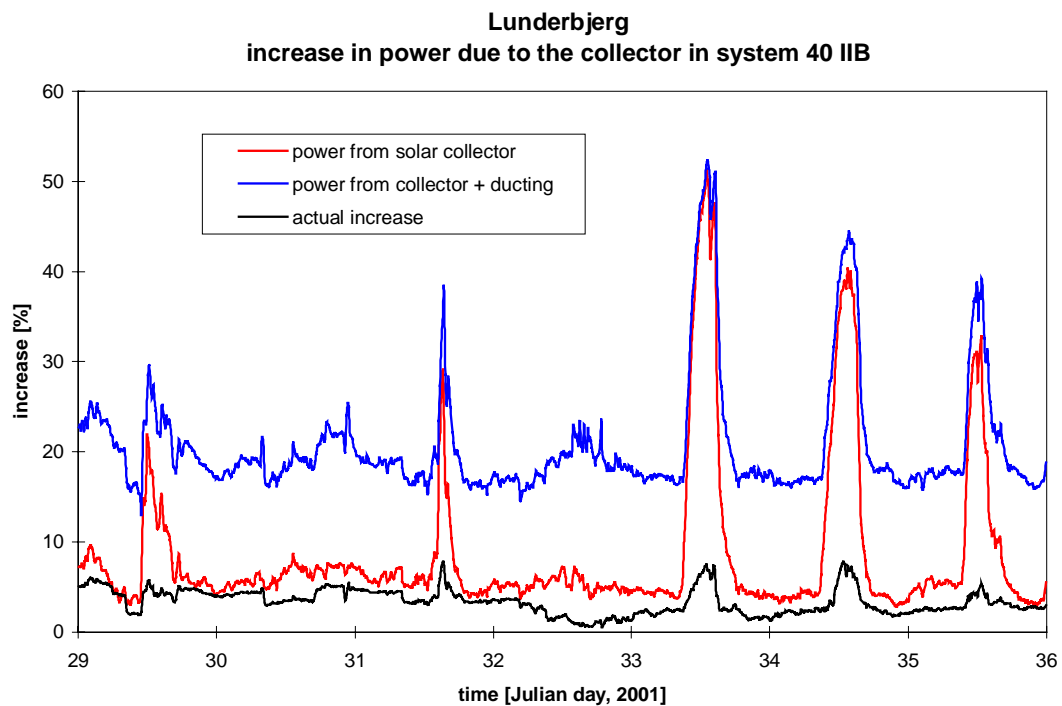


Figure 3.48. The possible and actual fraction the per-heating of the fresh air in the solar ventilation chimney and ducting is able to cover of the ventilation loss in apartment 40 IIB during week 6, 2001 (February 5 – February 11).

Figures 3.45-48 show a higher power transfer to the fresh air in the solar ventilation chimney than in the facades (figures 3.27-30) although a smaller collector area per dwelling: 1.3 m<sup>2</sup> for the chimney, while 1.7 m<sup>2</sup> in the facade. This is because no false air is let into the chimney in the top as for the facade and further because the solar ventilation chimneys are facing due south. During solar radiation nearly no heat loss occurs from the ductworks (red and blue curve in figures 3.45-46). It is further seen that the fresh air is pre-heated during the night when passing both the chimney and the attic. This is because the attic is heated by the heat losses from the dwellings below – the uninsulated backside of the collector is further directly connected to the attic (see figures 1.31-30).

The utilized fraction of the pre-heating in the solar ventilation chimney is higher than for the facade – partly because of the higher power transfer to the air, partly due to the lower efficiency of the heat exchanger.

The tenants of 40 IIB was persuaded to run the system in normal mode during a period in April in order to allow for a study of the system in this mode. Figure 3.49-54 show the results from the first week in April 2001 – April 2 – 8. The rather low efficiency of the heat exchanger is again due to the unbalance of the system – i.e. a too large difference between the flow rate of exhaust and fresh air.

#### **3.1.4. Common ventilation system in 40 C**

Figures 3.55-56 show the air flow rates through the heat exchanger while figures 3.57-58 show the temperatures around the heat exchanger in 40 C. The location of the sensors is shown in figures 2.15-16.

Figure 3.55-56 show that the system has been run wrongly – i.e. that the flow rate of fresh air is only half of the flow rate of exhaust air. And further that the fresh air fan wrongly was switched off in the night during the first three nights of the shown period. The reason for the small air flow during the first three nights although the fan was switched off is assumed to be a small under pressure in the dwellings, which is able to suck in some fresh air through the heat exchanger. The uncertainty at such low flow rates is further rather high.

The above illustrates the problem experienced with the common ventilation systems. There have been many complaints from the tenants in no. 38. First of all due to a malfunction of one for the bypasses, which allowed ambient air in being blown directly into some of the dwellings during a cold period. Further it has been very difficult to balance the air flows in the systems. Although balanced in the ventilation system the dwellings experienced an overpressure, while an under pressure was expected, leading to an often strong smell in the staircase from the cooking in the apartments. The difficulties in balancing the systems are supposed to be due to the very low pressure drops on which the systems are operating. However, low pressure losses in the systems are wanted in order to reduce the power demand of the fans.

When comparing figure 3.55 with 3.37 for the days 29-31 it is seen that the system of 40 C has a strong influence on the flow rate of fresh air to the system in 40 IIB. When the fresh air fan is switched off in system 40 C, the air flow rate of fresh air in system 40 IIB increases and opposite when the fan is switched on. This is because the two systems share the same fresh air duct from the chimney. The fans in system 40C are more powerful than the fans in the systems in 40 B.

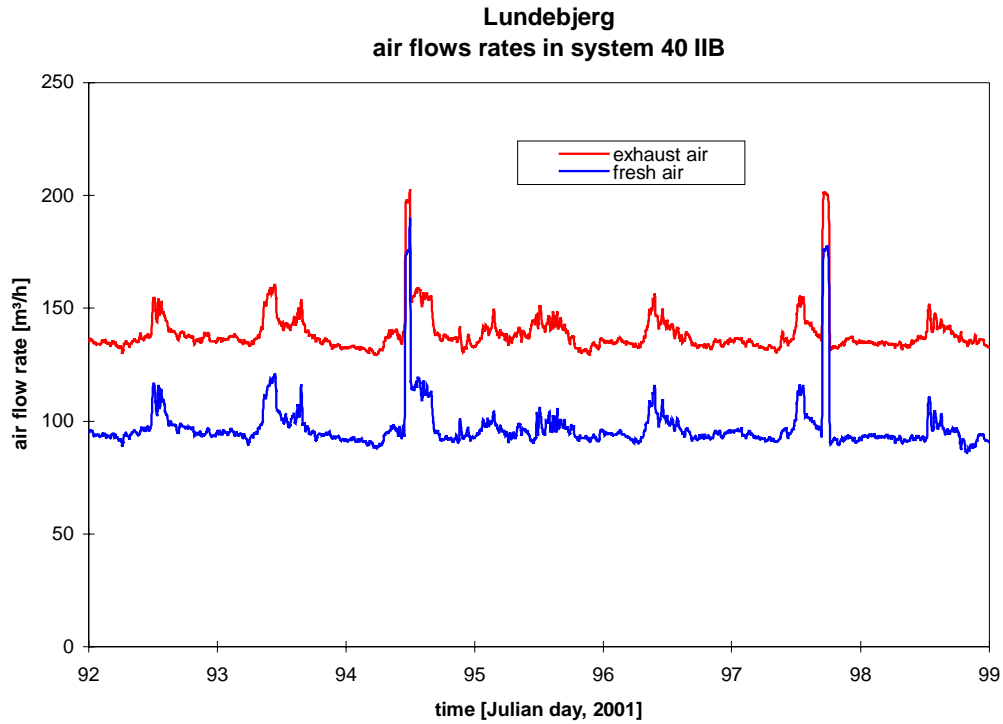


Figure 3.49. The air flow rates in the system of apartment 40 IIB during week 14, 2001 (April 2 - 8).

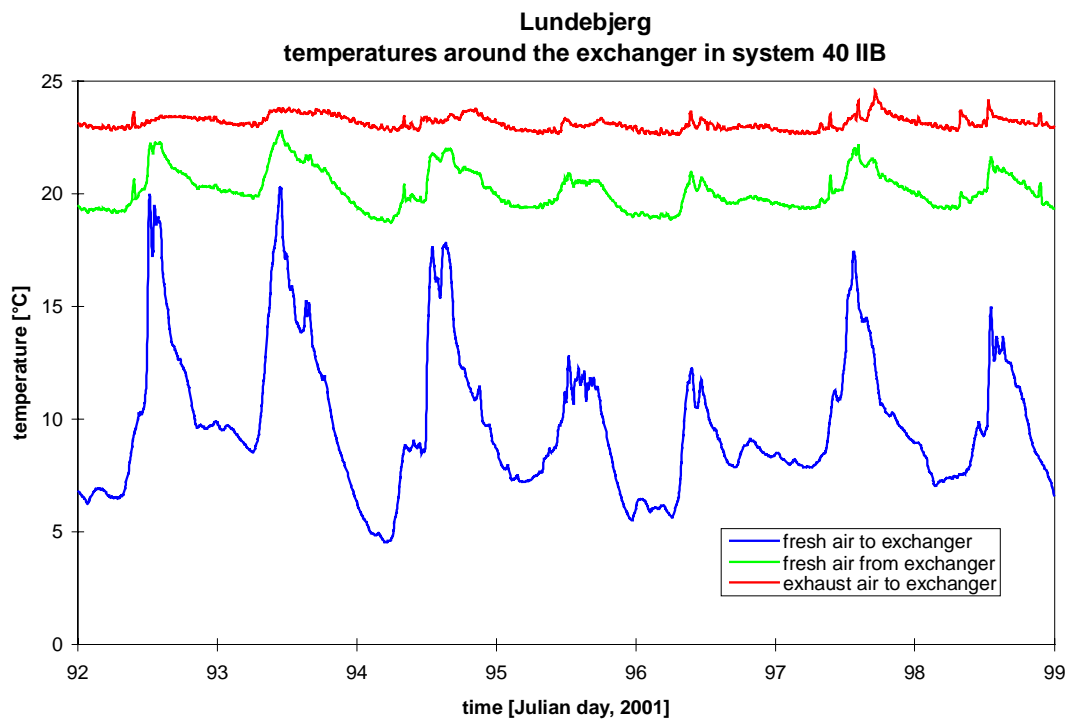


Figure 3.50. The air temperatures around the heat exchanger of apartment 40 IIB during week 14, 2001 (April 2 - 8).



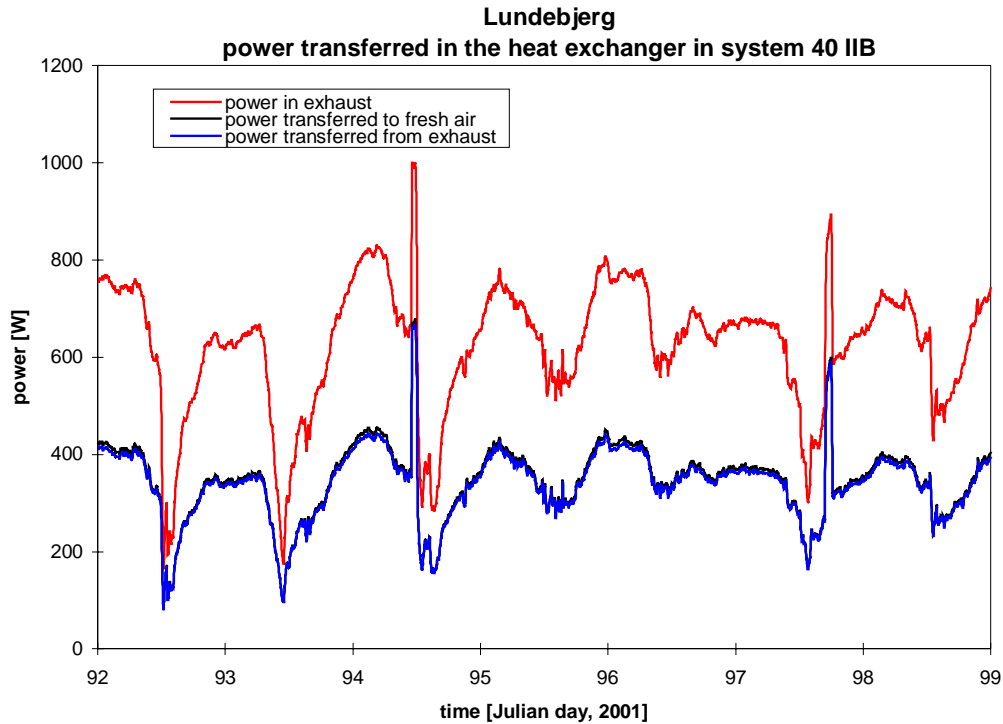


Figure 3.51. The heat flows in the heat exchanger of apartment 40 IIB during week 14, 2001 (April 2 - 8).

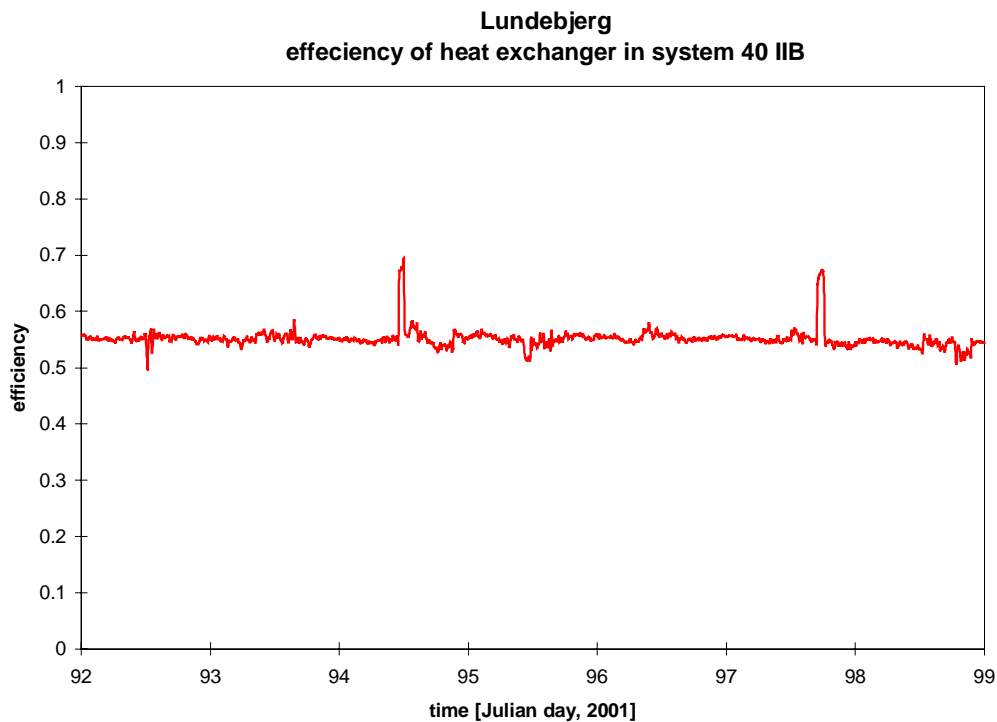


Figure 3.52. The efficiency of the heat exchanger of apartment 40 IIB during week 14, 2001 (April 2 - 8).

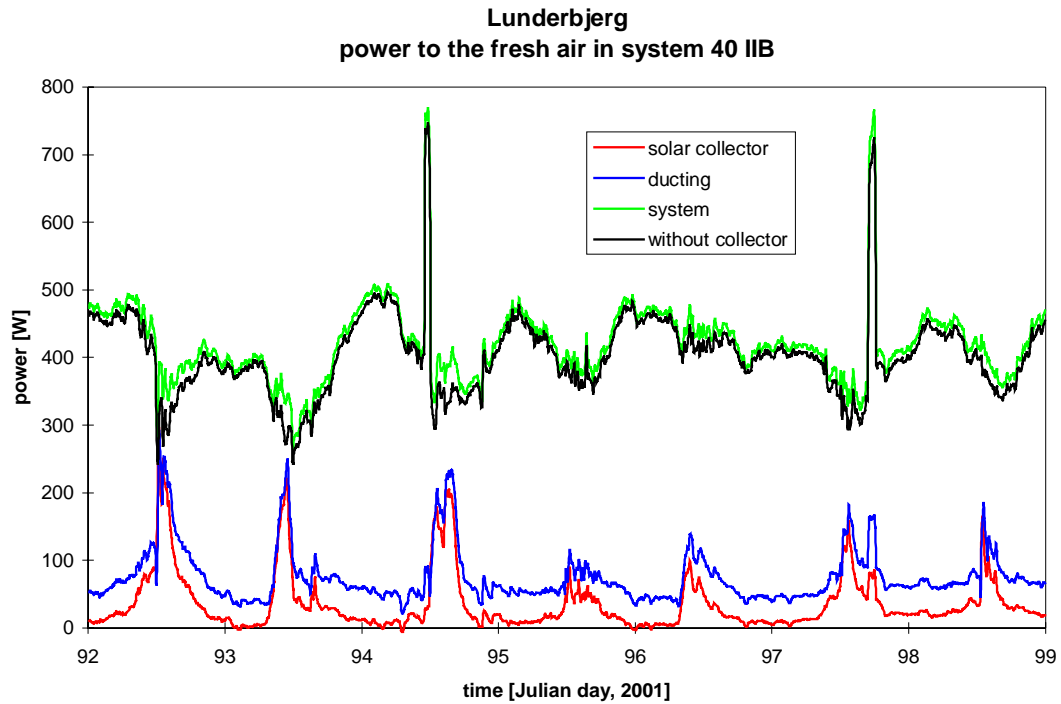


Figure 3.53. Power transferred to the fresh air in the collector, ducting and heat exchanger of apartment 40 IIB during week 14, 2001 (April 2 - 8).

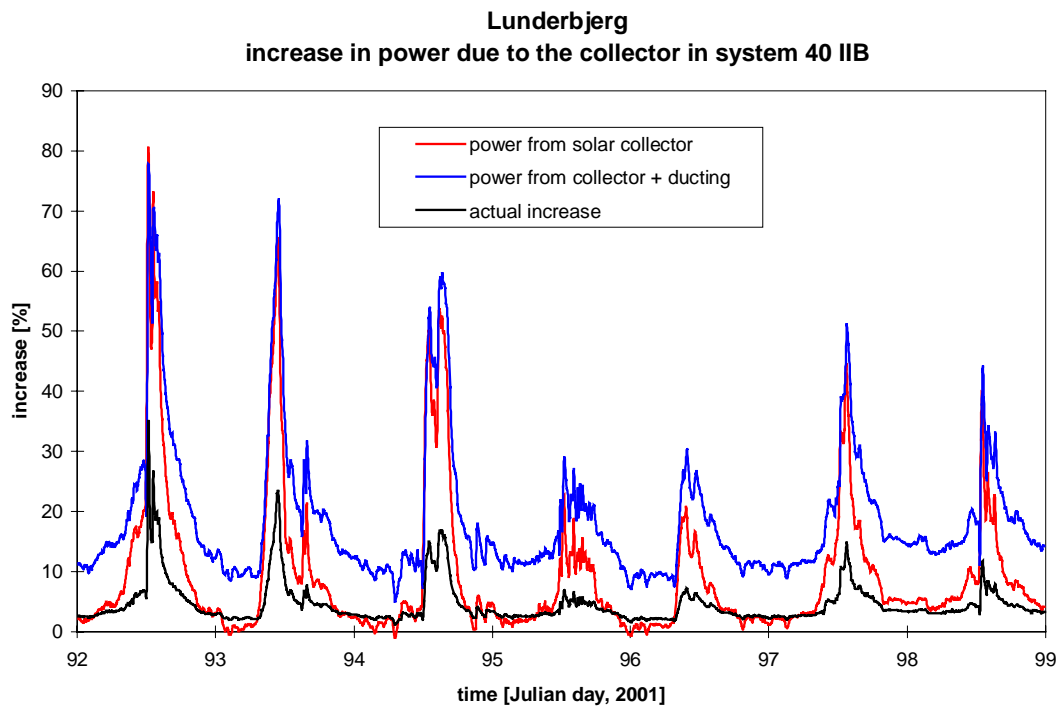


Figure 3.54. The possible and actual fraction the per-heating of the fresh air in the solar ventilation chimney and ducting is able to cover of the ventilation loss in apartment 40 IIB during week 14, 2001 (April 2 - 8).

Figures 3.57-58 show a strange pattern during the three first days. The two fresh air temperatures to and from the heat exchanger change levels between day and night. This is of course due to the switching off of the fresh air fan in the night during these three days. For the rest of the period the temperature profiles are very similar to the temperature profiles for the system in apartment 40 IIB – see figures 3.39-40. The conclusions are, therefore, the same as in section 3.1.3.

Figures 3.59-60 show the calculated heat flows in the heat exchanger. A lot of heat is of course wasted due to the unbalance of the air flow rates. However, the preheating of the fresh air in the solar ventilation chimney has as for apartment 40 IIB a major impact on the energy flows in the heat exchanger. The actual savings due to the preheating in the solar ventilation chimney are dealt with in section 3.2.

Figure 3.61-62 show the calculated efficiency of the heat exchanger, which due to the unbalance of the air flow rates is rather low and further negative during the first nights due to a lower fresh air temperature “from” the heat exchanger than “to” the heat exchanger. The efficiency of the heat exchanger will further be dealt with in section 3.2.

Figures 3.63-64 show as for apartment 40 IIA and B the power transfers to the fresh air in the solar ventilation chimney, the ducting and in the heat exchanger, while figures 3.65-66 show the fraction of the pre-heating in the solar ventilation chimney and ducting compared to the pre-heating over the total system. These fractions are compared with the actual benefit of the of the solar ventilation chimney compared to a system with no pre-heating before the heat exchanger. Please be aware for different y-axis.

The conclusions on figures 3.63-66 is similar to those drawn on the system in 40 IIB – i.e. a higher utilization of the solar energy than in 40 IIA. It is, however, difficult/impossible to separate the effect of the preheating in the solar ventilation chimney and in the ductwork. This will further be investigated in section 3.3.

The power to and from the PV-mixer of this system have been measured but will be investigated together with the measurements on the other solar ventilation chimneys in the following section.

Both on February 27 and March 5 an attempt was made in tuning the common ventilation systems. The results from the adjustment of system 40 C is shown in figures 3.67-74. Figures 3.67-68 show the air flow rates where the flow rate of fresh air was reduced to half the flow rate on February 27 (day 58) and later increased by approx. 50 % on March 5 (day 64). The flow rate of exhaust air was left unchanged until March 5 where it was reduced to 200 m<sup>3</sup>/h during night-time and with drops as far down as 100 m<sup>3</sup>/h during day-time ending up with a more stable air flow rate by the end of the period of below the air flow rate of fresh air. As the ventilation system serves three dwellings the air flow rates should be: exhaust  $126 \cdot 3 = 378$  m<sup>3</sup>/h and exhaust  $378 \cdot 0.9 = 340$  m<sup>3</sup>/h.

The above clearly indicates the problem in balancing the common ventilation systems.

Figures 3.69-70 show the air temperatures around the heat exchanger. From the figures it seems that the fresh air fan has been switched of during the period February 27 – March 5 as the fresh air temperature from the heat exchanger drops below the fresh air temperature to the

heat exchanger in the same way as seen in figure 3.57 where the fresh air fan was switched of during the night.

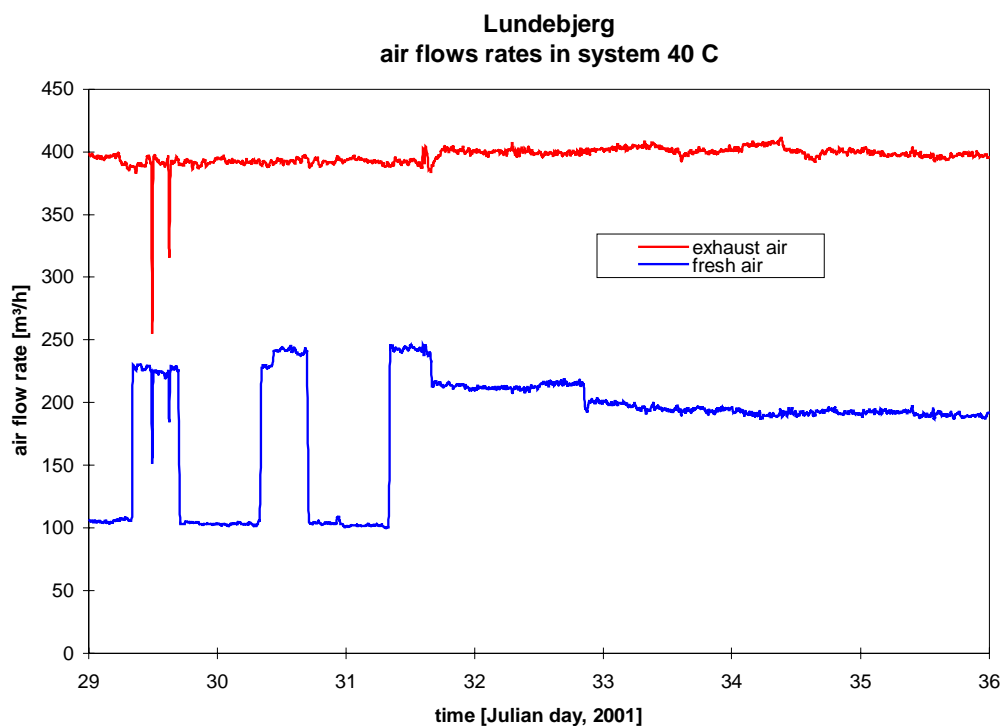


Figure 3.55. The air flow rates in the heat exchanger of the common system in 40 C during week 5, 2001 (January 29 – February 4).

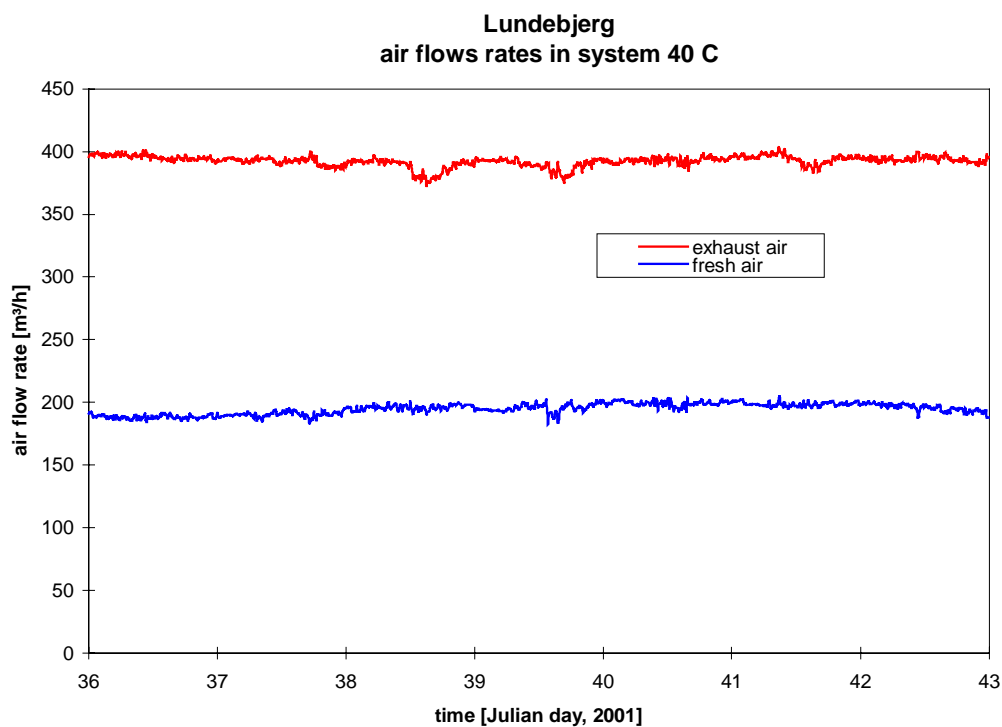


Figure 3.56. The air flow rates in the heat exchanger of the common system in 40 C during week 6, 2001 (February 5 – February 11).

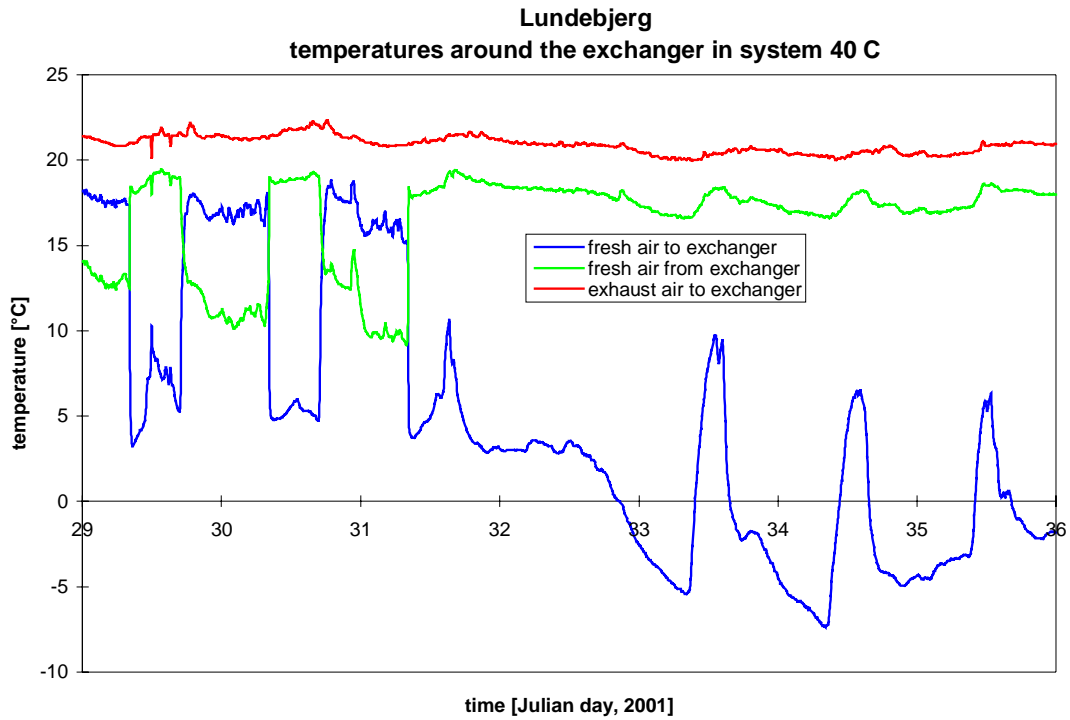


Figure 3.57. The air temperatures around the heat exchanger of the common system in 40 C during week 5, 2001 (January 29 – February 4).

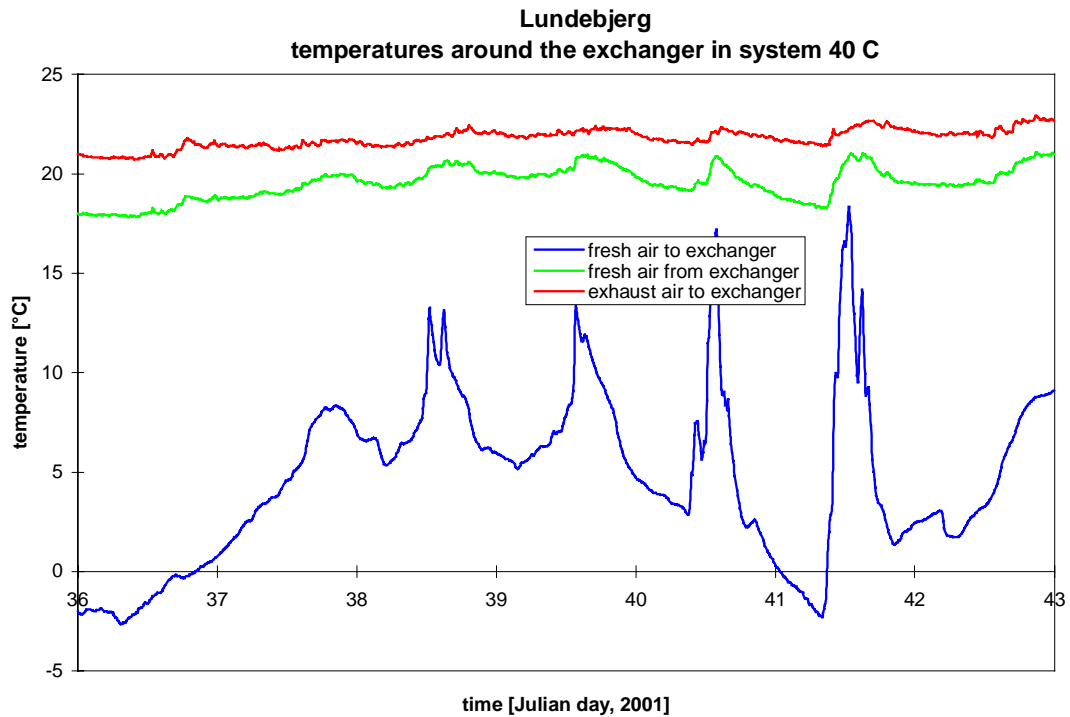


Figure 3.58. The air temperatures around the heat exchanger of the common system in 40 C during week 6, 2001 (February 5 – February 11).

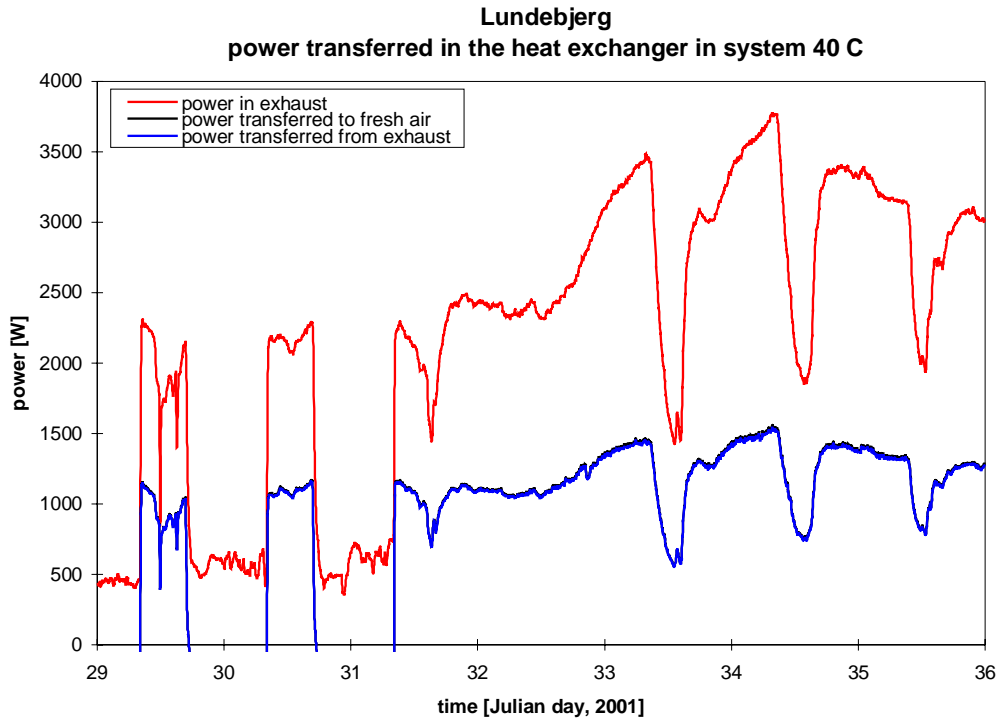


Figure 3.59. The heat flows in the heat exchanger of the common system in 40 C during week 5, 2001 (January 29 – February 4).

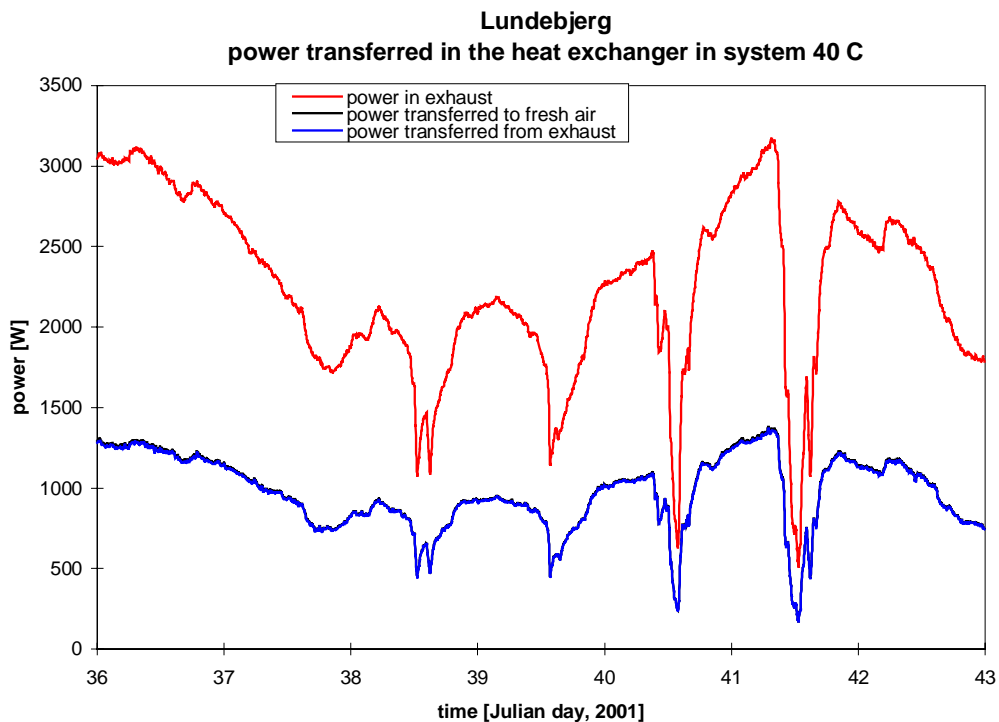


Figure 3.60. The heat flows in the heat exchanger of the common system in 40 C during week 6, 2001 (February 5 – February 11).

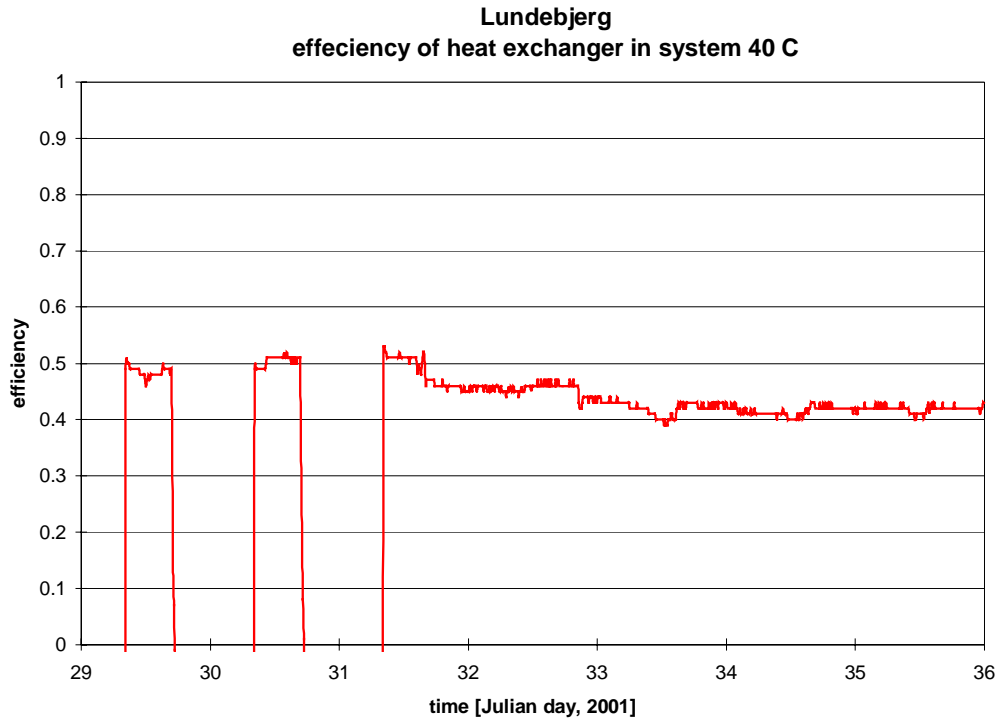


Figure 3.61. The efficiency of the heat exchanger of the common system in 40 C during week 5, 2001 (January 29 – February 4).

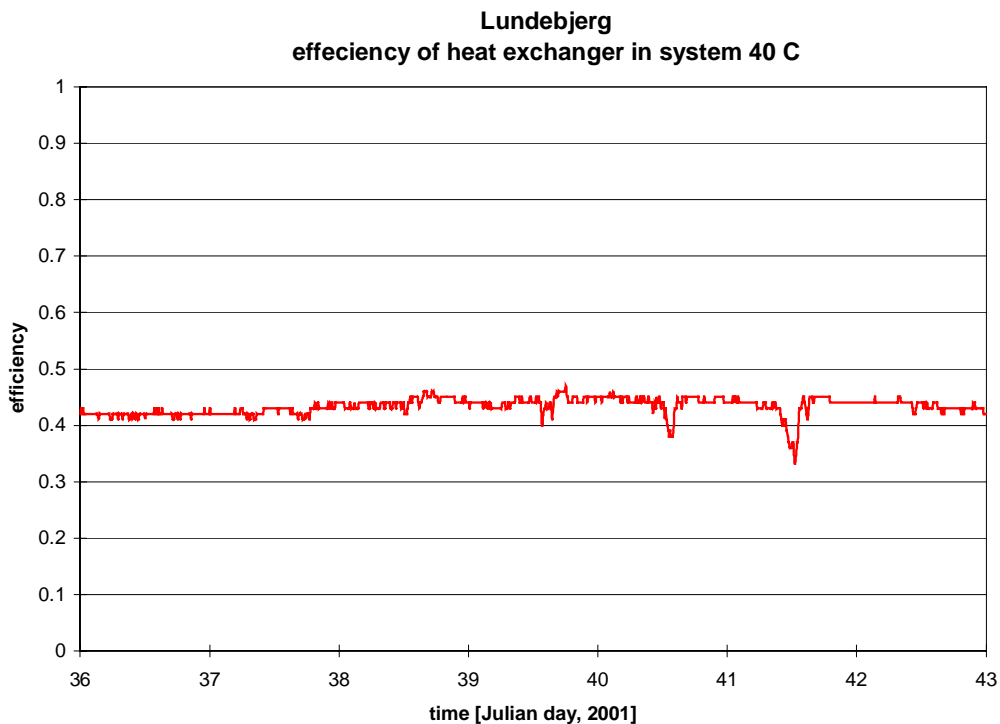


Figure 3.62. The efficiency of the heat exchanger of the common system in 40 C during week 6, 2001 (February 5 – February 11).



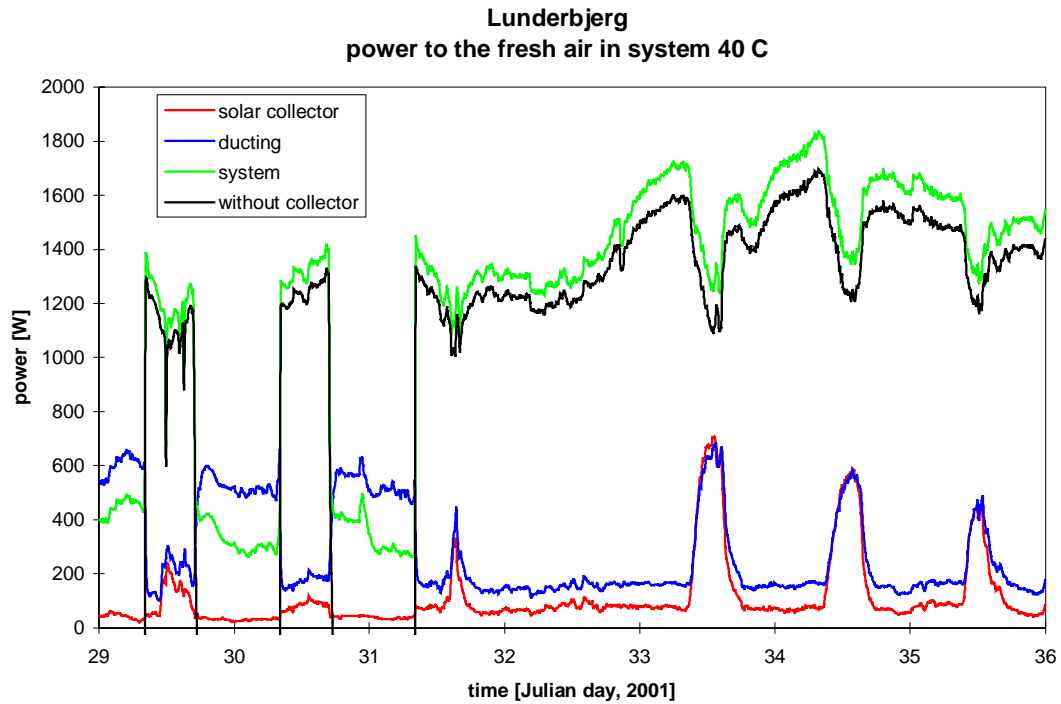


Figure 3.63. Power transferred to the fresh air in the collector, ducting and heat exchanger of apartment 40 C during week 5, 2001 (January 29 – February 4).

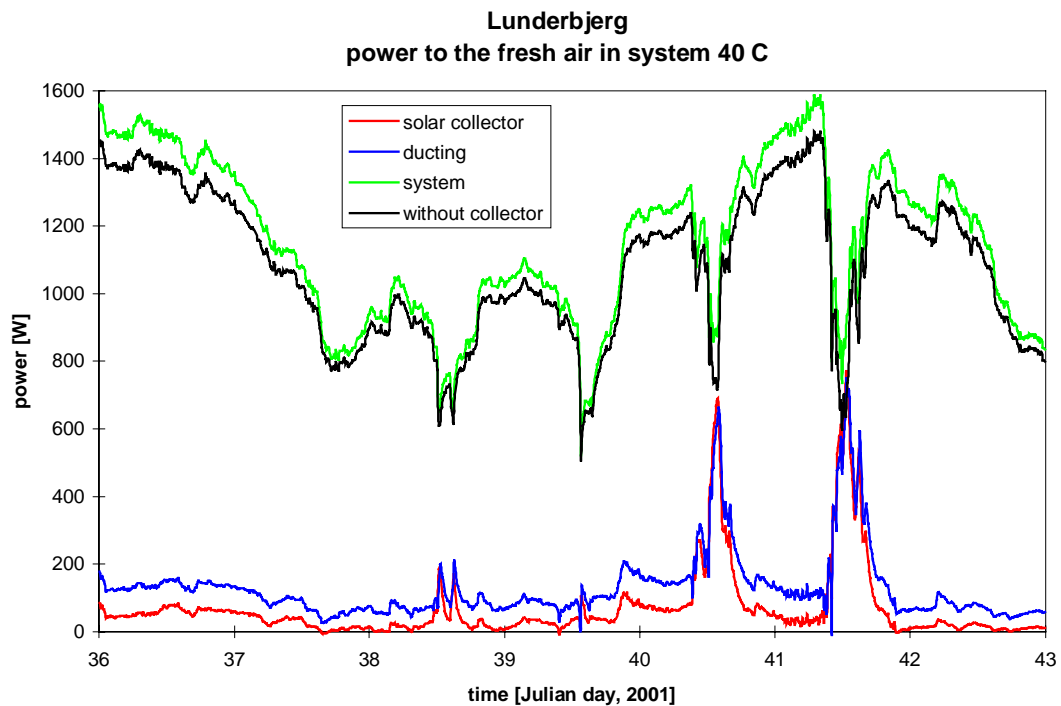


Figure 3.64. Power transferred to the fresh air in the collector, ducting and heat exchanger of apartment 40 C during week 6, 2001 (February 5 – February 11).

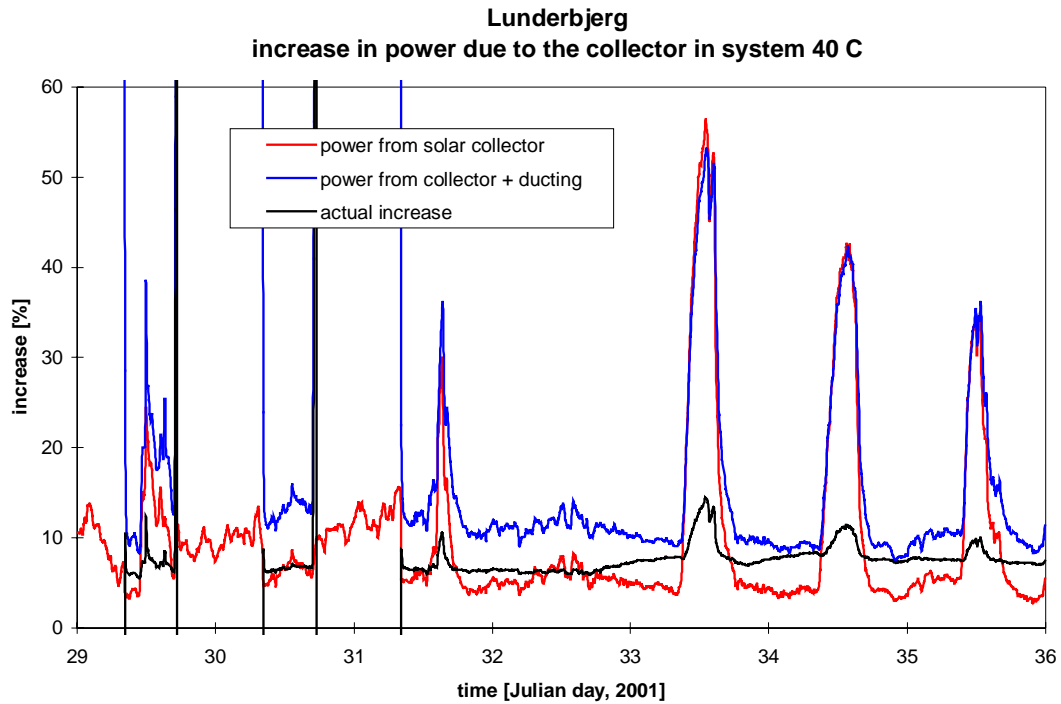


Figure 3.65. The possible and actual fraction the per-heating of the fresh air in the solar ventilation chimney and ducting is able to cover of the ventilation loss in apartment 40 C during week 5, 2001 (January 29 – February 4).

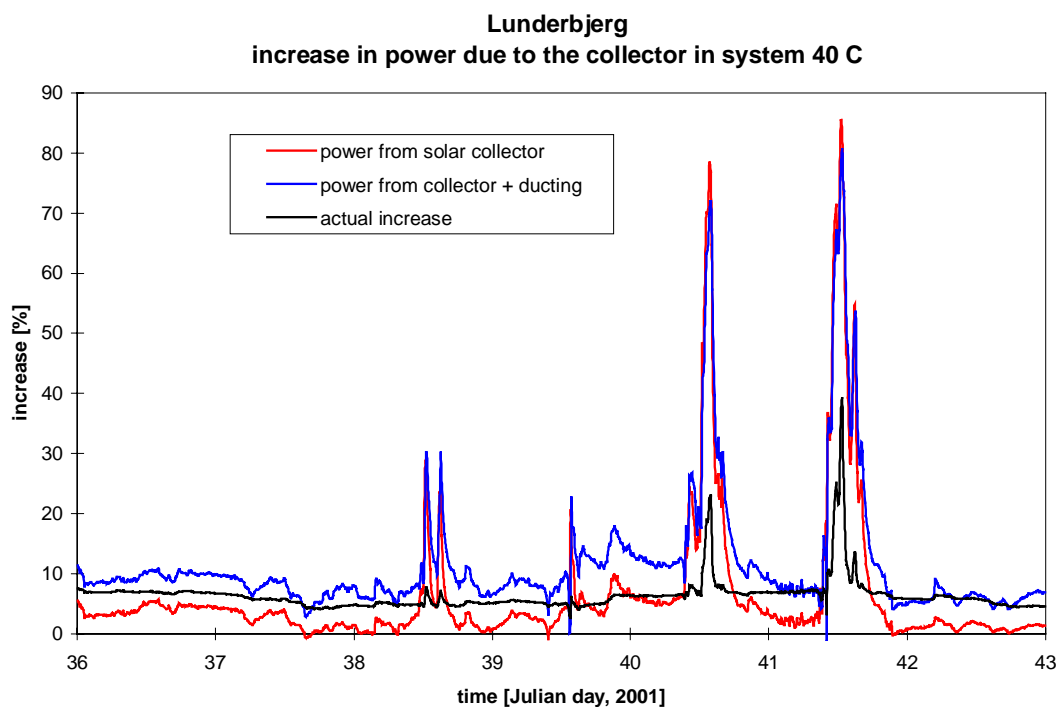


Figure 3.66. The possible and actual fraction the per-heating of the fresh air in the solar ventilation chimney and ducting is able to cover of the ventilation loss in apartment 40 C during week 6, 2001 (February 5 – February 11).

Figures 3.71-72 show the heat flows in the heat exchanger while figures 3.73-74 show the efficiency of the heat exchanger. The heat flow to the fresh air and the efficiency drops below zero between February 27 and March 5 is due to the measured higher fresh air temperature to the heat exchanger than from the heat exchanger. By the end of the period the efficiency of the heat exchanger is very high, which partly is due to the fact that the flow rate of fresh air is lower than the flow rate of exhaust air. The efficiency compensated for different air flow rates is investigated further in section 3.2.

### 3.1.5. The solar ventilation chimneys

The purpose of the solar ventilation chimneys of no. 38 and 40 is twofold: to preheat fresh air to the ventilation systems and to generate power for running the fans of the ventilation systems.

#### *Thermal performance of the solar ventilation chimneys*

Figure 3.75-78 show the temperatures in the solar ventilation chimney in no. 38 and 40, while figures 3.79-80 show the temperature at the backside of a PV-panel on all chimneys. Figures 3.81-82 show the temperature increase of the air due to the heating in the solar ventilation chimney in no. 38 and 40. Figures 3.83-84 show the air flow rate of fresh air through the solar ventilation chimney above no. 38 and 40. The locations of the sensors for the above measurements are shown in figures 2.17-21. Please be aware of the different y-axis applied.

Figures 3.75-78 show when comparing with figures 3.1-2 that the inlet temperature to the solar ventilation chimneys during solar radiation may be several degree above the ambient temperature at the north side of the building. For the chimney above no. 38: up to 8-16 K and for the chimney above no. 40: up to 10 K. The reason for this difference in "ambient" temperature is that the ambient air in front of the solar ventilation chimneys is heated due to the absorption of the solar radiation by the black roofing felt on the roof.

Although different air flow rates in the chimneys above no. 38 and 40 (see figures 3.83-84) figures 3.79-80 show very little difference between the PV-panel temperature of the two chimneys. There is on the other hand a noticeable difference between the PV-panel temperature of the chimney above no. 36 and the other two chimneys. The PV-panel temperatures will be investigated further in section 3.2.

When comparing figures 3.81-82 with 3.83-84 it is as expected seen that the temperature increase of the air across the chimneys is very flow rate dependent. High temperature increases at low air flow rates and low temperature increases at high air flow rates. By means of the measurements in figures 3.81-84 and the useful solar radiation (calculated as described in section 3.1.1) it is possible to calculate the efficiency of the solar ventilation chimneys when acting as solar air collectors in the following way:

$$\eta = Q_c / (E_{\text{useful}} \cdot A_c) \quad (3.4)$$

where  $Q_c$  is the energy transferred to the air when passing through the solar ventilation chimney [W]

$E_{\text{useful}}$  is the useful solar radiation on the chimney calculated as described in section 3.1.1 [W/m<sup>2</sup>]

$A_c$  is the area of the PV-array [m<sup>2</sup>]

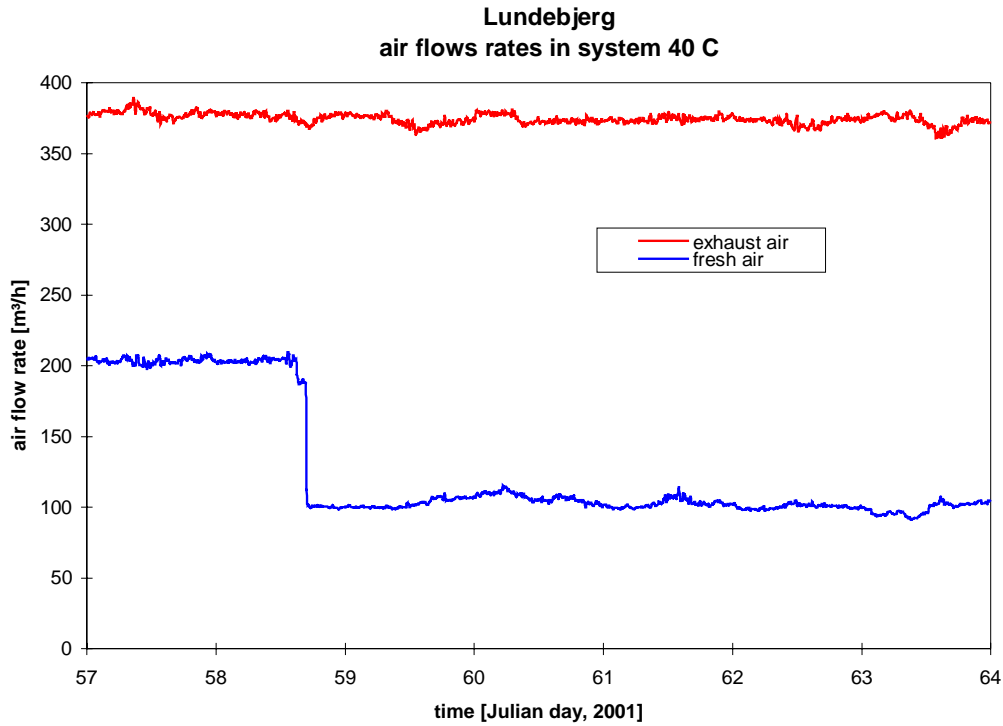


Figure 3.67. The air flow rates in the heat exchanger of the common system in 40 C during week 9, 2001 (February 26 – March 4).

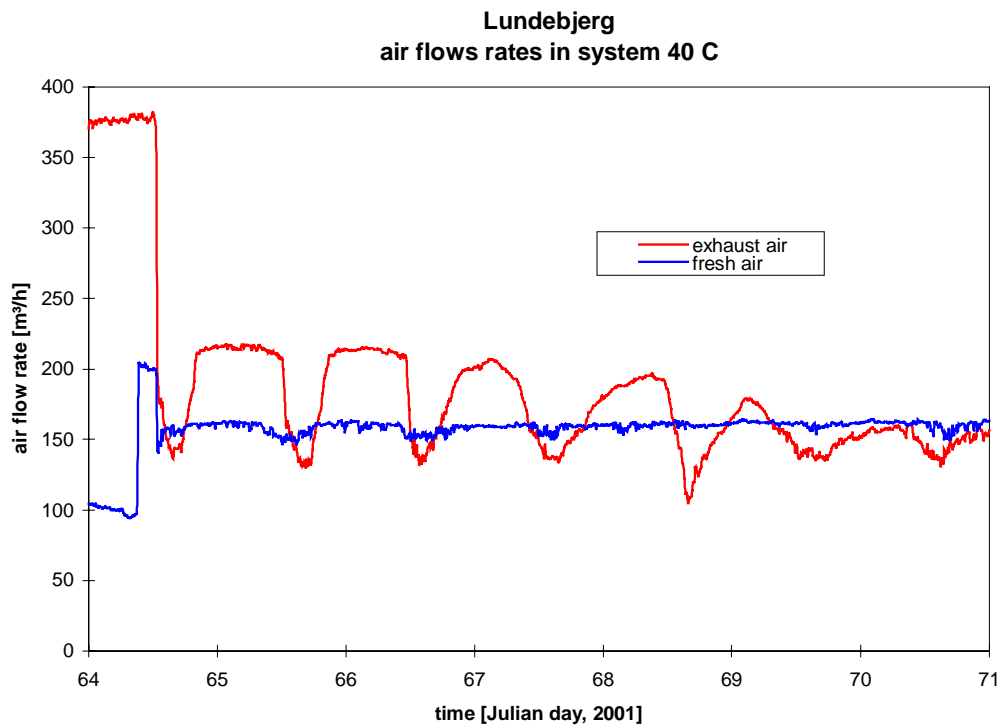


Figure 3.68. The air flow rates in the heat exchanger of the common system in 40 C during week 10, 2001 (March 5 – March 11).

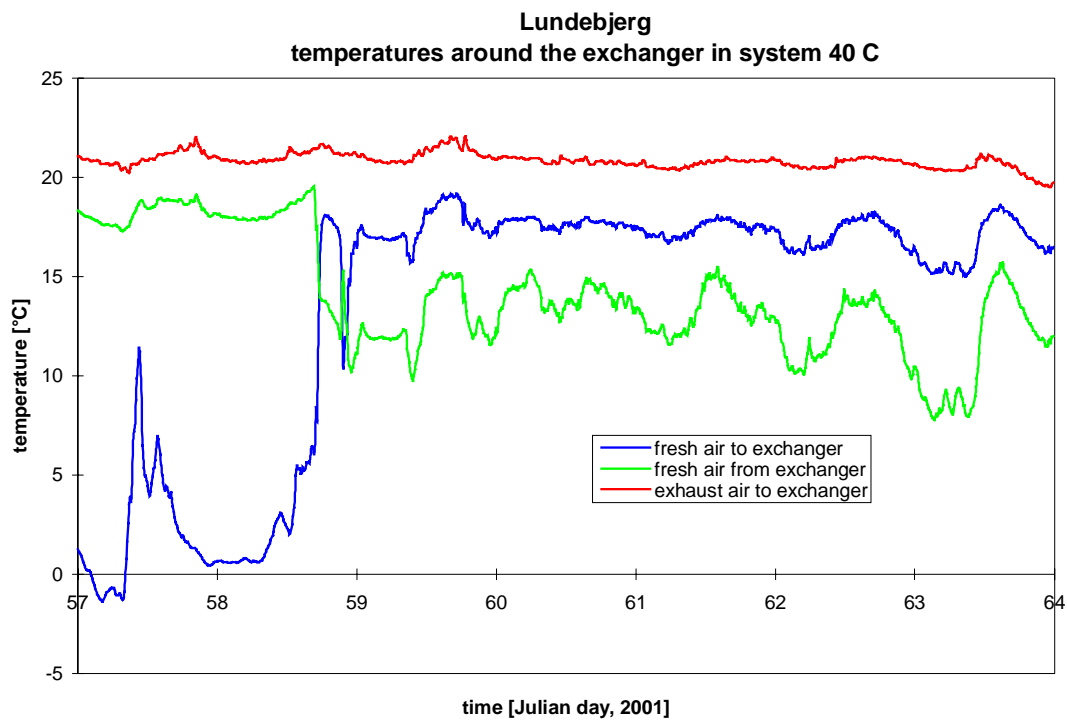


Figure 3.69. The air temperatures around the heat exchanger of the common system in 40 C during week 9, 2001 (February 26 – March 4).

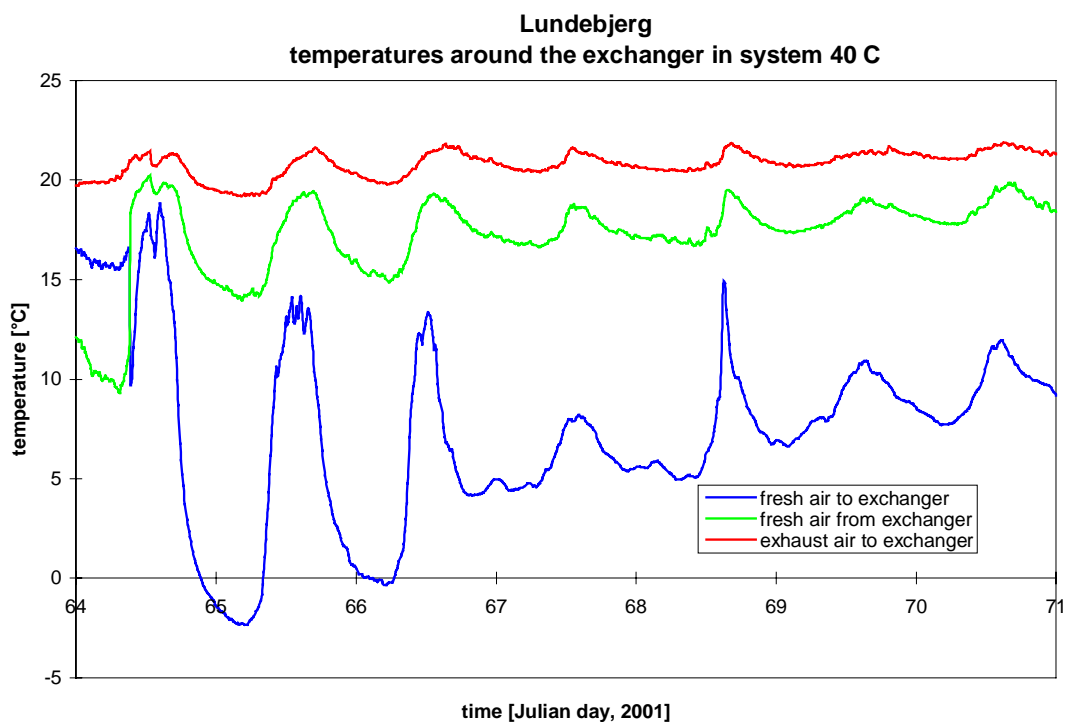


Figure 3.70. The air temperatures around the heat exchanger of the common system in 40 C during week 10, 2001 (March 5 – February 11).

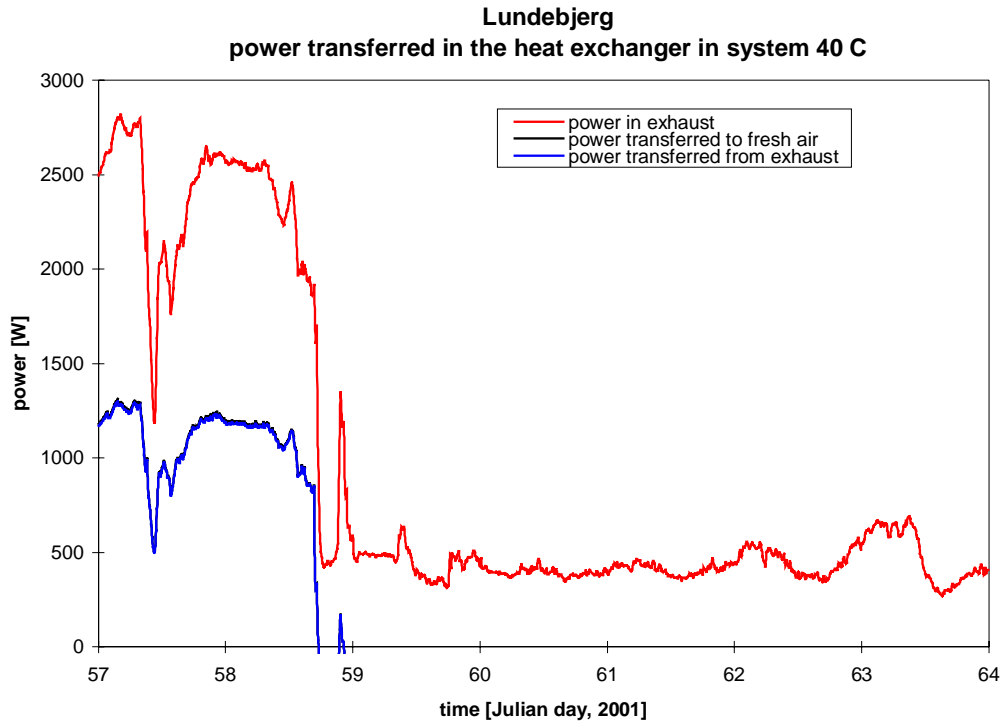


Figure 3.71. The heat flows in the heat exchanger of the common system in 40 C during week 9, 2001 (February 26 – March 4).

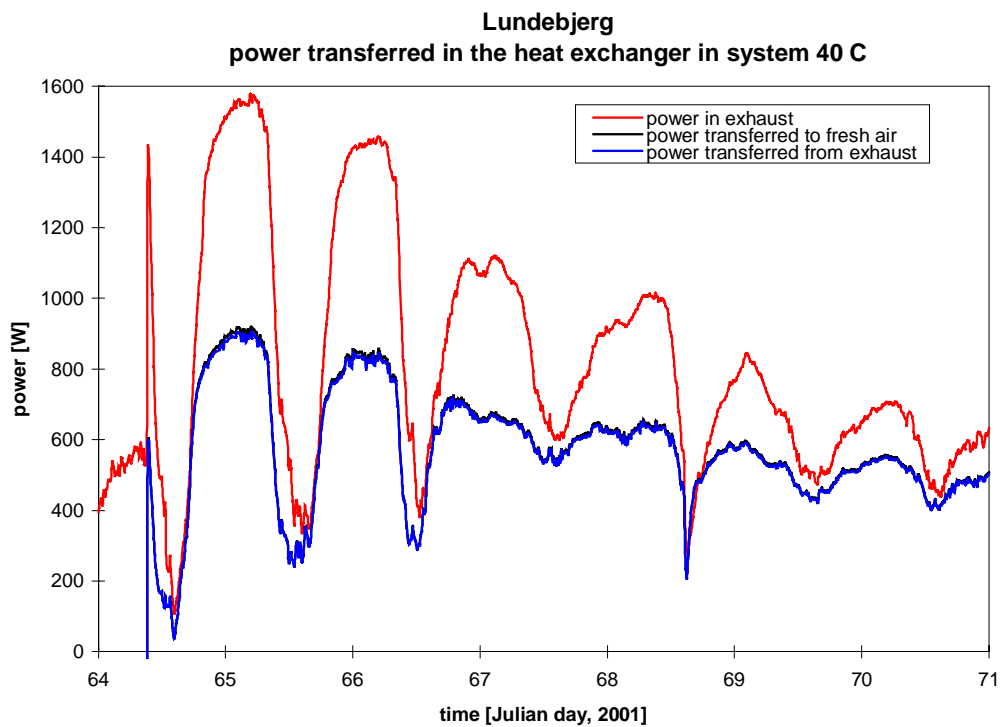


Figure 3.72. The heat flows in the heat exchanger of the common system in 40 C during week 10, 2001 (March 5 – March 11).

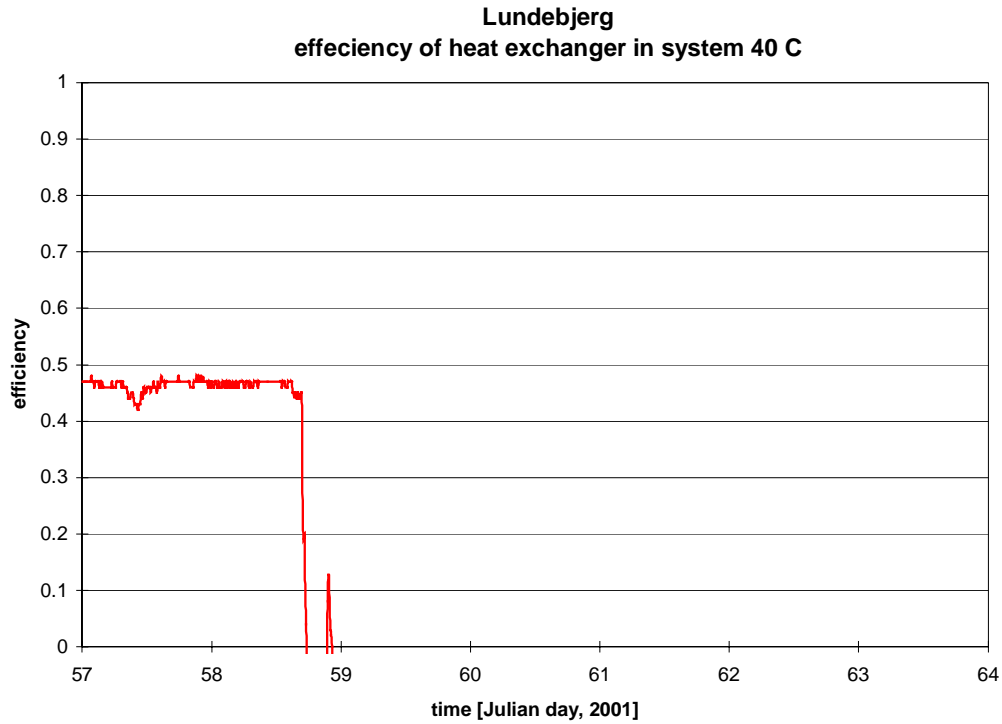


Figure 3.73. The efficiency of the heat exchanger of the common system in 40 C during week 9, 2001 (February 26 – March 4).

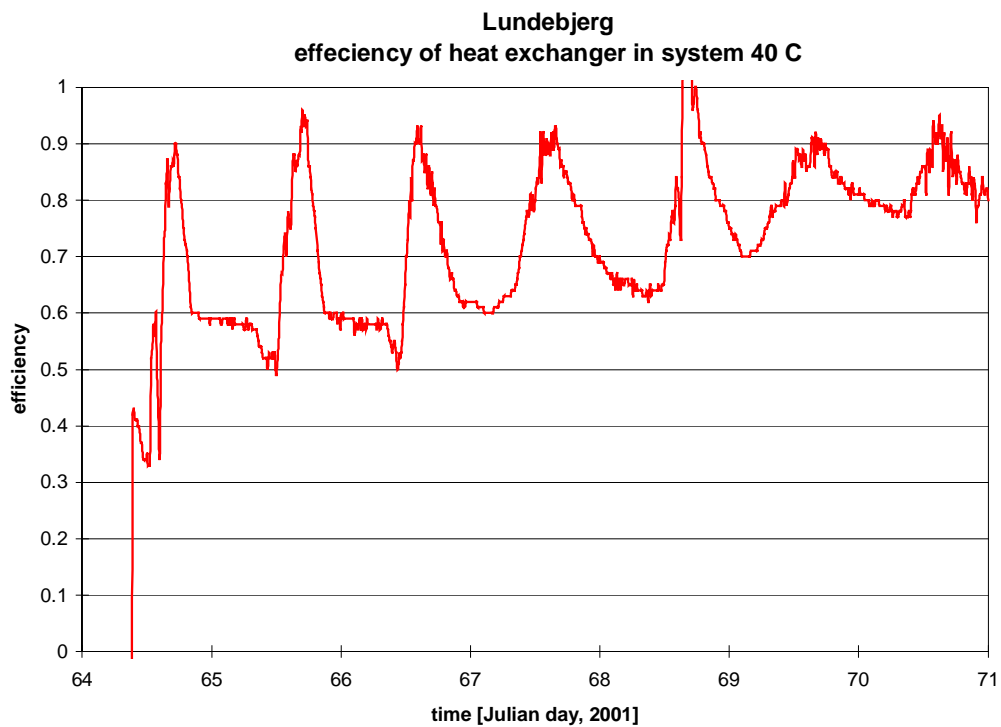


Figure 3.74. The efficiency of the heat exchanger of the common system in 40 C during week 10, 2001 (March 5 – March 11).



Figures 3.85-86 show that the calculated efficiencies are very scattered due to scattered solar radiation, scattered air flow rates and the thermal mass of the chimneys. The efficiencies for day 33-35 which are most reliable due to less scattering seems rather low, however, it has to be remembered, that the solar ventilation chimneys actually are solar air collectors without a cover, as the solar radiation is absorbed by the PV-panel. The efficiency of the solar ventilation chimneys are further investigated in section 3.2, where an equation for the efficiency dependency on the air flow rate is derived.

Figures 3.83-84 show that the air flow rates has been very fluctuating – especially for the chimney above no. 38. This is as already mentioned in section 3.1.4 due to the problems in balancing the common ventilation systems in staircase no. 38. The very high air flow rate on day 37-40 for no. 38 was caused by the tube connected to the pressure transducer controlling the fresh air fan had fallen off. In order to maintain the pre-set pressure difference the pressure transducer ran the fresh air fan at full speed. This illustrates how vulnerable the system is.

### ***PV performance of the solar ventilation chimneys***

One PV-mixer connected to each of the three solar ventilation chimneys has been monitored. The three ventilation systems thus monitored were all common ventilation systems: 36 B, 38 B and 40 C. The three PV-arrays monitored was the middle array on no. 38 and 39 (see figure 1.32) and the top array on no. 40 (see figure 1.33).

Figures 3.87-92 show the power to and from the PV-mixer, figures 3.93-98 show the utilized PV-power and the potential power from the PV-panels (the loss in the wiring is not considered as it is in the order of 2-3% and thus far less than the uncertainty of the measurements), while figures 3.99-104 show the utilization of the potential PV-power. The figures have been generated in the same manner as the figures for apartment 40 IIA in section 3.1.2. The conclusions are further similar to the conclusions from section 3.1.2.

From figures 3.87-92 it is seen that when solar power is available an immediate drop occurs in the power consumption from the grid. When the PV-panels can supply all the power to the fan no power is taken from the grid – i.e. the power demand of the PV-mixer itself is in these situations taken from the PV-panel. The difference between fan and grid power at no solar power gives the efficiency of the PV-mixer in grid mode, which according to table 1.3 should be 96 %. In pure PV mode the necessary PV power is higher than the fan power – the difference gives the efficiency of the PV-mixer in pure PV mode. From figures 3.87-92 it is seen that the efficiency in pure PV mode is lower than in pure grid mode. This is dealt with in table 1.4 and further in section 3.2.

Figures 3.93-98 show the utilized PV power and the potential power from the PV-panels (the loss in the wiring is not considered as it is in the order of 2-3% and thus far less than the uncertainty of the measurements). The potential power is calculated as for the PV-gable – see section 3.1.1, equation 3.1. Figures 3.93-98 show that the utilization of the potential PV power is very dependent on the actual demand as seen when comparing figures 3.93-98 with figures 3.87-92.

How large a fraction actually utilized of the potential power from the PV-panels is shown in figures 3.99-104. The very high utilized fraction appearing in figures 3.99-104 is caused by the rather high uncertainty of both the measurements and of the model at low solar radiation levels and should, therefore, not be considered. At high levels of potential power from the

PV-panels the utilized PV-power goes down to: 36: 20%, 38: 3-4% and 40: 25%. The reason for the low utilization is the very low power demand by the fans. The utilized fraction increases at lower potential power from the PV-panels because the fan power remains the same.

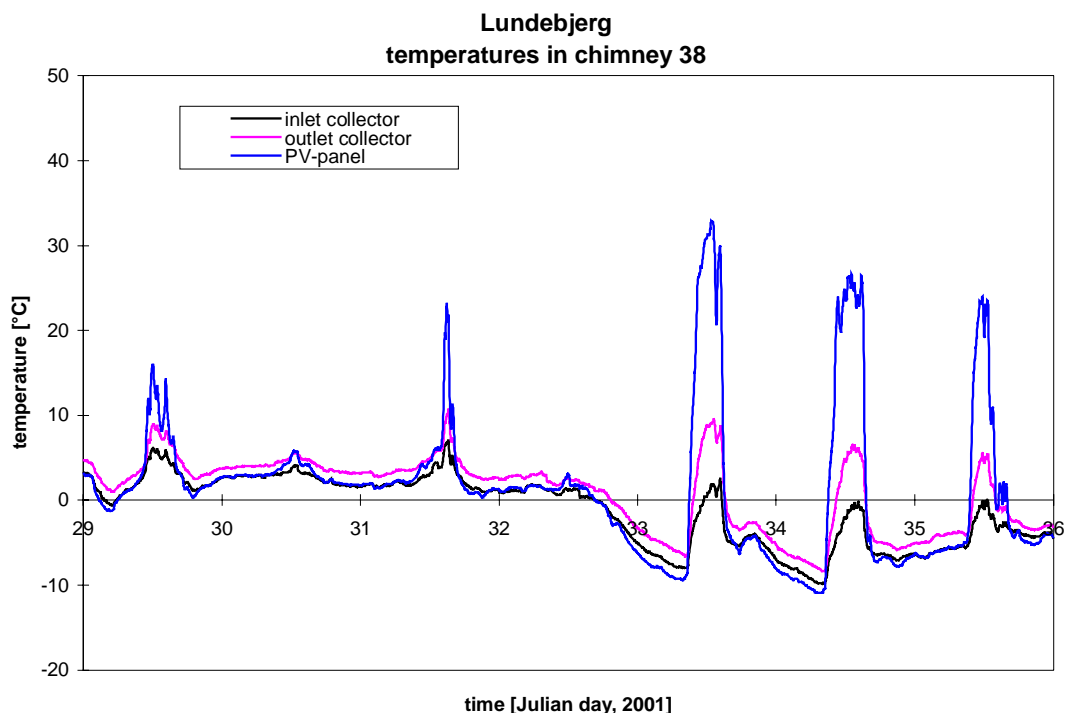


Figure 3.75. The temperatures in the solar ventilation chimney above no. 38 during week 5, 2001 (January 29 – February 4).

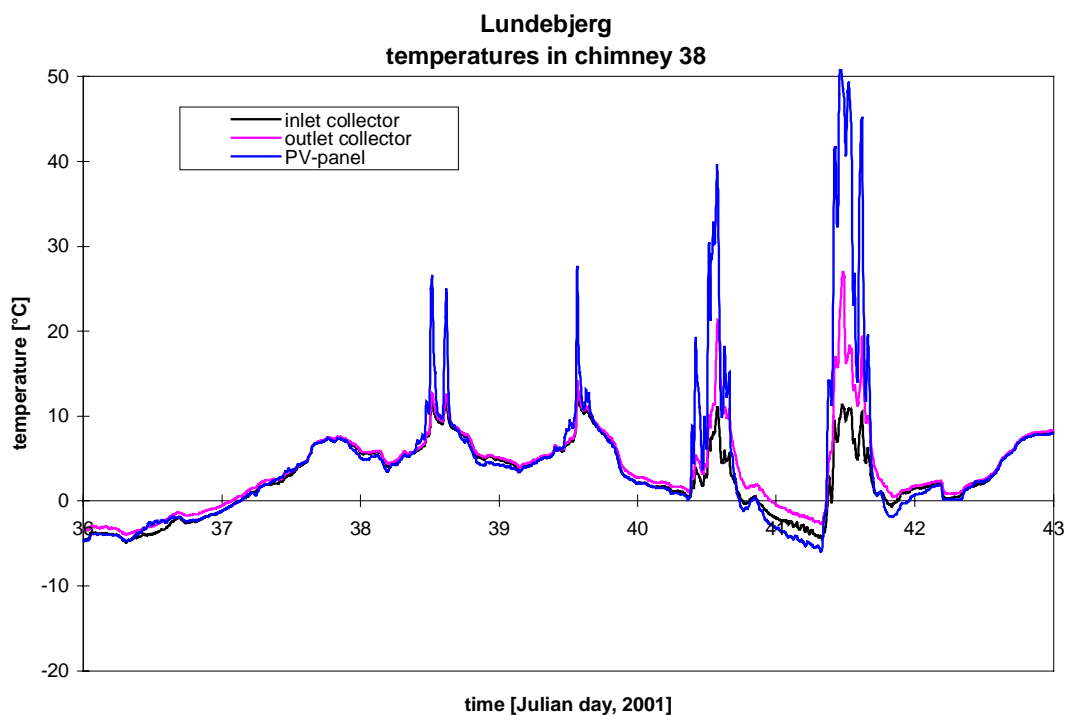


Figure 3.76. The temperatures in the solar ventilation chimney above no. 38 during week 6, 2001 (February 5 – February 11).

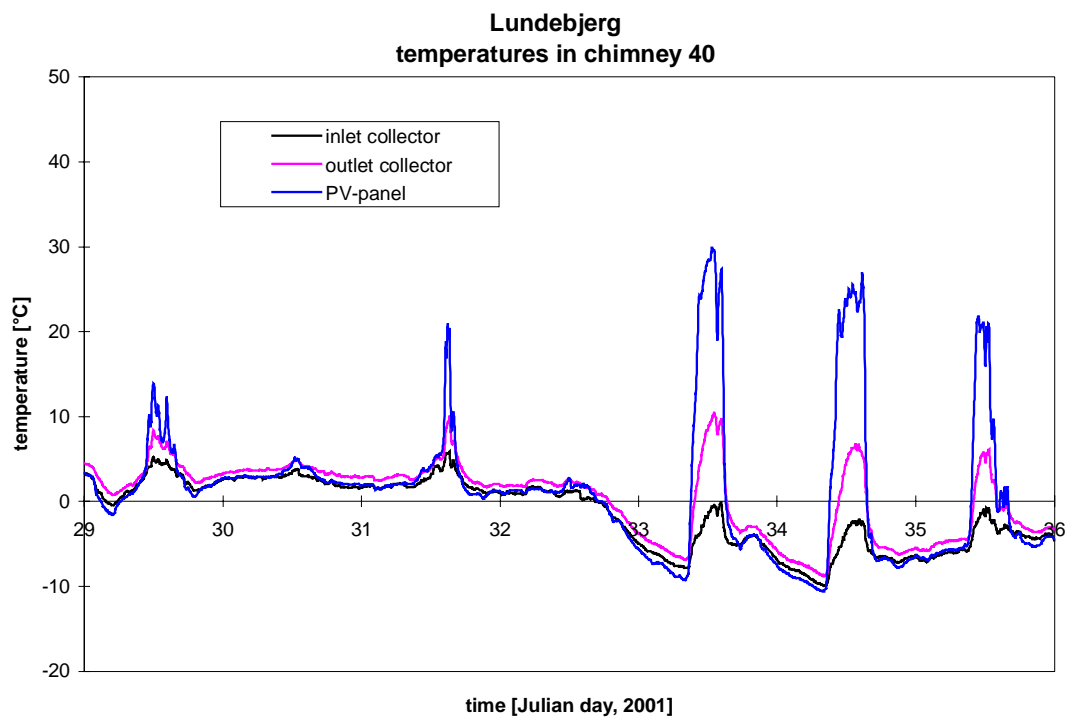


Figure 3.77. The temperatures in the solar ventilation chimney above no. 40 during week 5, 2001 (January 29 – February 4).

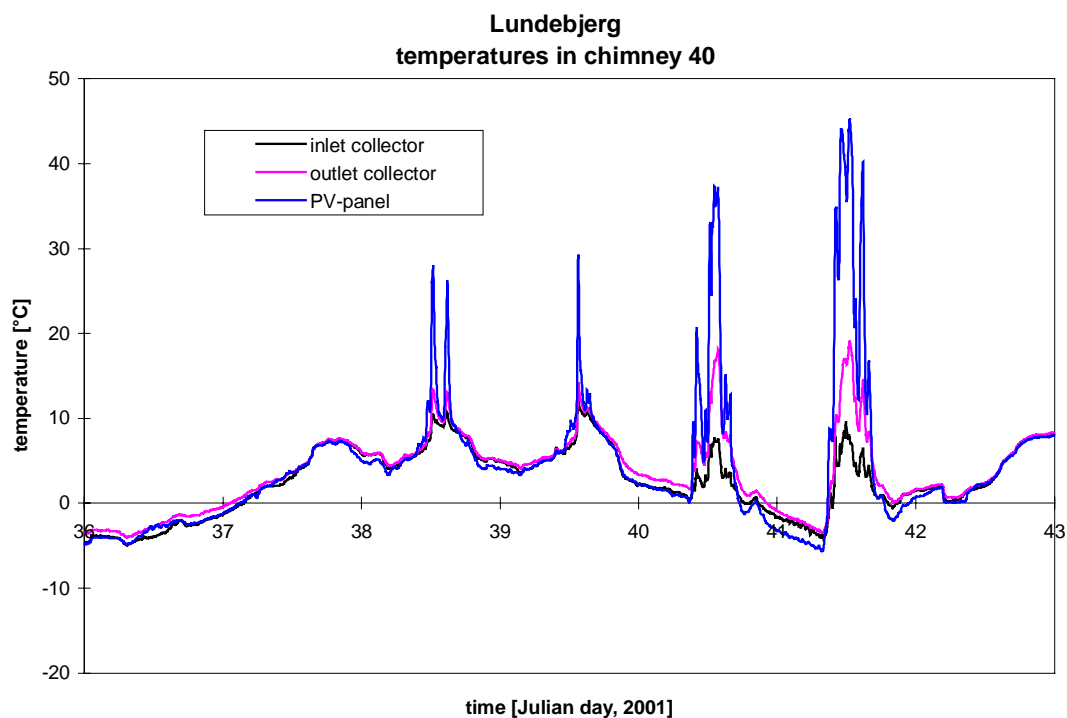


Figure 3.78. The temperatures in the solar ventilation chimney above no. 40 during week 6, 2001 (February 5 – February 11).

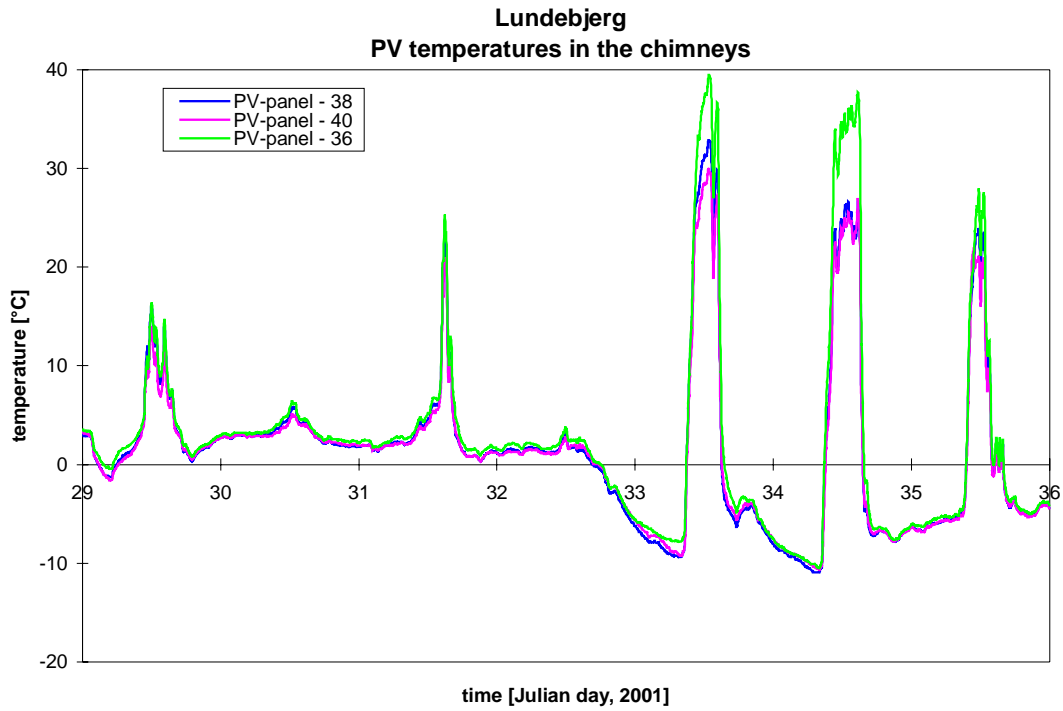


Figure 3.79. The temperatures on the backside of a PV-panel on all three chimneys during week 5, 2001 (January 29 – February 4).

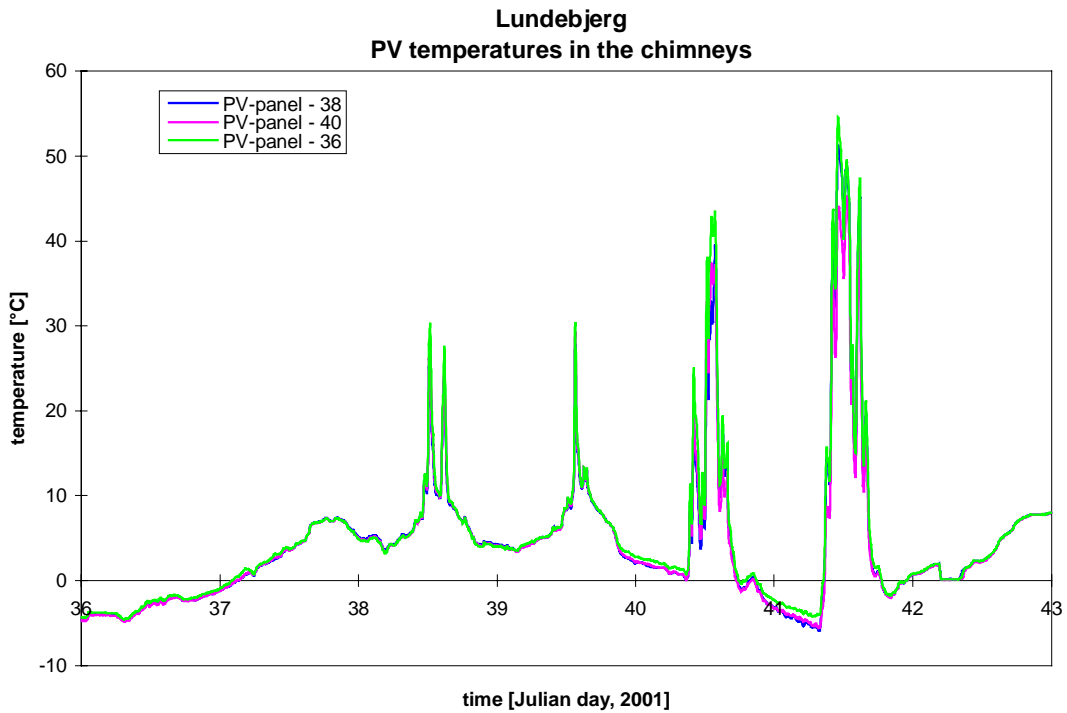


Figure 3.80. The temperatures on the backside of a PV-panel on all three chimneys during week 6, 2001 (February 5 – February 11).

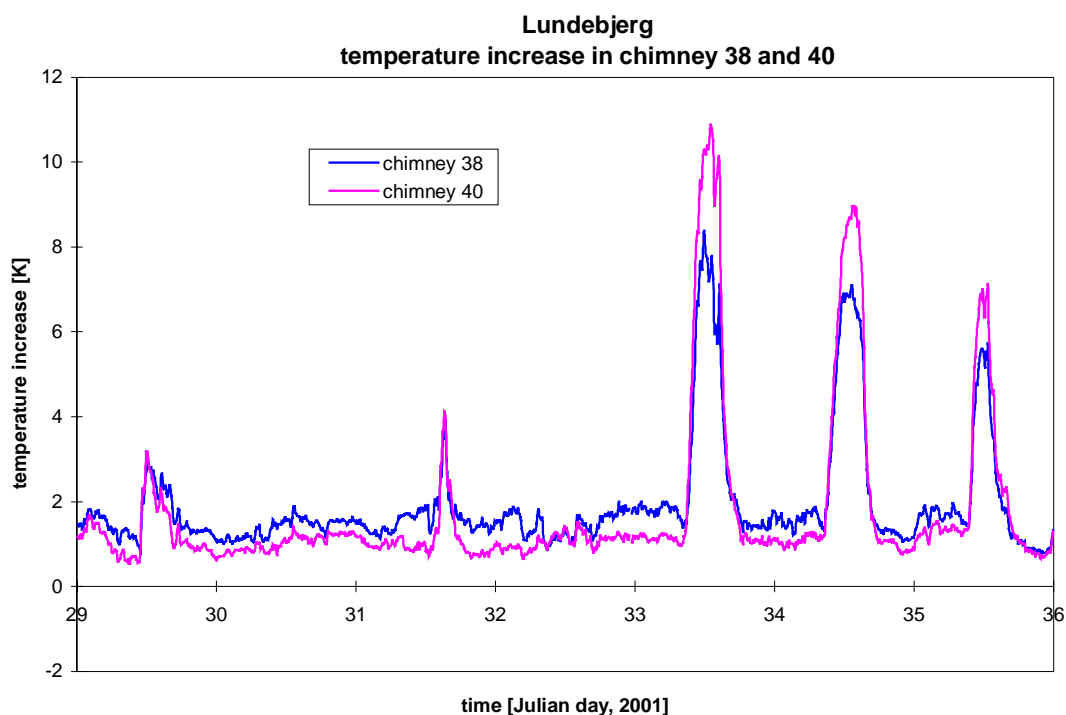


Figure 3.81. The temperature increase of the fresh air due to the heating in the chimneys above no. 38 and 40 during week 5, 2001 (January 29 – February 4).

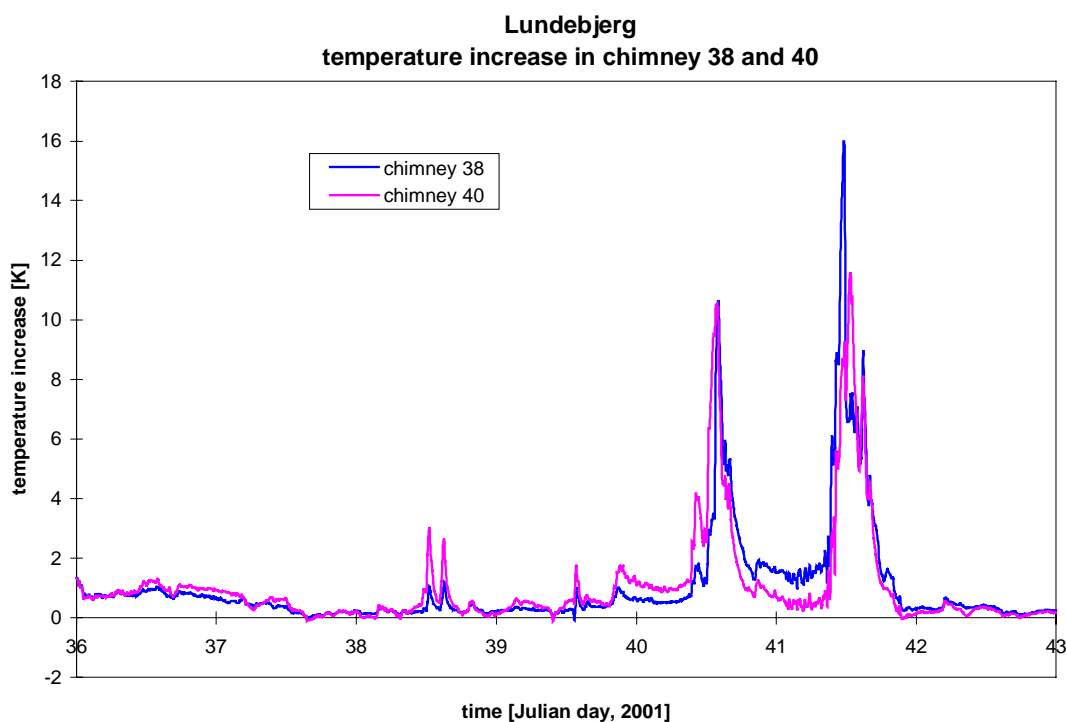


Figure 3.82. The temperature increase of the fresh air due to the heating in the chimneys above no. 38 and 40 during week 6, 2001 (February 5 – February 11).

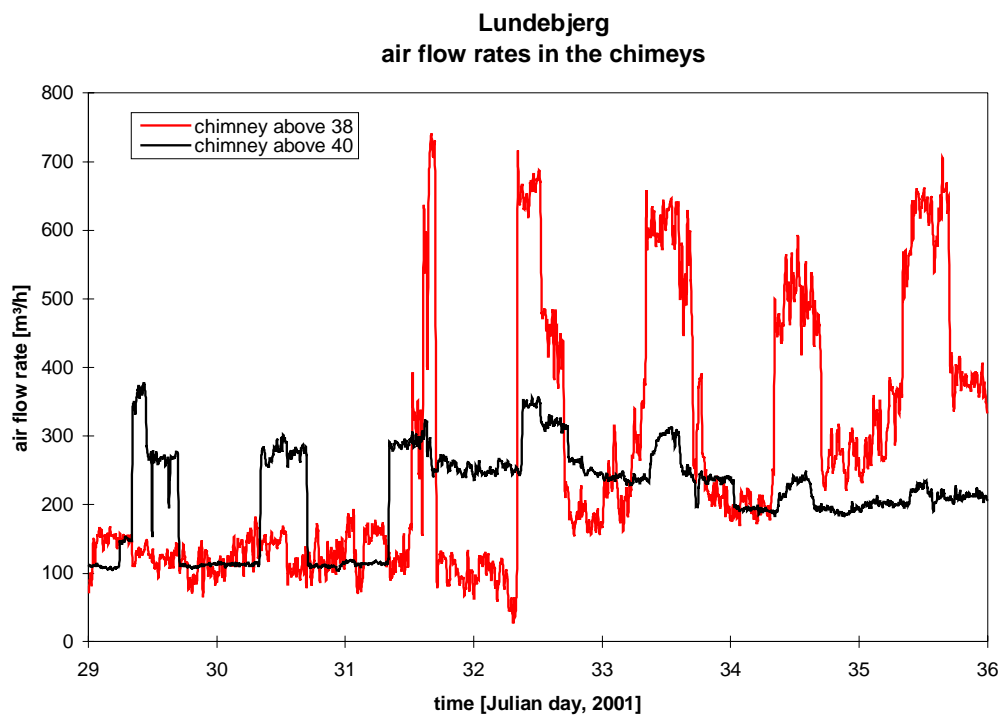


Figure 3.83. The flow rates of fresh air in the chimneys above no. 38 and 40 during week 5, 2001 (January 29 – February 4).

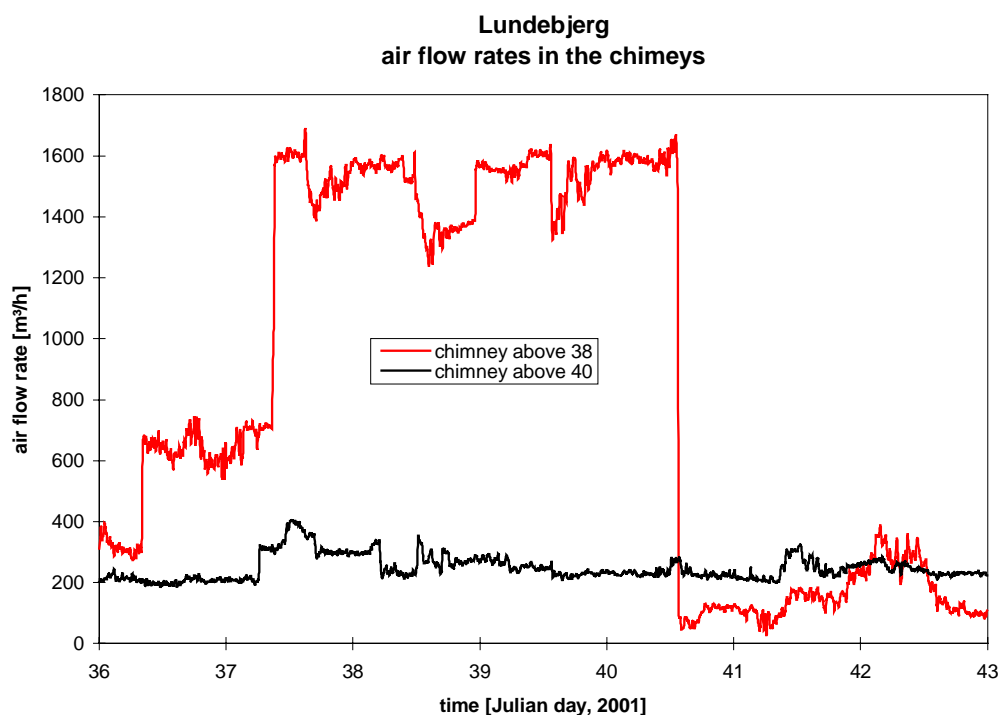


Figure 3.84. The flow rates of fresh air in the chimneys above no. 38 and 40 during week 6, 2001 (February 4 – February 11).

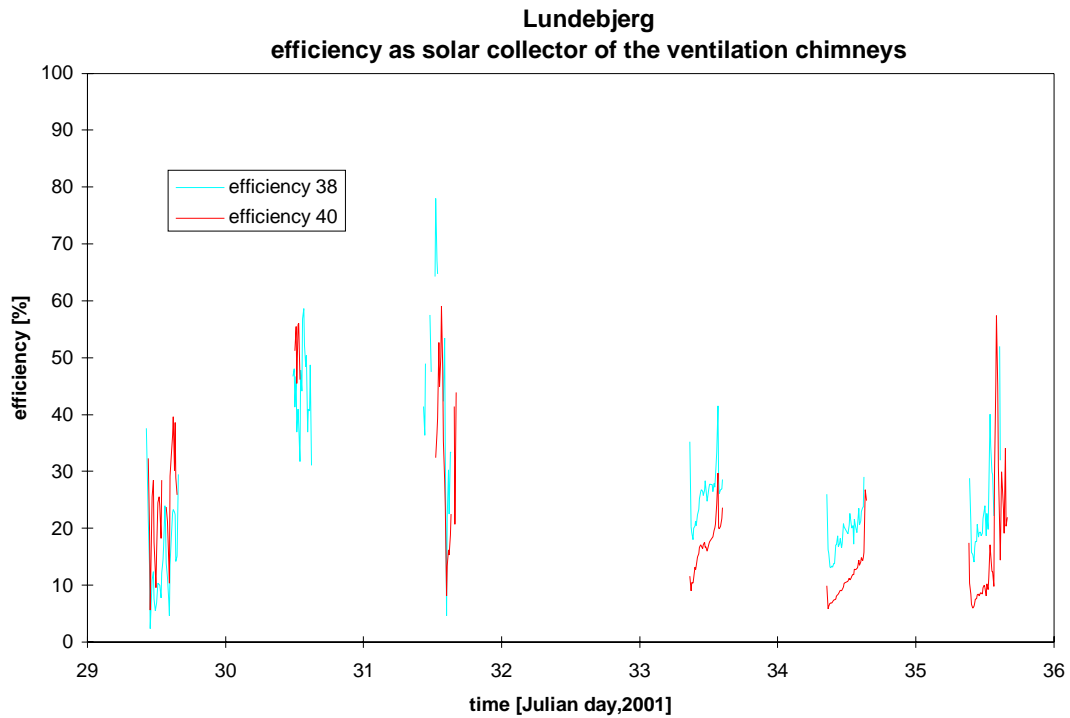


Figure 3.85. The efficiency as solar collector of the chimneys above no. 38 and 40 during week 5, 2001 (January 29 – February 4).

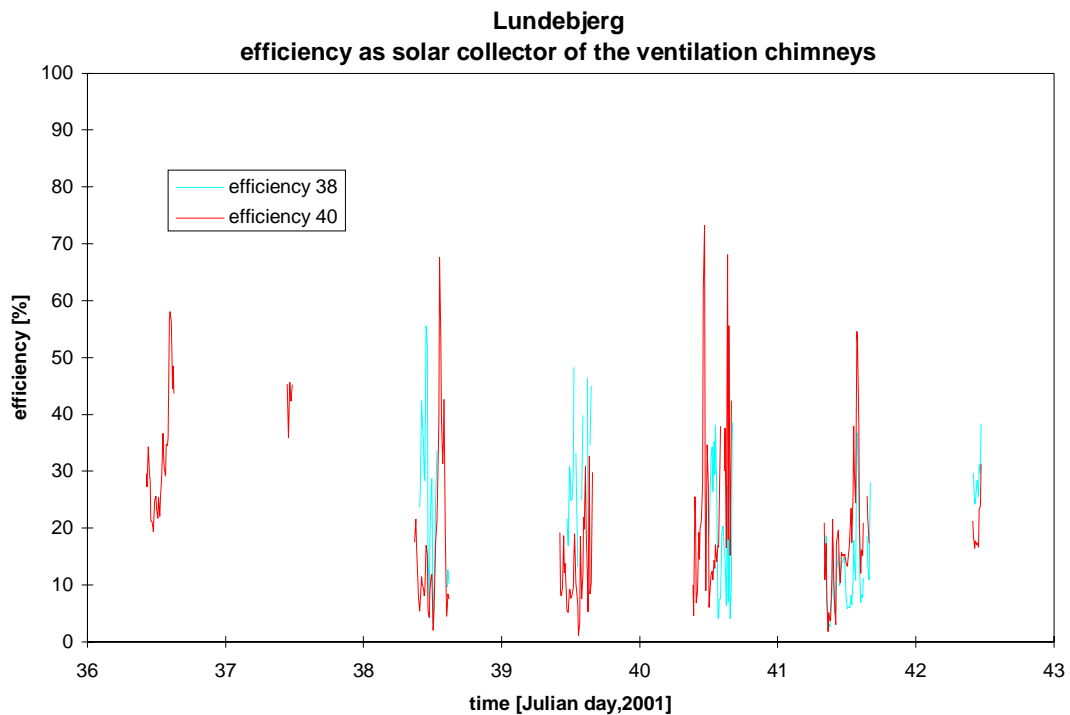


Figure 3.86. The efficiency as solar collector of the chimneys above no. 38 and 40 during week 6, 2001 (February 5 – February 11).



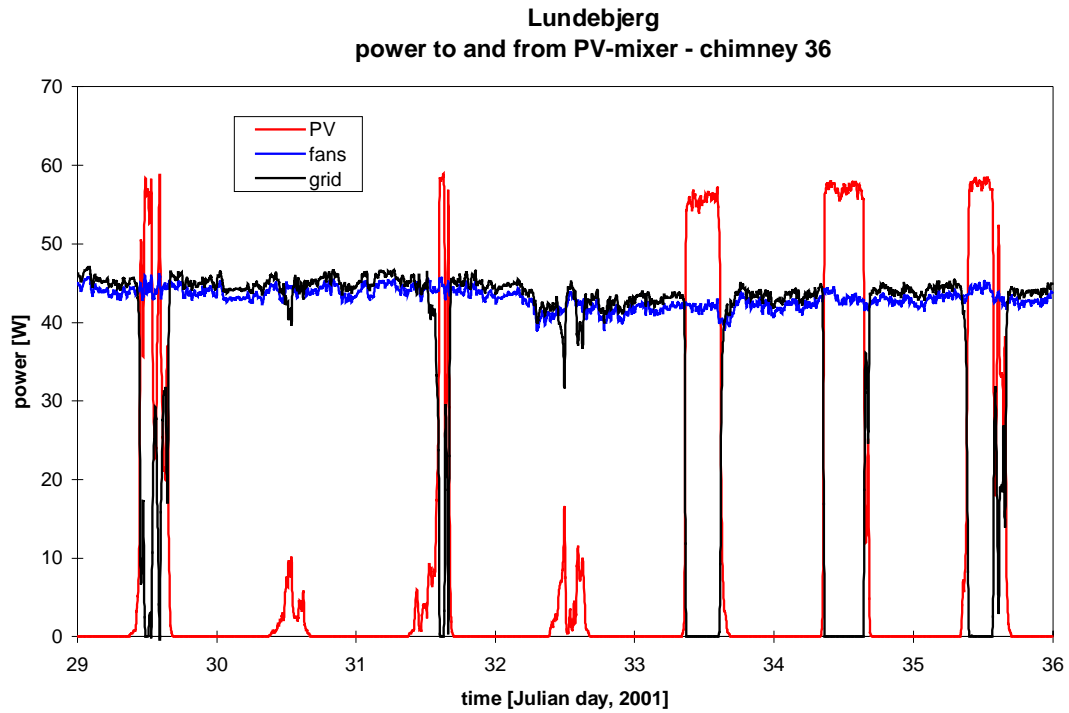


Figure 3.87. Power to and from the PV-mixer of the middle PV-array of chimney 36 during week 5, 2001 (January 29 – February 4).

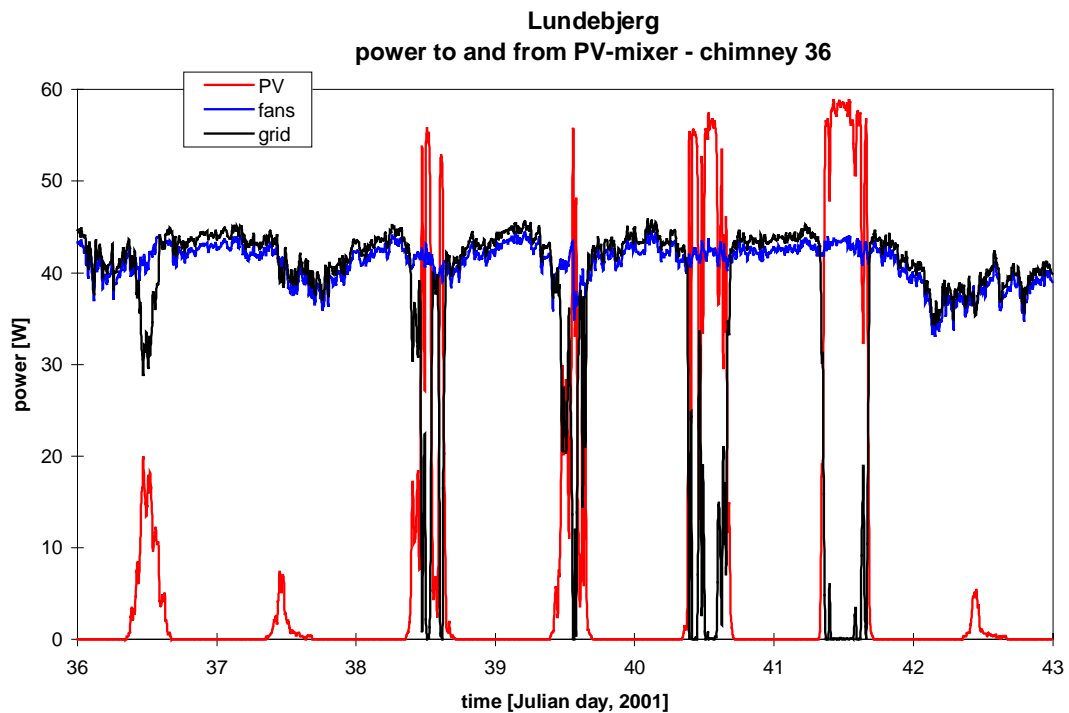


Figure 3.88. Power to and from the PV-mixer of the middle PV-array of chimney 36 during week 6, 2001 (February 5 – February 11).

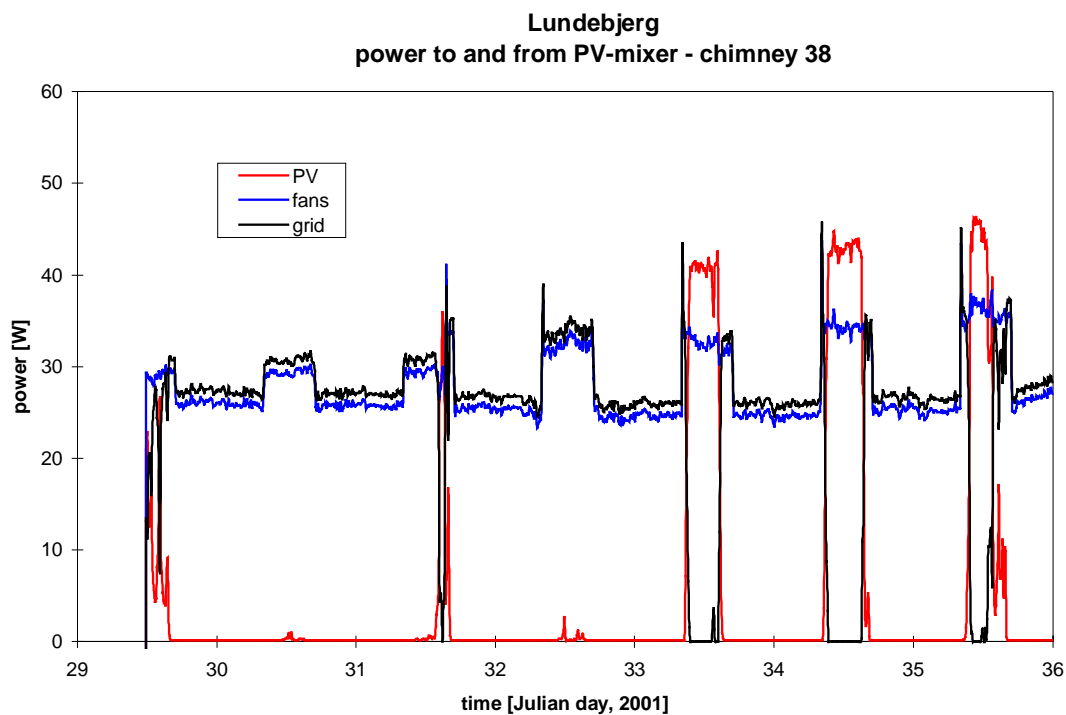


Figure 3.89. Power to and from the PV-mixer of the middle PV-array of chimney 38 during week 5, 2001 (January 29 – February 4).

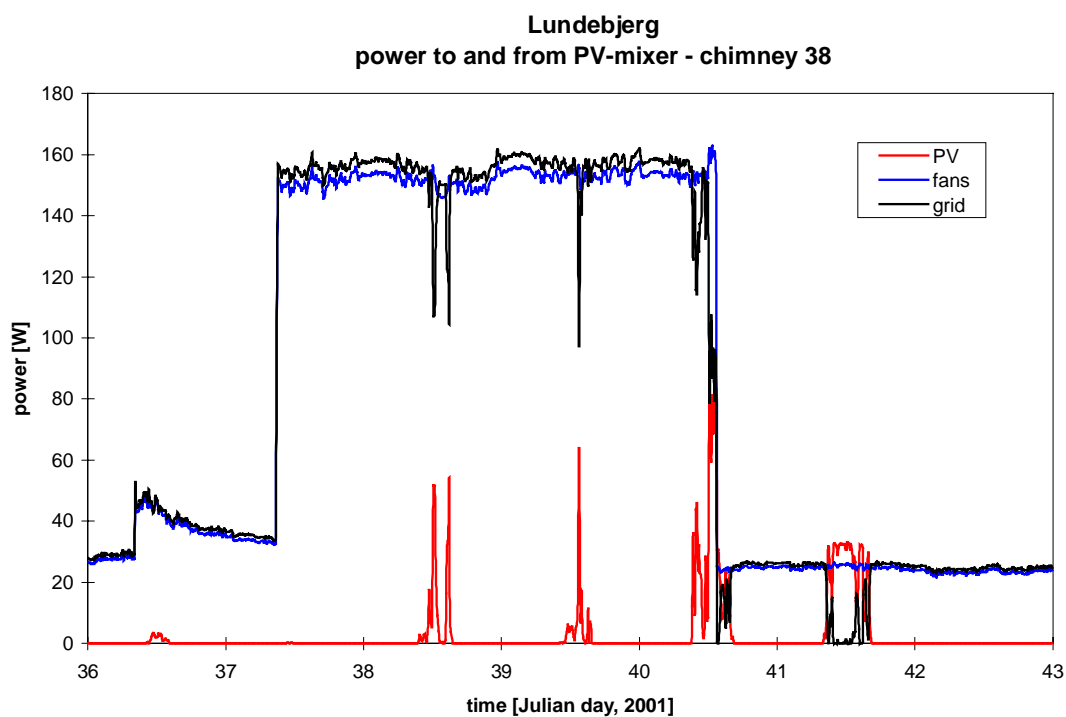


Figure 3.90. Power to and from the PV-mixer of the middle PV-array of chimney 38 during week 6, 2001 (February 5 – February 11).

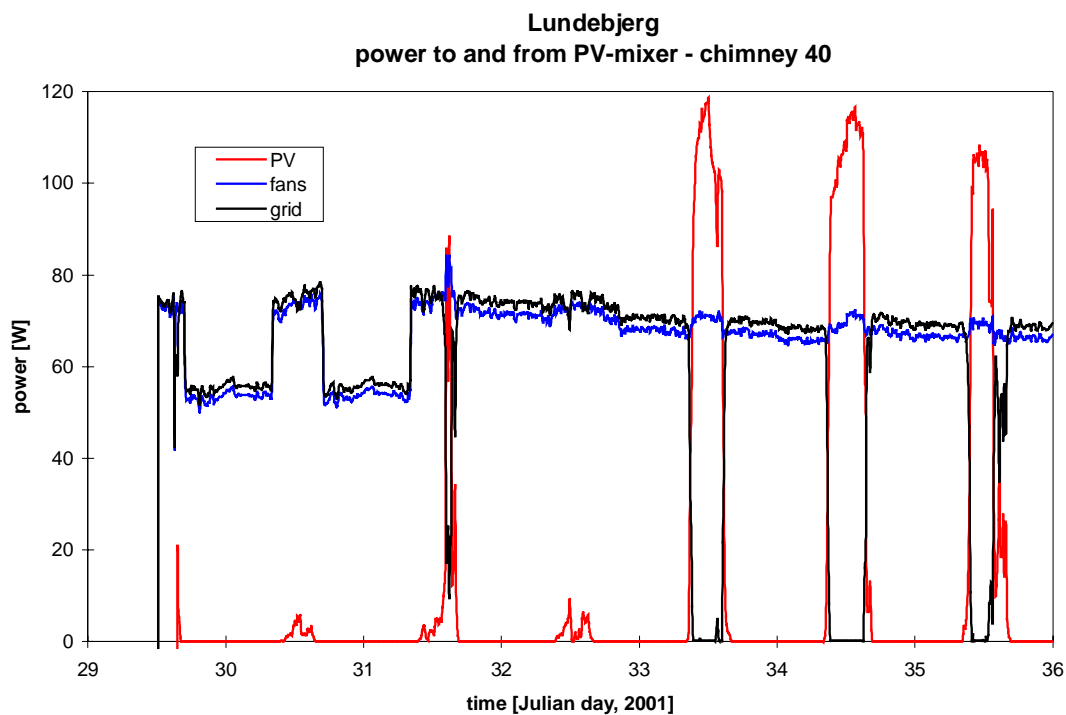


Figure 3.91. Power to and from the PV-mixer of the top PV-array of chimney 40 during week 5, 2001 (January 29 – February 4).

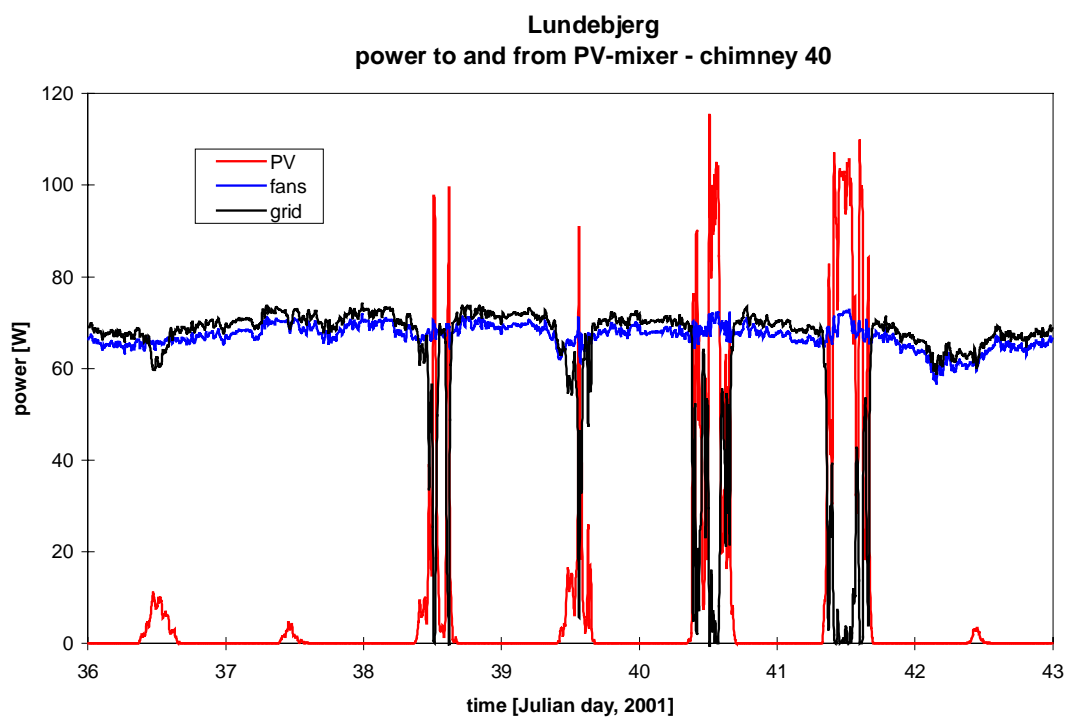


Figure 3.92. Power to and from the PV-mixer of the top PV-array of chimney 40 during week 6, 2001 (February 5 – February 11).

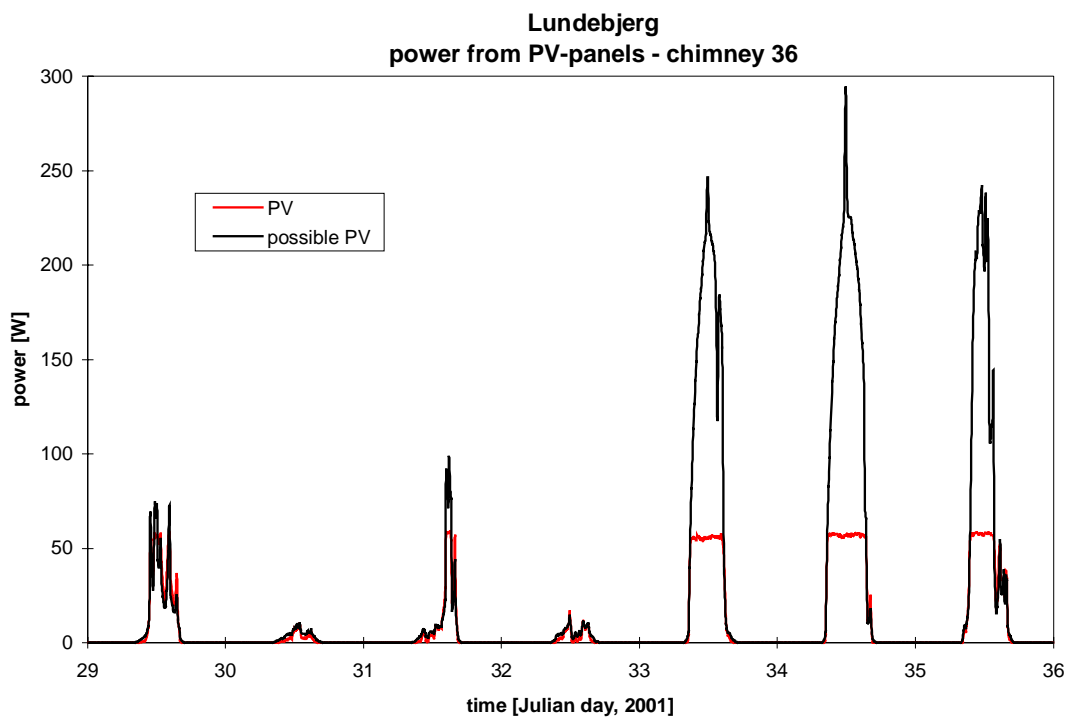


Figure 3.93. Actual power and potential power of the middle PV-array of chimney 36 during week 5, 2001 (January 29 – February 4).

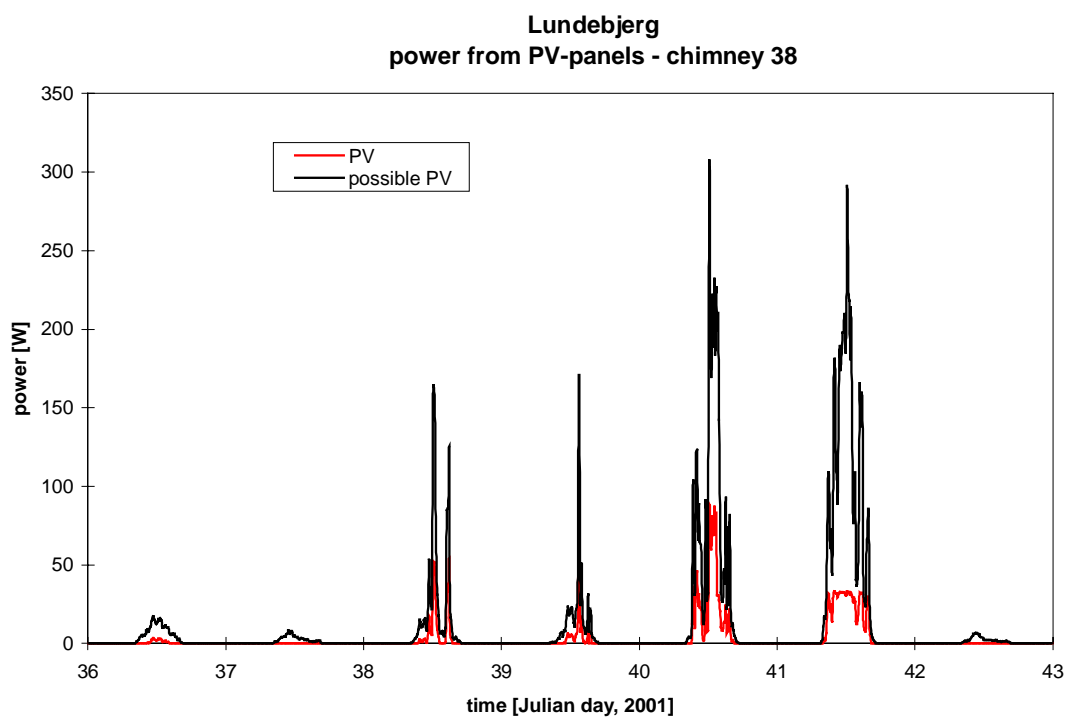


Figure 3.94. Actual power and potential power of the middle PV-array of chimney 36 during week 6, 2001 (February 5 – February 11).

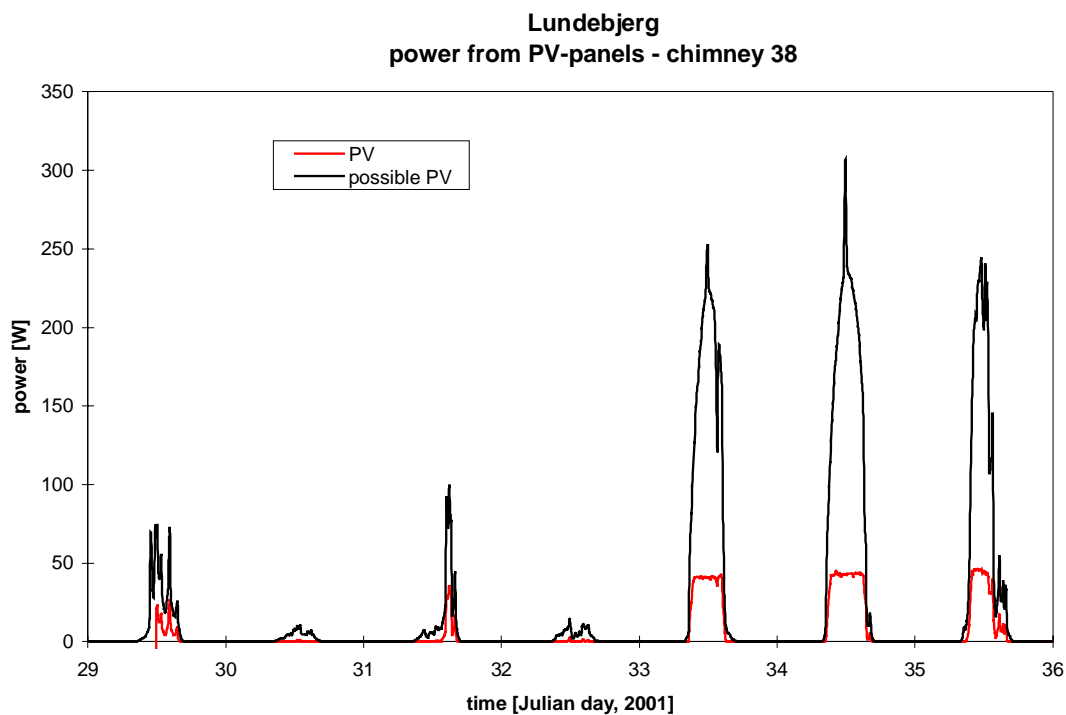


Figure 3.95. Actual power and potential power of the middle PV-array of chimney 38 during week 5, 2001 (January 29 – February 4).

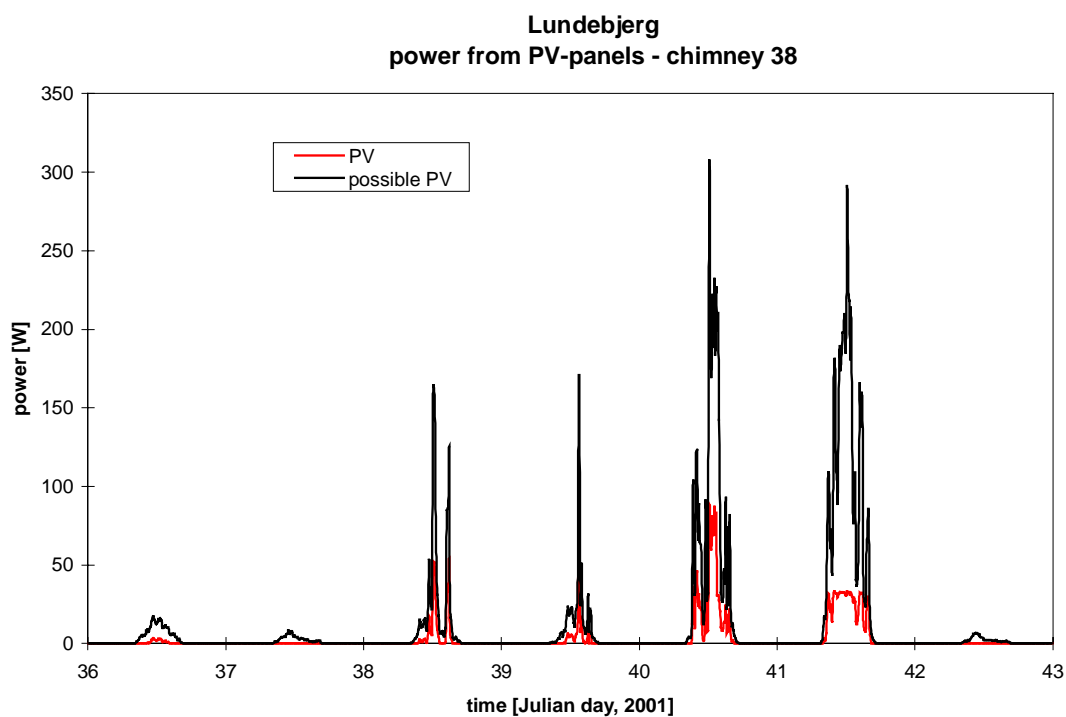


Figure 3.96. Actual power and potential power of the middle PV-array of chimney 38 during week 6, 2001 (February 5 – February 11).

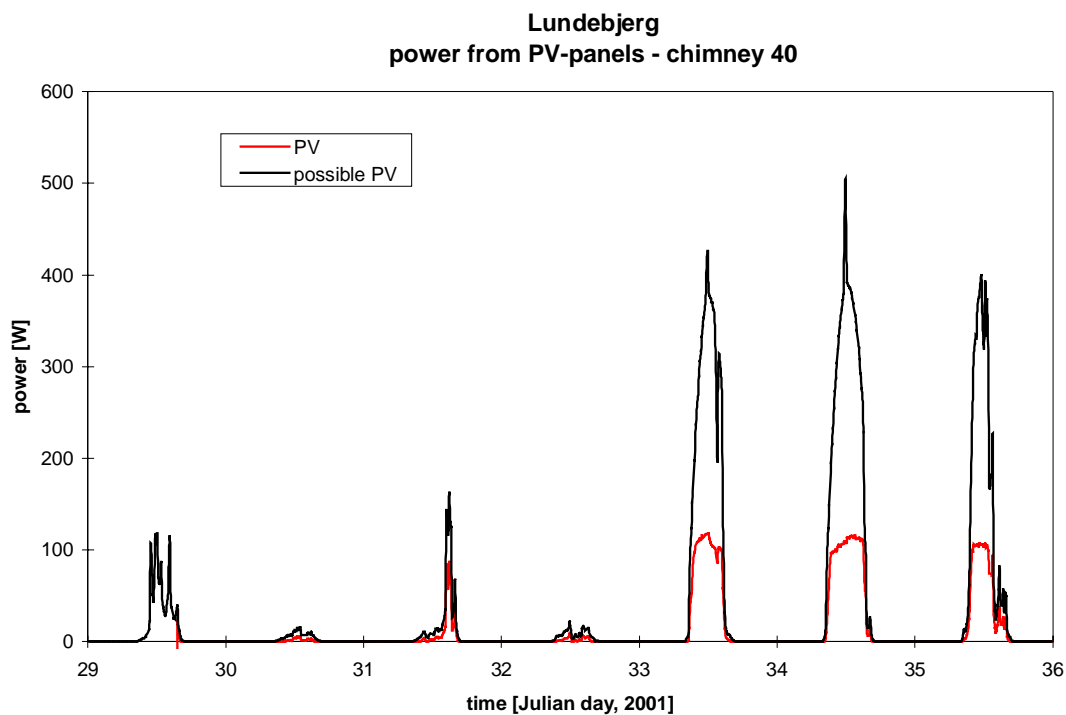


Figure 3.97. Actual power and potential power of the top PV-array of chimney 40 during week 5, 2001 (January 29 – February 4).

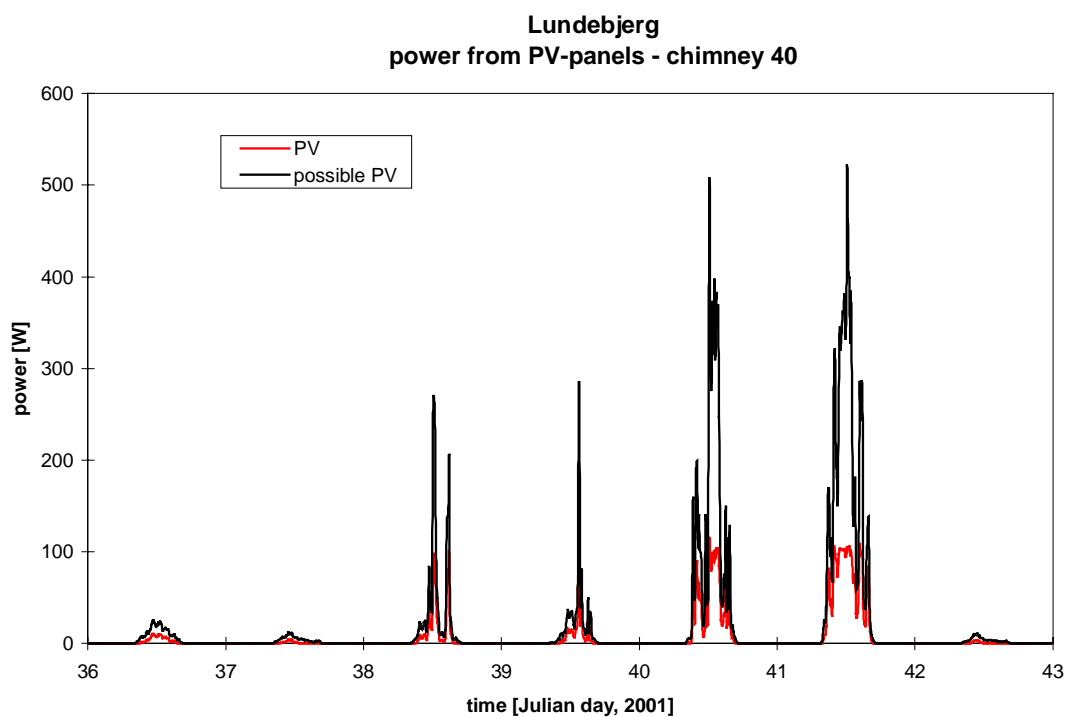


Figure 3.98. Actual power and potential power of the top PV-array of chimney 40 during week 6, 2001 (February 5 – February 11).

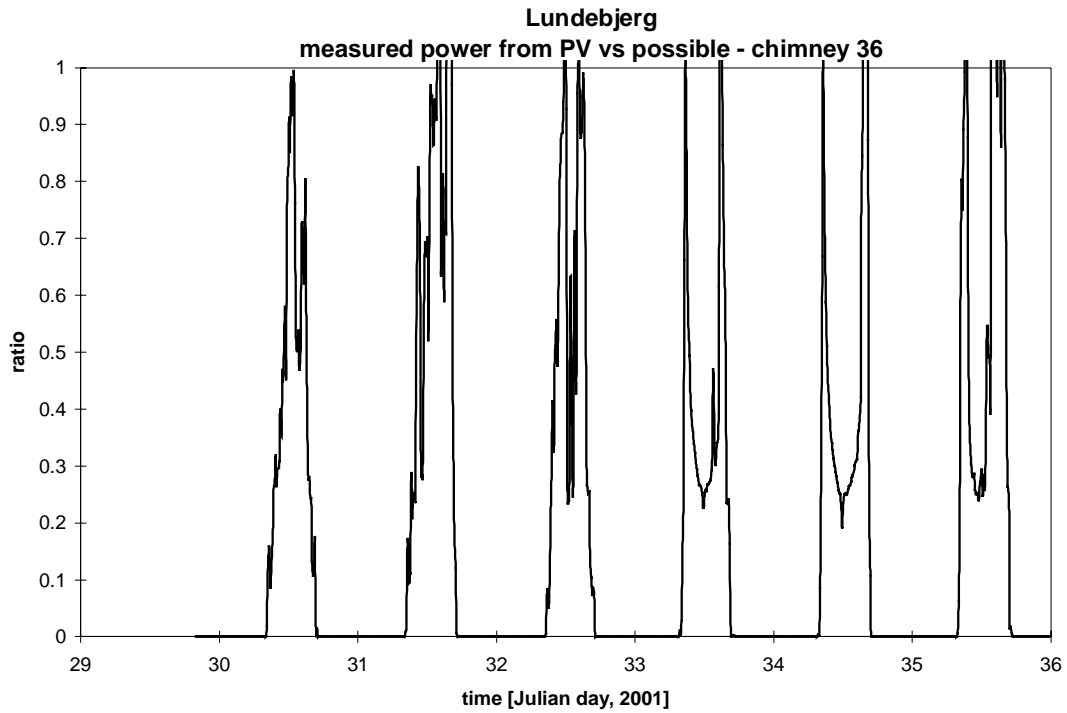


Figure 3.99. Actual power divided with potential power of the middle PV-array of chimney 36 during week 5, 2001 (January 29 – February 4).

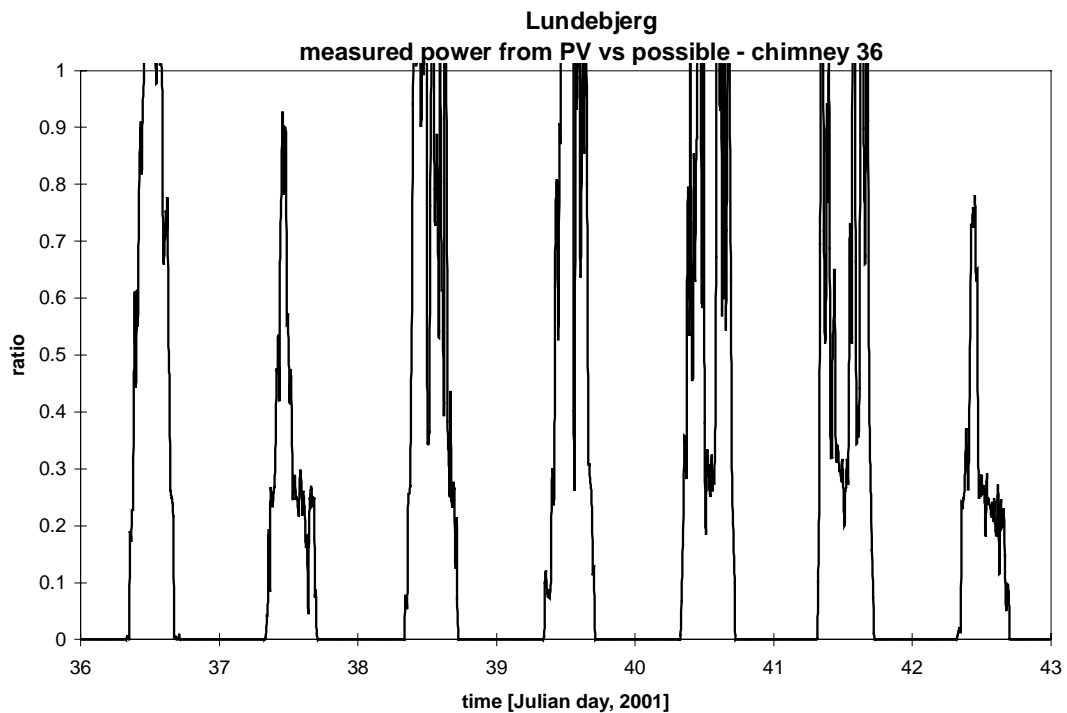


Figure 3.100. Actual power divided with potential power of the middle PV-array of chimney 36 during week 6, 2001 (February 5 – February 11).



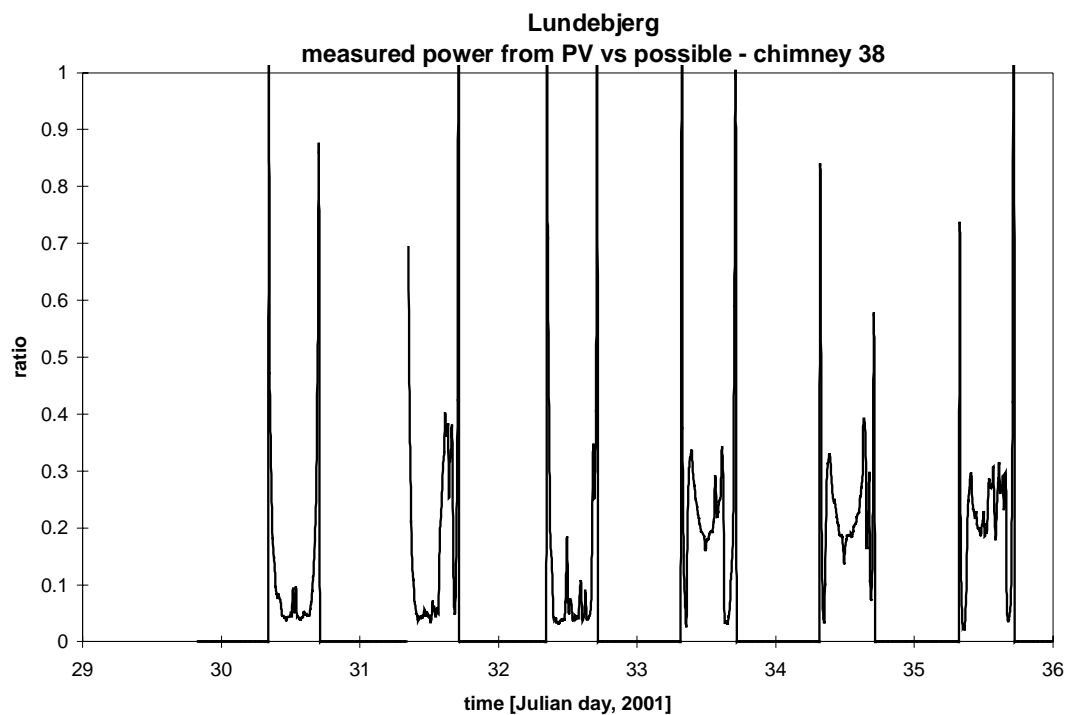


Figure 3.101. Actual power divided with potential power of the middle PV-array of chimney 38 during week 5, 2001 (January 29 – February 4).

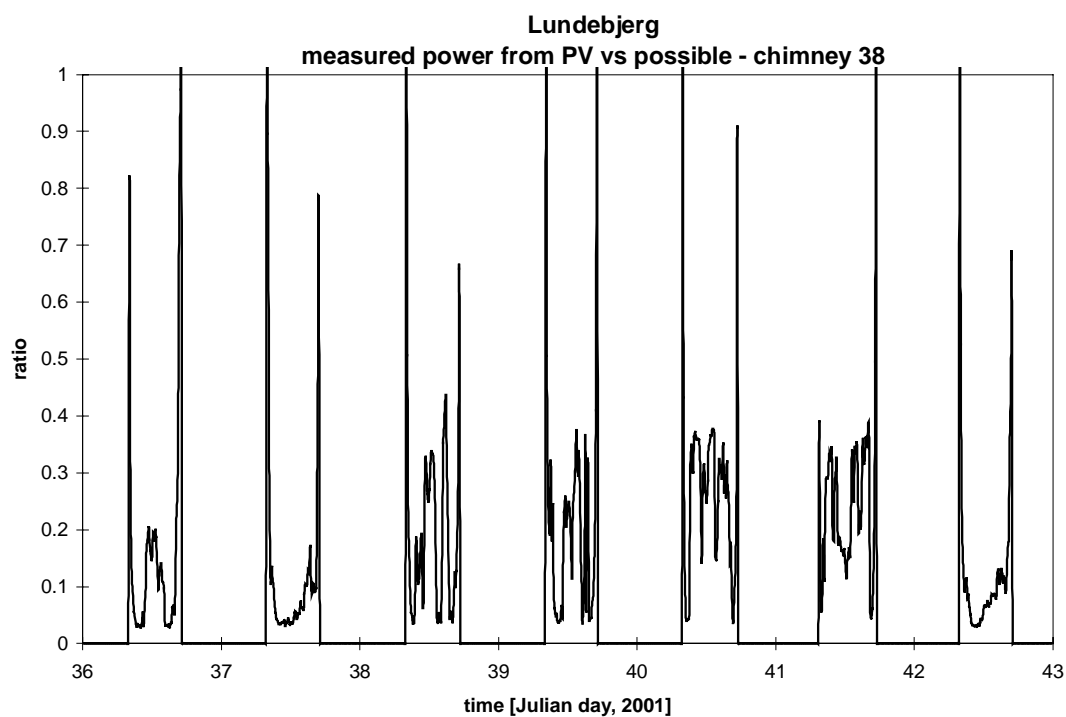


Figure 3.102. Actual power divided with potential power of the middle PV-array of chimney 38 during week 6, 2001 (February 5 – February 11).

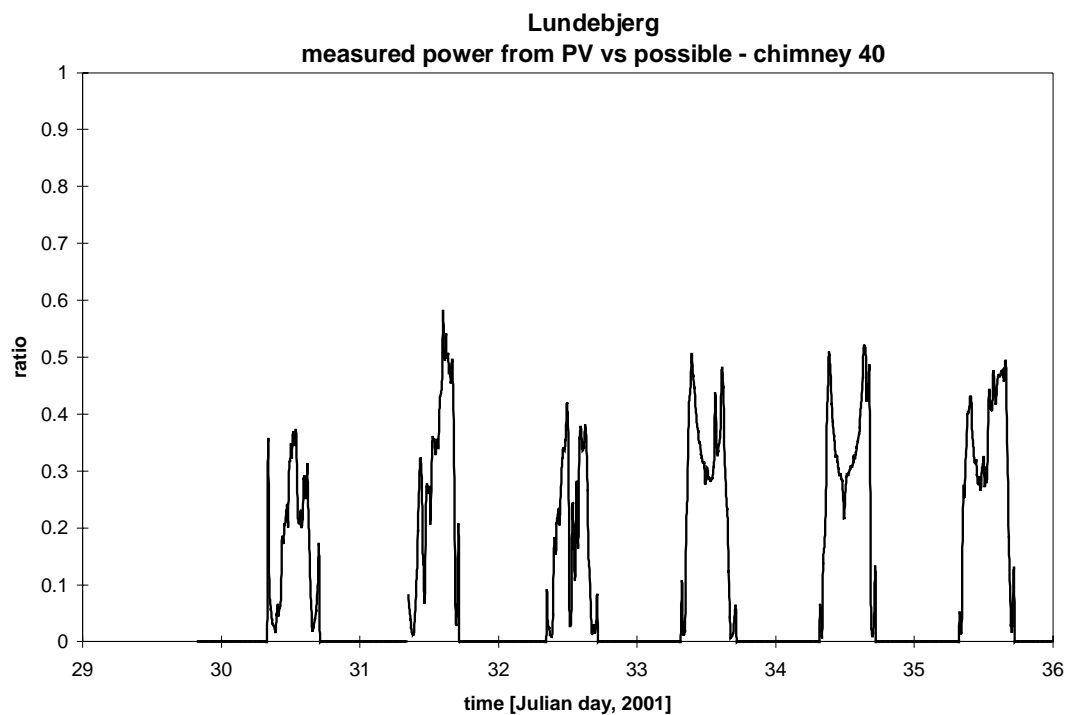


Figure 3.103. Actual power divided with potential power of the top PV-array of chimney 40 during week 5, 2001 (January 29 – February 4).

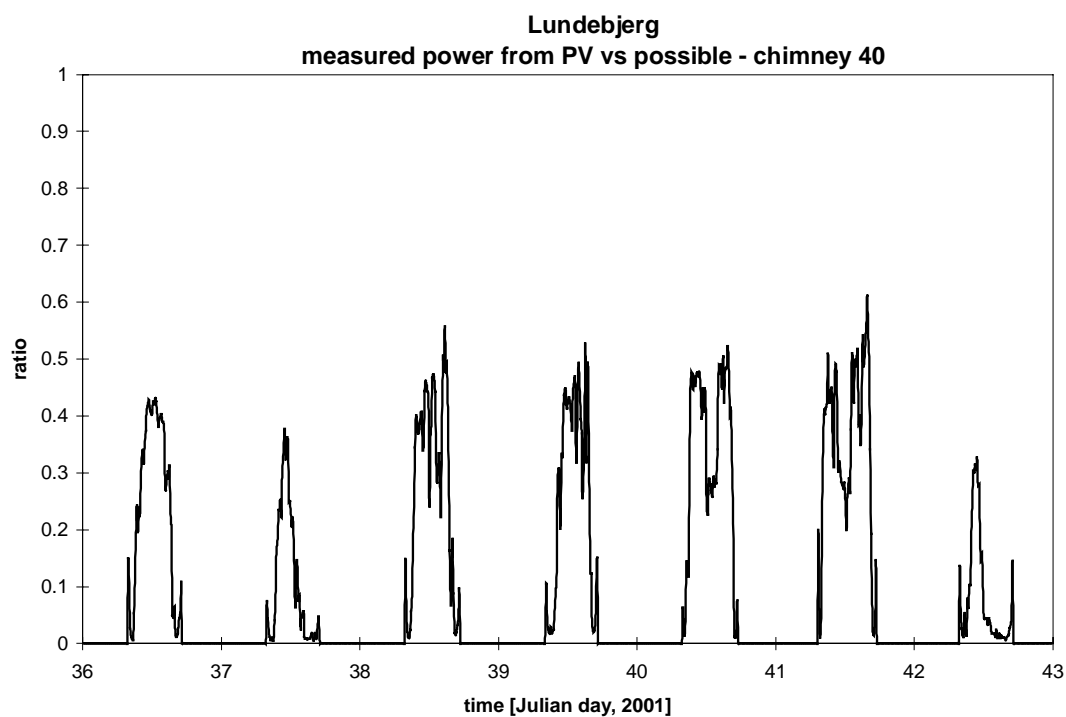


Figure 3.104. Actual power divided with potential power of the top PV-array of chimney 40 during week 6, 2001 (February 5 – February 11).

Figure 3.90 and figure 3.84 reveals a problem for the considered PV-panel on chimney 38 on day 38-40. Although high fan power demand the PV-mixer fails to utilize most of the potential PV-power even if this should have been possible. This is believed to be due to a malfunction of the PV-mixer – the PV-mixer has often a strange buzzing sound.

### **3.2. Calculations based on the measurements and more general conclusions**

The section deals with the function of the air to air heat exchanger, the fan power, the efficiency of the solar ventilations chimneys as solar air collectors, the temperatures of the PV-panels, the air temperature behind the PV-panels in the PV-gable and the PV-mixer, while the next section deals with the actual savings due to these components.

#### **3.2.1. The efficiency of the air to air heat exchangers**

The efficiency of the air to air heat exchangers is shown for two weeks in the former section. The shown efficiencies don't necessarily show a correct picture of the efficiency of the heat exchangers. In the following the efficiency is evaluated based on a larger set of data rather than on only two weeks.

Determination of the efficiency of the heat exchangers is not an easy task as condensation may occur. If condensation occurs the heat flow to the fresh air is higher than the heat flow from the exhaust air if the calculations of the heat flows are based on dry temperatures. The three heat exchangers on which the measurements have been carried out on will in the following be treated separately, however, with more common conclusions at the end.

#### ***Heat exchanger of apartment 40 IIA***

Figure 3.105 shows the calculated heating of the fresh air divided with the calculated cooling of the exhaust air (based on dry temperatures) in the heat exchanger as a function of the inlet temperature to the heat exchanger in apartment 40 IIA using data from 2000 (no data from 2001 has been used as the fresh air fan has been switched off during most of 2001). Only data at an inlet temperature below 17 °C are included in figure 3.105. The reason for this is to avoid values where the air to the heat exchanger has been heated too much by the sun – when the inlet temperature gets above the exhaust temperature the function of the heat exchanger changes totally. High inlet temperatures further lead to small temperature differences across the heat exchanger, which again increase the uncertainty of the calculations.

Figure 3.105 shows a rather strong dependency on the inlet temperature to the heat exchanger indicating that condensation did occur in the heat exchanger.

Figures 3.106-107 show the efficiency of the heat exchanger at normal and min. air flow mode. The values in figure 3.106 lay nicely around a line – the regression equation of that line is also shown in the figure. Figure 3.106 shows that condensation did occur as efficiencies above 100% occurs. The values in 3.107 are much more scattered. The reason for the scattering of the values of especially figures 3.107 and in less degree of figures 3.106 is that the two air flow rates in the heat exchanger fluctuate non-correlated - mainly for the values of figure 3.107.

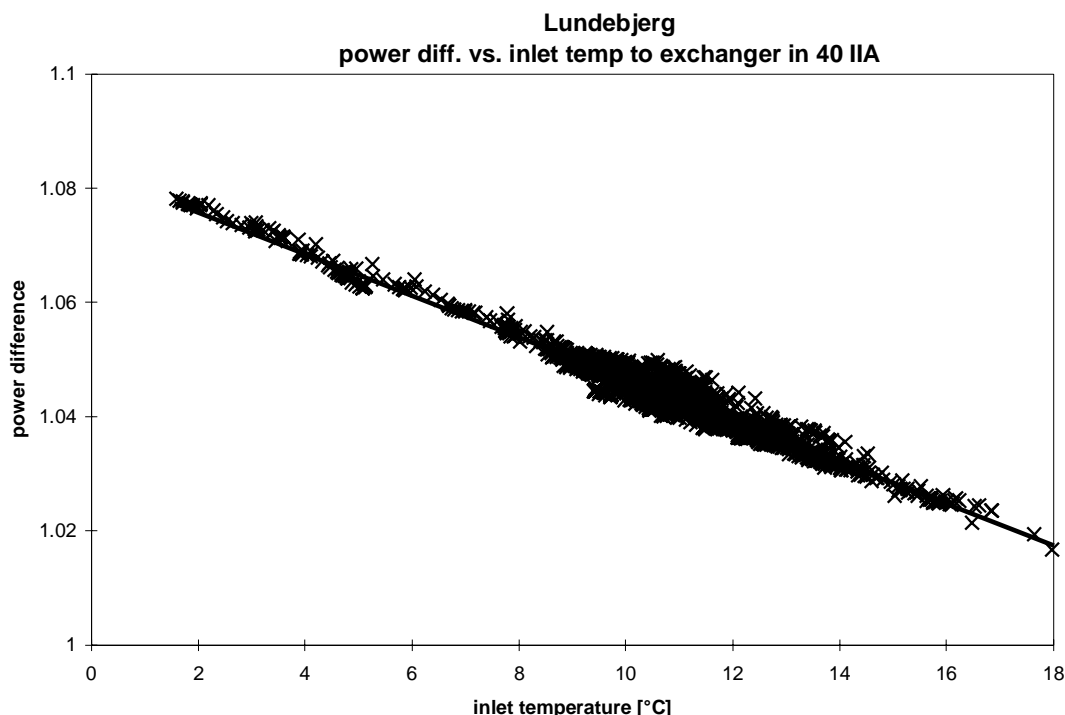


Figure 3.105. The calculated heating of the fresh air divided with the calculated cooling of the exhaust air (based on dry temperatures) in the heat exchanger for year 2000 at normal and min. flow rates.

At normal indoor air humidities condensation should not occur below an inlet temperature of 17 °C to the heat exchangers, however, the air from the bathroom may be very humid. In order to compensate for condensation in the heat exchanger the efficiency should, therefore, be found close to the axis to the right in the graphs. For normal flow rates this gives an efficiency of about 77 %. Figure 3.107 is less conclusive due to the scattering. However, the efficiencies at min. air flow mode should be lower than at normal air flow rate mode, which figure 3.107 also indicates.

But in order to compare the above efficiencies with the efficiency of other heat exchangers it is necessary to bring them on a form where the two air flow rates are identical, as this is the way which normally is used when comparing efficiencies of air to air heat exchangers. As the heat exchanger is identical to the one in 40 IIB, this will be done for both apartments together after the presentation of the measurements of 40 IIB.

### ***Heat exchanger of apartment 40 IIB***

Figures 3.108-111 show the calculated heating of the fresh air divided with the calculated cooling of the exhaust air (based on dry temperatures) in the heat exchanger as a function of the inlet temperature to the heat exchanger in apartment 40 IIB using data from 2000 and 2001. Figures 3.108-109 for min. air flow mode for year 2000 and 2001 respectively, while figures 3.110-111 are for normal and max air flow mode for year 2000 and 2001 respectively. Only data at an inlet temperature below 17 °C are included in figures 3.108-111. The reason for this to avoid values where the air to the heat exchanger has been heated too much by the sun – when the inlet temperature gets above the exhaust temperature the function of the heat

exchanger changes totally. High inlet temperatures further lead to small temperature differences across the heat exchanger, which again increase the uncertainty of the calculations.

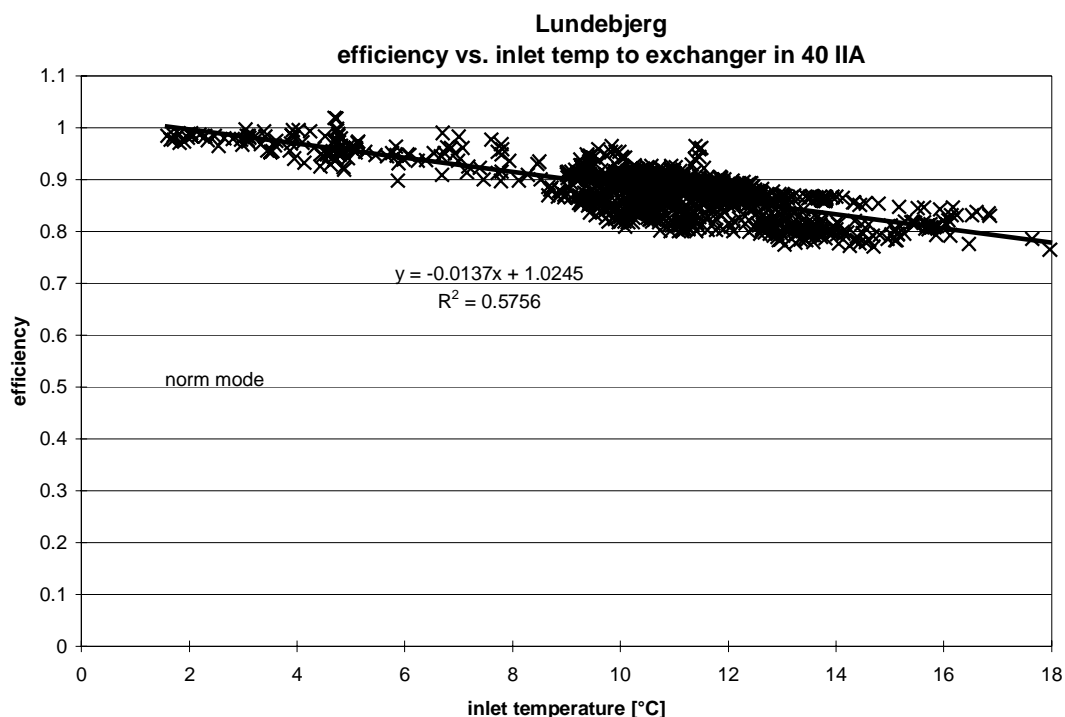


Figure 3.106. The calculated efficiency of the heat exchanger of apartment 40 IIA for year 2000 at normal flow rate.

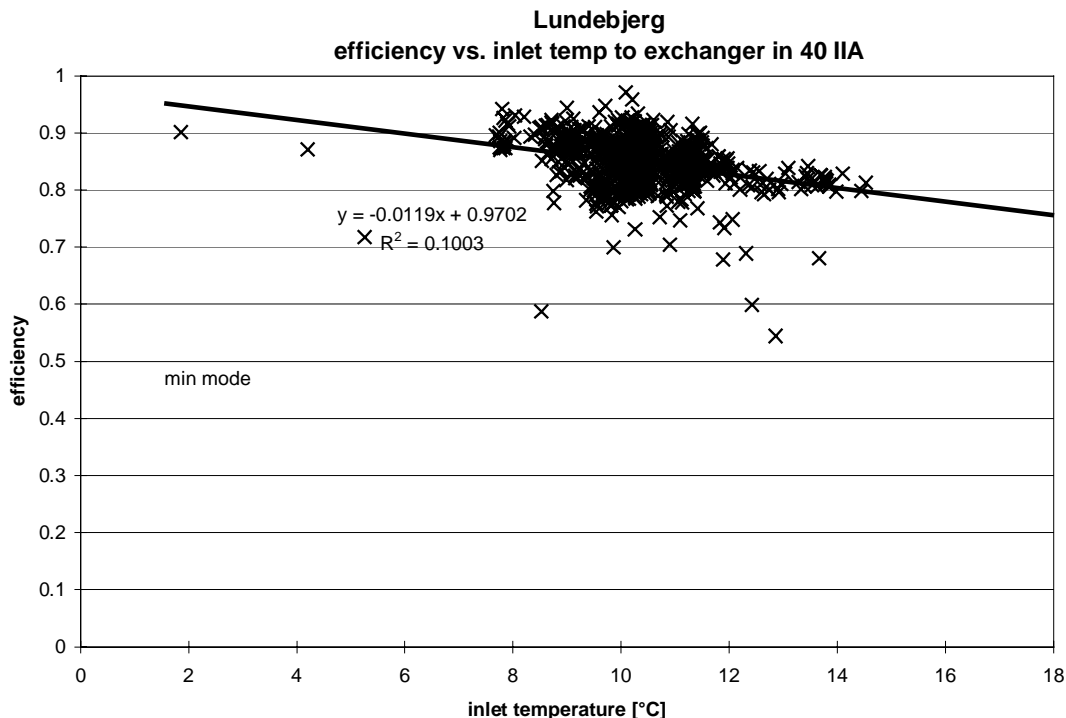


Figure 3.107. The calculated efficiency of the heat exchanger of apartment 40 IIA for year 2000 at min flow rate.

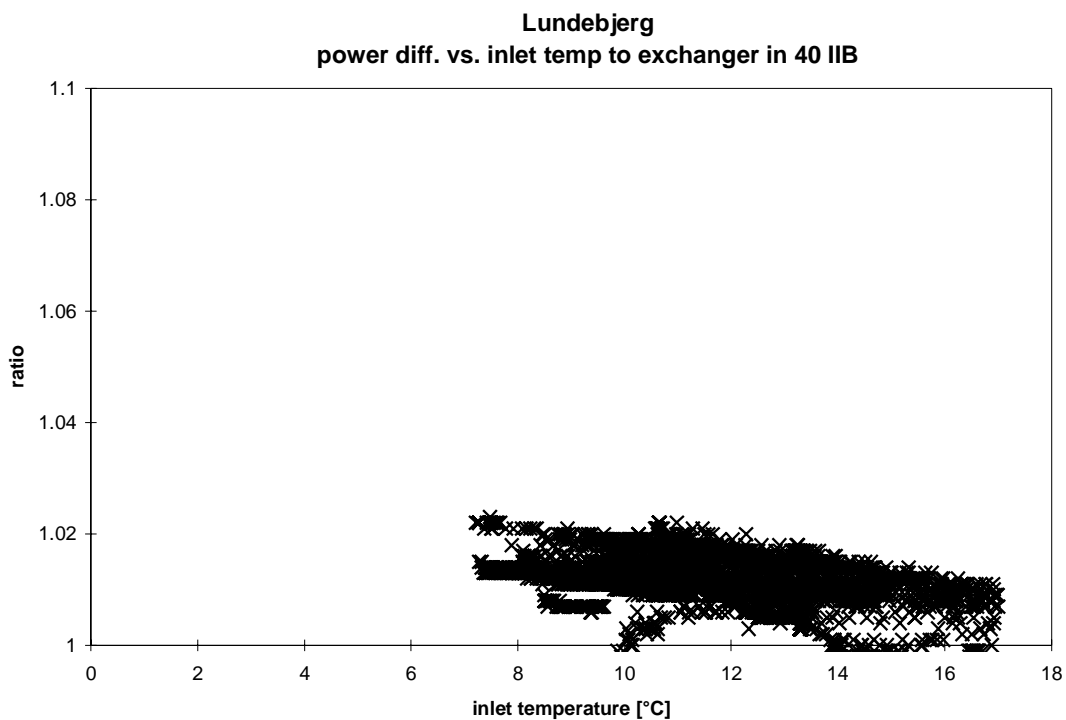


Figure 3.108. The calculated heating of the fresh air divided with the calculated cooling of the exhaust air (based on dry temperatures) in the heat exchanger of apartment 40 IIB for part of year 2000 at min. flow rates.

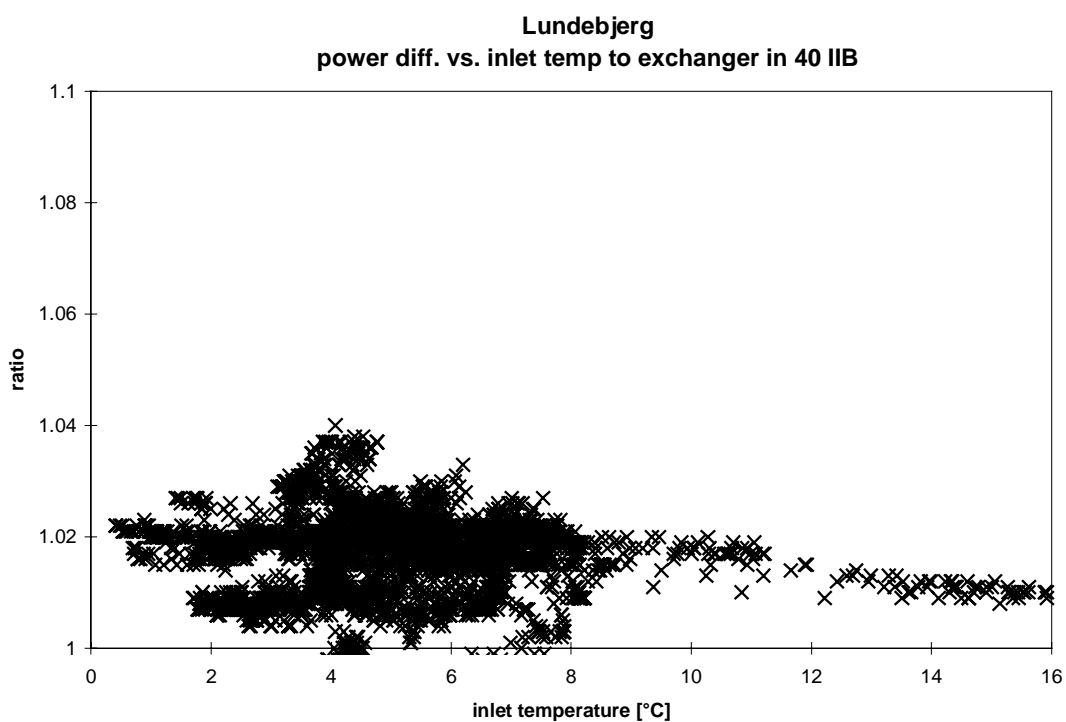


Figure 3.109. The calculated heating of the fresh air divided with the calculated cooling of the exhaust air (based on dry temperatures) in the heat exchanger for apartment 40 IIB for part of year 2001 at min. flow rates.

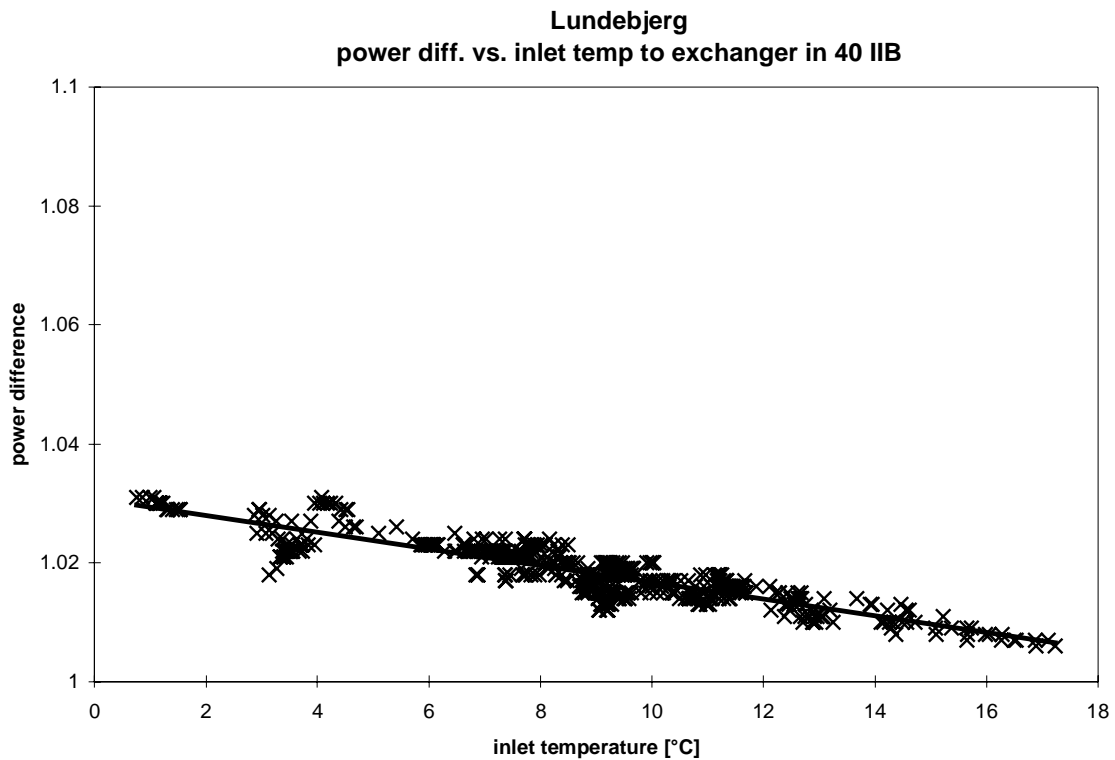


Figure 3.110. The calculated heating of the fresh air divided with the calculated cooling of the exhaust air (based on dry temperatures) in the heat exchanger for apartment 40IIB for year 2000 at normal and max. flow rates.

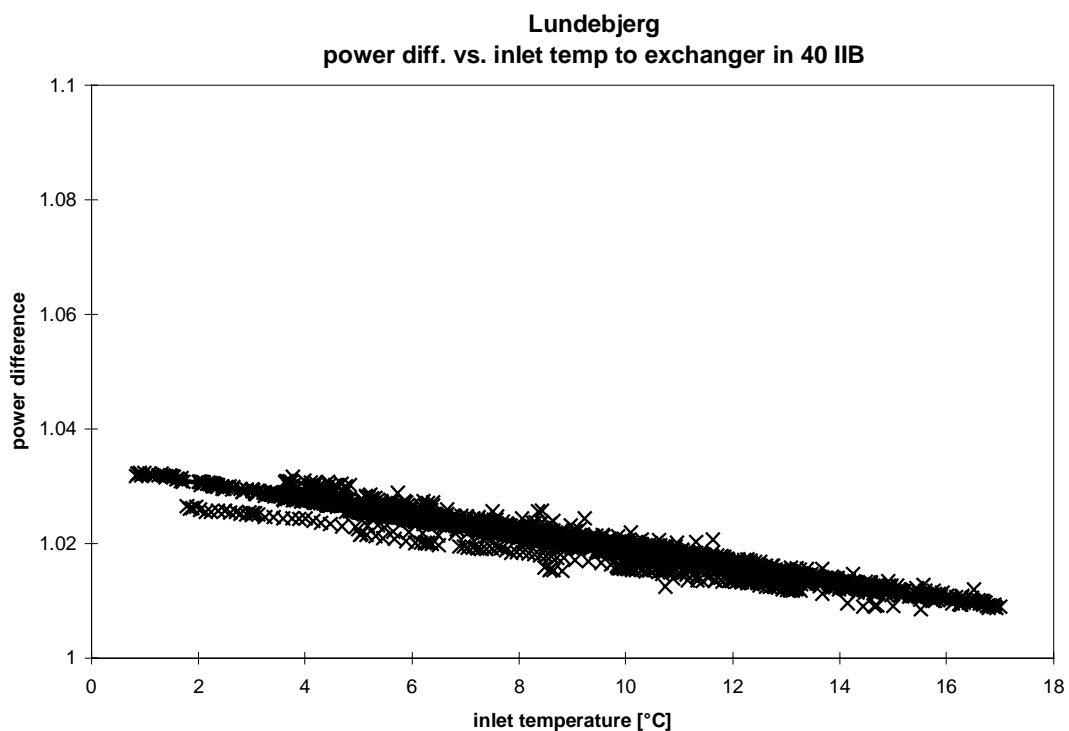


Figure 3.111. The calculated heating of the fresh air divided with the calculated cooling of the exhaust air (based on dry temperatures) in the heat exchanger for apartment 40 IIB for year 2001 at normal and max. flow rates.

Figures 3.108-111 show hardly any condensation – the ratio is between 0.99 and 1.04, however, a little temperature dependent. Figures 3.110-111 show a clear pattern (as for apartment 40 IIA), but with a smaller dependency on the inlet temperature. This supports the statement of the tenants – that the air in the apartment is very dry.

Figures 3.112-117 show the efficiency of the heat exchanger at min., normal and max air flow mode for 2000 and 2001. The values in figures 3.112-113 show no clear pattern while the values in figures 3.114-117 lay nicely around a line – the regression equations of these lines are also shown in the figures. The large scattering seen in figure 3.112-113 is caused by a large non-correlated fluctuation of the two air flows in the heat exchanger at min. flow rate mode as seen in figures 3.37-38. This is shown in figure 3.118, where the efficiency at min. flow rate mode is shown dependent on the ratio between the two air flow rates. Figure 3.118 shows a very strong correlation between the efficiency and the ratio between the two air flow rates. Figures 3.112-117 shows similar pattern for the efficiency for both 2000 and 2001.

Figures 3.114-117 show a very weak dependency of the efficiencies on the inlet temperature to the heat exchanger indicating that not much condensation had taken place in the heat exchanger.

Figures 3.112-117 show that the efficiencies in the three air flow modes were:

min. mode:	60? % (2000) and 55? % (2001) - found at an inlet temperature of 17°C
normal mode:	54 % (2000) and 56 % (2001) - found at an inlet temperature of 17°C
max. mode:	63 % (2000) and 64 % (2001) - found at an inlet temperature of 17°C

The efficiencies shown in figures 3.112-117 are the actual exchanger efficiencies during the measuring campaign, but do not give a clear picture of the function of the heat exchanger because of the large difference between the flow rate of exhaust and fresh air, the non-correlated fluctuations of these two parameters (especially at min. flow rates) and due to the short period the system have been allowed to run in max. mode.

In order to overcome this and in order to be able to compare the efficiency of the heat exchanger with the efficiency of other heat exchangers it is necessary to bring the efficiencies on a form where the two air flow rates are identical, as this is the way which normally is used when comparing efficiencies of air to air heat exchangers. As the heat exchanger is identical to the one in 40 IIA, this will be done for both apartments in the following.

### ***Normalized efficiency of the heat exchangers in 40 IIA and B***

It can be shown (Hansen, Kjerulf-Jensen and Stampe, 1997) that the exchanger efficiency at identical flow rates equal to the lowest flow rate is identical to the temperature efficiency at the lowest flow rate. The temperature efficiency is calculated based on the actual measured temperatures in the system.

$$\eta_{1t} = (T_{1o} - T_{1i}) / (T_{2i} - T_{1i}) \quad (3.5)$$

where:  $\eta_{1t}$  is the temperature efficiency at the smallest flow rate

$T_{1i}$  is the inlet temperature to the exchanger for the air with the smallest flow rate

$T_{1o}$  is the outlet temperature from the exchanger for the air with the smallest flow rate

$T_{2i}$  is the inlet temperature to the exchanger for the air with the largest flow rate



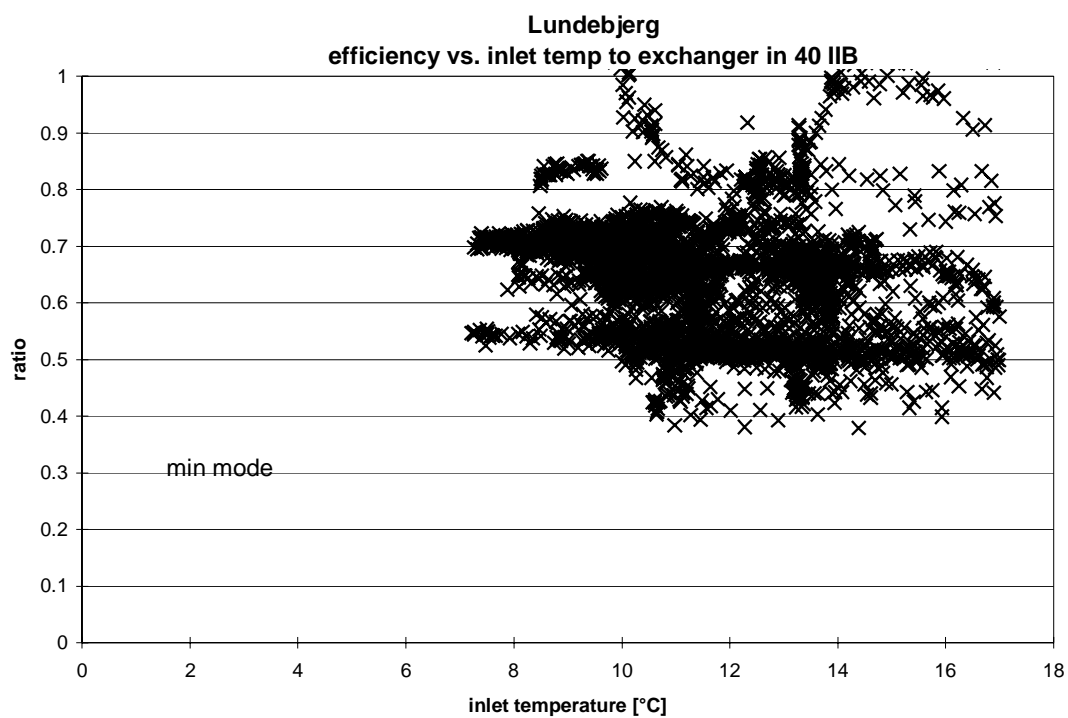


Figure 3.112. The calculated efficiency of the heat exchanger of apartment 40 IIB for part of year 2000 at min. flow rate.

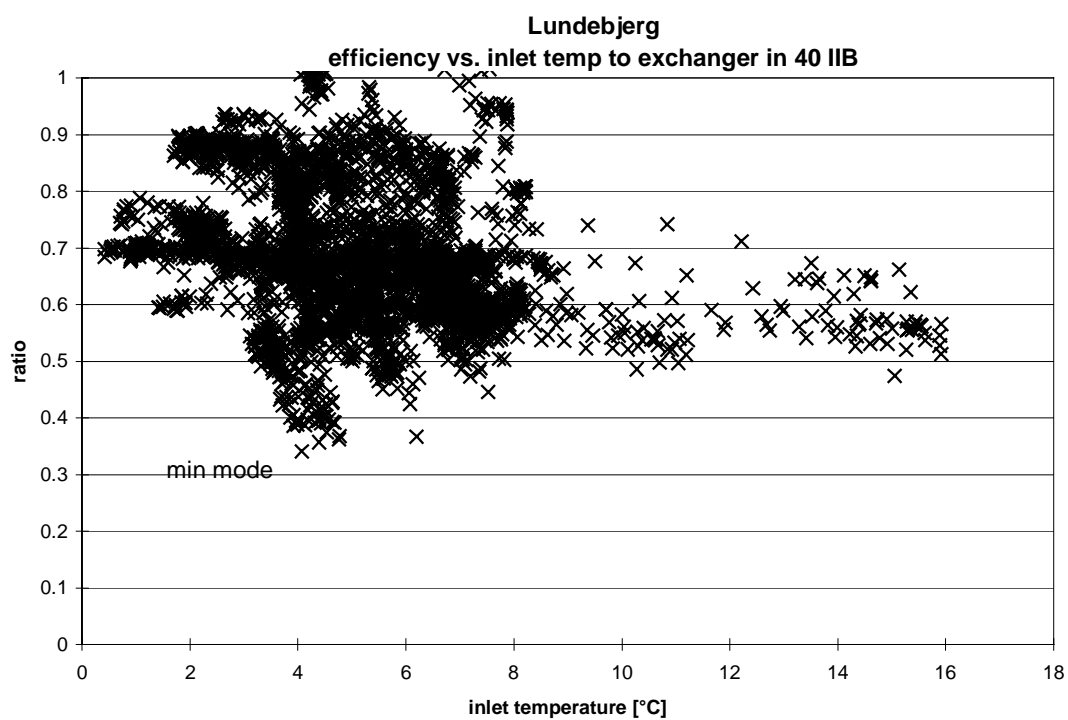


Figure 3.113. The calculated efficiency of the heat exchanger of apartment 40 IIB for part of year 2001 at min. flow rate.

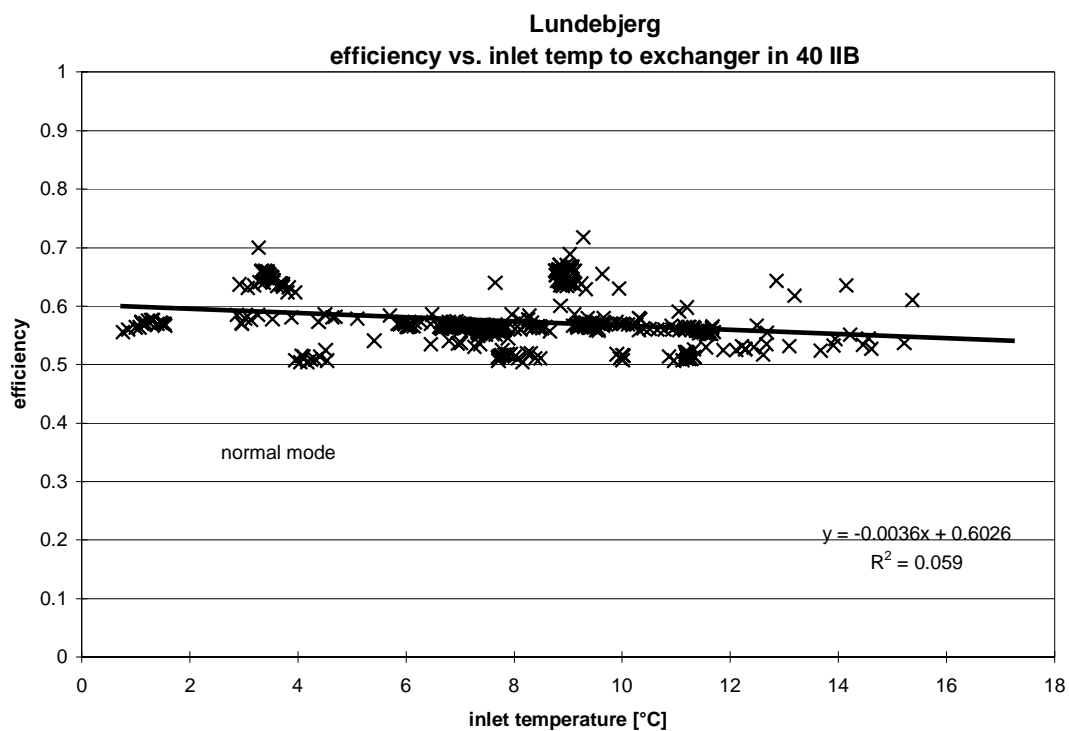


Figure 3.114. The calculated efficiency of the heat exchanger of apartment 40 IIB for year 2000 at normal flow rate.

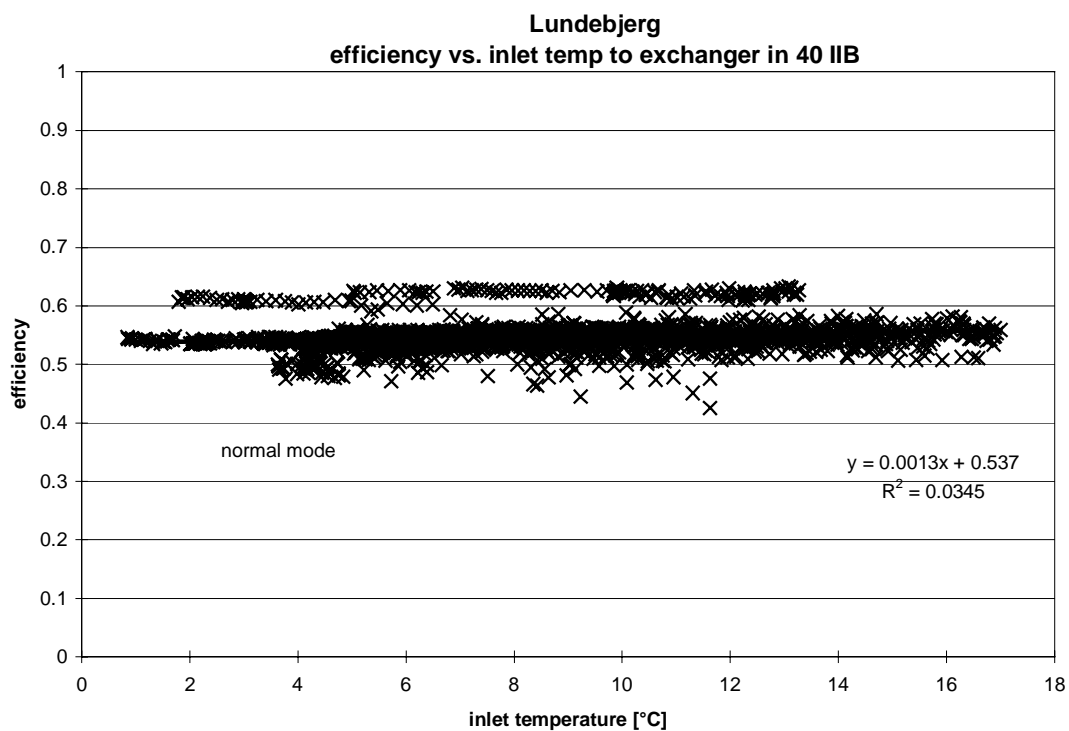


Figure 3.115. The calculated efficiency of the heat exchanger of apartment 40 IIB for year 2001 at normal flow rate.

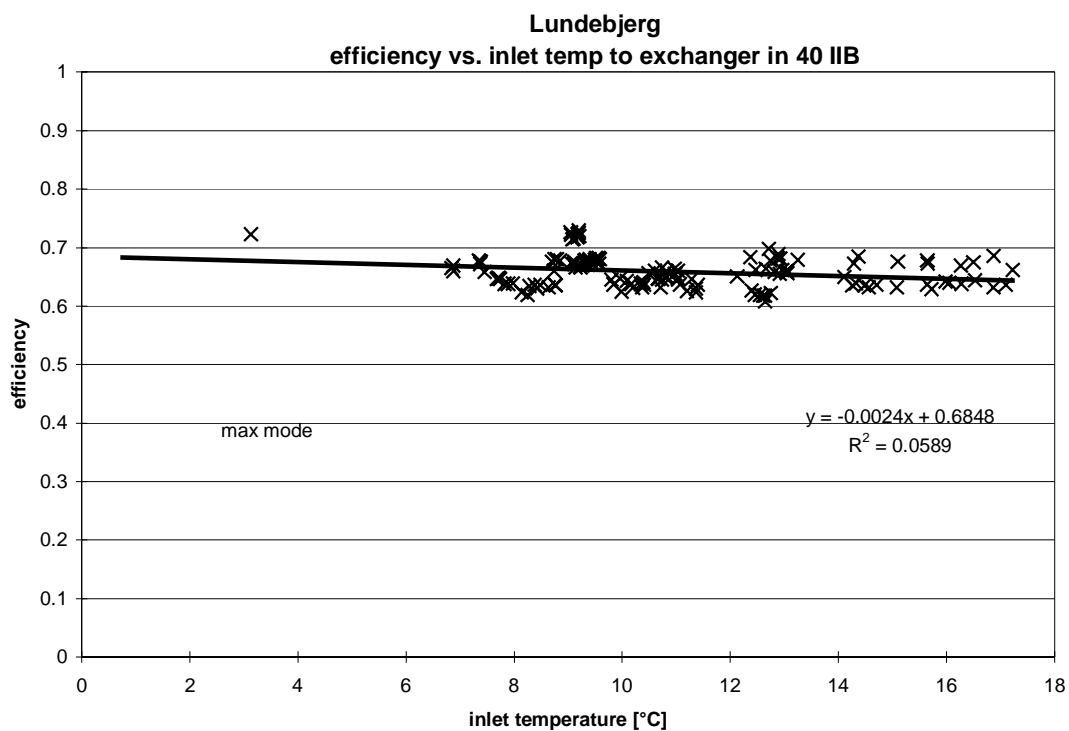


Figure 3.116. The calculated efficiency of the heat exchanger of apartment 40 IIB for year 2000 at max. flow rate.

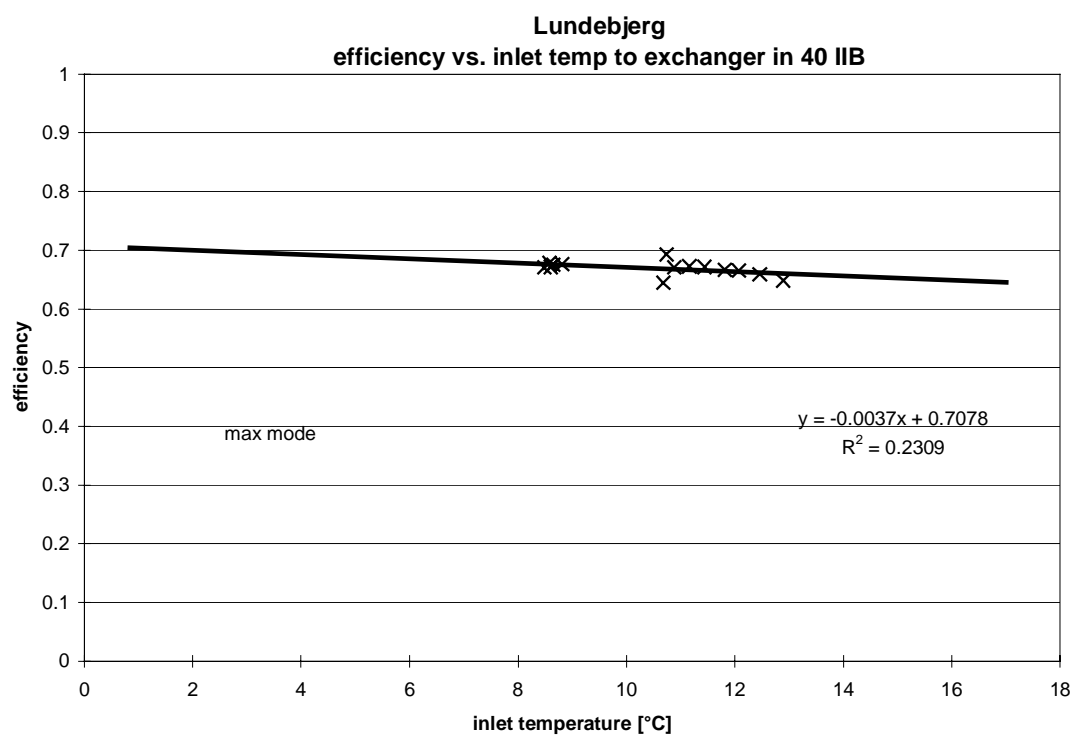


Figure 3.117. The calculated efficiency of the heat exchanger of apartment 40 IIB for year 2001 at max. flow rate.

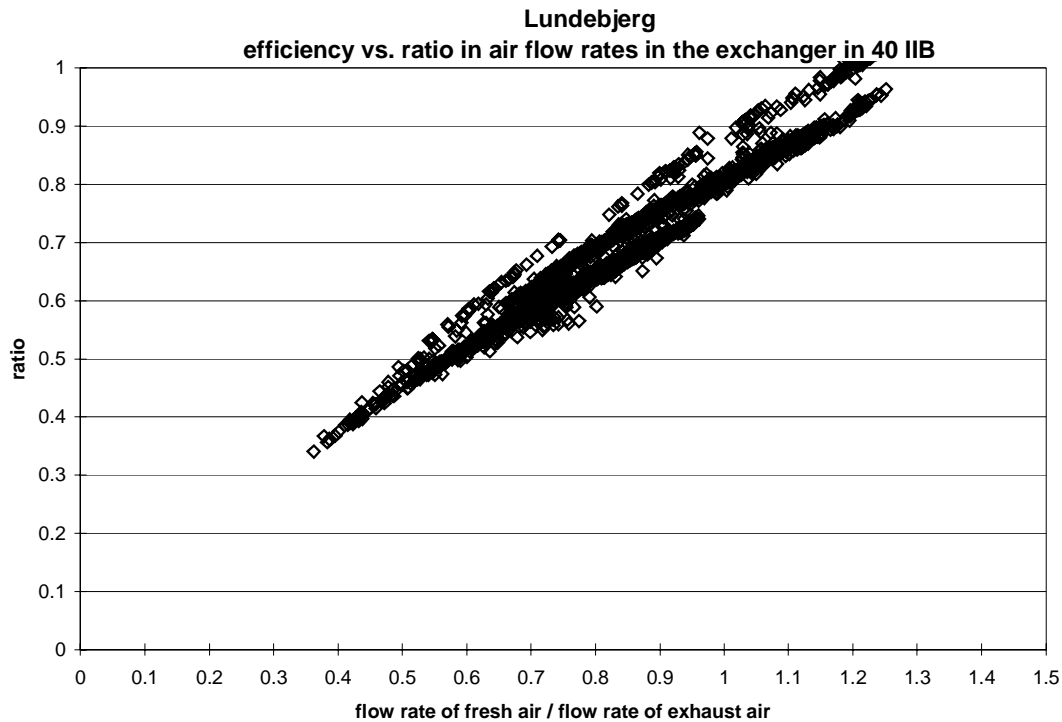


Figure 3.118. The calculated efficiency of the heat exchanger of apartment 40 IIB for year 2000 at min. flow rate as a function of the ratio between the two air flow rates.

Figure 3.119 shows an example of the result when applying equation 3.5 on values from normal air flow mode in 40 IIB during 2001. When comparing figure 3.119 with figure 3.115 a considerable increase in the efficiency of the exchanger is seen. The much lower efficiency in figure 3.115 is due to the unbalance in the air flow rates, but is what actually was experienced in the apartment. Figure 3.119 is the ideal case – however, the air flow rate of fresh air should always be about 10 % lower than the flow rate of fresh air in order to avoid humid air in penetrating the constructions of the building.

Similar calculations as shown in figure 3.119 have been performed on the different flow patterns experienced in the two heat exchangers. Combined efficiencies and flow rates have been obtained for an inlet temperature to the heat exchangers of 17°C. The result of this is shown in figure 3.120 together with the efficiency measured in laboratory (Olsen, 1998). The two points for each group of flow rates is for 2000 and 2001 respectively. The found efficiencies lay except for 40 IIA 75-80 m<sup>3</sup>/h rather nicely on a line. The scattering of 40 IIA 75-80 m<sup>3</sup>/h is believed to be the low number of data points to generate these points. The pattern of the efficiencies is not as expected. It was expected that the efficiency would be highest at high air flow rates and lowest at low air flow rates in a similar way as shown for the efficiencies found in laboratory. The reason for this strange pattern may be a high uncertainty at low flow rates and too few data points at high flow rates.

However, figure 3.120 shows that the efficiency of this type of heat exchanger is between 75 and 85 % and that this efficiency occurs at lower flow rates than measured in laboratory. The exchangers in Lundebjerg have been changed a bit compared to the exchanger tested in laboratory in order to increase the efficiency (Pedersen, 2001). The measured efficiency is rather high and close to aim of the project – an efficiency between 80 and 90 %.

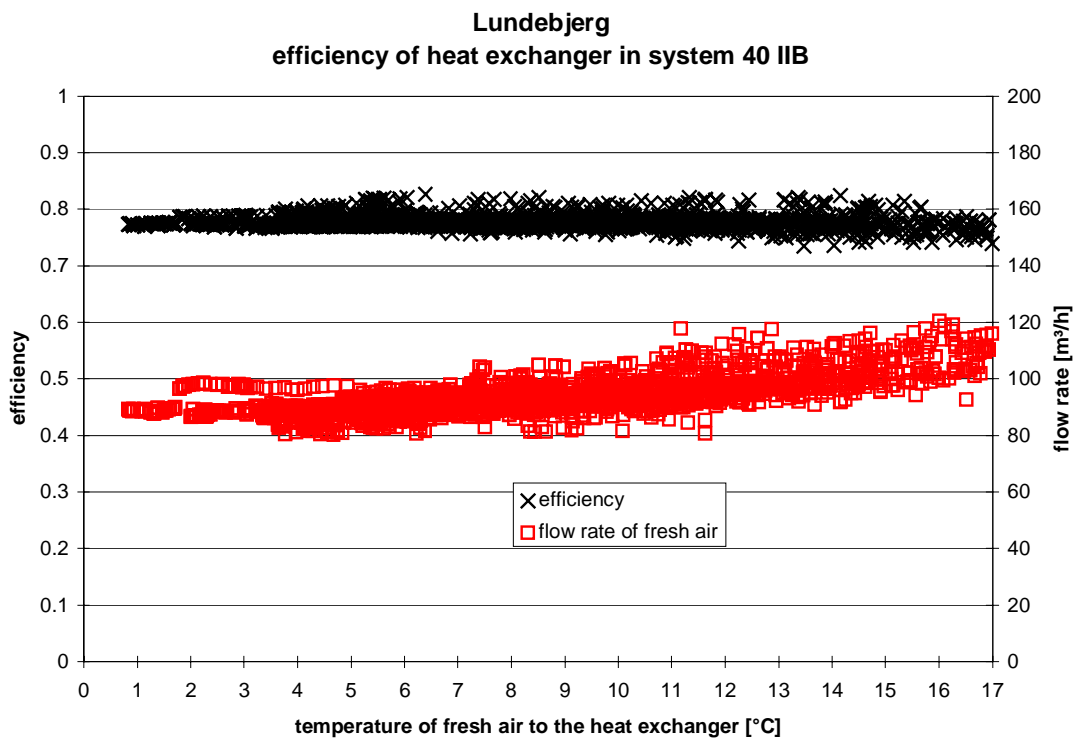


Figure 3.119. The calculated temperature efficiency and smallest air flow rate (here fresh air) of the heat exchanger of apartment 40 IIB for year 2001 at normal flow rate.

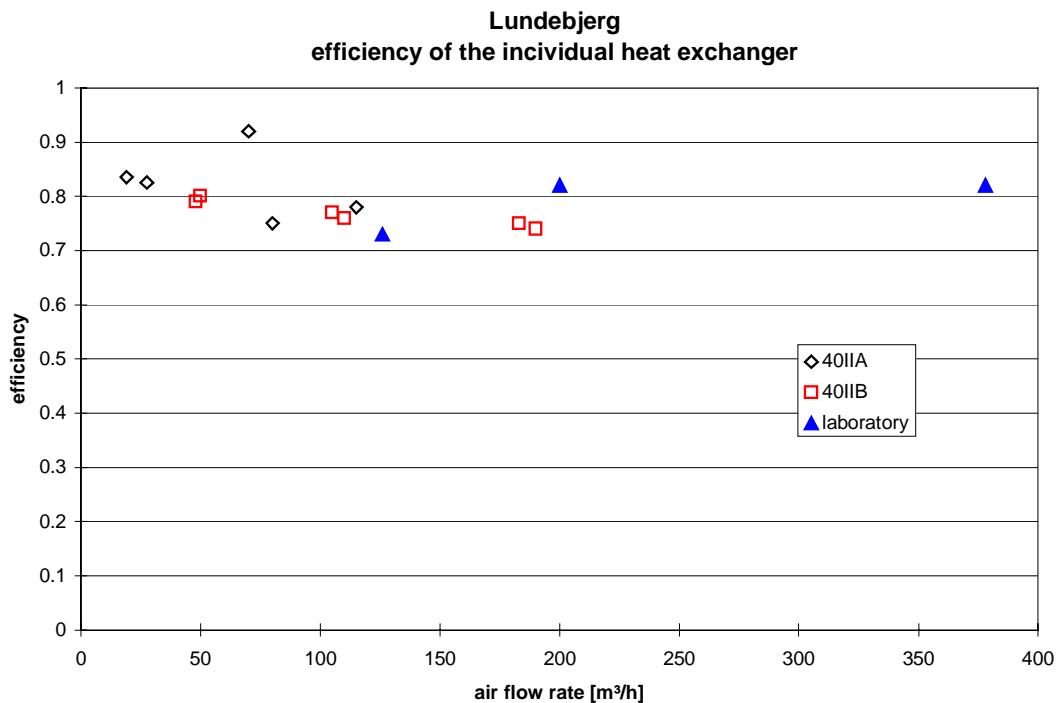


Figure 3.120. The calculated temperature efficiency found at an inlet temperature of 17°C for the heat exchanger of apartment 40 IIA and B for different flow rates together with the efficiencies measured in laboratory on an earlier version of the exchanger.

### Heat exchanger of system 40C

Figure 3.121 shows the calculated heating of the fresh air divided with the calculated cooling of the exhaust air (based on dry temperatures) in the heat exchanger as a function of the inlet temperature to the heat exchanger in system 40 C using data from 2001 (nearly no data are available from 2000). Only data at an inlet temperature below 17°C and air flow rates of fresh air above 200 m<sup>3</sup>/h are included in figures 3.121-122. The reason for the latter is to avoid data from the periods which is very low and/or very fluctuating or when the flow air of fresh air often gets above the flow rate of exhaust air – see figures 3.67-68.

Figure 3.121 shows hardly any condensation – the ratio is between 1.0 and 1.01, however, a little bit temperature dependency is seen.

Figure 3.122 shows the efficiency of the heat exchanger. The very low efficiency (around 50 %) is caused by the low air flow rate of the fresh air side of the heat exchanger – only about half of the air flow on the exhaust side of the heat exchanger.

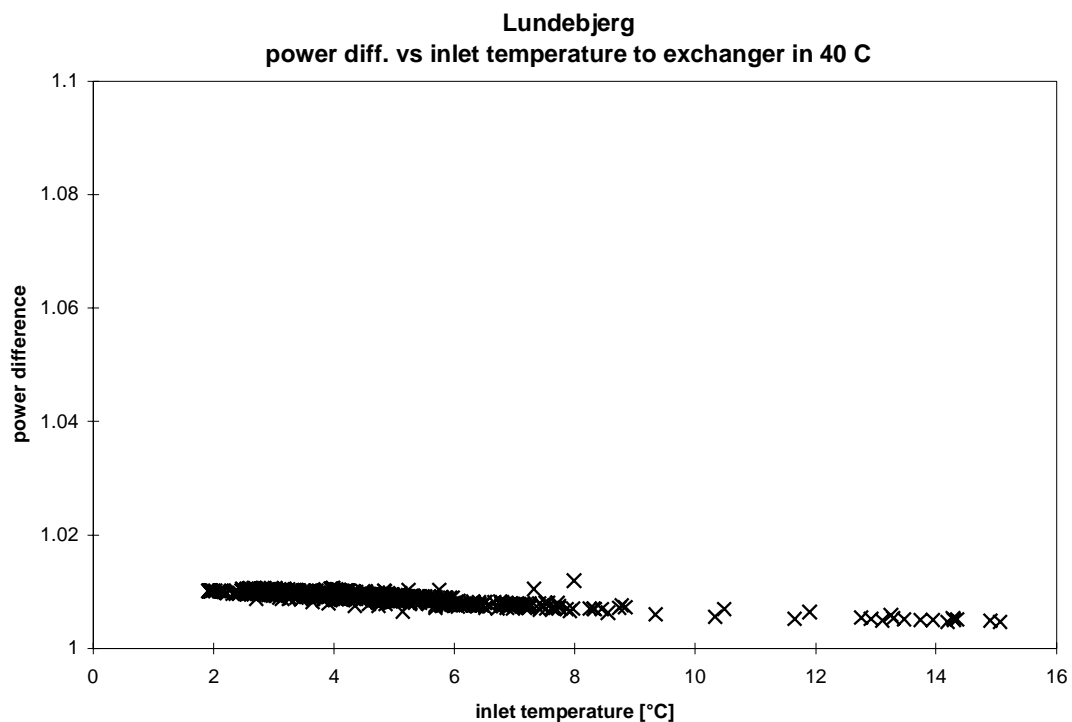


Figure 3.121. The calculated heating of the fresh air divided with the calculated cooling of the exhaust air (based on dry temperatures) in the heat exchanger for year 2001.

As for the heat exchangers in 40 IIA and B the efficiency of the heat exchanger in 40 C has been normalized with respect to the air flow rates – i.e. same air flow rates on both sides of the heat exchanger. This is shown in figure 3.123 where also the smallest air flow rate is shown. As for the heat exchangers in 40 IIA and B the efficiency is now rather high, however, a strange unexplained phoneme is shown in figure 3.123. The efficiency drops rather suddenly at inlet temperatures above 12°C. It is, therefore, difficult to state the efficiency of the heat exchanger, however, the experience from the small exchangers (40 IIA and B) is that the efficiency only drops slowly going towards 17°C (see figure 3.119). If this also is assumed to

be true for the exchanger in 40 C the efficiency at identical flow rates will from figure 3.123 be just above 80 %.

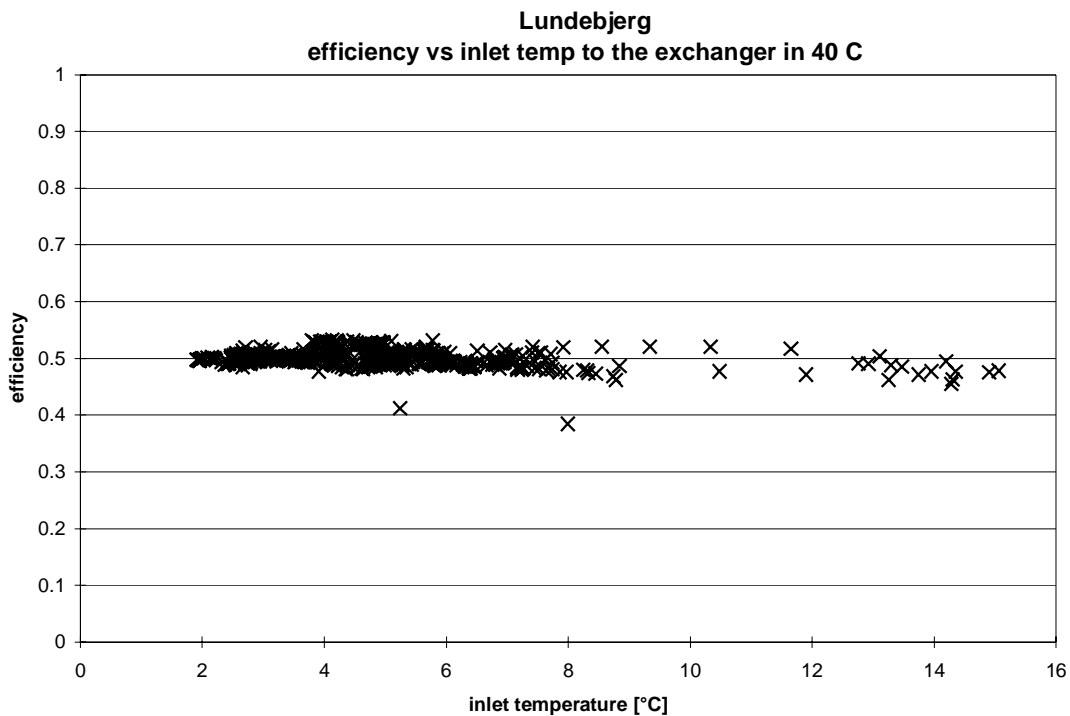


Figure 3.122. The calculated efficiency of the heat exchanger of system 40 C for year 2001.

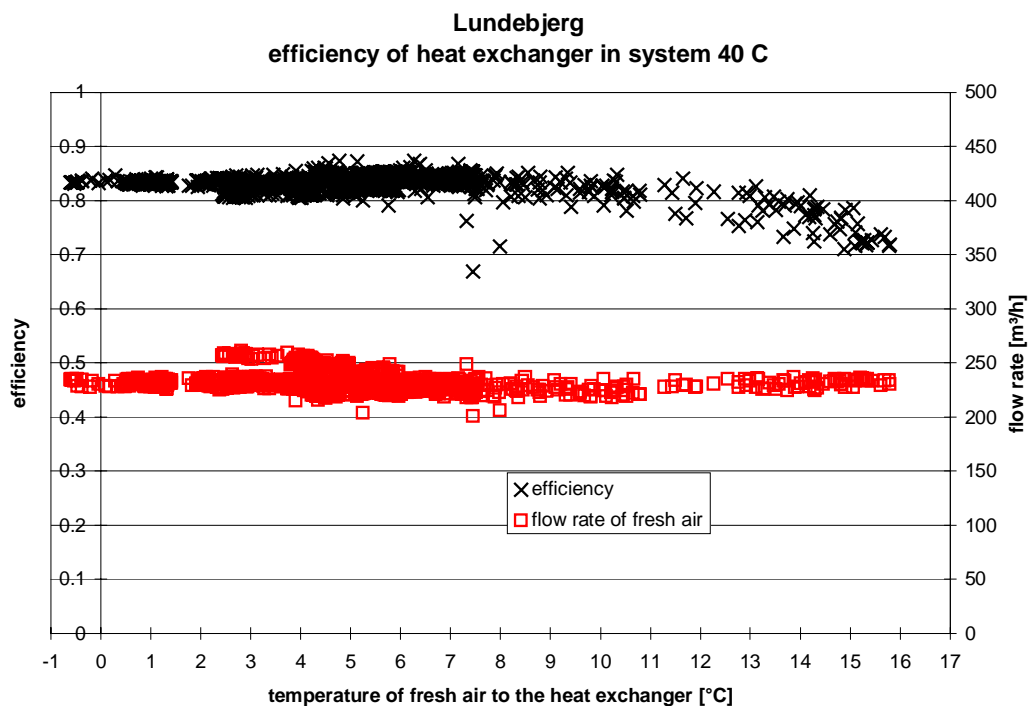


Figure 3.123. The calculated temperature efficiency and smallest air flow rate (here fresh air) of the heat exchanger of 40 C for year 2001.

Figure 3.123 shows that the flow rate of fresh air was around 230 m<sup>3</sup>/h while the design flow rate is up to 1000 m<sup>3</sup>/h. It should thus be possible to reach a higher efficiency if the flow rates are increased.

### 3.2.2. Fan power

The power to the fans of the ventilation systems was measured during February and March 2001. Figures 3.124-126 show the dependency of the fan power on the total flow rate (exhaust flow rate for 36 B) through the three systems: 36 B, 40 IIA and 40 C. The total flow rate is the sum of the flow rate of fresh air and exhaust air.

System 36 B has mainly been run at one flow rate so it is not possible to obtain an equation based on regression. This is, however, done for system 40 IIA and 40 C. The regression lines are also shown in figure 3.97-98.

$$\text{System 40 IIA: fan power} = 0.000243 \cdot \text{flow}^2 + 0.0727 \cdot \text{flow} \text{ [W]} \quad (3.6)$$

$$\text{System 40 C: fan power} = 0.000218 \cdot \text{flow}^2 - 0.0105 \cdot \text{flow} \text{ [W]} \quad (3.7)$$

where flow is the total flow rate – i.e. the sum of fresh air and exhaust air

The flow rates given in the Danish building code for exhaust ventilation is 126 m<sup>3</sup>/h while it for balanced systems is 126 + 113 = 239 m<sup>3</sup>/h. Using the above equations the fan power for the flow rates given in the building code may be found for the three systems – the uncertainty for system 36 B and 40 C is high as 3 · 126 m<sup>3</sup>/h = 378 m<sup>3</sup>/h and 3 · 239 = 717 m<sup>3</sup>/h is outside the validity of figures 3.124 and 3.126.

To the found fan power the power loss of the ac/dc converter has to be added. The power loss of the ac/dc converter is:

$$\text{power loss} = 5.6 + 0.0278 \cdot P \text{ [W]} \quad (3.8)$$

where P is the total power consumption from the grid of the fans incl. the loss of the ac/dc converter

The total power consumption of the three ventilation systems at flow rates given in the Danish building code is shown table 3.1.

System	total flow rate W	fan power W	losses in ac/dc con- verter W	total power demand W	total power demand per dwelling W
36 B	378	70	8	78	26
40 IIA	239	31	7	38	38
40 C	717	105	9	114	38

Table 3.1. The power consumption of the fans of the three ventilation systems at the air flow rates specified by the Danish building code.



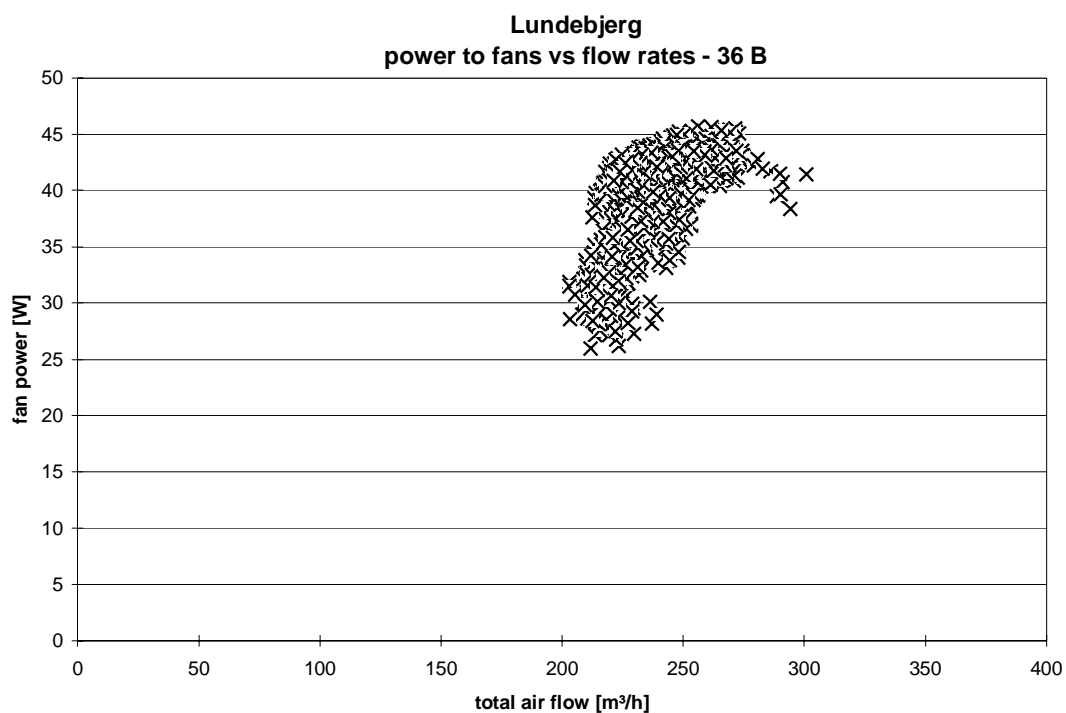


Figure 3.124. The dependency of the fan power to system 36 B on the exhaust flow rate.

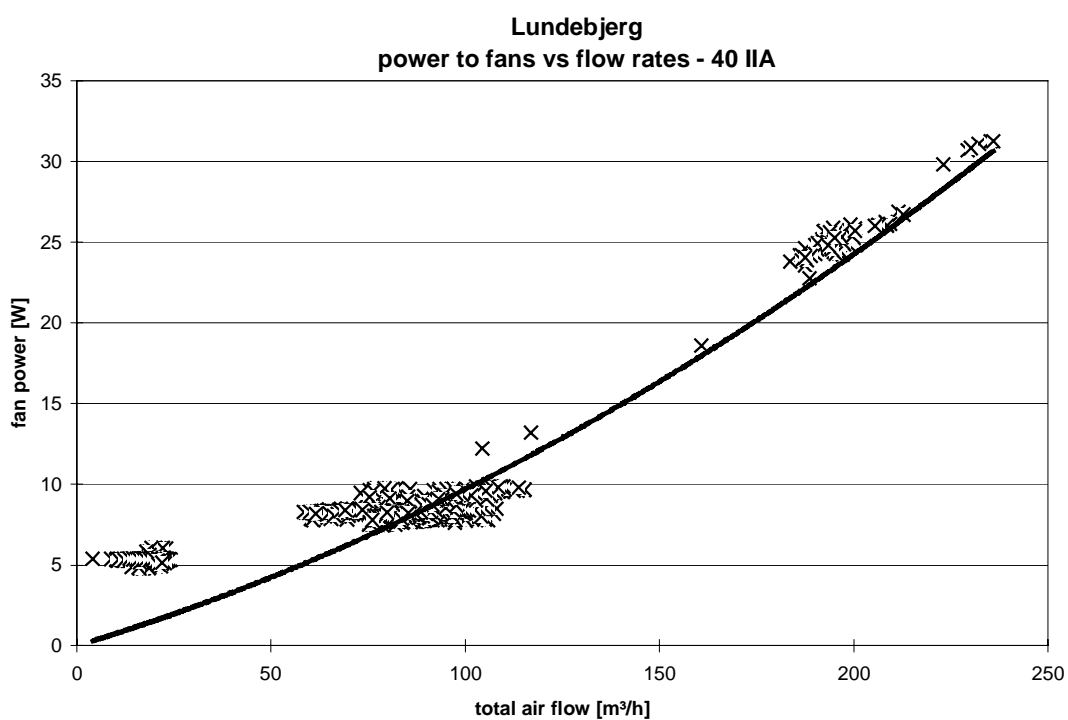


Figure 3.125. The dependency of the fan power to system 40 IIA on the total flow rate.

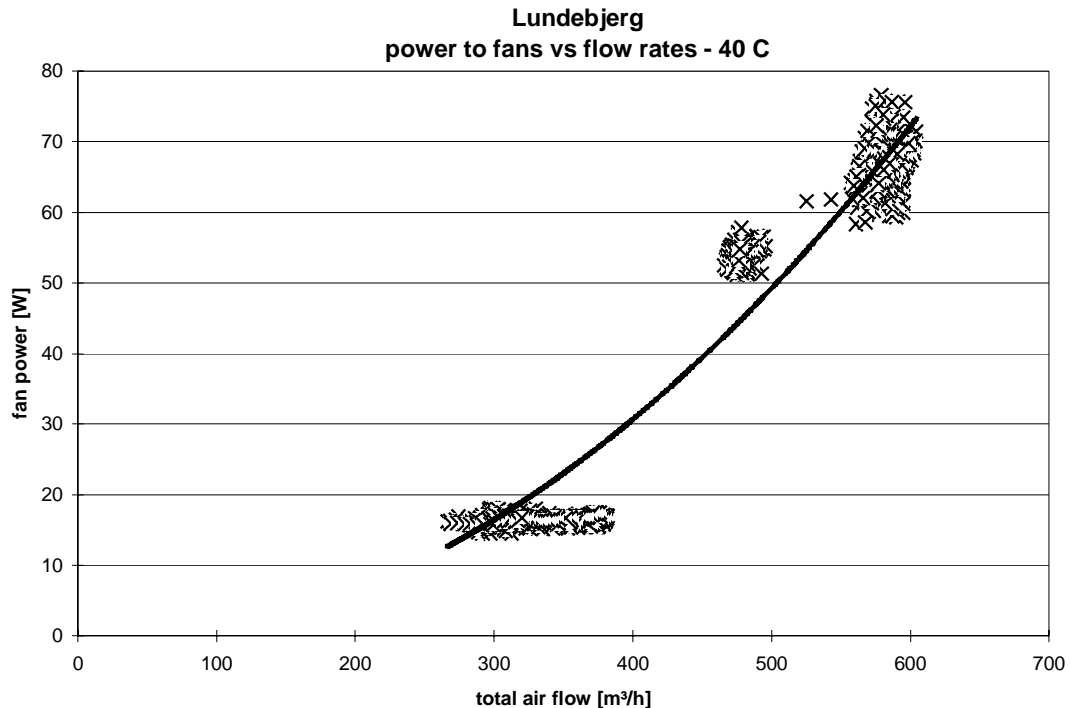


Figure 3.126. The dependency of the fan power to system 40 C on the total flow rate.

The max fan power for balanced ventilation systems are in the Danish building code given to 87 W – there is no demand for exhaust ventilation. The fan power at the actual systems is thus 44% of the requirements in the building code. The fan powers in figures 3.124-126 and table 3.1 should be divided with 0.96 (efficiency of the PV-mixer in grid mode – see later) when then the power is delivered entirely from the grid via the PV-mixer.

When comparing figures 3.124-126 with table 1.6 one reason for the difficulties in balancing the ventilation systems is seen. The fans were during the measuring period only run at 5-33 % of their max power. In a constant pressure system this will create problems as the fans are run far away from their optimum. It is, thus, difficult for the fans to obtain a constant pressure leasing to the fluctuations in the air flow rates as seen in section 3.1.

### 3.2.3. Efficiency of the solar ventilation chimneys as solar air collectors

Figures 3.85-86 show that the efficiency of the chimneys as solar air collector over the day and for different days appears rather differently. This is as already explained due to scattering in the solar radiation and the air flow rates, the thermal mass of the chimneys but also due to the wind on the PV-panels. In order to determine the efficiency of the chimneys as solar air collectors it is necessary to find periods with nearly stationary conditions. An example of a day with almost steady state conditions is shown in figure 3.127 for February 15, 2001.

The efficiency of chimney 40 is in figure 3.127 found to be 13% at a flow rate of 37 m³/h. Several of such coupled values have been found for both chimneys and are shown in figure 3.128. In figure 3.128 are also shown the regression line and the regression equation based on the shown values. The air flow rates are normalized – i.e. divided by the area of the PV-array of the solar ventilation chimneys. The scattering of the values in figure 3.128 is due to differ-

ent wind speeds along the PV-panels. Figure 3.128 further shows the corresponding percentage of the useful solar radiation, which was utilized in the PV-panels for generation of electricity.

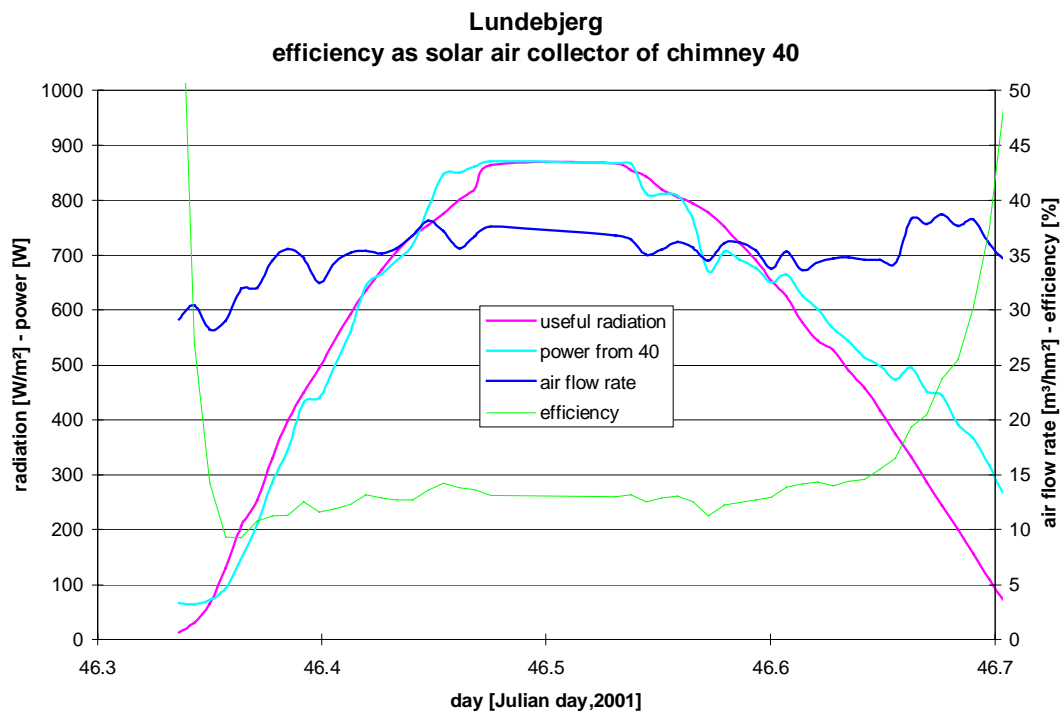


Figure 3.127. Day with nearly steady state conditions for determination of the efficiency of the solar ventilation chimneys as solar air collector.

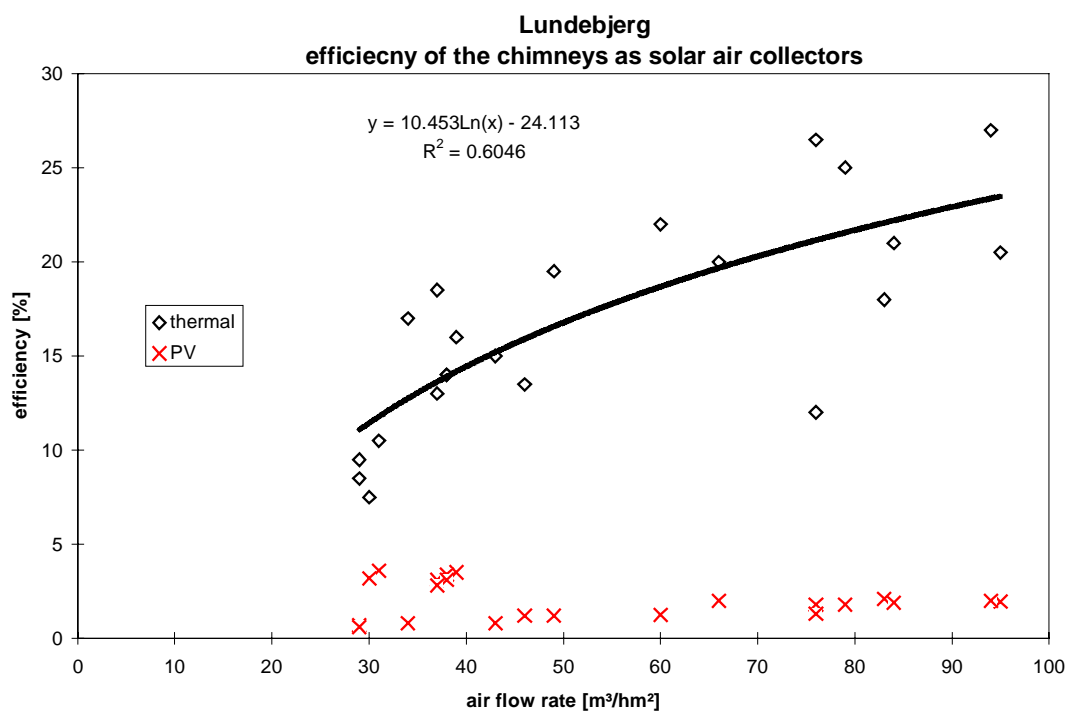


Figure 3.128. The efficiency of the solar ventilation chimneys as solar air collectors.

Figure 3.129 show the efficiency of the solar ventilation chimneys as solar air collectors from figures 3.128 together with a commercial Danish solar air collector (Jensen, 1994) – one of the most efficient solar air collectors in the world (Fechner, 1999). The solar air collector has a double cover and a very efficient absorber, so it is no wonder that the solar ventilation chimneys are less efficiency, as they have no cover to protect the absorber and that no attempt has been made to increase the heat transfer between the absorber and the air by e.g. fins.

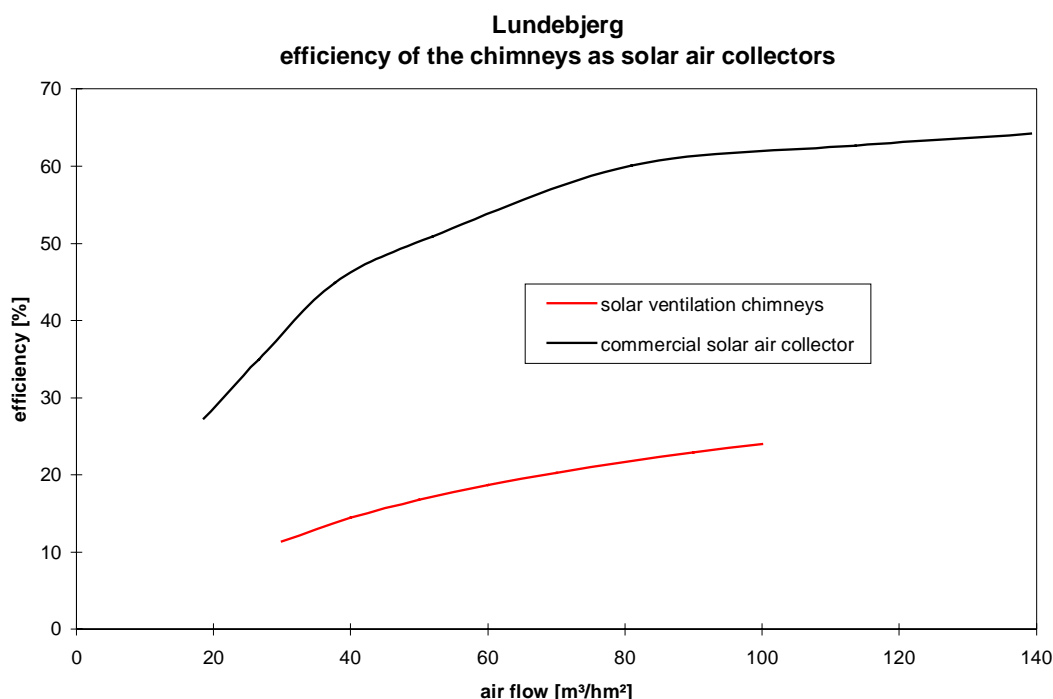


Figure 3.129. The efficiency of the solar ventilation chimneys as solar air collectors compared with a commercial Danish solar air collector.

In order to evaluate if the solar ventilation chimneys thermally perform as they should the efficiency from figure 3.128 has been compared with calculations with a new simulation tool based on TRNSYS (Bosanac et al, 2001).

The solar ventilation chimney has as closely as possible been modelled with the new tool. One problem with the model is, however, that is developed for smaller air gaps behind the PV-panels – i.e. always a fully developed turbulent flow behind the PV-panels – it is not possible to model laminar flows as was present in the chimneys as described later.

The results from the simulations are shown together with the curve from figure 3.128 in figure 3.130. Although not perfect a better match is shown in figure 3.130 than in 3.129. In figure 3.128 it is seen that the utilized solar radiation for electricity production is 2-4 %. The efficiency of the solar ventilation chimneys in figure 3.130 (the red curve) should, therefore, be compared with the green curve in figure 3.130 (3 % PV). The difference between these two curves is partly due to the fact that the green curved is calculated using equations for turbulent flow rather than laminar flow and partly because the model assumes an even air flow behind the PV-panels while this hardly may be the case in the solar ventilation chimneys due to the low air speed in the solar ventilation chimneys (below 0.5 m/s – see later), the obstruction

created by the vertical profiles carrying the PV-panels (see figure 1.29) and the central location of the outlet from the air cap of the chimneys (see figure 1.27).

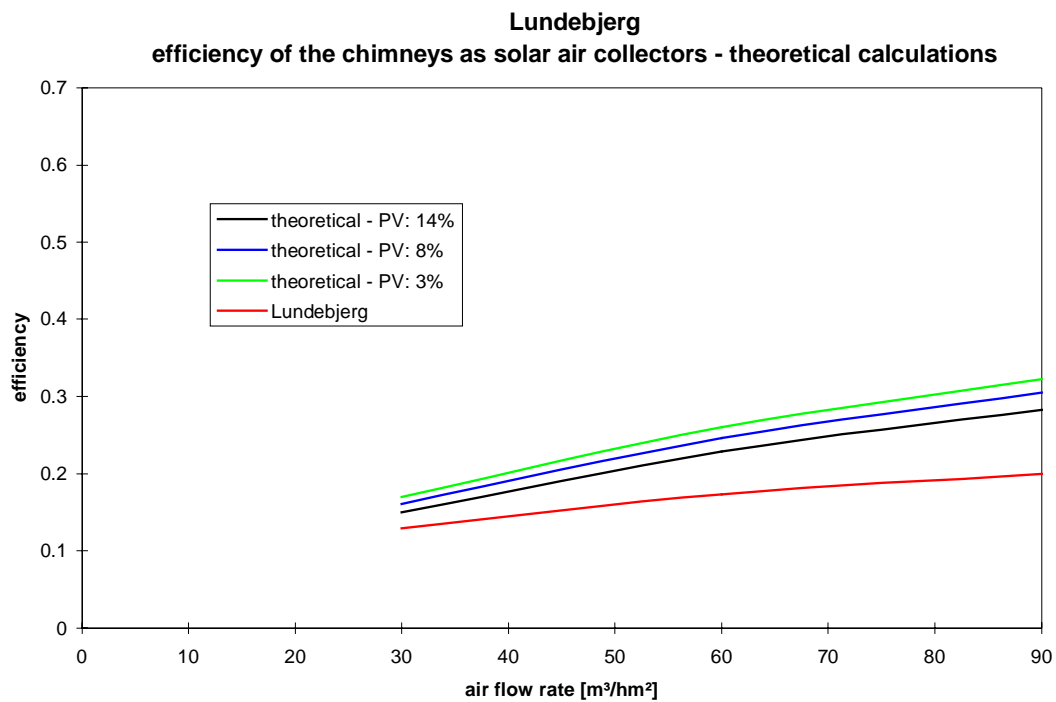


Figure 3.130. The measured and modelled efficiency of the solar ventilation chimneys. The modelled efficiency is shown for three efficiencies of the PV-panels.

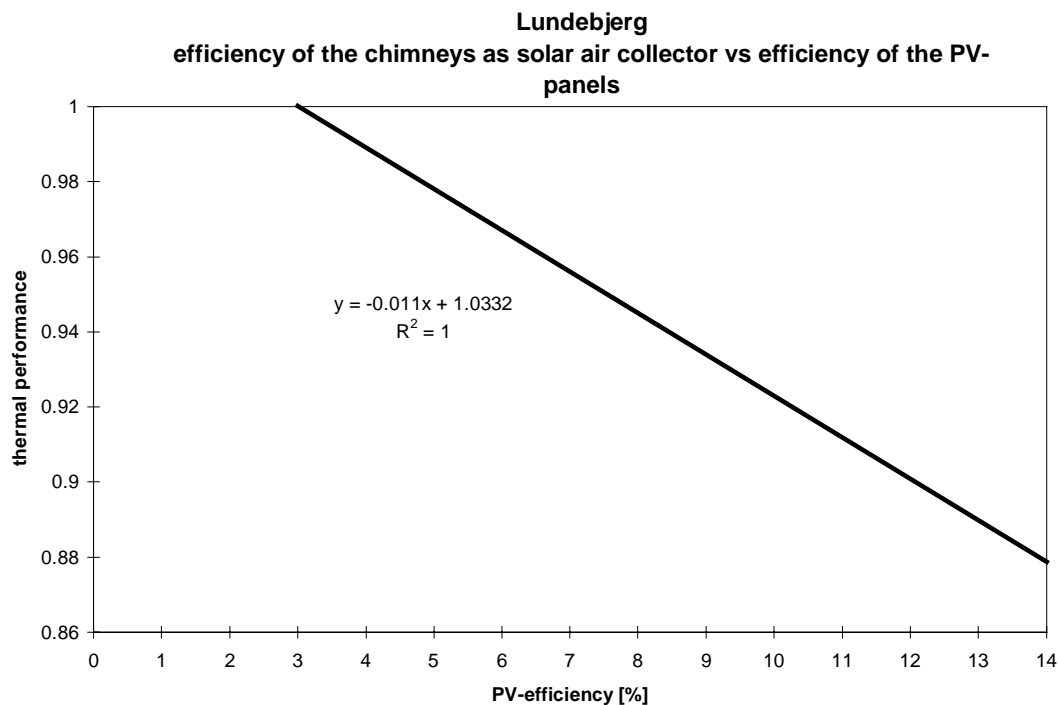


Figure 3.131. The dependency of the modelled efficiency on the efficiency of the PV-panels.

Although the match is not perfect it is believed that effect of the percentage of produced PV-power on the thermal efficiency of the solar ventilation chimneys shown with the model also is valid for the actual chimneys within a reasonable uncertainty. The modelled influence of the produced PV-power on the thermal efficiency of the solar ventilation chimneys is shown in figure 3.131. Figure 3.131 shows a linearly dependency. The thermal efficiency of the solar ventilation chimneys will thus decrease from 20 % at a flow rate of about 70 m<sup>3</sup>/hm<sup>2</sup> to 17.5 % when going from 3 % utilization of the solar radiation as PV-power to 14 %.

The equation in figures 3.128 and 3.131 will be used in section 3.3 to evaluate the savings due to the pre-heating of the fresh air in the solar ventilation chimneys.

The PV-facade at 40 IIA is also run as a solar air collector, however, due to the incorrect running of that system nearly only data at min. air flow rate are available as shown in figure 3.132. The figure also show the regression line for the efficiency of the solar ventilation chimneys. The figure indicates that the PV-facade is as efficient as the solar ventilation chimneys at low flow rates – however, no data are available for the chimneys at this low flow rates and the efficiency of the PV-facade is further rather uncertain due to the large uncertainty on the air flow measurement at such low flow rates. Figure 3.132 further indicates that the PV-facade is less efficient at higher air flow rates (around 70 m<sup>3</sup>/hm<sup>3</sup> equal to 119 m<sup>3</sup>/h), however, the few data points here makes the figure inconclusive. The lower efficiency at higher air flow rates was, however, expected due to the missing damper in the top of the PV-facade – i.e. the pressure drop across the PV-facade is expected to increase more rapidly than across the inlet grid where the damper is missing. The percentage of air taken from behind the PV-panels is expected to decrease with increasing air flow rates.

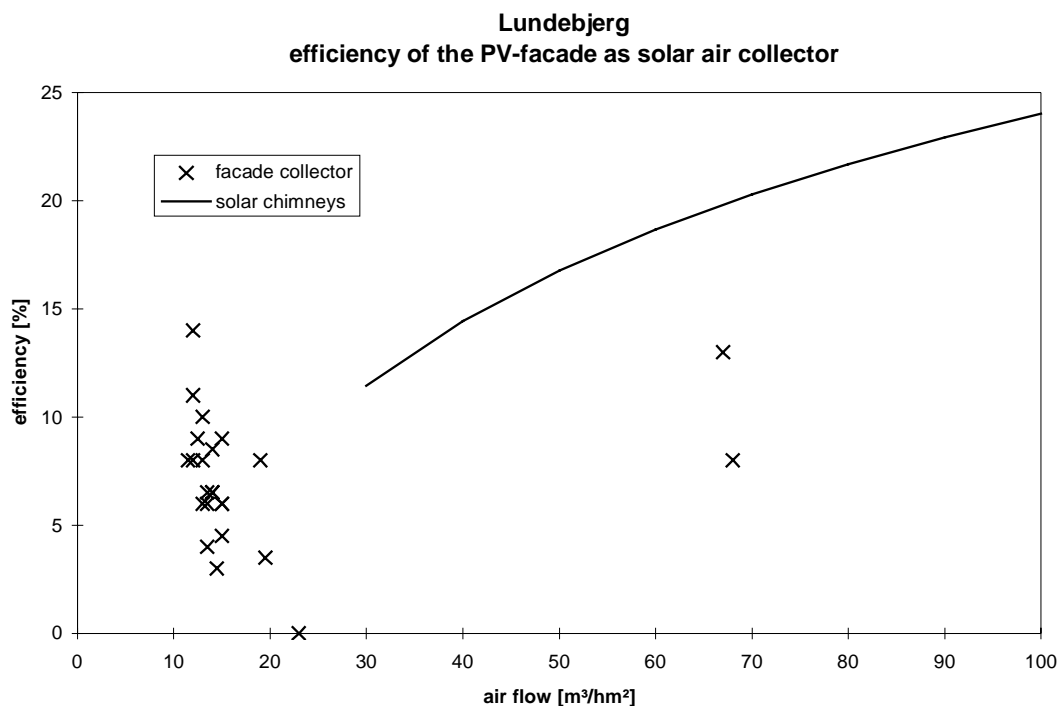


Figure 3.132. The efficiency of the PV-facade as solar air collector.

Figure 3.133 shows instead the heating of the air (the temperature increase) across the PV-facade – the figure shows that the heating hardly gets above 5 K, which supports the conclu-

sion in section 3.1.3 about the benefit of the PV-facade as solar air collector. However, the low heating of the air in the PV-facade is also due to the east facing of the PV-facade. The facade is hit by far less solar radiation than the solar ventilation chimneys and the peak value of the solar radiation occurs during a shorter period than for the solar ventilation chimneys. Due to the thermal mass of the PV-panels lower peak temperatures may be expected for the PV-facade. However it have to be concludes that with the present construction of the PV-facades and the present orientation the PV-facades are of little benefit.

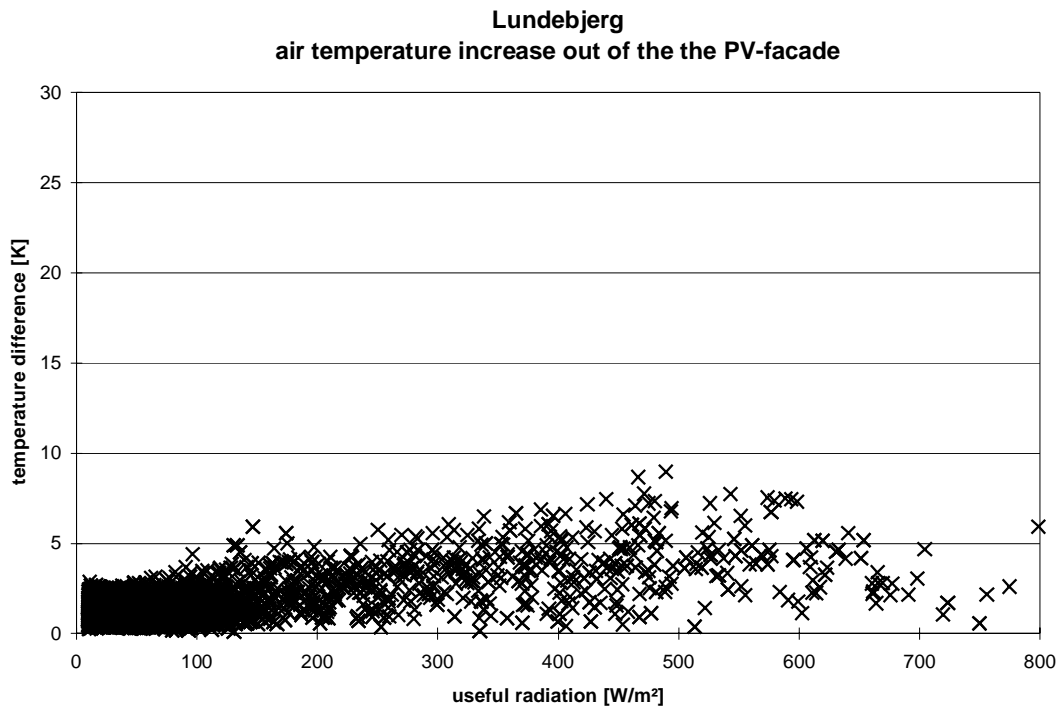


Figure 3.133. The temperature increase of the fresh air when passing through the PV-facade dependent on the useful solar radiation on the PV-facade.

### 3.2.4. Temperatures of the PV-panels

One of the objectives of the project was to investigate the possible increase in electrical performance of the PV-panels due to the cooling of the PV-panels by the air flow behind the PV-panels.

Figures 3.134-136 show the temperature difference between the PV-panels in the three chimneys and in the PV-gable measured at the backside of the PV-panels shown in figures 2.17 and 2.5. The temperature difference is shown dependent on the useful solar radiation on the PV-panels. The shown values lay for each PV-panel temperature nicely around a line, which is shown in the figures together with the equation for the line found by regression. The scattering around the lines is partly due to the thermal mass of the PV-panels, which brings the PV-panel out of phase with the solar radiation. However, the main reason for the scattering is although believed to be the influence of the wind on the PV-panels.

The temperature of the PV-panels on chimney 38 and 40 are almost identical although the air flow rate behind the PV-panels are very different as shown in figure 3.137. That the two temperatures are identical is shown in figure 3.138 where the two temperature differences from

same scans are plotted against each other. The reason for the identical temperatures is the very low air speed behind the PV-panels – less than 0.5 m/s. The air speed is thus in the same order of magnitude as a buoyancy driven air flow. The difference in air flow due to the fans of the systems is thus of no importance. The dampers in the top of the PV-gable and chimneys have due to the low temperatures not been open during the period, where the values in figures 3.134-136 have been obtained – only internal air circulation has thus occurred in chimney 36 and the PV-gable. When comparing the regression lines of the four cases – figure 3.139 it is seen that the PV-panel temperature difference of chimney 36 and the PV-gable also are identical and 16 % higher than the PV-panel temperature of chimney 38 and 40.

Based on the findings in figures 3.134-139 it can be concluded that:

- the air speed behind the PV-panels in the chimneys and the PV-gable is too low to cool the PV-panels more than a buoyancy driven air flow
- without forced air flow/open dampers in the top the PV-panels will obtain a temperature increase compared to ambient, which is 16 % higher than with an air flow - forced or buoyancy driven
- a decrease of 16 % in the temperature level due to the air flow behind the PV-panels will lead to an increase in electrical performance of the PV-panels of 2.5 % at a useful radiation level of 800 W/m<sup>2</sup>. The cooling of the PV-panels by the air flow behind the PV-panels is thus low leading only small increases in the PV generated power.
- a higher performance of chimney 38 and 40 as solar air collector would have been achieved with a smaller air gap behind the PV-panels (i.e. higher air speed) and thereby a better cooling of the PV-panels. However, a smaller air gap will create a higher pressure drop and thereby reduce the air flow and cooling of the PV-panels during the summer with only buoyancy driven flow

Please remember to add the ambient temperature to figures 3.134-36 and 3.139 in order to obtain the absolute temperature of the PV-panels.

The PV-panel temperature has also been found for the PV-facade dependent on the useful solar radiation – figure 3.140. For the location of the sensor see figure 2.11. Although main part of the available data are at low radiation levels figure 3.140 shows same pattern as figure 3.134-36. But the regression line is more like the regression lines for the gable and chimney 36 – i.e. without any air flow. This indicates opposite section 3.1.3 that no air has been sucked from behind the PV-facade. The numbers of data at higher radiation levels are, however, too few to make any firm conclusion on this.

### **3.2.5. Air temperatures in the PV-gable**

One of the aims of the PV-gable was to preheat fresh air to the dwellings behind the gable. The temperature level of the air behind the PV-panels is, therefore, investigated in the following. Figures 3.141-143 show the temperature difference between ambient and the air at the inlet to the three floors.

The air temperature behind the PV-panels in the PV-gable is as for the PV-panels very scattered due to the thermal mass of the PV-gable and the influence of wind. Regression lines has



based on the measured values been found for all the three temperatures – these are seen in the figures together with the equations. The regression lines are further compared in figure 3.144. Figure 3.144 shows that the air temperature behind the PV-panel increases with increasing height.

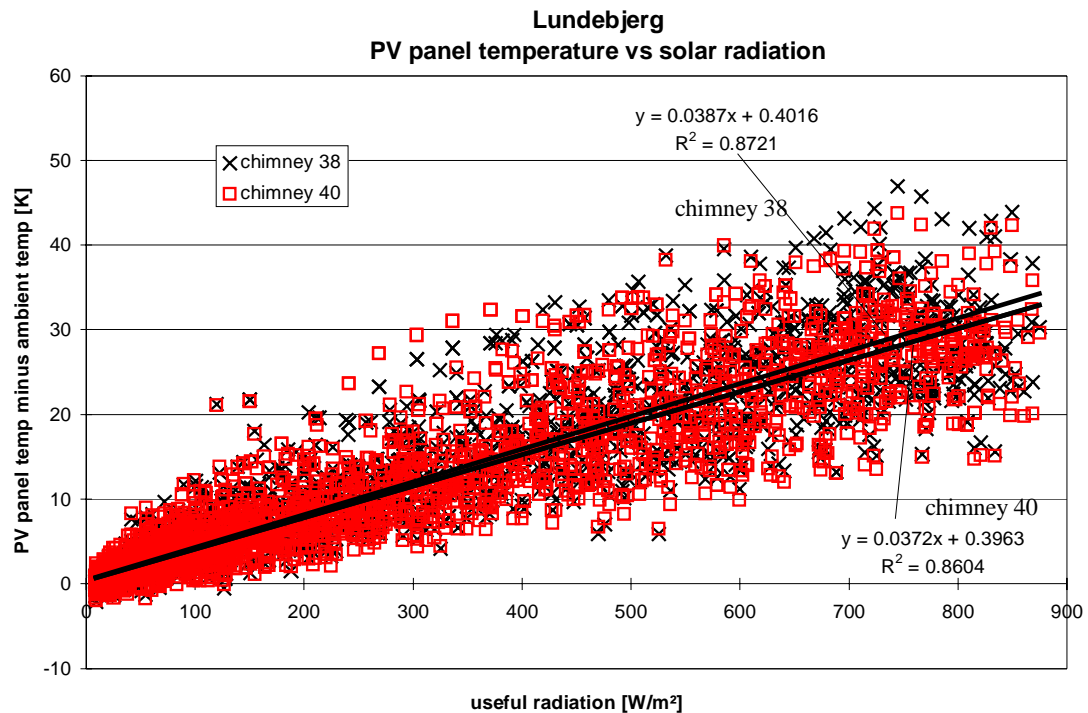


Figure 3.134. The temperature difference between a PV-panel on chimney 38 and 40 and ambient dependent on the useful solar radiation on the PV-panel.

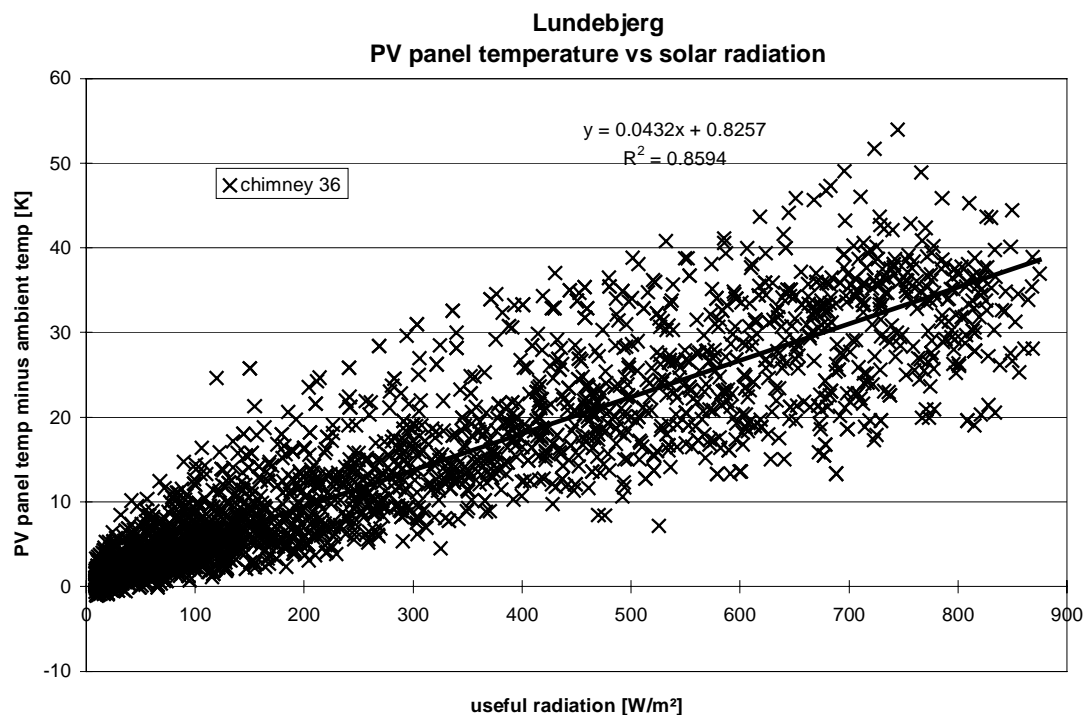


Figure 3.135. The temperature difference between a PV-panel on chimney 36 and ambient dependent on the useful solar radiation on the PV-panel.

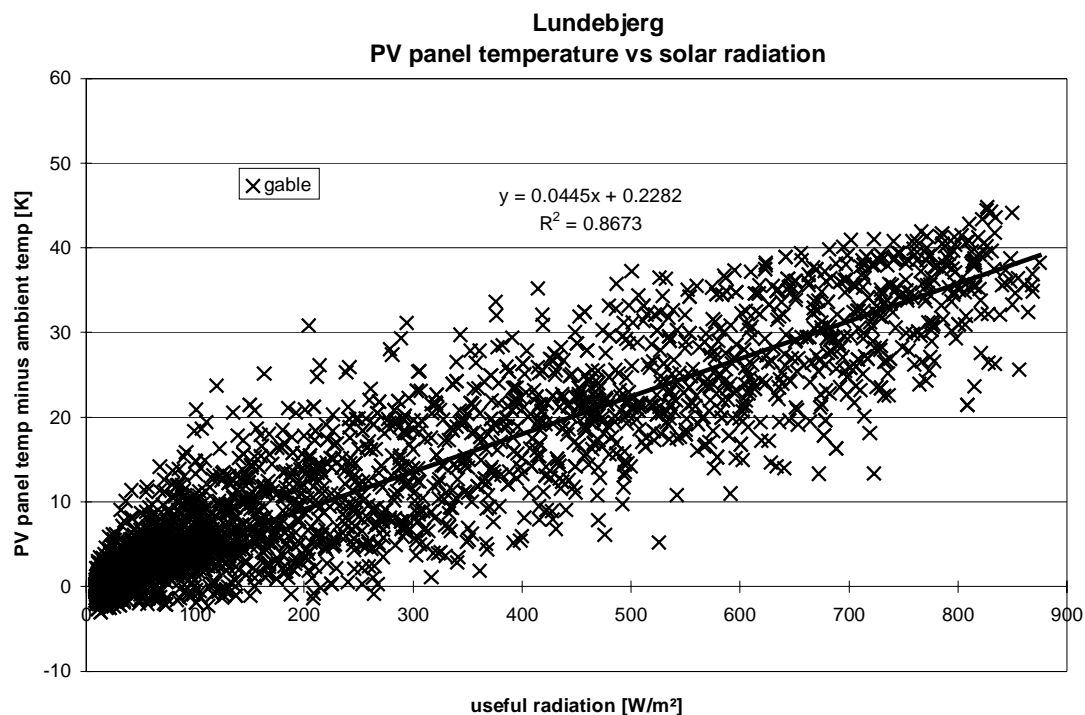


Figure 3.136. The temperature difference between a PV-panel on the PV-gable and ambient dependent on the useful solar radiation on the PV-panel.

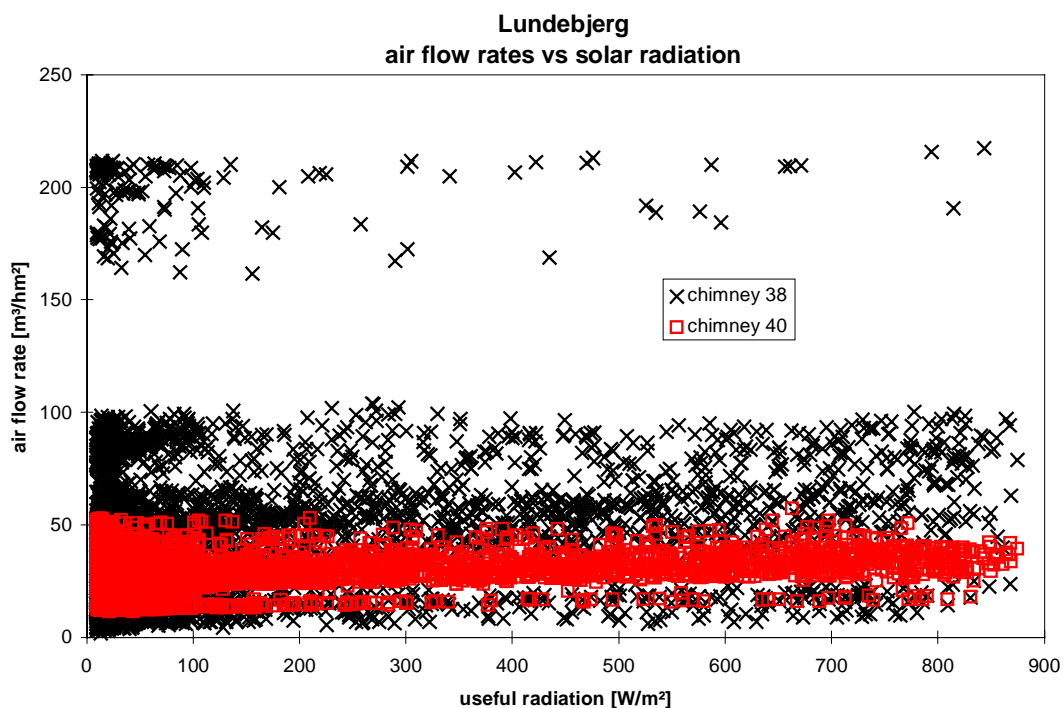


Figure 3.137. The air flow rate through chimney 38 and 40 as a function of the useful solar radiation on the PV-panel.

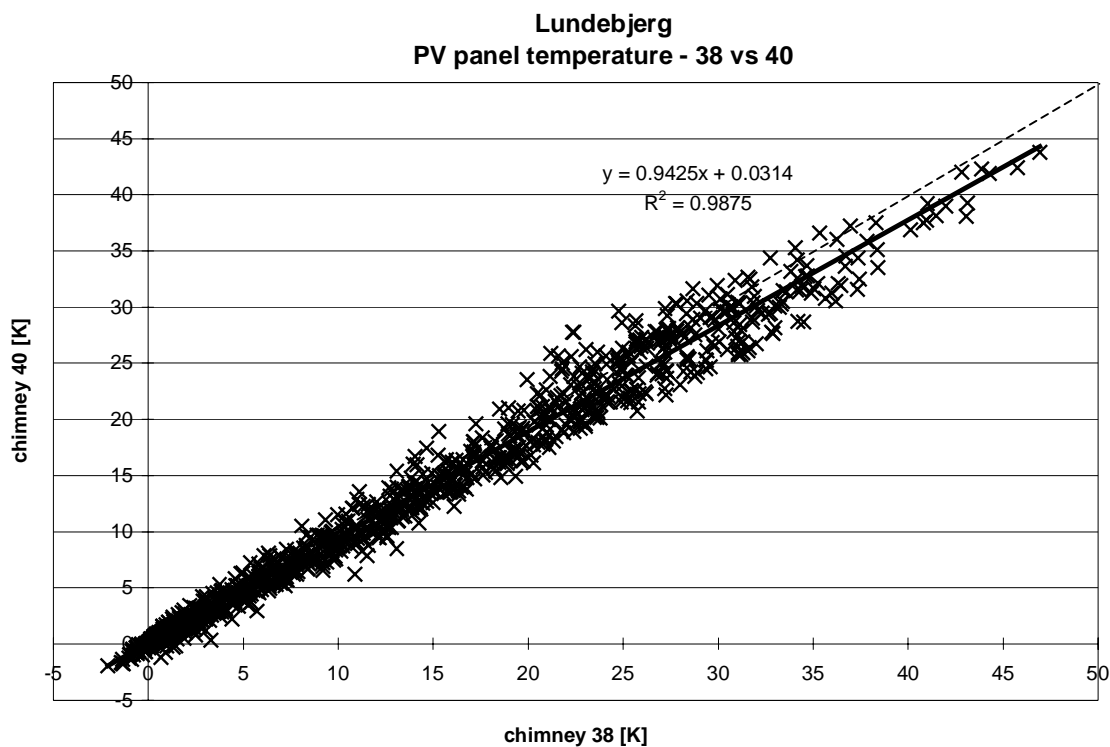


Figure 3.138. PV-panel temperatures minus the ambient temperature for chimney 38 and 40 from same scans plotted against each other.

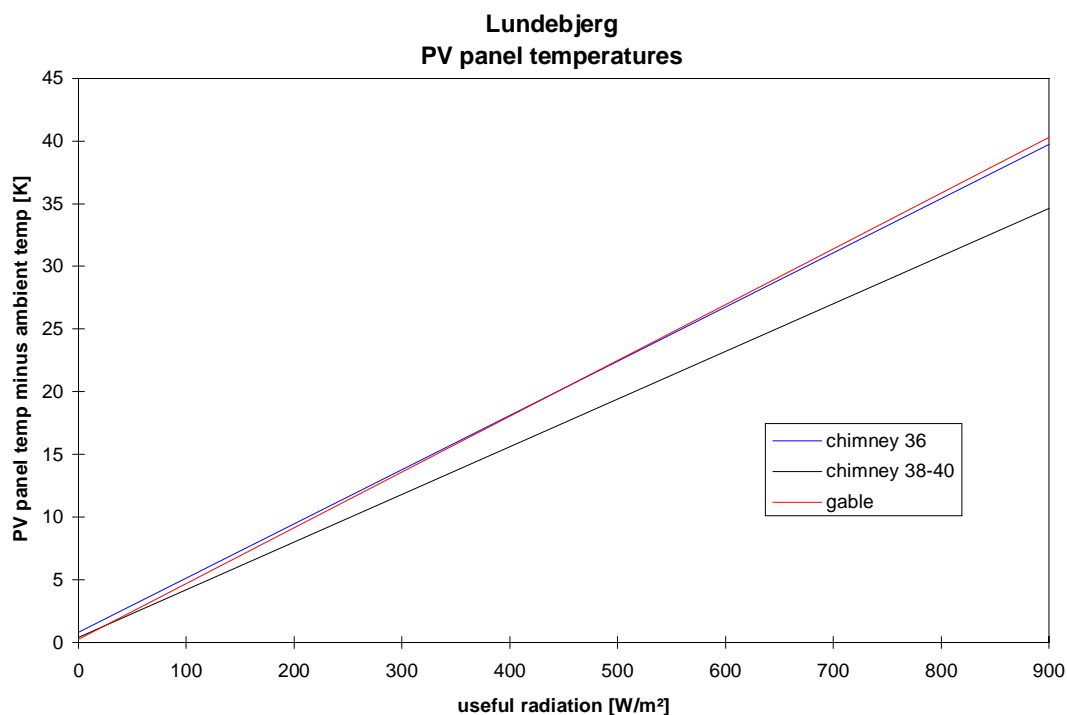


Figure 3.139. The temperature difference between a PV-panel on the three chimneys and the PV-gable and ambient dependent on the useful solar radiation on the PV-panel.

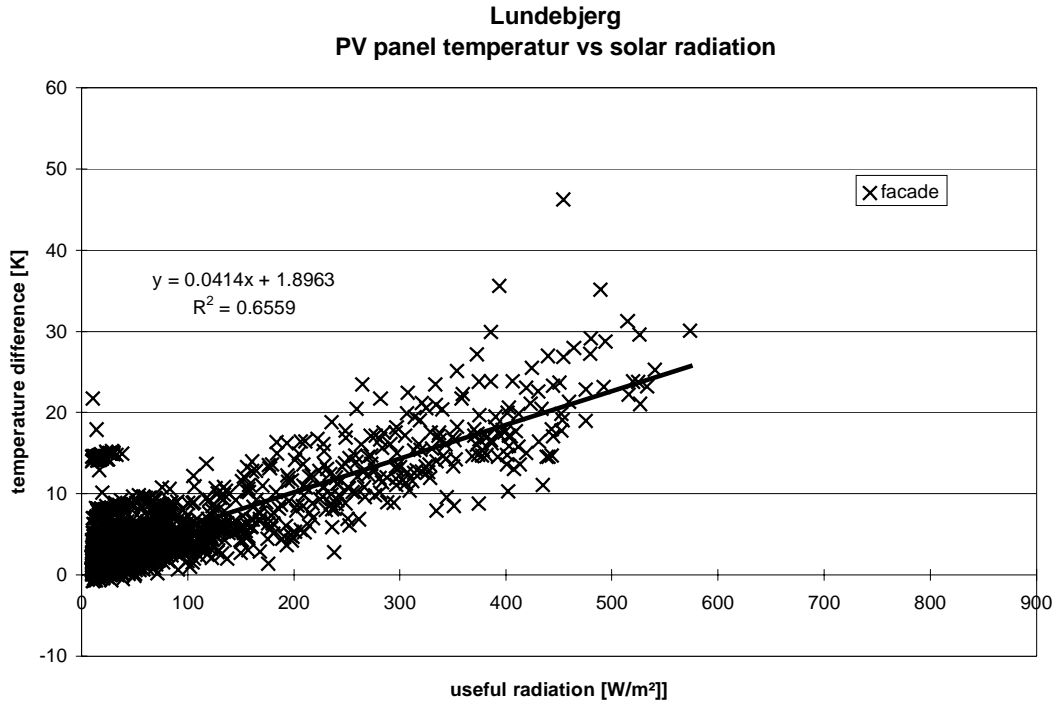


Figure 3.140. The temperature difference between a PV-panel on the PV-facade and ambient dependent on the useful solar radiation on the PV-panel.

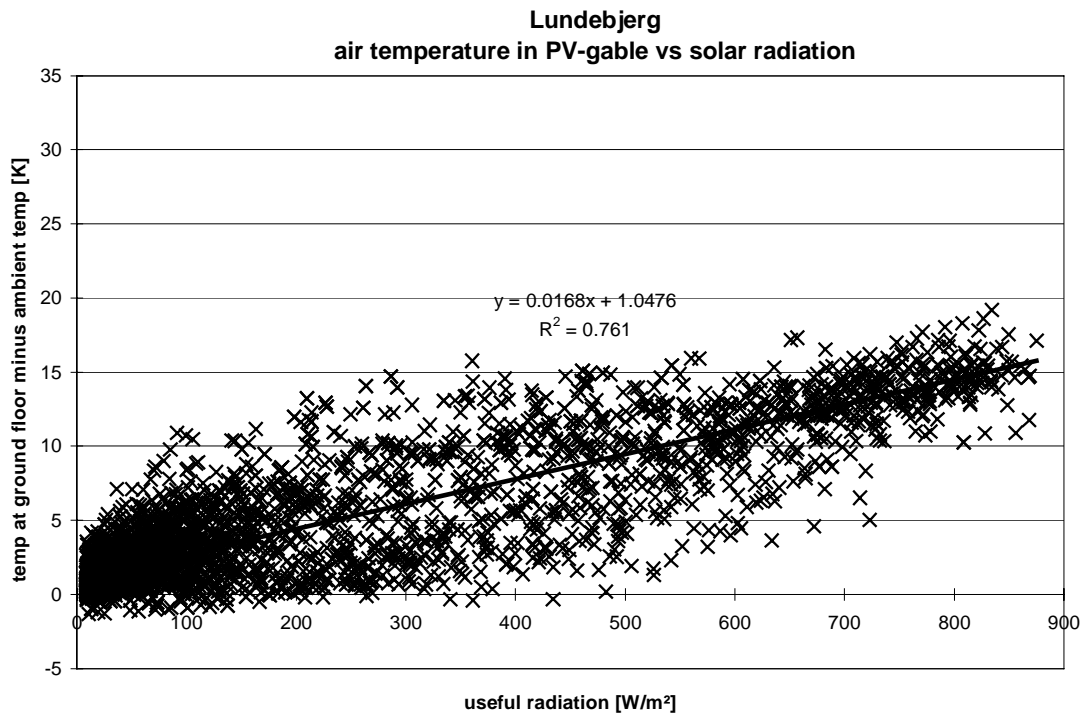


Figure 3.141. The temperature difference between the air at the ground floor in the PV-gable and ambient dependent on the useful solar radiation on the PV-panel.

The intended control of the inlet diffusers is that the diffusers should be open at an air temperature in the PV-gable of between 16 and 24°C. Figures 3.141-144 may be used to determine when the diffusers will be open under different conditions – however, it should be re-

membered to add the value of the actual ambient temperature in order to obtain the absolute temperature of the air at the three different levels behind the PV-panels of the PV-gable.

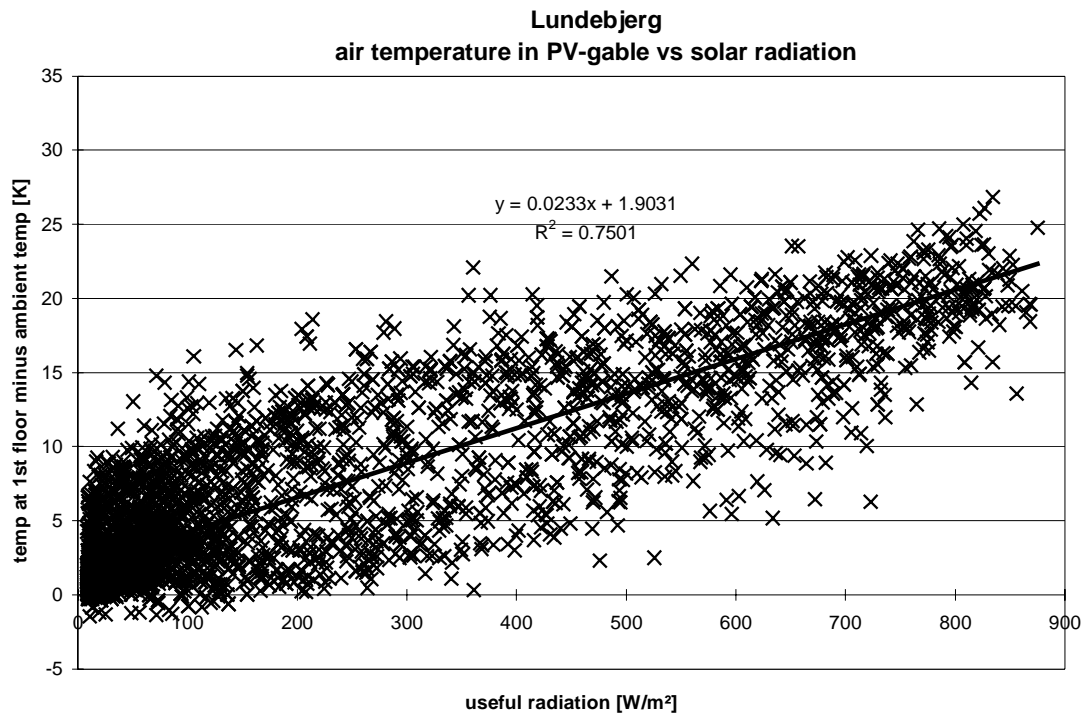


Figure 3.142. The temperature difference between the air at the 1<sup>st</sup> floor in the PV-gable and ambient dependent on the useful solar radiation on the PV-panel.

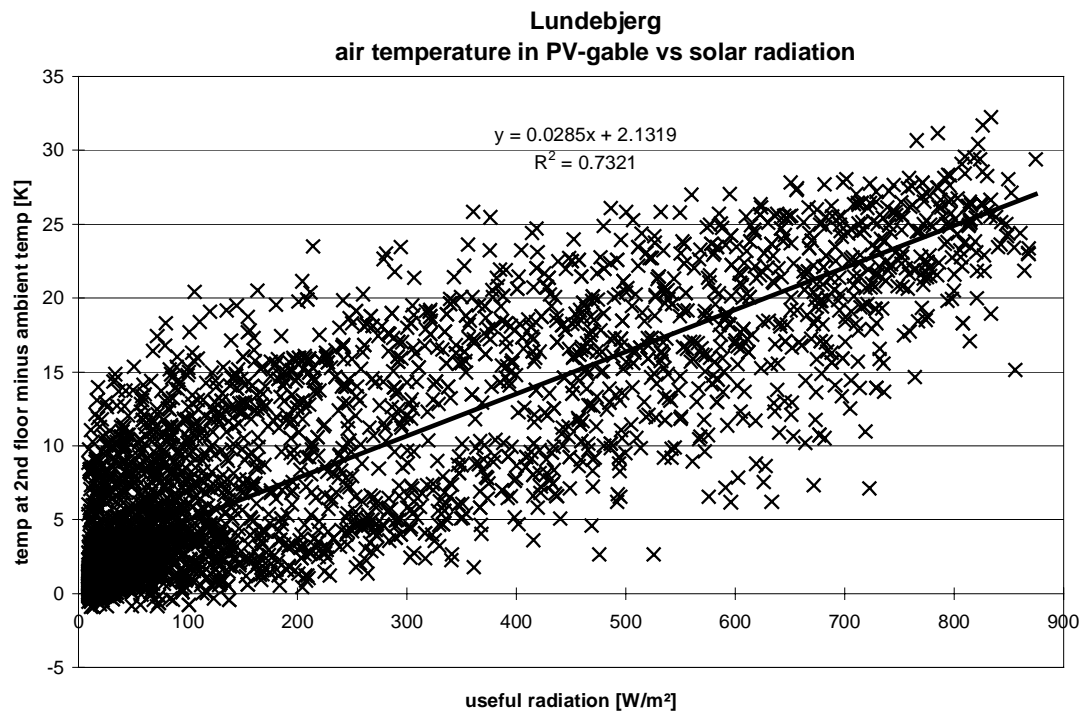


Figure 3.143. The temperature difference between the air at the 2<sup>nd</sup> floor in the PV-gable and ambient dependent on the useful solar radiation on the PV-panel.

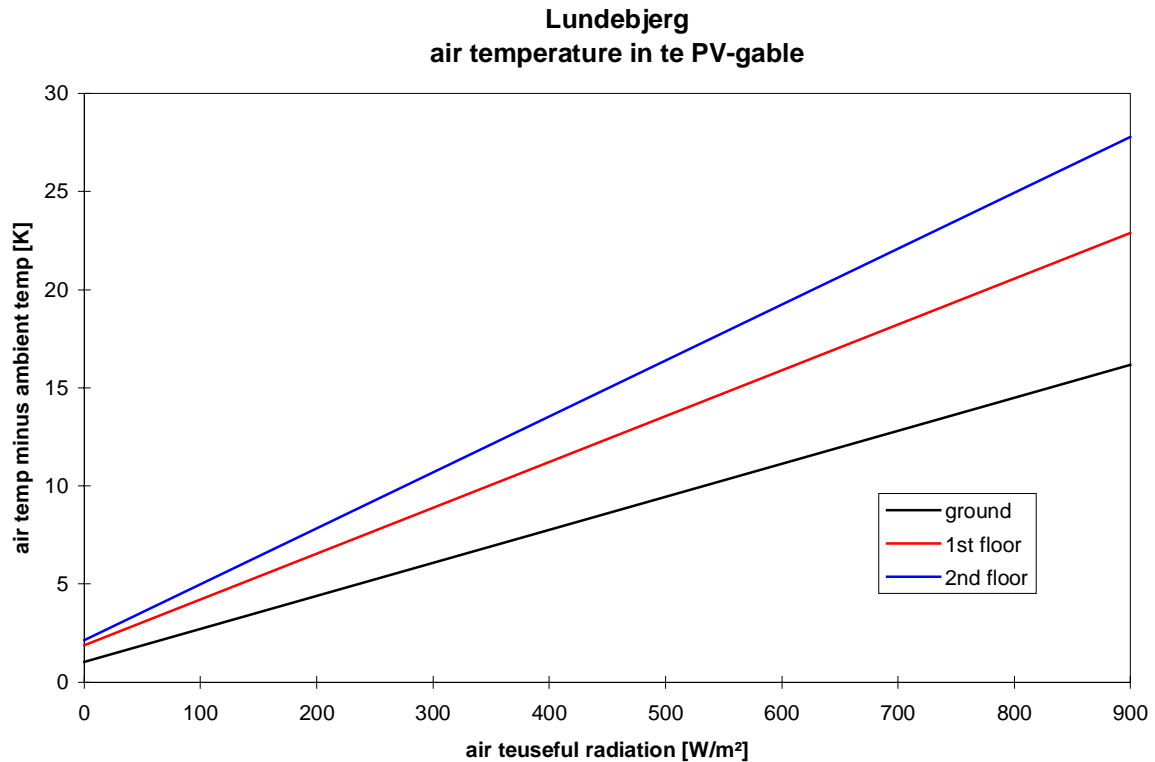


Figure 3.144. The temperature difference between the air in the PV-gable and ambient dependent on the useful solar radiation on the PV-panel.

### *Setpoint for the opening of the inlet diffusers in the gable*

It is not possible on the controller for the opening of the inlet diffusers in the gable to see the actual set points. The buttons for defining the set points are without a scale.

Based on the measurements from 2001 figure 3.145 has been generated. The figures shows the calculated power by the air from the gable to apartment 36 IIB (see also figures 3.11-12) as a function of the temperature in the gable at the second floor.

Figure 3.145 gives no clear picture of when the inlet diffusers open and close. From the figure it seems that the diffusers always are opens, which is not true – inspections have shown that the diffusers have been closed as temperatures below 16°C. Figure 3.145, thus, illustrate the very large uncertainty in measuring the power by the air from the gable to the apartment.

An attempt to calculate the performance of the gable as pre-heater of the fresh air to the building will, however, be made in section 3.3.

### **3.2.6. The PV-mixer**

The PV-mixer was one of the new features of the PV-VENT systems. It is therefore of special interest to evaluate this component. The objective of the PV-mixer is that it should be able to maintain the desired power to the fans while utilizing as much PV-power as possible.

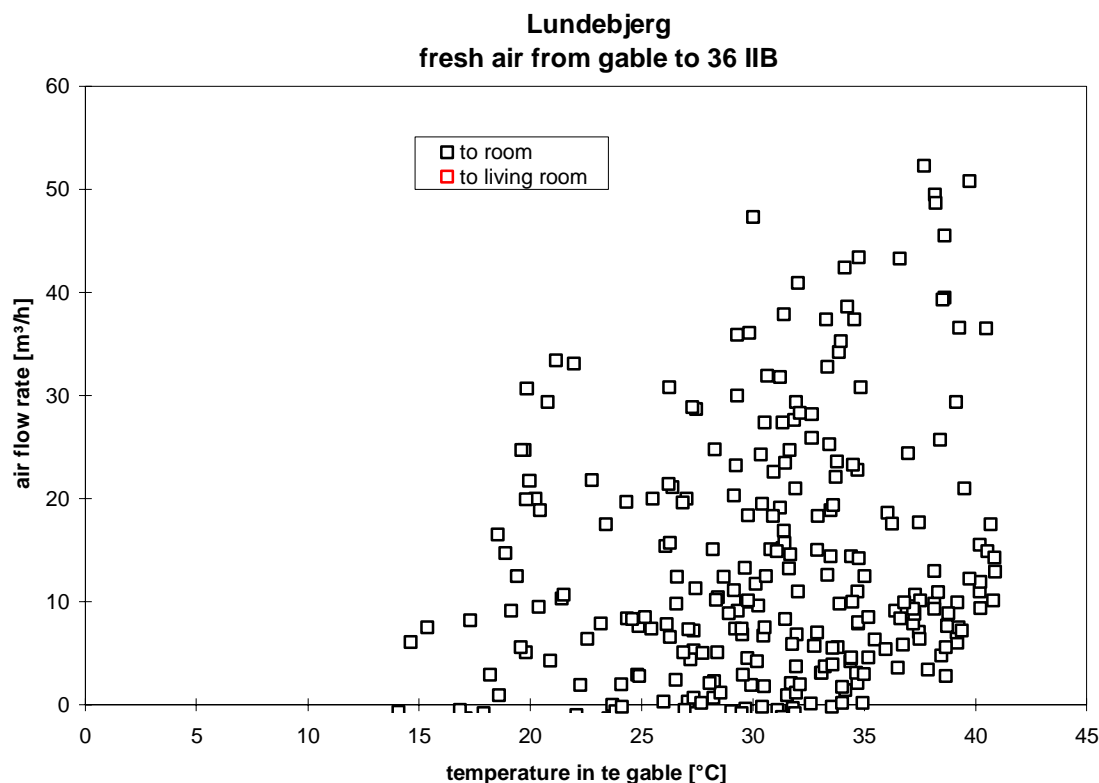


Figure 3.145. The air flow rates to the apartment 36 IIB dependent on the air temperature behind the PV-panels at the inlet to the dwelling.

The actual operation is shown in figures 3.31-36 and figures 3.87-104. The chosen concept of the PV-mixer does that it cannot utilize excess power from the PV-panel above the actual demand. The size of the PV-panel should therefore carefully be dimensioned in accordance with the actual power demand in order not to waste PV-power. If the power from the PV-panel is larger than the demand an inverter feeding the grid with the PV-power will most properly be a better solution.

The efficiency of the PV-mixer is evaluated in the following.

### ***Grid mode***

Table 1.3 shows the efficiency of the PV-mixer in pure grid mode. As the switch mode technology is utilized in the PV-mixer the shown efficiency of the PV-mixer of 96 % is constant.

### ***PV mode***

Table 1.4 shows the efficiency of the PV-mixer in pure PV mode. Table 1.4 indicates that the efficiency in pure PV mode is dependent on the actual power demand. Figures 3.146-149 show the measured efficiency of the PV-mixer in the systems at pure PV-mode. In figure 3.150 these values are shown together with the values from table 1.4 and values from Sundevadsgade/Tøndergade (Jensen, 2001). The equation for the regression line is further shown in the figure.

The max. power which the PV-mixer can deliver to the fans is 300 W. This means that the max. efficiency of the PV-mixer in pure PV-mode from figure 3.150 is 90 %, while slowly decreasing to 80 % at a demand of about 50 W. At lower demands figure 3.150 indicates that the decrease of the efficiency will be much faster – however, the measured values are rather scattered in this area indicating a large uncertainty.

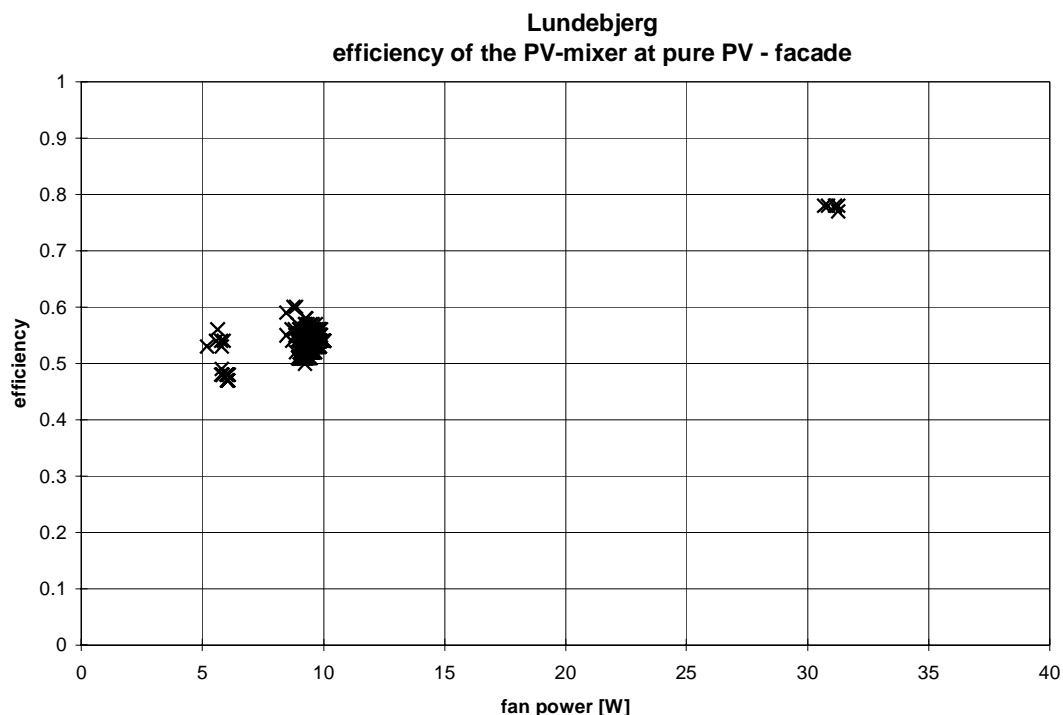


Figure 3.146. The efficiency of the PV-mixer at pure PV-mode as a function of the demand measured – PV-facade on apartment 40 IIA.

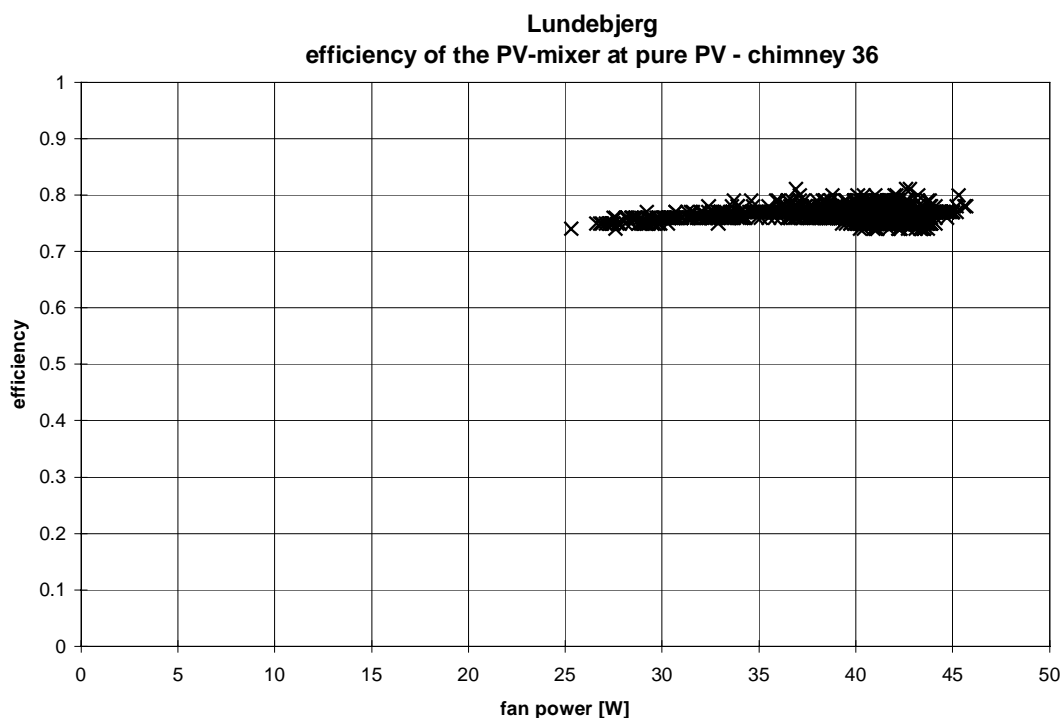


Figure 3.147. The efficiency of the PV-mixer at pure PV-mode as a function of the demand measured – chimney 36.



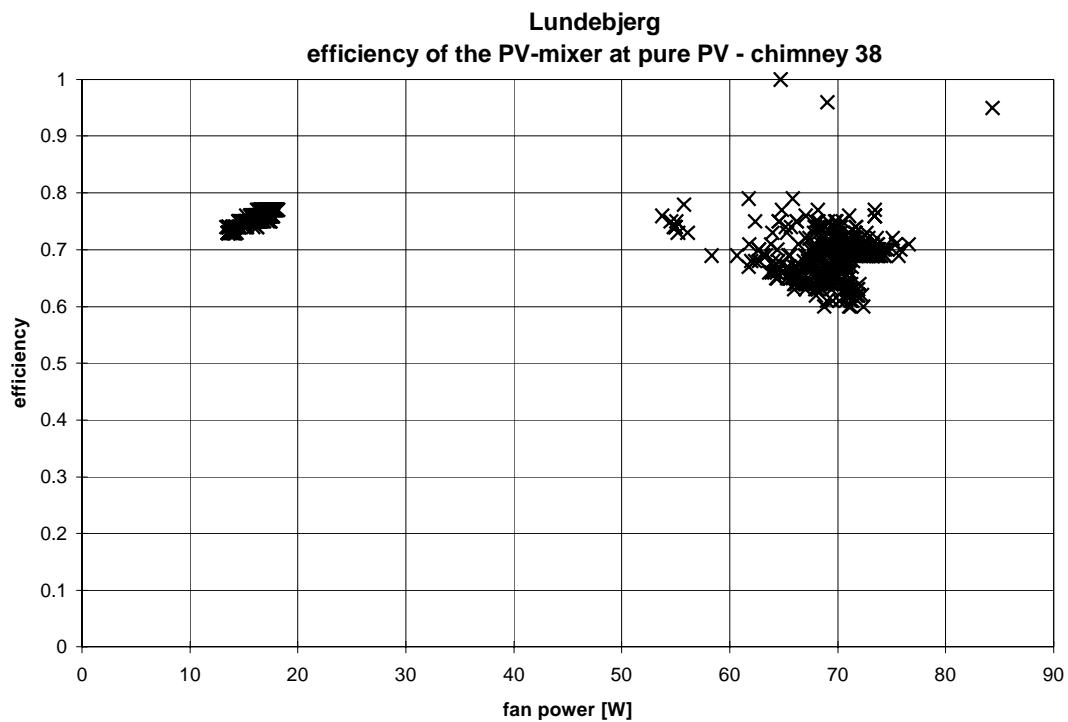


Figure 3.148. The efficiency of the PV-mixer at pure PV-mode as a function of the demand measured – chimney 38.

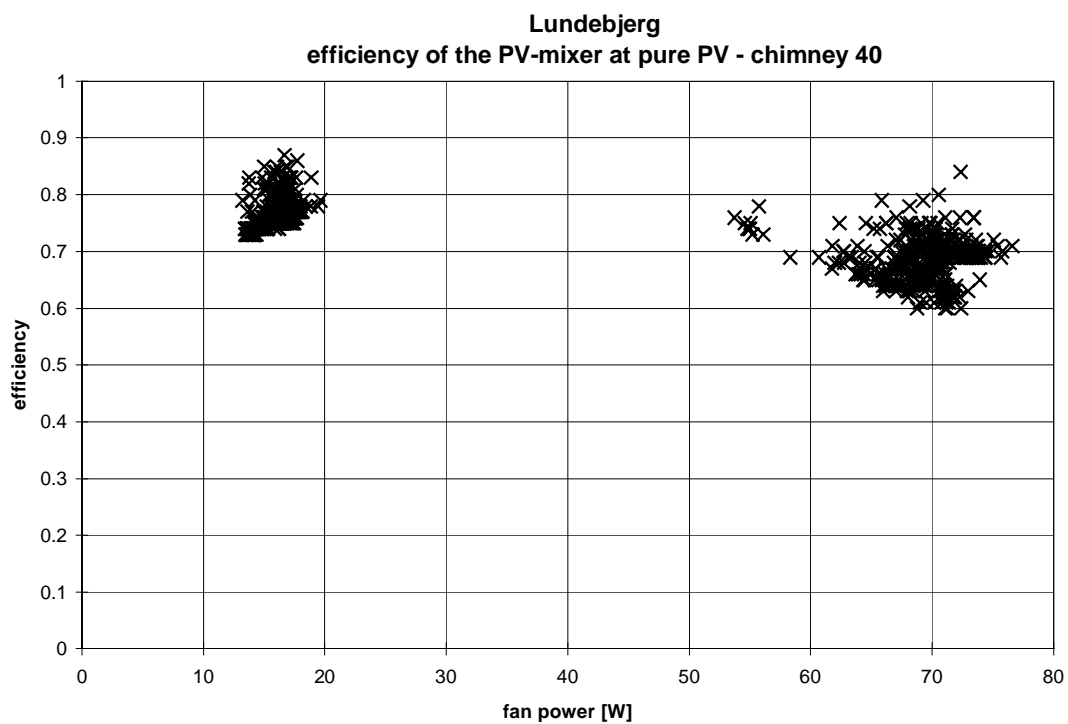


Figure 3.149. The efficiency of the PV-mixer at pure PV-mode as a function of the demand measured – chimney 40.

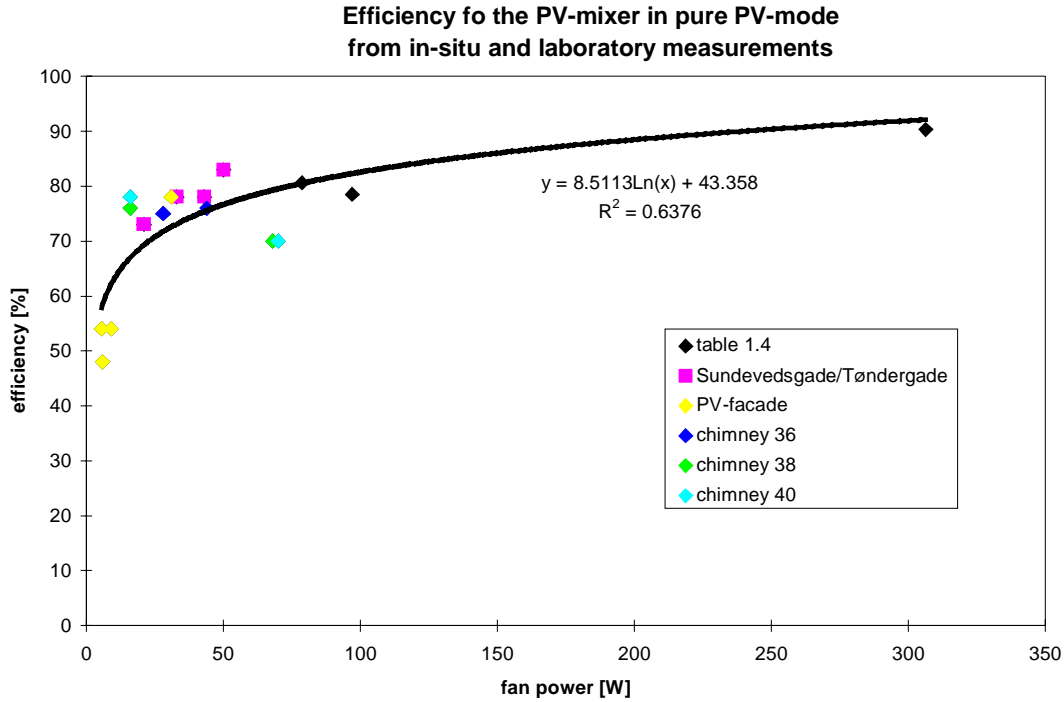


Figure 3.150. The efficiency of the PV-mixer at pure PV-mode as a function of the demand measured in Lundebjerg, Sundevedsgade/Tøndergade (Jensen, 2001) and in laboratory (table 1.4).

### **Mixed PV and grid mode**

The efficiency of the PV-mixer in mixed mode is rather difficult to obtain. The efficiency of the grid part will always be 96 %. Based on this the efficiency can be found based on the measured inputs from the grid and the PV-panels and the measured output to the fans. However, the measured values are too scattered to give an answer. In order to give an impression of the efficiency of the PV part during mixed mode operation the values from table 1.2 and test 3 from table 1.3 has been used in the following way:

$$\eta_{PV} = (P_{fan} - P_{grid} * 0.96) / P_{PV} \quad (3.9)$$

where  $\eta_{PV}$  is the efficiency of the PV part in mixed mode  
 $P_{fan}$  is the measured consumption of the fan  
 $P_{grid}$  is the measured power from the grid:  $U_{grid} * I_{grid}$   
 $P_{PV}$  is the measured power from PV:  $U_{pv} * I_{pv}$   
 0.96 is the efficiency of the grid part of the PV-mixer

The results are shown in figure 3.151. The values are for a demand of about 276 W and the value on the x-axis is the PV-power divided with the demand in order to obtain a normalized expression which may be used in other situation – e.g. the simulations in the next section.

Figure 3.151 indicate that the efficiency of the PV-mixer is linear dependent on the ratio between the power of PV and the power demand of the fans. At zero PV power the efficiency is about the efficiency of the PV-mixer at pure grid mode – 0.96, while it when going towards

pure PV-mode decreases linearly towards the efficiency in pure PV-mode as shown in figure 3.150.

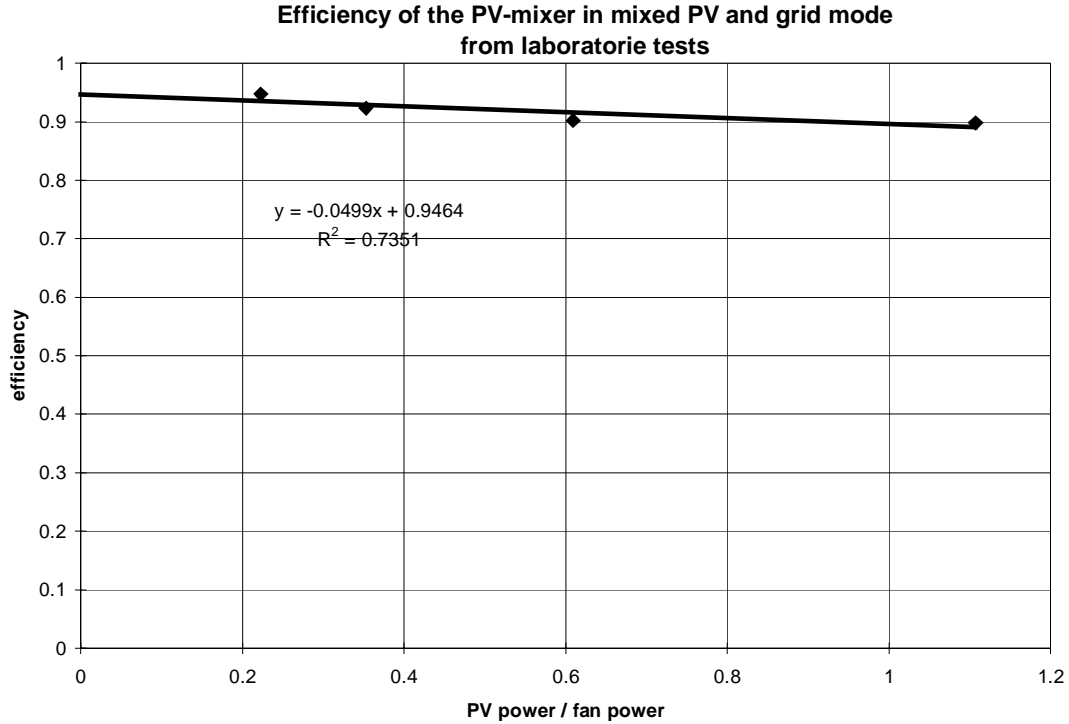


Figure 3.151. The efficiency of the PV-mixer at mixed PV and grid mode as a function of the PV power divided with the fan power - measured in laboratory (table 1.2).

This means that the efficiency for the PV part of the PV-mixer for other fan powers may be found as a linearly function based on two points: 0.96 at no PV-power and a value found in figure 3.150 for pure PV-mode dependent on the actual power demand of the fans. When combining the information from figures 3.150 and 3.151 the following equation appears:

$$\eta = a \cdot (\text{PV power} / \text{fan power}) + 0.96 \quad (3.10)$$

where:  $\eta$  is the efficiency of the PV-part at mixed PV/grid mode

$$a = (b + c \cdot \text{fan power} + d \cdot \text{fan power}^2) / (1 + e \cdot \text{fan power} + f \cdot \text{fan power}^2 + g \cdot \text{fan power}^3)$$

$$b = -0.2405$$

$$c = -0.00593$$

$$d = 1.36 \cdot 10^{-5}$$

$$e = 0.04232$$

$$f = 1.1646 \cdot 10^{-4}$$

$$g = -1.1374 \cdot 10^{-7}$$

0.96 is the efficiency of the grid part

It is not possible to prove that the above conclusion is correct, however, it is believed that the relationship is sufficiently correct in order to allow for the calculations in the next section.

### 3.3. Obtainable savings of the systems

This section deals with the obtainable savings from the system under different conditions. Measurements have been carried out for less than one half year and the systems have most of the time not been run as intended. It gives, therefore, no meaning to determine the actual savings of the systems. Based on the findings in section 3.2 a simulation program has instead been created – a simulation program which allows to calculate the savings on a yearly basis for different conditions of e.g. air flow rates, fan powers, sizes of PV-arrays, etc.,

The following will be calculated:

- savings in ventilation losses due to the heat exchanger
- savings due to the pre-heating of the air in the PV-facade, PV-gable and solar ventilation chimneys
- savings in electricity consumption due to the PV-panels
- waste of PV-energy due to a lower demand than the peak power of the PV-panels

#### 3.3.1. Simulation program

The simulation program is based on the Danish Test Reference Year (TRY) (SBI, 1982) and the applied solar processor (for calculation of solar incidence angle, direct and diffuse solar radiation) is the one from (Dutr , 1985).

No thermal model of the building – i.e. calculations of the actual heating demand of the building – has been included. However, in order to exclude periods without heating demand the calculations on the thermal part of the system has been skipped outside the Danish heating season (September 22 – May 8) and when the ambient temperature is above 17 C.

#### *Pre-heating*

##### PV-gable

The three apartments facing the PV-gable has exhaust ventilation. The flow rate of the system is day and night as defined in the Danish building code: exhaust 126 m<sup>3</sup>/h. The flow rate of fresh air from the PV-gable is driven by the under pressure in the dwellings. The air flow rate is, therefore, very fluctuating due to different wind pressure and if the tenants opens a window. This is shown in figure 3.152. Figure 3.152 shows the ratio between the measured air flow rate from the PV-gable and the flow rate of exhaust air as a function of the air temperature in the PV-gable – only values at air temperatures above 16 C are shown.

Figure 3.152 shows a very scattered picture. A linear regression suggests as shown a mean value of 0.6. This value will be used in the simulation program

The actual energy to the dwellings will be found based on the air flow rate of exhaust air multiplied with 0.6, the temperature of the air in the solar wall found in figures 3.141-144 (page 133-135) (+ the ambient temperature) and the ambient temperature from the Danish TRY. It is here assumed that the PV-gable is an infinite reservoir – i.e. that the temperatures found in figures 3.141-144 is the air temperatures in the PV-gable no matter the size of the air flow drawn from the PV-gable and no matter the time when the air flow occurs. This is of

course not correct but is the only way to handle the PV-gable here. It is judged that although the rather high uncertainty on the calculations the found trends will rather well characterize the PV-gable as solar air collector.

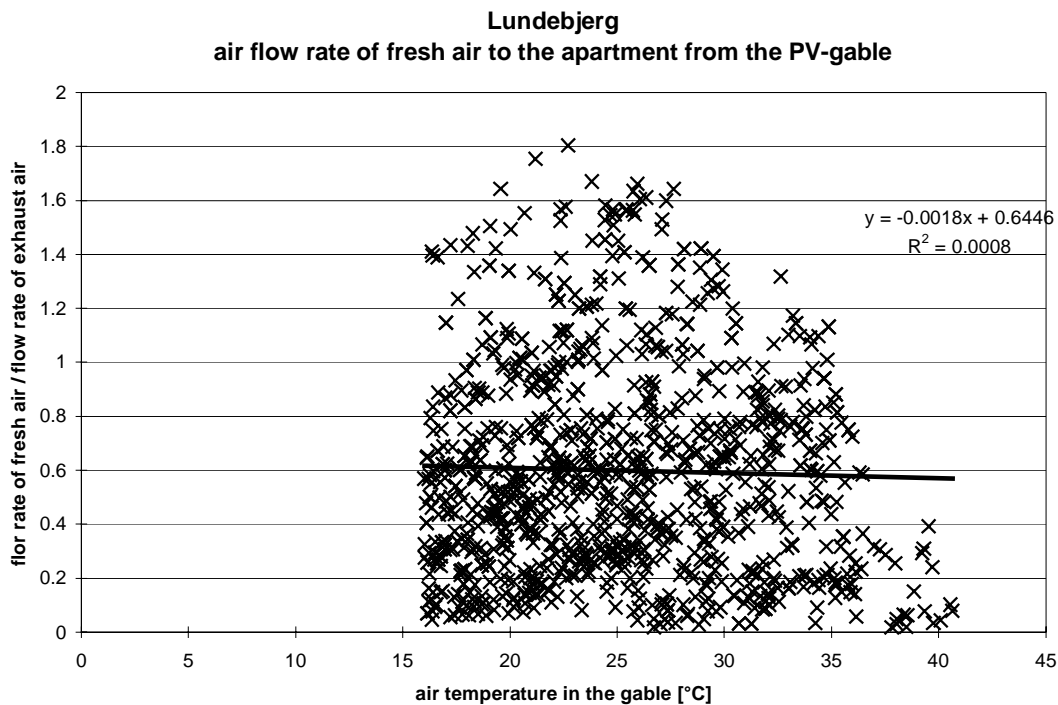


Figure 3.152. Ratio between measured air flow rates from the PV-gable and corresponding flow rates of exhaust air.

#### PV-facade, solar ventilation chimneys and heat exchangers

The flow rates of the systems are day and night as defined in the Danish building code: exhaust 126 m<sup>3</sup>/h and fresh air  $126 \cdot 0.9 = 113.4$  m<sup>3</sup>/h.

The inlet temperature of fresh air to the heat exchangers is either the ambient temperature (i.e. no pre-heating before the heat exchanger) or (in the case of pre-heating in the PV-facade or a solar ventilation chimney) calculated using the equation in figure 3.128 (page 124) corrected for the actual PV production using the equation in figure 3.131 (page 126). It is assumed that the efficiency of the PV-facade as solar air collector (if constructed as intended) is the same as for the solar ventilation chimneys, which figure 3.132 indicates would have been the case.

The performance of the heat exchanger with and without pre-heating in PV-facade/chimney can be calculated/simulated in the following way:

The actual efficiency of the heat exchanger are calculated using figure 3.106 (page 110) for 40 IIA, figure 3.114 (page 115) for 40 IIB and an apartment in 38. It has been chosen to simulate an apartment in 38, because the area of PV-panel per dwelling here is lower than for the apartments in 40. The area of PV-panels is 1.28 and 0.85 m<sup>2</sup> per dwelling for 40 and 38 respectively. The PV-facade has an area of 1.73 m<sup>2</sup>. The chimneys are facing south while the PV-facade is facing east. Identical equation for the efficiency of the heat exchanger has been

chosen for 40 IIB and 38 in order to be able to evaluate the influence of the area of the PV-panels.

The temperature of the fresh air after the heat exchanger has been calculated in the following way:

$$T = T_{in} + \eta \cdot (T_{exh} - T_{in}) \cdot \rho_{exh} / \rho_{fr} \cdot cp_{exh} / cp_{fr} \cdot V_{exh} / V_{fr} \quad (3.11)$$

where  $\eta$  is the actual efficiency of the heat exchanger – figures 3.106 and 3.114

$\rho$  is the density of air

$cp$  is the heat capacity of air

$V$  is the flow rates of air

subscript in indicate the inlet temperature of fresh air to the heat exchanger

subscript exh indicate exhaust air

subscript fr indicate fresh air

The actual heating of the fresh air in the heat exchangers may then be found. It is also possible to calculate the overall heating of the fresh air in the system with and without pre-heating in the PV-facade/chimney. In this way it is possible to determine the actual benefit of the pre-heating of the fresh air in the PV-facade/chimney, which of course is lower than the heating in the PV-facade/chimney.

#### Fan power and savings due to the PV-panels

The actual fan power may be calculated using equations 3.6 and 3.7 (page 121), which gives identical fan powers for the flow rates in the Danish building code – see table 3.1 (page 121).

The losses due to the transformer may be calculated using equation 3.8 (page 121). Losses in the wiring are not considered, as these should be as low as 2-3% and thus far less than the uncertainty of the calculations.

The potential power from the PV-panels can be calculated using equation 3.1 (page 47). The temperature of the PV-panels are found using figure 3.134 (page 130) (+ the ambient temperature).

How large part of the fan power which actually can be covered by PV has been calculated using the equation in figure 3.150 (page 139) and equation 3.10 (page 140).

The peak power for the three cases: PV-facade, 40 IIB and 38 are: 100, 150 and 100  $W_p$  respectively.

Based on the above the following energy flows has been calculated: Energy to fans with and without PV, energy delivered to the PV-mixer from the PV-panels and PV energy not utilized due to too low demands.

### **3.3.2. Simulation results**

The results from simulation with the developed simulation program are described in the following.

### ***Pre-heating in the PV-gable***

The pre-heating has been evaluated for three cases – i.e. three set points for the inlet diffusers connecting the PV-gable with the dwellings. The chosen set point were:

- as in the actual case: open at an air temperature in the PV-gable between 16 and 24°C
- always open
- open at an air temperature in the PV-gable below 20°C

The two latter control strategies may lead to problems. The always-open strategy will most properly lead to overheating from time to time and if not taken care of draft during periods with low temperatures in the PV-gable. The always open below 20°C mode does not cause overheating, but may cause draft if proper actions to prevent this are not taken. The two latter control strategies are evaluated in order to determine the max. obtainable pre-heating in the PV-gable.

The simulations have further been carried out for all three apartments: ground floor, 1<sup>st</sup> floor and 2<sup>nd</sup> floor. Table 3.2 shows the results from the simulations.

Open diffuser	Exhaust kWh	Ground floor		1 <sup>st</sup> floor		2 <sup>nd</sup> floor	
		kWh	%	kWh	%	kWh	%
16-24°C	4129	64	1.6	111	2.7	124	3.0
Always	4129	246	6.0	365	8.8	432	10.5
<20°C	4129	209	5.1	256	6.2	256	6.2

Table 3.2. The possible preheating in the PV-gable dependent on the set points for the diffusers. In the “%-columns” the savings are shown as a percentage of the heat loss due to the exhaust ventilation “Exhaust-column”.

Table 3.2 shows a rather low potential for savings from a PV-gable. However, the applied model is rather simple – i.e. no building model included and only regression lines to represent the air temperatures in the PV-gable. So if the above technology is considered in a building project more advanced modeling of the construction including modeling of the heat demand of the building should be applied in order to obtain a better basis for choosing this type of solar energy technology.

### ***Balanced ventilation systems with pre-heating in a PV-facade/solar ventilation chimney***

Table 3.3 shows the yearly results from the simulations of the three cases.

Table 3.3 shows that the amount of recovered heat in 40 IIA is much larger than in 40 IIB and 38. This is of course because of the higher efficiency of the heat exchanger in 40 IIA – compare figures 3.106 and 3.114.

Table 3.3 shows surprisingly that the pre-heating in the PV-facade leads to a lower overall performance of the system. To explain this one has to look at figure 3.106. The efficiency is as seen very strongly dependent on the inlet temperature to the heat exchanger in such a way that the efficiency (due to condensation) decreases with increasing inlet temperature. So the small increase in the inlet temperature caused by the PV-facade actually leads to a decrease in

the efficiency of the heat exchanger, which more than overrule the benefit of the pre-heating by the sun. The values in brackets show the result if the efficiency of the heat exchanger is replaced with the efficiency in figure 3.114 with a much lower dependency on the inlet temperature. Doing this the result looks more reasonable.

	40 IIA kWh	40 IIB kWh	38 kWh
<b>Heat exchanger</b>			
Energy in the exhaust air	4129	4129	4129
Energy in the inlet air incl. pre-heating by the sun	4056(2502)	2517	2508
Energy in the inlet air exc. pre-heating by the sun	4070(2478)	2478	2478
Benefit of pre-heating by the sun <sup>1)</sup>	-14( 24)	39	30
<b>PV-facade/chimney</b>			
Energy to the air from the sun	70	114	88
<b>Fans and PV</b>			
Energy to the fans from the grid - without PV	236	236	236
Energy to the fans from the grid - with PV	211	191	198
Benefit of PV <sup>2)</sup>	25	45	38
PV energy delivered to the PV-mixer	29	55	46
Not utilized PV energy	4	32	12

Table 3.3. Yearly calculated energy flows in the ventilation system.

<sup>1)</sup> energy in the inlet air with pre-heating in the solar wall minus without pre-heating.

<sup>2)</sup> energy to the fans from the grid without PV minus with PV

When comparing the three sets of simulations (40 IIA with the same exchanger efficiency as for 40 IIB and 38) it is seen that the benefit of the pre-heating by the sun is rather low – below 1 %, which of cause is due to the rather small “solar air collector” – 0.85 and 1.73 m<sup>2</sup> - and the heat exchanger – only 34 % of the energy supplied the fresh air by the sun is utilized as pre-heating of the air after the heat exchanger. The performance of the PV-facade/chimneys as solar air collectors (before the heat exchanger) is as expected – around 100 kWh/m<sup>2</sup> for the southern orientation and 40 kWh/m<sup>2</sup> for the eastern orientation. Only about one third of the pre-heating occurring in the solar ventilation chimney ends up as utilized energy after the heat exchanger.

Between 11 and 19 % of the energy to the fans is covered by the PV-panels. Nearly no PV power is lost in 40 IIA, which is due to the low solar radiation on the PV-panels due to the eastern orientation – the PV-panels are seldom able to deliver more power than needed. For 40 IIB the PV-panels covers 19 % of the energy to the fans, but 37 % of the potential energy from the PV-panels is not utilized. In 38 16 % of the energy to the fans is covers while only wasting 21 % of the potential PV-power. It seems based on this not reasonable to cover more than 15 % of the energy to the fans if a PV-mixer is applied. If larger percentages is wished it might be more beneficial to apply an inverter connected to the public grid.



The reason for the low part of PV power not utilized in 38 (although the peak power of the PV-panels is three times as high as the required fan power (31 W)) is of course that the radiation level at vertical south seldom is 1000 W/m<sup>2</sup> and the temperature of the PV-panels seldom is 25°C or below.

### ***Parameter variations***

The above simulation model is rather general, which means that it is possible to perform parameter variations for some of the main parameters of the system. Parameter variations are in the following carried out for the efficiency of the heat exchanger and the peak power of the PV-panels. The solar ventilation chimney is in the simulations facing south.

#### Efficiency of the heat exchanger

The efficiency of the heat exchanger is in the following fixed values – i.e. not dependent on the inlet temperature of fresh air as this makes it much easier to display the results graphically without losing too much realism. The simulations are carried out in order to evaluate the influence of the efficiency of the heat exchanger on the utilized fraction of the pre-heating in the solar ventilation chimney. Figure 3.153 shows the results from the simulations with two areas of solar ventilation chimney per apartment – 1.28 m<sup>2</sup> as in 40 IIB and 5 m<sup>2</sup>.

Figure 3.153 shows as expected a decreasing utilization of the pre-heating in the solar ventilation chimney with increasing efficiency of the heat exchanger. Due to the rather simple model without a building part, the utilized part of the pre-heating in the solar ventilation chimney is at low exchanger efficiencies a bit too high, as it here compete with the direct solar gains through the windows. On the other hand - the utilized part of the pre-heating in the solar ventilation chimney is a bit too low at high exchanger efficiencies as the solar energy also may cover a part of the transmission loss of the apartment.

The utilization of the pre-heating of the fresh air in the solar ventilation chimney is in general low and specially at high heat exchanger efficiencies and should in such cases carefully be evaluated before chosen.

#### Utilized and not utilized PV power

Figure 3.154 shows the results from simulations where the peak power of the PV-panels has been varied. The necessary fan power during the heating season is in the simulations 31 W – as were the case in the former simulations.

Figure 3.154 may be used for other fan powers if the x-axis is replaced with the peak power divided with 31 (fan power in figure 3.154) as done in figure 3.155. However, the efficiency of the PV-mixer is dependent on the fan power as shown in figure 3.150 and equation 3.10. So the found values in figure 3.155 should be multiplied with the following factor:

$$f = \eta / 72.6 \quad (3.12)$$

where  $\eta$  is the efficiency of the PV-mixer at the actual fan power found in figure 3.150  
72.6 is the efficiency at a fan power of 31 W as used in figures 3.153-54

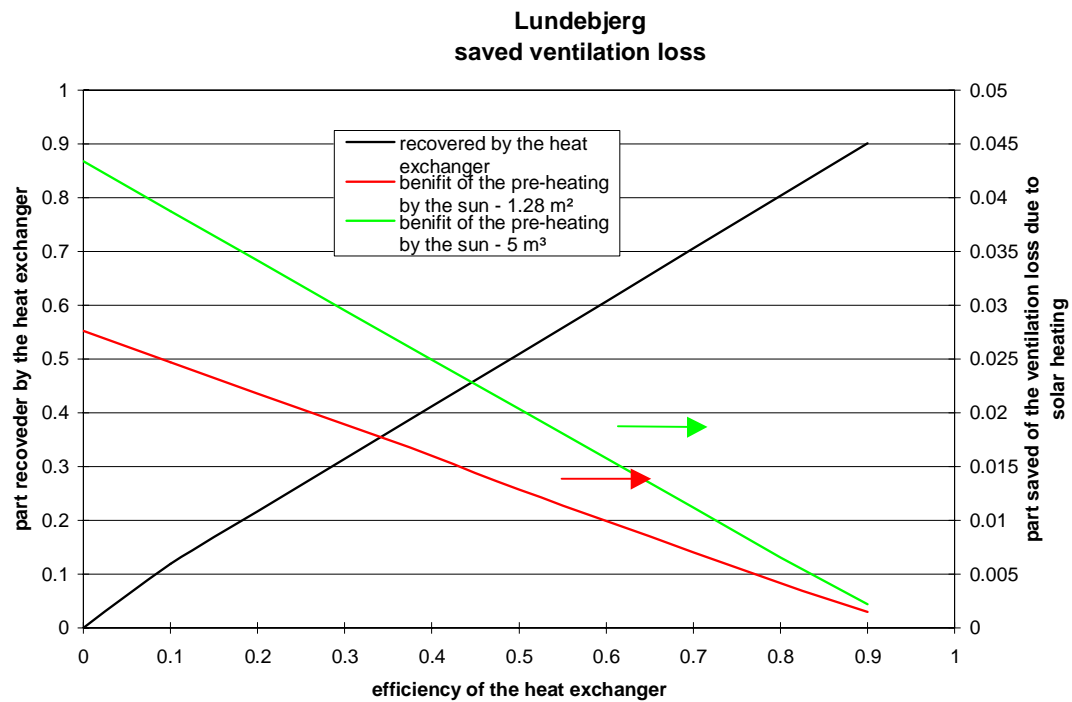


Figure 3.153. The recovered fraction of the mechanical ventilation loss and the utilized fraction of the pre-heating in the solar ventilation chimney dependent on the efficiency of the heat exchanger.

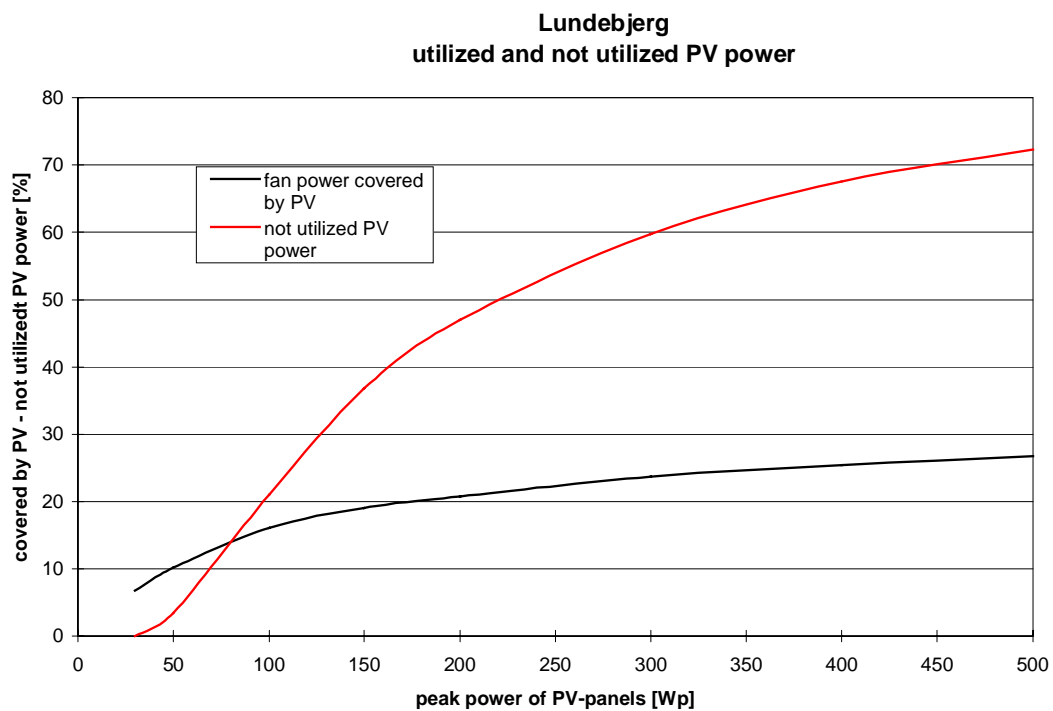


Figure 3.154. Utilized and not utilized PV power dependent on the peak power of the PV-panels.

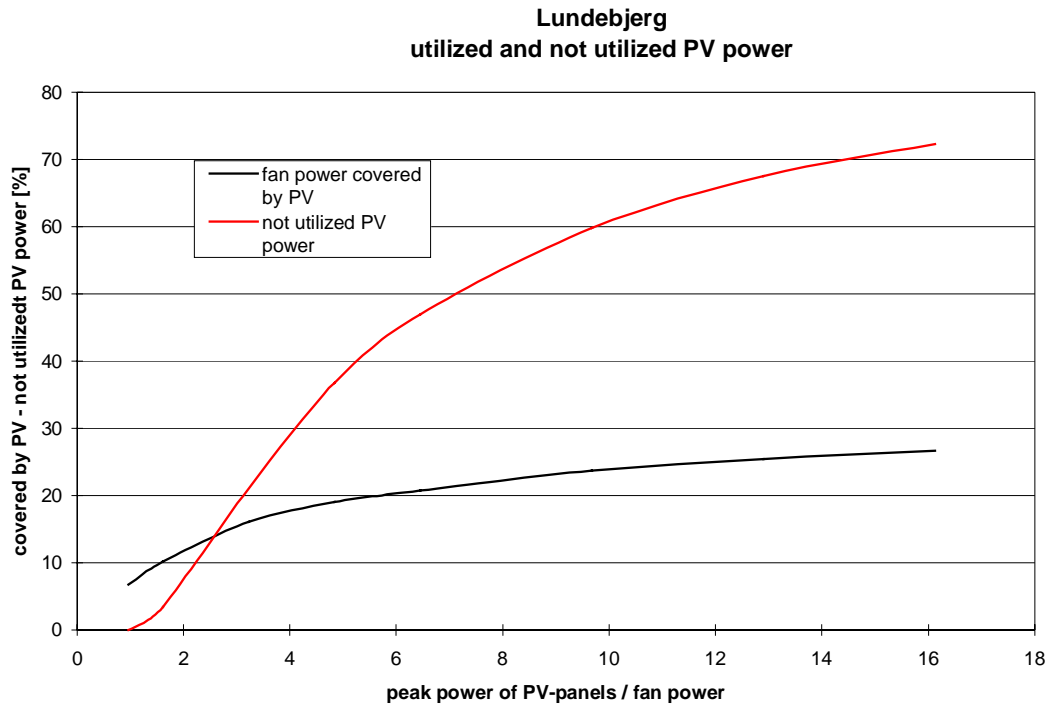


Figure 3.155. Utilized and not utilized PV power dependent on the ration between the peak power of the PV-panels and the actual fan power.

Figures 3.154-55 show that a considerable area of PV-panels is necessary to cover e.g. 25 % of the necessary fan power. The problem is, however, that the not utilized PV power increases more rapidly than the utilized part of the PV power. So if the aim is to cover a large fraction of the necessary energy to the fans it would be wise to apply an inverter rather than a PV-mixer. Figures 3.154-55 indicate as stated above that when applying a PV-mixer one should not attempt to cover more than 15 % of the energy to the fans – above this percentage the not utilized PV power increases too fast.

## 4. Conclusions

The following conclusions are common for both measuring projects under PV-VENT: Lundebjerg and Sundevedsgade/Tøndergade (Jensen, 2001).

### 4.1. Aims of the PV-VENT project

The aims of the projects was research, development and tests in the following areas:

- develop and illustrate different ways of architectural integration of solar energy systems with combined PV power production and pre-heating of ventilation air in buildings
- investigate the potential in pre-heating fresh air to the building by cooling the PV-panels with the fresh air and further to determine how much this cooling will increase the electrical performance of the PV-panels
- develop and test air to air heat exchangers with an efficiency of 80 % or above
- develop and test fans and ventilation systems with an overall fan power demand of about 35 W
- develop and test a direct coupling of the PV-panels to the fans in order to avoid the losses in an inverter
- develop and test different ventilation systems utilizing the above-mentioned features

### 4.2. Results from the PV-VENT project

#### 4.2.1. Architectural results

Different ways of integrating PV-VENT systems in the building envelope has been developed and tested:

##### *Lundebjerg*

Three different ways of integrating PV-panels with pre-heating of fresh air to the building have been demonstrated in Lundebjerg: a large PV-gable with amorphous PV-panels, a PV-facade with polycrystalline (c-Si) PV-panels and solar ventilation chimneys with polycrystalline (c-Si) PV-panels. Especially the latter feature – the solar ventilation chimney is a new and interesting concept as it allows for increased PV areas although the orientation of the building is not optimal for utilization of solar energy - as was the case in Lundebjerg.

However, the Lundebjerg project is not only interesting due to the demonstrated methods for architectural integration of PV systems in buildings. As a part of the project an architectural competition on the renovation of the building including PV-VENT systems was held in 1998 with five well known Danish architect firms. The result of the competition is seen at Lundebjerg today, but many other ways of introducing PV-VENT systems was proposed in the

not winning contributions – way of introducing PV-VENT systems that may be utilized by others in future projects.

### ***Sundevedsgade/Tøndergade***

In this building only one way of integrating PV-VENT systems is tested. The integration technique is, however, very interesting as the PV-panels are integrated in a solar wall also containing the heat exchangers. The solar wall is further integrated with a new sun space for each dwelling.

### ***General conclusions on architecture***

Several new and interesting ways of solving building integration of PV-VENT systems have been developed. Several of these have further been demonstrated in the project. It is believed that the results from the project will influence future projects in this field.

#### **4.2.2. Pre-heating of fresh air – cooling of PV-panels**

The aim of pre-heating fresh air by cooling the PV-panels is twofold: reduce the ventilation losses of the building while increasing the performance of the PV-panels.

The actual benefit of the pre-heating of the fresh air to the buildings has been low. The reasons for this are several:

- The absorber of the “solar air collectors” is the PV-panels. There is no cover in front of the absorbers as cooling of the PV-panels with ambient air is desirable in order to keep the cell temperature down and thereby the efficiency of the PV-panels up. This decreases the efficiency of the system as solar air collector – the efficiency is less than half of the efficiency of a good traditional solar air collector
- The very high efficiency of the heat exchangers in the system – see later – decreases the utilizable part of the pre-heating in the solar wall, PV-facade and solar ventilation chimneys. The projects showed that only about one third of the pre-heating by the sun actually was utilized
- It was decided that the PV-panels should be cooled on the backside by natural ventilation during the summer – in order to save fan power. This means that the air gap behind the PV-panels has to be rather wide in order to decrease the pressure loss across the PV “solar air collectors”. The air speed in forced air flow mode will then be low leading to a low heat transfer coefficient between the backside of the PV-panels and the air. This again results in a low efficiency of the solar air collectors

The solar wall at Sundevedsgade/Tøndergade showed a higher benefit of the pre-heating in the solar wall than shown at Lundebjerg. The reason for this is the high heat loss from the building to the solar wall rather than utilization of solar radiation.

The measured temperature of the PV-panels was often rather high – 50°C – due to the low air speeds behind the PV-panels. The benefit of the cooling of the PV-panels was therefore low.

Due to the low benefit of the pre-heating by the sun this feature should carefully be evaluated before chosen in future projects.

#### **4.2.3. Air to air heat exchangers**

Based on the measurements in the two projects the normalized efficiency of the air to air heat exchangers has been found. The normalized efficiency is when the two air flow rates are identical – this is the normal way to state the efficiency of air to air heat exchangers. The normalized efficiency was found to lay around 80 %. The actual efficiency was shown to be both much below or much above 80 % due to too large differences between the two air flows and due to condensation in the heat exchangers.

The aim of the project regarding efficient heat exchangers was thus fulfilled.

#### **4.2.4. Low fan power**

The necessary fan power in the balanced ventilation systems with heat recovery was shown to be 38 W per dwelling for Lundebjerg and 52 W per dwelling for Sundevedsgade/Tøndergade. The higher fan power at Sundevedsgade/Tøndergade is caused by the higher pressure loss in the heat exchanger arrangement. The high pressure loss of the heat exchangers at Sundevedsgade/Tøndergade is due to the many bendings in the duct works necessary due to the location in the solar wall.

38 W is very close to the aim of 35 W. If further the contribution from the PV-panels is subtracted (10-15 % of the necessary fan energy) the average necessary fan power is 32-34 W.

#### **4.2.5. Direct coupling of PV-panels to fans**

Electricity from PV-panels cannot be the only supply to the fans as the fans run day and night and because hardly any solar radiation is available during large part of the winter meaning that a battery bank and the area of PV-panels should be large.

Instead it was decided to develop a so-called PV-mixer, which is in charge of utilizing as much as possible of the available PV power while topping up with power from the grid when the PV power is too low or not present.

The measurements show that the developed PV-mixer works as intended. The efficiency in grid mode is 96 % but below 90 % is pure PV mode. The latter efficiency can maybe be increased by further development of the concept.

The main problem with the concept of coupling of the PV-panels to the fans via a PV-mixer rather than an inverter is that excess power from the PV-panels is not utilized – i.e. if the PV-panels are able to supply more power than the demand of the fans this excess power is lost. For this reason one should not aim at cowering more than 15 % of the energy to the fans by PV via a PV-mixer. Below 15 % the waste of PV energy will stay below 20 %. If the wish is to cover a larger fraction of the energy to the fans by PV it may be wiser to apply an inverter rather than a PV-mixer.

#### **4.2.6. Total systems**

Several total ventilation system utilizing the above described features and techniques has been developed and tested in the project – both individual and common ventilation systems.

The individual systems were all equipped with a control panel in the dwellings. The tenants are thus able to change the way the systems run. The tenants are happy that they themselves can decide how the systems should run. But there is a high risk that the systems are run improperly – i.e. at too low air flow rates because e.g. the noise from the fans (although very silent) annoys the tenants.

The tenants are not allowed to control the common ventilation systems – one ventilation system per three dwelling. This has, however, not lead to a more proper running of these systems than the individual systems. Due to the low pressure drops in the systems and the thereby low speed of the fans, the systems has been very difficult to balance. There has for that reason been several complaints. This illustrates that special care should be taken when dimensioning this type of systems with low pressure losses – especially the fans should fit the actual demands.

The testing of the complete systems rather than components has revealed much valuable information on the influence of one component on the other components of the systems which in the future may lead to better systems.

#### **4.2.7. General conclusions**

It is believed that the PV-VENT project has added important information and experience to the field of combining PV and ventilation systems. Information and experience that future systems of this type may benefit from. Several of the components from the project are believed to be able to contribute to set the standards for future PV and ventilation systems. Several of the components from the project is today commercial available and are used in ordinary building projects.

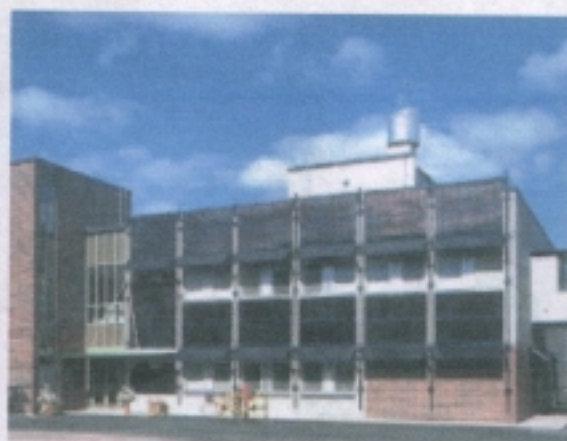
## 5. References

- Duffie, J.A. and Beckman, W.A., 1991. Solar Engineering of Thermal Processes. John Wiley & Sons, New York. ISBN 0-47-51056-4.
- Dutr  W.L., 1985. A Thermal Transient Simulation Model for Thermal Solar Systems – EMGP2. Solar Energy R&D in the European Community, series A, volume 5. D. Reidel Publishing Company. ISBN 90-277-2051-7.
- Hansen, H.E., Kjerulf, P. and Stampe, O.B. (ed), 1997. Heating and climate technology (in Danish). Danvak Aps. ISBN 87-982652-8-8.
- Jensen, S. ., 1994. Test of the Summer House Package from Aids Milj . Thermal Insulation Laboratory, Technical University of Denmark. Report no. 94-1.
- Jensen S. and Pedersen, J.S., 1999. PV-VENT, Technical Progress Report, first two years – TemoVex Denmark.
- Jensen, B.K., 2000. Measuring report – PV-mixer (in Danish). Solar Energy Centre Denmark, Danish Technological Institute. August 2000.
- Jensen, S. ., 2001. Results from measurements on the PV-VENT systems at Sundevedsgade/T ndergade. Solar Energy Centre Denmark, Danish Technological Institute. SEC-R-15. ISBN 87-7756-614-9.
- Lepp nen, J., 1999. PV-VENT, Technical Progress Report, first two years – Neste/NAPS.
- Lepp nen, J., 2000. Solar panels Maintenance and Operation Guide. Lundebjerg, Copenhagen, Denmark. Forum.
- Lien, A.G. and Hestness, A.G., 1999. Architectural Integration of PV for ventilation in three buildings in Denmark – PV-VENT, Low cost energy efficient PV-Ventilation in retrofit housing. Department of Building Technology, Norwegian University of Science and Technology.
- Mehr, U., 2000, Evaluation report – PV-mixer (in Danish). Solar Energy Centre Denmark, Danish Technological Institute. January 2000.
- Nielsen, J.E., 1995. Documentation of KVIKSOL – a program for simulation of solar heating systems (in Danish). Version 5.0. Solar Energy Laboratory, Danish Technological Institute Energy.
- Olsen, H., 1998. Measuring report on heat exchangers from Temovex (in Danish). Danish Technological Institute.
- Petersen, S.N., 2001. The AirVex contribution to the PV-VENT report. AirVex.
- SBI, 1982. Weather Data for HVAC and Energy – Danish Test Reference Year. Danish Building Research Establishment. SBI Report n. 135.



# **Appendix A**

## **Data sheets for the PV-panels**



Above: 3.5 kWp a-Si facade system at Neste Chemicals R&D building at Porvoo, Finland

Left: 1 kWp a-Si facade block at NAPS Customer Service Centre in Vantaa Finland

## PV-gable

# Amorphous Silicon PV Cladding System for Facades

The main advantages of using amorphous silicon PV modules in vertical facade applications are a more acceptable cost per unit area than crystalline silicon PV modules, and a more attractive uniform appearance over large areas. Although less efficient than crystalline silicon modules, amorphous silicon modules have advantages in that they are less affected by shadowing and are less affected by high operating temperatures.

For vertical PV facades on office and commercial buildings, NAPS has developed a new amorphous silicon module with an inexpensive mounting structure that fulfils the special safety and aesthetic requirements of glass facades. Attention has been paid to the design to the ease of mounting and maintenance. An inexpensive yet reliable wiring and connector system is used. This approach leads to a modular PV facade system that

can be a cost-effective PV building surface already today. Future developments of improved thin film PV modules can be easily incorporated into this design of module and structure.

Modules are mounted by sliding them into a special profile. Retrofit PV facades can have any number of modules in a horizontal row, although it is usual to group modules in multiples of one series string (normally 10). There is no limit to the number of rows that can be stacked vertically. Spaces at the ends of rows can be filled with a suitably coloured metal panelling, using the same mounting profiles.

The system is ideal for the refurbishment of old concrete-clad buildings which are now showing severe deterioration. It is also suitable for fitting to the surfaces of newer buildings.



**Fortum**

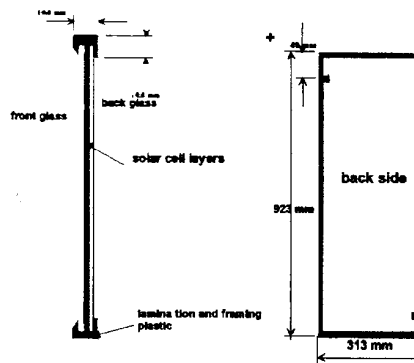
### The new a-Si facade module construction

NAPS has developed a special version of its 12Wp amorphous silicon module especially for vertical mounted building facades. This module has an improved encapsulation method which will give a longer service life than the 'normal production' amorphous silicon PV module. The new encapsulation method uses a polyurethane-based material between the two glasses which is also an integral frame.

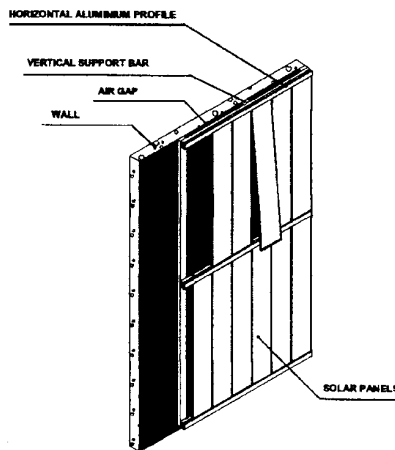
The frame is designed to be compatible with a specially-developed aluminium mounting channel. The module rests on one short side within the mounting profile. It is easy to replace single modules at any time should the need arise. Two short flying leads make series interconnections very simple.

- Increased service lifetime compared to conventional metal-framed a-Si modules with older encapsulation methods.
- Improved resistance to wind loading, allowing a low cost mounting system with easy replacement of individual modules if required.
- No possibility of the module frame becoming live and leading to a potential safety hazard or corrosion of the frame.
- Increased safety in the case of the module glass being broken in use or during installation, also in the case of fire (no large sharp glass fragments).
- Improved aesthetics, since the encapsulant is black rather than clear, which leads to a more uniform appearance of the modules.

### Module dimensions



### Mounting System



### Electrical specifications

(Under standard test conditions of: 1000W / sq m irradiance, cell temperature of 25°C and Air Mass 1.5 standard simulated solar spectrum)

Maximum power: 12Wp typically: 0.75A at 16.0V  
Open circuit: 23.2V, Short circuit: 0.94A  
Fill factor: 0.55, Module efficiency: 4.2%  
Cell efficiency (in module): 4.5%

Note: Maximum power Watts and efficiencies (subject to thermal and other module history conditions) are subject to a +/- 10% variation. All other figures are typical values.

Amorphous silicon PV modules give more than their rated maximum power during the first few weeks of their service life, which is a phenomenon common to the a-Si products of all manufacturers. Thereafter, the maximum power stabilises, but is somewhat dependent on the long term ambient temperatures to which the a-Si modules are exposed. The figure of 12Wp per module refers to the stabilised maximum power, measured under standard test conditions, if the module experiences an average ambient (air) temperature of 20-25°C for some weeks. In the southern parts of the Nordic countries, for instance, the year-round average ambient temperature is approximately 5-10°C, which is considerably less than 20-25°C. Under these conditions we would estimate the average stabilised module power to be reduced from 12Wp per module to approximately 11Wp per module.

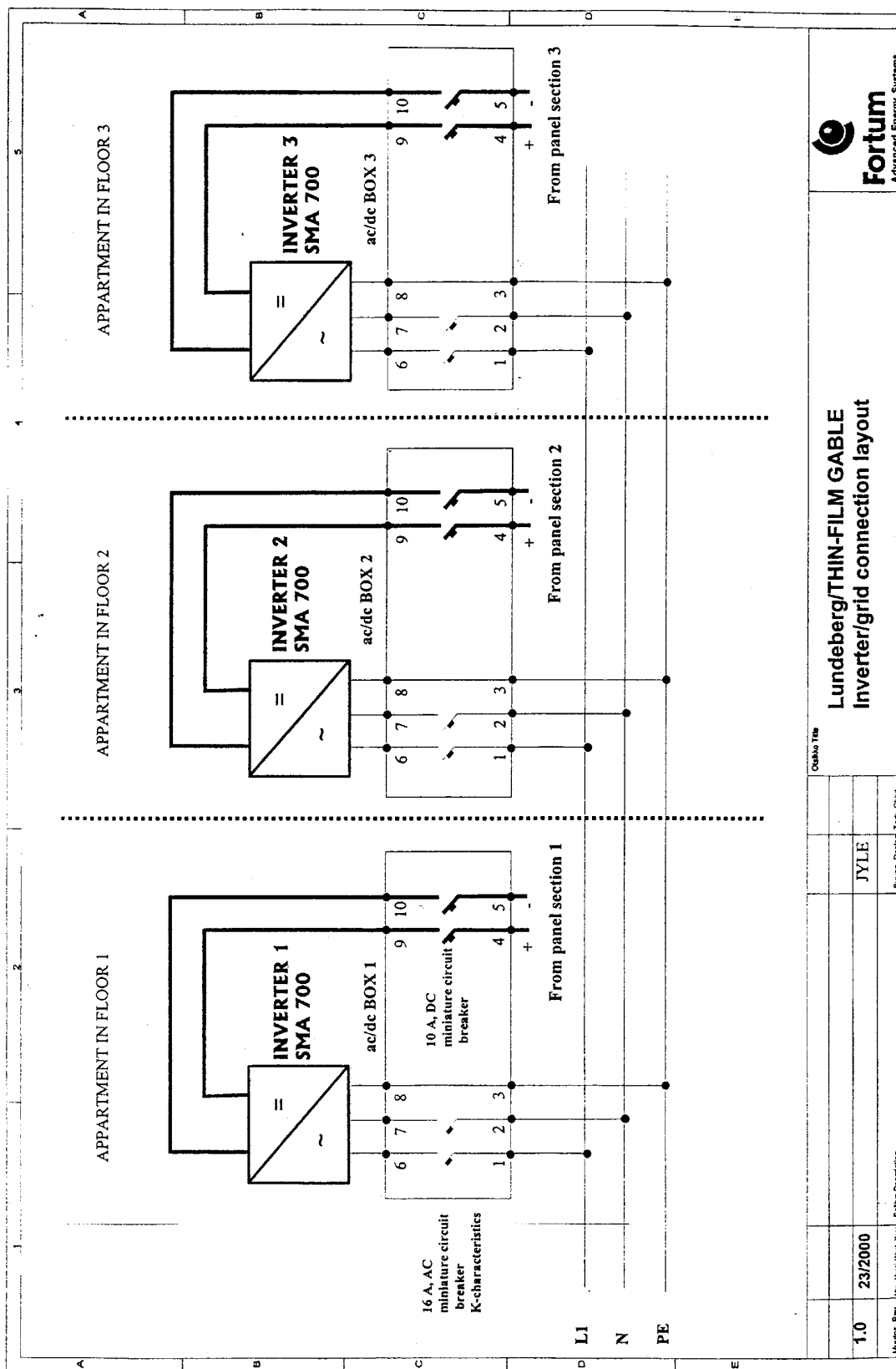


NAPS Systems Oy  
POB 90  
FIN-00048 FORTUM  
FINLAND  
Tel. +358 10 45 25547  
Fax +358 10 45 25744  
www.fortum.com

Your local NAPS office or Distributor is:

NAPS has sales and representative offices in Finland, France, Norway, Sweden, Kenya and UK.  
NAPS is part of Fortum Group. Fortum Group has worldwide interests in oil, energy and petro chemicals.





Osaka Tite

# Lundeberg/THIN-FILM GABLE Inverter/grid connection layout



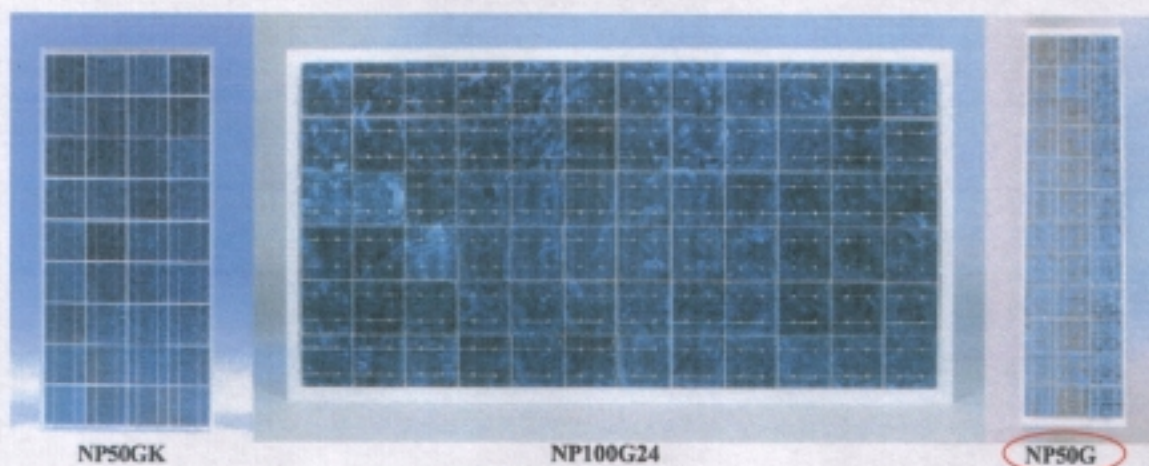
JYLE

1.0 23/2000

Shawn, Design, Test, Check

Multiple Rev. / No. / Date / Year / Subject Description





## Solar ventilation chimneys

### Polycrystalline solar modules type NPG

---

NPG range of high efficiency solar (photovoltaic, PV) modules combine power, efficiency and quality construction in highly dependable solar generators. These modules are designed for easy installation a for a wide range of applications, including battery charging, direct drive of solar water pumps and grid connection via a suitable inverter.

Most modules in the NPG range contain 36 polycrystalline silicon cells in series; the optimum module configuration for 12 Volt battery charging under the most demanding conditions. Charging of 24 and 48 Volt batteries is easily achieved by suitable series connection of modules.

The NP61GK module contains 44 polycrystalline silicon cells in series and is especially designed for use with one of our charge controllers with dc/dc conversion and current boosting, such as Genio and Max-Power.

Featuring the highest standards of construction, NPG Series modules are able to withstand the harshest environments and continue to perform efficiently. Properly installed, these modules have a design life of at least 20 years. Cells are protected from dirt, moisture and impact by a tempered, low-iron glass front. The solar circuit is laminated using EVA between tempered glass and a durable, multi-layered polymer back-sheet for superior moisture resistance.

NPG Series modules are tested to meet or exceed international standards, quality and performance requirements. The modules' test performance and our years of experience providing dependable power in locations throughout the world assure you that NPG modules can meet your solar power needs today. NPG Series modules carry a 10 year limited power warranty.





## NPG series modules

- Electrically-matched, polycrystalline silicon solar cells for efficient conversion of both direct and diffuse light.
- Cells chemically coated for reduced reflection.
- Double redundant contacts on each cell for greater circuit reliability.
- Low iron content 3mm tempered glass cover provides mechanical protection and high light transmission.
- Circuit laminated between layers of ethylene vinyl acetate (EVA) for moisture resistance, UV stability, and electrical isolation.
- Tough, multi-layered polymer backsheet for resistance to abrasion, tears and punctures.
- Rugged, lightweight anodised aluminium frame with 4 mounting slots (7 x 12mm) and 2 central 4mm diameter holes for grounding screws.
- One or two junction boxes, designed for easy field wiring, safety and environmental protection.
- Wired-in bypass diodes reduce potential loss of power or damage from partial array shading.
- Laboratory tested for a wide range of operating conditions (-40°C to +85°C).
- Designed to meet or exceed the environmental requirements of IEC61215 (equivalent to Ispra CEC503). Tested and certificated by TÜV.

## Power Specifications

	NP50G	NP50GK	NP61GK	NP75GK	NP75G	NP100G12	NP100G24	
Maximum Power ( $\pm 10\%$ )	50	50	61.1	75	75	100	100	Watts
Current (typical at max power)	3.00	3.00	3.00	4.57	4.57	6.00	3.00	Amps
Voltage (typical at max power)	16.7	16.7	20.4	16.4	16.4	16.7	33.3	Volts
Short Circuit Current (typical)	3.35	3.35	3.35	4.95	4.95	6.7	3.35	Amps
Open Circuit Voltage (typical)	21.6	21.6	26.3	21.1	21.1	21.6	43.1	Volts

The above values refer to standard test conditions of 1000 W/m<sup>2</sup> solar irradiance, 25°C cell temperature, Air Mass 1.5.

## Mechanical Details

	NP50G	NP50GK	NP61GK	NP75GK	NP75G	NP100G12	NP100G24
Overall length mm	1293	985	1198	1200	1580	1293	1293
Overall width mm	330	440	448	532	405	650	650
Thickness at edge mm	34	34	34	34	34	34	34
Weight kg	5.2	5.0	6.2	7.2	7.5	9.3	9.1
<b>Integral mounting slots 7 x 12 mm</b>							
Long sides: centre to centre mm	643	505	795	600	790	643	643
Long sides: centre to frame end mm	325	240	201.5	300	395	325	325
Short sides: centre to centre mm	287	409	409	489	362	607	607
Short sides: centre to frame end mm	21.5	15.5	19.5	21.5	21.5	21.5	21.5

## Construction

	NP50G	NP50GK	NP61GK	NP75GK	NP75G	NP100G12	NP100G24
Cells	36	36	44	36	36	72	72
Cell dimensions mm	101.25x101.25		125 x 125		125 x 125		101.25x101.25
Cell layout	3 x 12	4 x 9	4 x 11	4 x 9	3 x 12	6 x 12	6 x 12
Cell electrical circuit	36S x 1P	36S x 1P	44S x 1P	36S x 1P	36S x 1P	36S x 2P	72S x 1P
Junction boxes	2	1	1	1	2	2	1
Junction box type	A	G	G	G	A	A	G
Bypass diodes factory fitted	2	2	0	2	2	2	3

## NOCT

	NP50G	NP50GK	NP61GK	NP75GK	NP75G	NP100G12	NP100G24
Normal Operating Cell Temperature	43	43	43	42	42	44	44

Cell temperature at 800 W/m<sup>2</sup> solar irradiance, 20°C ambient temperature, wind speed  $\leq 1 \text{ m/s}$ , free air access to module rear

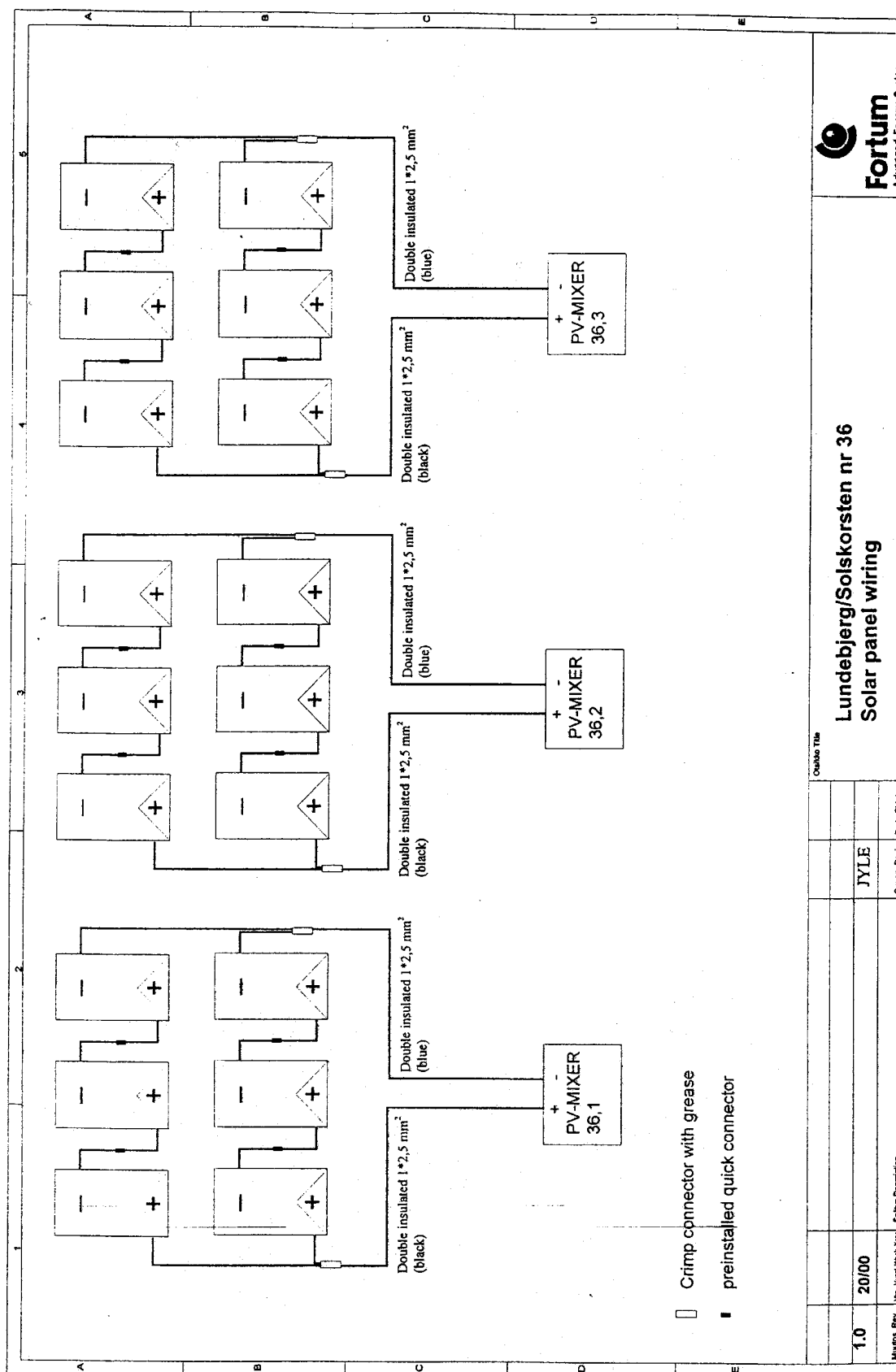


**Fortum**

NAPS Systems Oy POB 90 FIN-00048 FORTUM FINLAND  
Tel. +358 10 45 25547 Fax +358 10 45 25744 www.fortum.com

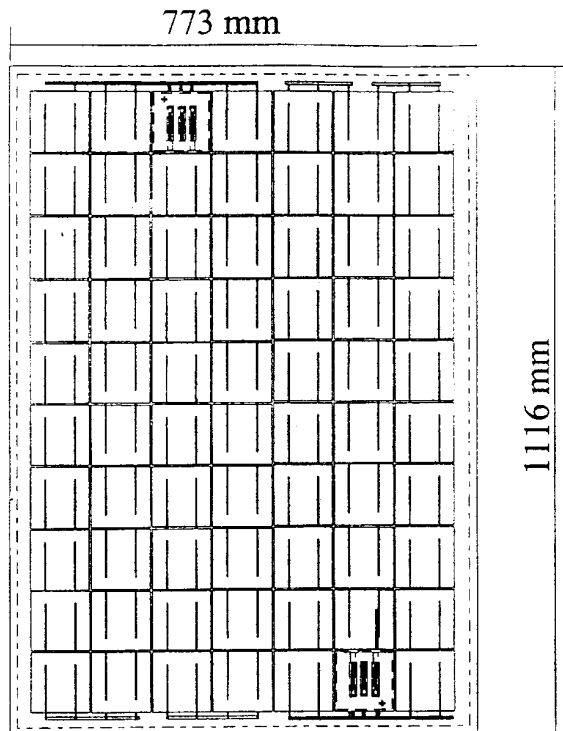
All product rights belong exclusively to NAPS Systems Oy. NAPS Systems Oy reserves the right to make changes without prior notice to the specifications of new versions of the product. To meet customers' needs we continuously develop our products. Therefore the specifications of the latest product versions should be checked before purchase.

GB-SE-P194-1-0300











Viewed from backside



Module Type	NP97G B
Max Power (+/- 10%)	97 Watts
Typical Imp	3 Amps
Typical Vmp	32,8 Volts
Typical Isc	3,25 Amps
Typical Voc	42 Volts

Specification based on 1 Kw/sq m solar irradiance  
25 deg C cell temperature, Air Mass 1.5



Potential electrical Hazard,  
when exposed to sunlight


Manufactured in Finland

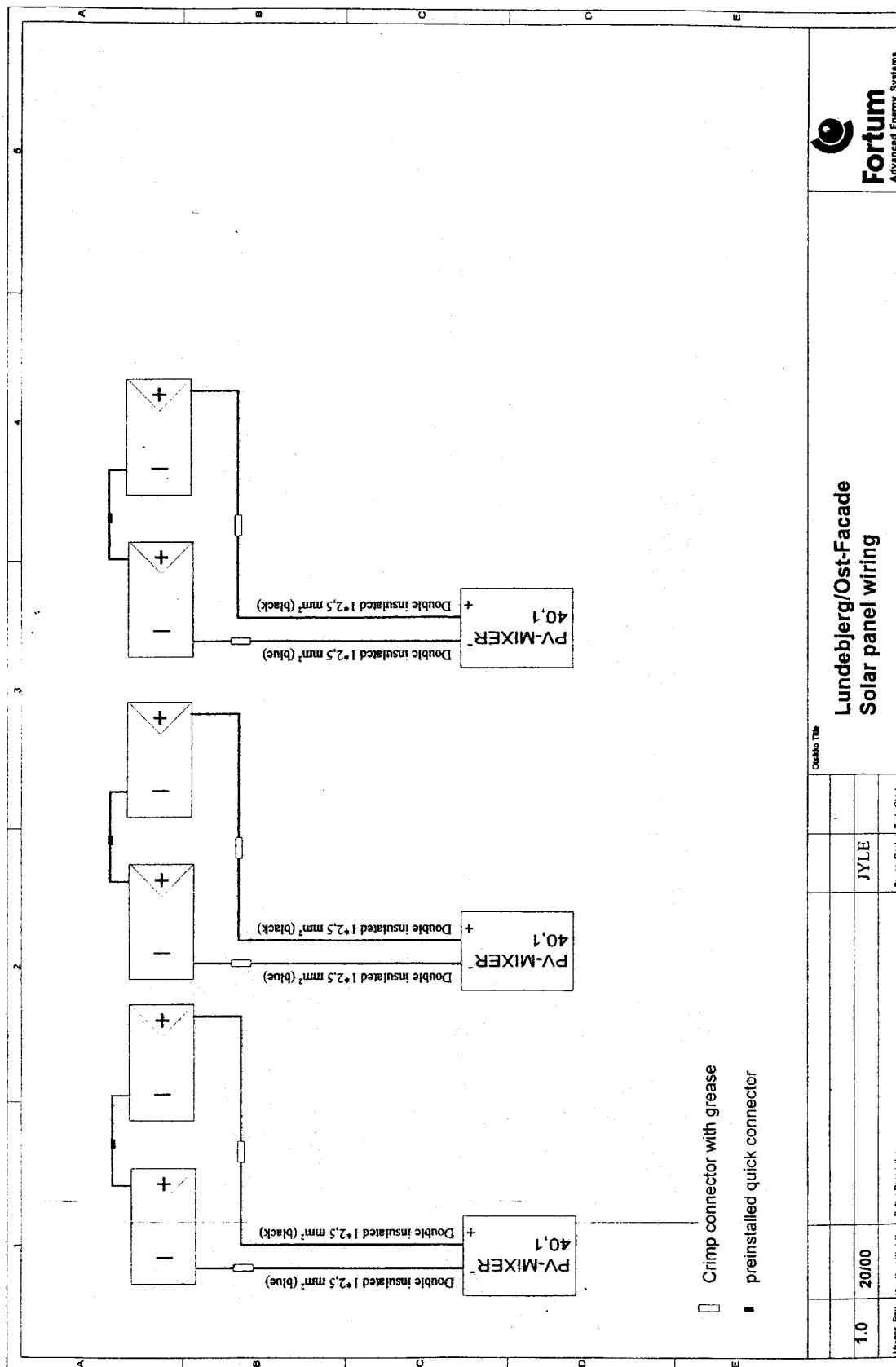
Phone +358 20 4501  
Fax +358 20 450 5744

Serial No

Panel electrical specification label

**6 modules of this type**

Rev.		Description	Title	 <b>Fortum</b> <small>Advanced Energy Systems</small>
	Jan 00		Lundebjerg Appartment building East facade panel	Solar panels, design



# **Appendix B**

## **Data sheets for the heat exchangers and fans**

(unfortunately only available in Danish)

# JoVex H300

## Tekniske data

AirVex er altid behjælpelig med projektering og beregning. Det sikrer, at vore kunder får netop det ventilationssystem de har brug for!

JoVex H300 er velegnet til effektiv ventilation af bygninger/lokaler op til 150 m<sup>2</sup>.

Systemet består af en varmegenvindingsenhed, to ventilatorkasser, to filterkasser, strømforsyning, styring og automatik.

JoVex H300 findes i 3 varianter:

- **JoVex H300-175 DC**
- **JoVex H300-190 AC**
- **JoVex H300-190 DC**

Ventilatorer med **AC-motorer** har bagudkrummede skovlblade for et lavere energiforbrug, trykstabilitet og lavt lydniveau.

**DC-ventilatorer** er med børsteløse elektronisk kommuterede motorer og bagudkrummede skovlblade.

Energiforbruget er ca. 20% mindre end for traditionelle AC-motorer.

## Fysiske data

Kabinettet er konstrueret med dobbelt galvaniseret stålplade og mellemiggende isolering.

Højde	220 mm
Dybde/bredde	500 mm
Længde, vekslerdel	1300 mm
Isolering	30 mm
Vægt vekslerdel	30 kg
Kondensafløb (rustfri studs)	1/2"
Vekslerareal	2x16 m <sup>2</sup>
Vekslermateriale	Søvandsbestandig aluminium
Temperaturvirkningsgrad	op til 90%

## Motorspecifikationer

	H300-175DC	H300-190AC	H300-190DC
2 stk. radialventilatorer med bagudkrummede vinger	Ø175 mm	Ø190 mm	Ø190 mm
Nettilslutning	230 V/50 Hz	230 V/50 Hz	230 V/50 Hz
Driftspænding ventilatorer	56 V DC	70-230 V	56 V DC
Forbrug W/m <sup>3</sup> luft pr. ventilator	0,11	0,18-0,38	0,16
Max. omdr./min	3500	2700	2950
Luftmængde ved 100 Pa	max. 200 m <sup>3</sup> /h	max. 200 m <sup>3</sup> /h	max. 250 m <sup>3</sup> /h
Max. optagen effekt inkl. Regulator	90 W	150 W	190 W
Max. lufttemperatur	60°C	60°C	60°C
Reguleringsområde	20-100%	70-230 V	20-100%
Styresignal	0-10 V DC	Spænding	0-10 V DC

## Tilbehør

Alle systemer fra AirVex kan udbygges med et omfattende program af tilbehør. Se særskilt løsesblad.

## AirVex ventilationssystemer

	Max. ydelse ved 100 Pa	Bygningsareal op til	Installation				Bemærkninger
			Lodret	Vandret	Udendørs	Indendørs	
JoVex H300	250 m <sup>3</sup>	100 m <sup>2</sup>	*	*	*	*	Ende på række
JoVex H450	450 m <sup>3</sup>	300 m <sup>2</sup>	*	*	*	*	Ende på række
JoVex L450	450 m <sup>3</sup>	300 m <sup>2</sup>	*	*	*	*	Ende på række
JoVex S450	350 m <sup>3</sup>	200 m <sup>2</sup>	*	*	*	*	Ende på række
JoVex S800	1000 m <sup>3</sup>	700 m <sup>2</sup>	*	*	*	*	Ende på række
JoVex H1000	1000 m <sup>3</sup>	700 m <sup>2</sup>	*	*	*	*	Ende på række
JoVex L1000	1000 m <sup>3</sup>	700 m <sup>2</sup>	*	*	*	*	Ende på række
JoVex S1500	1500 m <sup>3</sup>	800 m <sup>2</sup>	*	*	*	*	Ende på række

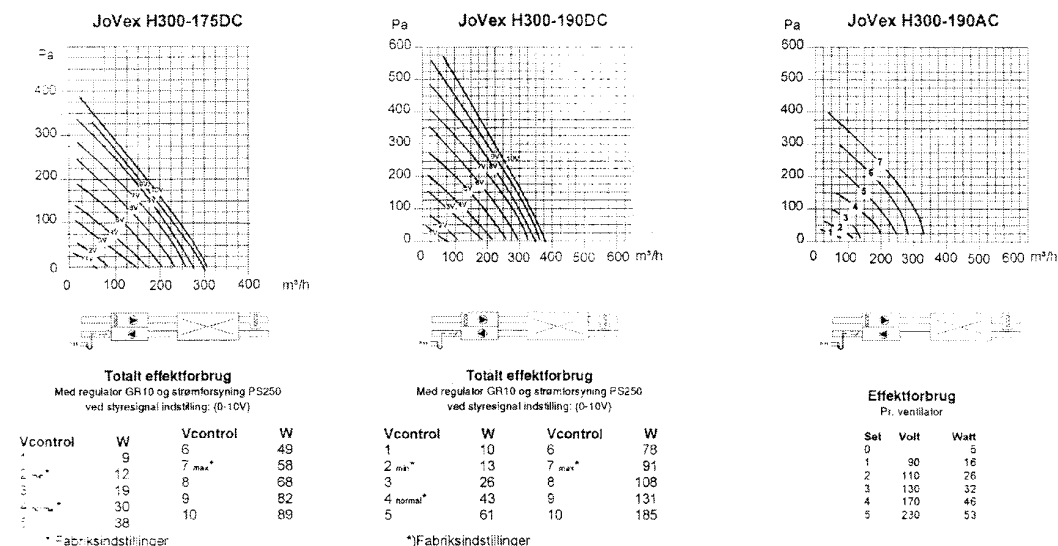
# JoVex H300

## Tekniske data

AirVex er altid behjælpelig med projektering og beregning. Det sikrer, at vore kunder får netop det ventilationssystem de har brug for!

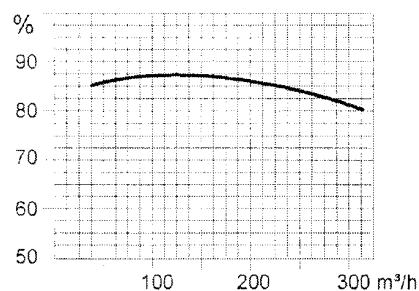
### Ydelsesdiagrammer og forbrug for JoVex H300 Anlæg:

Ydelserne er disponibelt tryk uden for aggregat med standard filtre.



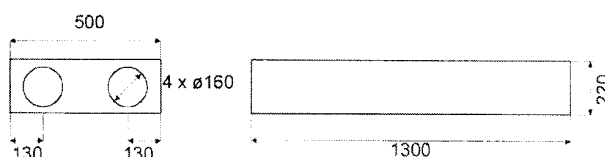
### Varmegenvinding for JoVex H300:

Bemærk at denne kan svinge som funktion af fugtighed, temperaturdifferens og luftmængder ind/ud.

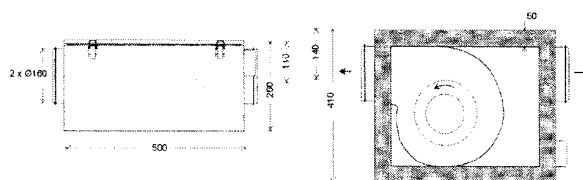


### Målskitse for H300

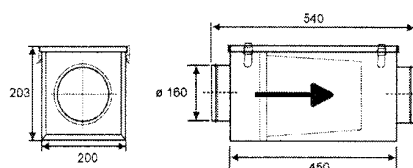
Mål mm



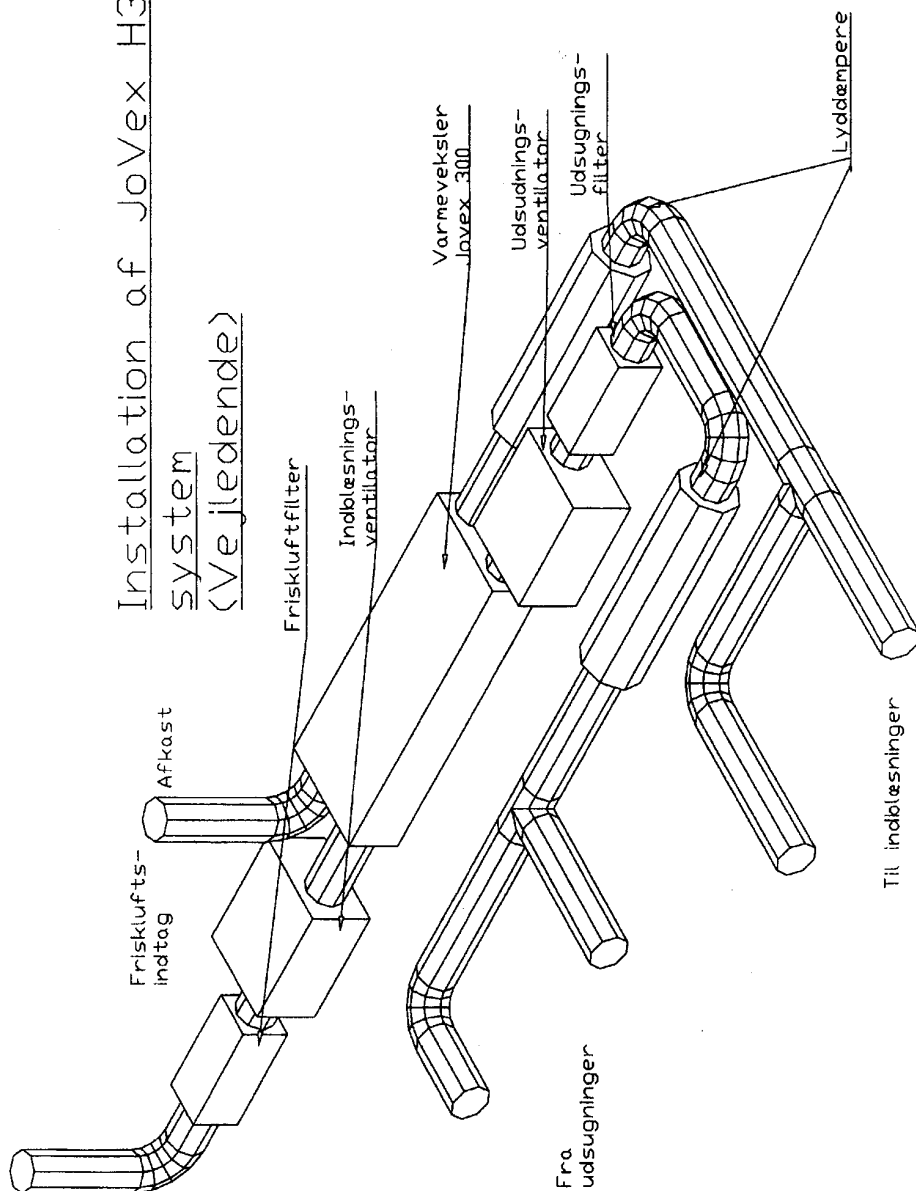
### Målskitse for ventilatorer (LMK160)



### Målskitse filterkasser



# Installation af JoVex H300 system (Vejledende)



Opstilling af JoVex H300 med  
tilhørende komponenter.

JoVex H300 DEMO	AirVex Danmark Norgesvej 3 DK-8450 Hammel	Tlf: 70231077 Fax: 70232180 www.airvex.dk
1/08/00		

# JoVex H1000

## Tekniske data

JoVex H1000 er velegnet til effektiv ventilation af bygninger/lokaler op til 1000 m<sup>2</sup>.

Systemet er velegnet til eksempelvis centralt udluftningssystem til etageejendomme eller til kontor/industri-bygninger.

Systemet består af en varmgenvindingsenhed, hvor på der med standard ventilationsfittings påsættes eksterne ventilator-kasser og filterkasser. Aggregaterne kan udstyres med vand eller el-varmeblader. Aggregaterne har internt bypass

JoVex H1000 findes i 2 varianter:

- JoVex H1000-280DC
- JoVex H1000-280AC

Begge versioner er med ventilatorer med bagudkrummede skovlblade for et lavere energiforbrug, trykstabilitet og lavt lyd-niveau.

DC-ventilatorer er med børsteløse elektronisk kommuterede motorer og bagudkrummede skovlblade. Energiforbruget er ca. 20% mindre end for traditionelle AC-motorer.

## Fysiske data

Kabinettet er konstrueret med dobbelt galvaniseret stålplade med mellemliggende isolering.

Højde/bredde/længde - veksler.....	630/940/1800 mm
Højde/bredde/længde/tilslutning - ventilatorer .....	390/550/600/ø315 mm
Højde/bredde/længde/tilslutning - filterkasser .....	500/500/450/ø315 mm
Længde, samlet .....	afhængig af opsætning
Isolering .....	50/100 mm
Vægt - veksler/motorer/filterkasser .....	110/30/10 kg
Kondensafløb (rustfri studs) .....	1/2"
Vekslerareal .....	2x64 m <sup>2</sup>
Vekslermateriale .....	Søvandsbestandig aluminium
Temperaturvirkningsgrad .....	op til 90%

## Motorspecifikationer

	H1000-280DC	H1000-280AC
2 stk. radialventilatorer	Ø280 mm Bagudkrummet	Ø280 mm Bagudkrummet
Nettilslutning	230 V/50 Hz	230 V/50 Hz
Driftspænding ventilatorer	56 V DC	70-230 V
Forbrug W/m <sup>3</sup> luft pr. ventilator	0,11	0,18-0,38
Max. omdr./min	3500	2700
Luftmængde ved 100 Pa	max. 1200 m <sup>3</sup> /h	max. 1100 m <sup>3</sup> /h
Max. optagen effekt inkl. Regulator	300 W	500 W
Max. lufttemperatur	60°C	60°C
Reguleringsområde	20-100%	70-230 V
Styresignal	0-10 V DC	Spænding

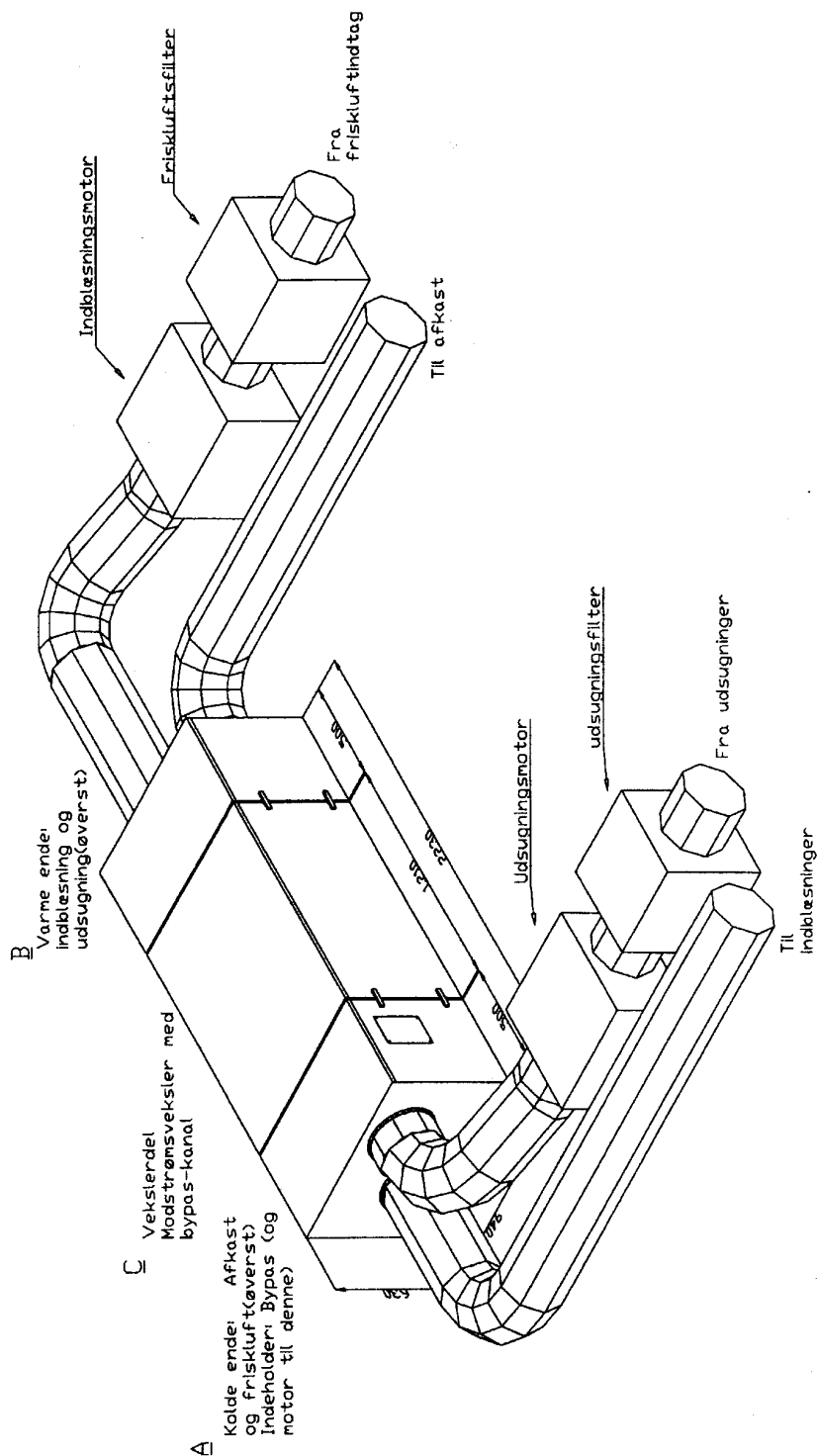
## Tilbehør

Alle systemer fra AirVex kan udbygges med et omfattende program af tilbehør. Se særskilt løbsblad.

## AirVex ventilationssystemer

	Max. ydelse ved 100 Pa	Bygningsareal op til	Installation				Bemærkninger
			Lodret	Vandret	Udendørs	Indendørs	
JoVex H450	450 m <sup>3</sup>	300 m <sup>2</sup>	*	*	*	*	
JoVex L450	450 m <sup>3</sup>	300 m <sup>2</sup>	*	*	*	*	
JoVex S450	350 m <sup>3</sup>	200 m <sup>2</sup>	*	*	*	*	
JoVex S600	1000 m <sup>3</sup>	700 m <sup>2</sup>	*	*	*	*	
JoVex H1000	1000 m <sup>3</sup>	700 m <sup>2</sup>	*	*	*	*	
JoVex L1000	1500 m <sup>3</sup>	700 m <sup>2</sup>	*	*	*	*	
JoVex S1500	1500 m <sup>3</sup>	800 m <sup>2</sup>	*	*	*	*	





H1000 ventilationsvarmeveksler  
for tilslutning til eksterne  
motorer og filtre

JoVex H1000	TermoVex Danmark	Tlf: 70231077
11/08/00	Norgesvej 3	Fax: 70232180
	DK-8450 Hammel	www.termovex.dk